

Crosslinked (Poly)vinylamine Copolymers

Von der Fakultät für Mathematik, Informatik und Naturwissenschaften der RWTH Aachen University zur Erlangung des akademischen Grades eines Doktors der Naturwissenschaften genehmigte Dissertation

vorgelegt von

Thorsten Fischer, M.Sc.

aus

Willich, Deutschland

Berichter: Prof. Dr. Martin Möller

Prof. Dr. Andrij Pich

Tag der mündlichen Prüfung: 06.03.2025

Diese Dissertation ist auf den Internetseiten der Universitätsbibliothek verfügbar.

Eidesstattliche Erklärung

Ich, Thorsten Fischer, erkläre hiermit, dass diese Dissertation und die darin dargelegten Inhalte die eigenen sind und selbstständig, als Ergebnis der eigenen originären Forschung, generiert wurden.

Hiermit erkläre ich an Eides statt

- 1. Diese Arbeit wurde vollständig oder größtenteils in der Phase als Doktorand dieser Fakultät und Universität angefertigt;
- 2. Sofern irgendein Bestandteil dieser Dissertation zuvor für einen akademischen Abschluss oder eine andere Qualifikation an dieser oder einer anderen Institution verwendet wurde, wurde dies klar angezeigt;
- 3. Wenn immer andere eigene- oder Veröffentlichungen Dritter herangezogen wurden, wurden diese klar benannt;
- 4. Wenn aus anderen eigenen- oder Veröffentlichungen Dritter zitiert wurde, wurde stets die Quelle hierfür angegeben. Diese Dissertation ist vollständig meine eigene Arbeit, mit der Ausnahme solcher Zitate;
- 5. Alle wesentlichen Quellen von Unterstützung wurden benannt;
- 6. Wenn immer ein Teil dieser Dissertation auf der Zusammenarbeit mit anderen basiert, wurde von mir klar gekennzeichnet, was von anderen und was von mir selbst erarbeitet wurde;

7. Ein Teil oder

Teile dieser Arbeit wurden zuvor veröffentlicht, und zwar in

- 1. Fischer, T., Köhler, J., Keul, H., Singh, S., Möller, M., Highly Swellable Hydrogels from Waterborne Poly(Vinylamine-*co*-Acetamide), *Macromol. Chem. Phys.* **2018**, 1800399.
- 2. Fischer, T. Köhler, J., Möller, M., Singh, S., Physical Gels of Poly(Vinylamine) by Thermal Curing, *RSC Adv.*, **2020**, *10*, 21933-21939
- 3. Fischer, T. Demco, D.E., Fechete, R., Möller, M., Singh, S.; Poly(vinylamine-co-N-isopropylacrylamide) linear polymer and hydrogels with tuned thermoresponsivity, *Soft Matter*, **2020**, *16*, 6549-6562
- 4. Fischer, T., Tenbusch, J., Möller, M., Singh, S., A Facile Method for Grafting Functional Hydrogel Films on PTFE, PVDF, and TPX Polymers, *Soft Matter*, **2022**, *18*, 4315

Table of Contents

1.	Declar	ration of Authorship	i				
2.	Zusam	nmenfassung	iv				
3.	Summ	ary	vii				
4.	Chapte	er 1. Introduction and Overview	1				
	a.	Motivation	1				
	b.	Overview	2				
5.	Chapte	er 2. Literature Survey about Polymerization, Introducing Thermore	sponsiveness				
	and Gelation of Poly(vinylamine)						
	a.	Introduction and Overview	4				
	b.	Polymerization	7				
	c.	Hydrogels and Microgels	17				
	d.	References	28				
6.	Chapte	er 3. Chemical gels of P(VAm-co-VAA)	34				
	a.	Introduction	35				
	b.	Experimental Part	37				
	c.	44					
		i. Polymer Synthesis	45				
		ii. Chemical Gelation	51				
		iii. Swelling Behavior	54				
		iv. Rheological Behavior	58				
	d.	Conclusion	60				
	e. References						
7.							
	a.	a. Introduction					
	b.	b. Experimental Part					
	c.	c. Results and Discussion					
	d. Conclusion						
	e.	References	82				
8.	Chapter 5. Thermoresponsive P(VAm-co-NIPAm) hydrogels						
	a. Introduction						
	b.	1					
	c.	Results and Discussion	93				
		i. Synthesis of the Polymer	93				
		ii. Temperature-Induced Phase Transition of the Polymer	96				
		iii. Temperature-Induced Phase Transition of the Hydrogels	105				
		iv. Water States and Side-Chain Dynamics by ¹ H-HRNMR	111				
		v. Polymer Diffusometry by ¹ H-HRNMR	114				
		vi. Hydrogel Morphology by Water Self-Diffusion	115				
	d.	Conclusion	119				
	e.	References	120				

9.	Chapte	er 6. A Facile Method for Grafting Functional Hydrogel Films on l	PTFE, PVDF
	and TI	PX Polymers	124
	a.	Introduction	125
	b.	Experimental Section	127
	c.	Results and Discussion	131
	d.	Conclusion	146
	e.	References	147
10.	Ackno	wledgements	152

Zusammenfassung

Die vorliegende Arbeit befasst sich hauptsächlich mit der Polymerisation von N-Vinylamiden und der anschließenden Gelierung. Dazu werden via Hydrolyse freie Amingruppen gebildet und die Präpolymere über Carbonat-Vernetzer geliert. Ferner wird eine Methode vorgestellt um inerte Oberflächen via Nitreninsertion mit primären Amingruppen zu versehen.

Während Gele basierend auf Acrylamid, ein Konstitutionsisomer von N-Vinylformamid, Gegenstand vielfältiger Literatur sind, gibt es deutlich weniger Beispiele für Gelsystem basierend auf NVF. Gele basierend auf NVF haben allerdings den Vorteil über eine einfache Hydrolyse eine (maßgeschneiderte) Anzahl freier primärer Amingruppen zu bilden. Primäre Amingruppen können über vielfältige Reaktionen weiter funktionalisiert werden, um spezielle Eigenschaften zu erhalten (z.B. Zellbindungspeptide). Allerdings ist eine direkte Polymerisation zu Polyvinylamin (PVAm) nicht möglich, da das entsprechende Monomer, Vinylamin, nicht stabil ist. PVAm wird bisher schon u.a. in der Papier- und Textilindustrie eingesetzt. Ein auf PVAm basierendes Gel könnte aufgrund der freien primären Amingruppen vielfältige weitere Anwendungsmöglichkeiten u.a. im medizinischen Bereich ermöglichen. Die Attraktivität der Gel- und Polymersysteme basiert auf der maßschneiderbaren Dichte von Amin-Gruppen, womit direkte Auswirkungen auf die erhaltenen Eigenschaften wie Ladungsdichte/pH-Responsivität, Vernetzungsgrad, Hydrophilie, etc. gesteuert werden können. Zudem erlaubt die Copolymerisation mit hydrophoben Monomeren die Darstellung thermoresponsiver Polymere und Gele. Diese gelten als attraktive Kandidaten z.B. für Wirkstofffreisetzungssysteme.

Kapitel 2 bietet einen umfassenden Überblick über die Gelierung von PVAm. Dafür wird zunächst auf die neusten Entwicklungen eingegangen, um PVAm zu synthetisieren, auf insbesondere im Hinblick definierte Molekulargewichte und Polydispersiätsindices (PDI). Weiterhin werden Methoden vorgestellt, um thermoresponsive Copolymere von Polyvinylamid bzw. PVAm zu erhalten, bzw. welche untere kritische Löslichkeitstemperatur (LCST) in Abhängigkeit des molaren Anteils von N-Vinylamin bzw. NVF mit verschiedenen Co-Monomeren erreicht werden kann. Der zweite Teil von Kapitel 2 befasst sich mit den unterschiedlichen Gelierungsmethoden von PVAm. Für die Darstellung der Gele wird einerseits eine in-situ Gelierung bei der Polymerisation in Anwesenheit eines Vernetzers mit abschließender Hydrolyse um freie Amingruppen zu erhalten diskutiert. Andererseits besteht die Möglichkeit einer nachträglichen Vernetzung eines Präpolymers über freie Amingruppen. Weiterhin werden auch thermoresponsive Gele betrachtet.

In Kapitel 3 wird die Copolymerisation von NVF mit N-vinylacetamid (NVA) betrachtet. Die Bestimmung der Polymerisationsparameter beider Monomere zeigt eine statistische Verteilung. Ferner zeigt die Kinetik und Selektivität der Hydrolyse in Bezug auf NVF bzw. NVA, dass unter gewählten Bedingungen NVF komplett selektiv hydrolysiert wird. Die Amin-funktionellen Präpolymere werden mittels Phenylcarbonat-telechelic Polyethylenglykol in Anwesenheit einer Base vernetzt. Die erhaltenen Hydrogele werden in Abhängigkeit der Restanteile primärer Amine, der Basenkonzentration, und der Vernetzerkonzentration hinsichtlich ihres Quellungsverhaltens und rheologischer Eigenschaften hin untersucht. Es zeigt sich, dass mit diesem System sehr hohe Quellungsgrade realisiert werden können. In Abwesenheit einer Base führt die elektrostatische Anziehung zwischen den Urethangrupen zu einer physikalischen Vernetzung. Dieses wird in Kapitel 4 besprochen. Hierfür konnte eine kritische Gelierungskonzentration über rheologische Experimente bestimmt werden, die sich daraus ergibt, dass eine Vernetzung bei Konzentrationen unterhalb des maximalen Quellungsgrades kein durchgehendes Gel ergibt. Die physikalischen Wechselwirkungen wurden mittels NMR und UV-Vis Spektroskopie untersucht. Außerdem wurd gezeigt, dass die schnelle Gelierung zu Inhomogenitäten führt, die über aufeinanderfolgende Heiz- und Kühlzyklen homogenisiert werden können, was sich durch ein deutlich erhöhtes Speichermodul zeigt. Eine chemische Vernetzung konnte über NMR ausgeschlossen werden. In Kapitel 5 werden temperaturresponsive Copolymere und Hydrogele besprochen. Hierzu wird NVF mit N-isopropylacrylamid copolymerisiert (NIPAm) und anschließend hydrolysiert. Die Copolymerisationparameter zeigen dabei eine leicht schnellere Polymerisation von NVF, d.h. innerhalb eines Polymers gibt es einen Gradienten von hoher zu niedriger NVF-Konzentration. Durch NMR konnte gezeigt werden, dass unter den gewählten Bedingungen selektiv NVF hydrolysiert wird. Die LCST der Copolymere lässt sich hierbei über das NVF zu NIPAm Verhältnis einstellen, was via UV-Vis Spektroskopie, NMR gezeigt wird. Die anschließende Gelierung über 1,2-Rheologie und Bis(Phenylcarbonat)-Ethylenglykol ergibt temperaturresponsive Hydrogele. Diese werden über UV-Vis Spektroskopie, Rheologie und NMR charakterisiert. Dabei wird ein two-state model angewendet, um den Phasenübergang zu beschreiben.

In Kapitel 6 werden chemisch inerte Oberflächen, d.h. Polymethyl-1-penten (TPX), Polyvinylidenfluorid (PVDF) und Polytetrafluoroethylen (PTFE) mit einer dünnen Hydrogelschicht oberflächenfunktionalisiert. Dazu wird ein PVAm basiertes Copolymer mit N-Succinimidyl-4-azidotetrafluorobenzoat funktionalisiert. Das vorhandene Azid reagiert unter UV-Licht zu einem hochreaktiven Nitrene. Diese können u.a. in die C-H Bindung

insertieren, wodurch eine stabile kovalente Bindung an die die aliphatischen und überraschenderweise auch an die PTFE Oberflächen erreicht wird. Ausgiebige Untersuchungen des Benetzungsverhalten der behandelten Oberflächen mit Wasser zeigen, dass die Oberflächen hydrophylisiert worden sind. Dynamische Kontaktwinkelmessungen mit der Wilhelmy-Waage legen hierbei nahe, dass die Polymerketten die Möglichkeit einer Re-Orientierung haben, d.h. das hydrophobe Polymerrückgrat ist in Luft nach außen gerichtet und dreht sich nach Wasserkontakt nach innen. Dieser Vorgang ist komplett reversibel. Folglich kann man die so funktionalisierten Oberflächen als amphiphil bezeichnen. Diese Arbeit bildet damit die Grundlage um chemisch inerte Oberflächen zu funktionalisieren um zum Beispiel die mechanischen Eigenschaften von **PTFE** mit Zellbindungspeptiden oder Wachstumshormonen/Medikamenten auszustatten.

Summary

This thesis deals mainly with the polymerization of N-Vinylamides and their subsequent gelation. Therefore, free amines are generated by hydrolysis of the pre-polymers, which are subsequently crosslinked by carbonate-based crosslinkers. Moreover, a method is presented to decorate inert surfaces with primary amin groups by nitren insertion.

While Gels based on acrylamide, a constitution isomer of N-vinylformamide (NVF), is subject of manifold literature, examples of gel systems based on NVF are scarce. Nevertheless, gel systems based on NVF have the advantage of a (tailored) number of free primary amine groups via simple hydrolysis. Primary amine groups can be further functionalized by numerous reactions to gain specific properties, e.g. cell binding sequences. Thus, PVAm based gels can find entrance in medical applications. In general, the attractiveness of PVAm based systems is caused by the tailorable number of primary amine groups which in turn influence properties such as charge density/pH responsiveness, crosslinking density, hydrophilicity, etc. However, a direct polymerization to poly(N-vinylamine) (PVAm) is not possible, since the respective monomer, vinyl amine, is not stable. Therefore at least two step synthesis is necessary including a hydrolysis step.

In Chapter 2, the latest methods are summarized to synthesize PVAm, especially with focus to defined molecular weights and a low polydispersity index. Moreover, methods are introduced to obtain thermoresponsive copolymers of polyvinlamide/PVAm. It is demonstrated how the lower critical solution temperature (LCST) can be tailored by the molar fraction of VAm or NVF with different co-monomers. The second part of Chapter 2 deals with the different gelation methods of PVAm. The synthesis of the gels is on the one hand discussed via an insitu gelation in the presence of a crosslinker during the polymerization with subsequent hydrolysis and on the other hand via the formation of prepolymers which are hydrolyzed and subsequently crosslinked via the free amine groups. Furthermore, thermoresponsive gels are presented.

In Chapter 3 the copolymerization of NVF with N-vinylacetamide (NVA) is shown. The copolymerization parameters of both monomers reveals a statistical distribution. Further show the kinetics and the selectitivity of the hydrolysis with respect to NVF and NVA that NVF is hydrolyzed completely under defined conditions. The amin-functional prepolymers are crosslinked by phenylcarbonate telechelic poly(ethylene glycol) (PEG-PC) in presence of a base. The formed hydrogels are characterized by their swelling ratio and rheological

properties in dependence on the concentration of primary amines, the concentration of the base, and the concentration of the crosslinker. It is shown that with this gel system very high swelling ratios can be realized. In absence of a base leads the electrostatic interaction between the urethane groups to physical crosslinking. These are discussed in Chapter 4. The critical gelation concentration is determined via rheology. The physical interactions were examined by NMR and UV-Vis spectroscopy. Furthermore, it is shown, that the fast gelation leads to inhomogenities, which could be cured by subsequent heating/cooling cycles as revealed by a significant increase of the storage modulus. A possible chemical crosslinking-reaction is ruled out by NMR.

In chapter 5 thermoresponsive copolymers and hydrogels are prepared. Therefore, NVF is copolymerized with N-isopropylacrylamide (NIPAm) und subsequently hydrolyzed. The copolymerization parameters reveal a slightly faster polymerization of NVF, which means within a polymer chain there is a gradient from a NVF rich to a NVF poor regime. NMR shows, that NVF can be selectively hydrolyzed under defined conditions. The LCST can be tailored via the ratio of NVF to NIPAm, what is shown in rheology and UV-Vis spectroscopy. The gelation via 1,2-bis(phenylcarbonate)-ethylene glycol yields in thermoresponsive hydrogels. These are characterized by NMR, UV-Vis spectroscopy, and rheology. A two-state model is applied to describe the phase transition.

In Chapter 6 the surface of chemically inert foils, that means polymethyl-1-penten (TPX), poly(vinylidene fluorid) (PVDF), and poly(tetrafluoro ethylene) (PTFE) are functionalized with a thin hydrogel layer. Therefore a copolymer based on PVAm is functionalized with N-succinimidyl-4-azidotetrafluoro benzoate. The azide reacts to a highly reactive nitrene under UV light. These nitrenes can insert in e.g. a C-H bond leading to a stable covalent binding to the aliphatic and surprisingly also PTFE surfaces. Thorough investigations of the wetting behavior of the treated surfaces show, that the surfaces are hydrophilized. Dynamic contact angle measurements with the Wilhelmy balance suggest that the polymerchains can reorientate, which means that the hydrophobic polymer backbone is directed to the outside while in contact with air turning to the inside while in contact with water. This process is reversible. Consequently, the treated surfaces are amphiphile. This work might be the base to functionalize chemically inert surfaces to combine e.g. the mechanical properties of PTFE with cell recognition sequences, growth factors, drugs, and so on and so forth.

List of Abbreviations

2EOENVF N-vinyl-N-ethoxyethoxyethyl formamide

AA Acrylic acid

AAm Acrylamide

AIBN Azo-bis(isobutylnitril)

APS ammonium peroxodisulfate

CHic C-H insertion crosslinking

CLSM Confocal laser scanning microscopy

CMRP Cobalt mediated radical polymerization

DLS Dynamic light scattering

DN Double network

DOI Degree of ionization

DSC Differential scanning calorimetry

ECMO Extracorporal membrane oxygenator

EDC 1-Ethyl-3-(3-dimethylaminopropyl)carbodiimide

EG-PC Ethylene glycol-1,2-bis(phenylcarbonate)

EOENVF *N*-vinyl-*N*-ethoxyethyl formamide

EWG electron withdrawing group

FTIR Fourier-transformation infra-red

G' Storage modulus

G" Loss Modulus

GA Glutaraldehyde

GMA Glycidyl methacrylate

HRMAS High resolution magic angle spinning

LCST Lower critical solution temperature

LVE Linear viscoelastic regime

MBAA *N,N'*-methylene bisacrylamide

MCH microgel composite hydrogel

MMA methyl methacrylate

M_n Number average molecular weight

M_w Weight average molecular weight

NHS N-Hydroxysuccinimide

NIPAm N-isopropyl acrylamide

NMR Nuclear magnetic resonance

NMVA N-methylvinylacetamide

NVA *N*-vinylacetamide

NVCl N-vinylcaprolactam

NVEE 2-(*N*-vinylformamido)ethyl ether

NVP N-vinylpyrrolidone

PAA Poly(acrylic acid)

PCF Phenyl chloroformate

PDI Polydispersity index

PE Poly(ethylene)

PEG Poly(ethylene glycol)

PEG-PC Poly(ethylene glycol) telechelic bis(phenyl carbonate)

PEI Poly(ethylene iminie)

PNVF Poly(*N*-vinylformamide)

PNVIBA Poly(*N*-vinylisobutyramide)

PNVNiPrF Poly(*N*-vinyl-*N*-isopropylformamide)

PTFE Poly(tetrafluoro ethylene)

PVAm Poly(vinylamine)

PVDF Poly(vinylidene difluoride)

PVPI Poly(*N*-vinylphtalimide)

SAOS Small amplitude oscillation shear

SEC Size exclusion chromatography

SEM Scanning electron microscopy

SN Single network

TBHP tert-butyl hydroperoxide

TEA Trietyl amine

TEMED *N,N,N',N'*- Tetramethylethan-1,2-diamine

THF Tetrahydrofuran

TPX Poly(1-methylpentene)

VA044 Azo-bis[2-(2.imidazolin-2-yl)propane] dihydrochloride

VAc Vinylacetate

Vam Vinylamine

VPTT Volume phase transition temperature

wt% weight%

Chapter 1.

Motivation and Introduction

The original aim of this thesis was to synthesize a double network hydrogel consisting of a chemical gel based on poly(vinyl amine) (PVAm) and a physical gel in order to completely cover a stent. This double network gel should solve the main problems caused by the stent, i.e. the restenosis caused by the change of the phenotype of the blood vessel surrounding smooth muscle cells to the proliferative type and the thrombosis caused by the lesion of the blood vessel. The hydrogel layer should accordingly form a mechanical barrier to stop the smooth muscle cells from proliferation and to "hide" the lesion avoiding thrombus formation. PVAm was used because of the variety of reactions the primary amine group can undergo. However, the gelation of PVAm itself posed an unexpected great challenge. A further obstacle was the occurrence of barely described phenomena such as physical gel via the formation of non-covalent carbonateamin bonds, the apparent covalent crosslinking/insertion of nitrenes with poly(tetrafluoro ethylene), etc. These effects made it necessary to generate new hypotheses, which had to be falsified or verified. Therefore, this thesis can be considered as fundamental research for the gelation of PVAm. In order to obtain a deeper understanding of PVAm and its behavior several different gel systems (chemical and physical) are synthesized and thoroughly investigated by various methods including Cryo-SEM, rheology, NMR, DSC, Contact Angle, UV-Vis spectroscopy, etc. obtaining valuable information about the structure-property relationship. Thus, the major contribution of this thesis is the understanding of PVAm based gel systems by prepolymerization with subsequent hydrolysis and crosslinking providing a platform for double network hydrogels.

Chapter Overview

This thesis is divided into 6 Chapters, which are briefly described in the following paragraphs:

Chapter 2. gives a comprehensive overview about the literature of P(VAm) and its thermoresponsive copolymers. Furthermore, microgels and hydrogels based on P(VAm) are presented. At last, thermoresponsive microgels and hydrogels are described.

Chapter 3. describes the chemical gelation of poly(*N*-vinylamine-*co*-acetamide) with poly(ethylene glycol) telechelic bis(phenylcarbonate). The polymerization and hydrolysis of the copolymer is analyzed. Afterwards the obtained hydrogels are described in terms of their swelling and rheological behavior.

Chapter 4. describes a physical gel formed by the components used in Chapter 3. The nature of the bonding is analyzed in terms of UV-Vis spectroscopy and rheology. Chemical crosslinking is ruled out. It is shown, that thermal curing can homogenize the gel.

Chapter 5. describes the synthesis of poly(N-vinylamine-co-N-isopropylacrylamide) and hydrogels thereof. The phase transition of the polymer and the hydrogel is characterized by UV-Vis spectroscopy, rheology, and advanced NMR spectroscopy.

Chapter 6. describes the formation of a hydrogel layer based on PVAm on chemical inert surfaces by C-H insertion crosslinking. To achieve this PVAm is functionalized with an azide moiety which reacts to a nitrene under UV light. The resulting hydrogel film is investigated by advanced wetting experiments.

Chapter 2

Literature Survey about Polymerization, Introducing Thermoresponsiveness and Gelation of Poly(vinylamine).

1. Introduction

Polyvinylamine (PVAm) is one of the most interesting and versatile polymers. Its versatility arises from its high density of primary amines, which can undergo multiple reactions as shown in Scheme 2.1.¹

Scheme. 2.1. Some chemical reactions of PVAm. Physical interactions (metal complexation, CO₂ attachment, etc. not shown). Adapted from Ref.² The reaction of PVAm with acetone is claimed by Trommler et al.³

Though in contrast to its simple structure, its polymerization was challenging for decades as already indicated by the titles of reviews by Jones (1944) "Attempted Preparation of Polyvinylamine" and Pinschmidt (2010) "Polyvinylamine at Last". The challenging character is caused by the instability of the according Vinylamine (VAm) monomer, which tautomerizes to the imine. The breakthrough came with the invention of two-step processes namely the route via hydrolysis of an alkylamide, Hofmann rearrangement of acrylamide, or, more recently, the hydrozinolysis of poly(N-vinylphtalimide) (PVPI).⁶⁻⁸ Among these methods the hydrolysis, which involves the polymerization of a *N*-vinylamide, for example *N*-vinylformamide (NVF) and the subsequent hydrolysis of the amide group, is the most straight forward. Knowledge about hydrolysis kinetics allows control of the hydrolysis degree and therefore the density of primary amine groups. 9,10 The second method to tailor the density of primary amines or to introduce further functionality is the copolymerization of N-vinylamide with a second monomer; for example NVF can be selectively hydrolyzed in presence of N-vinylacetamide (NVA) and NVA can be selectively hydrolyzed in presence of N-methylvinylacetamide (NMVA), respectively. 11-14 Besides the intrinsic pH responsiveness of PVAm advanced applications like triggered release systems require further stimuli-responsiveness. In this context thermoresponsiveness is the most relevant one. 15-17 Therefore, particular focus is given on thermoresponsive copolymers, where applicable.

This literature survey is divided in two parts. The first part deals with the developments from the last 5 years, on the polymerization and ways to obtain a defined molecular weight with a narrow PDI. Particularly, the focus is laid on thermoresponsive copolymers, where the complete literature is reviewed. The second part deals with microgels and hydrogels from PVAm. Since this topic was not considered in the review of Pinschmidt or Pelton, the complete literature is reviewed.

2. Polymerization

2.1 Controlled Polymerization

Although N-vinylamides, in particular, NVF is long known, their controlled polymerization remains challenging. The vast majority of polymerization techniques of NVF rely on radical polymerization. Cationic polymerization of NVF is also known, but mainly to obtain NVFoligomers. This is due to the limited solubility of poly(N-vinylformamide) (PNVF) in solvents other than water and due to the reactivity of the monomer itself which has three different nucleophilic sites (double bond, carbonyl group, amide group). 18 However, the controlled radical reaction of NVF obtaining a narrow PDI still presents a key challenge. Controlled polymerization techniques of N-vinyl monomers were extensively reviewed in 2013 by Nakabayashi et al.¹⁹ Consequently, in this survey, only the recent developments of the polymerization of acyclic N-vinylamides are considered. These polymerization techniques are based on organometallic mediated reaction mechanisms giving controlled molecular weight and dispersity. 12,20-24 In a systematic study by Debuigne et al. bis(acetylacetonato)cobalt(II) ([Co(acac)₂]) was used for the controlled radical polymerization in bulk of N-vinylamides.²⁴ In particular NVF, NVA, NMVA, N-vinylpyrrolidon (NVP), N-vinylcaprolactam (NVCl), and vinylacetate (VAc) were polymerized via cobalt mediated radical polymerization (CMRP)²⁴ The mechanism of CMRP relies on the reversible entrapment of the radical forming a cobaltpolymer bond (Scheme 2.2.). The rate of reaction is determined by the ratio of the rate of chelation k_c (species 1 "dormant") and the rate of dissociation k_d (species 2 "active"). Besides known factors such as solvent and temperature, ^{25,26} intramolecular chelation with the carbonylmoiety of the amide forming a five-membered ring (species 3)²⁷ and the presence of hydrogen on the secondary amine as in case of NVA and NVF play a crucial role.²⁴ While for the cyclic vinylamides and for NMVA narrow PDIs were reported, but the reaction is poorly controlled for NVA and NVF. It is believed that free monomers stabilize the radical by hydrogen bonding and the lability of the C-Co bond for the less substituted vinylamides are driving the equilibrium to the active species. 24 The reduction of the temperature to 0 °C for photointiation in solution further improves the control of the reaction yielding for example to a PDI of 1.18 with molecular weight M_n of 56.3 kDa and 23 % conversion. $^{12,21-24}$ However, the controlled polymerization of NVF still remains unsolved. This challenge was overcome recently changing the central-atom of the metal-organic species to tellurium for an organotellurium-mediated radical polymerization (TERP). 20 NMVA, NVA, and NVF were polymerized in the presence of an organotellurium chain transfer reagent and thermally initiated by an azo-initator, resulting in a pseudo-first-order kinetics of polymerization and attainment of low dispersity (< 1.25). This study is the first reported case of a controlled radical polymerization of NVF. The PNVF was subsequently hydrolyzed to the corresponding amine. 20

homolytic bond cleavage
$$k_{d}$$

$$k_{c}$$

$$k_{d}$$

$$k_{d$$

Scheme 2.2. Mechanism of CMRP. The reaction rate k_d and k_c determines the reaction rate of the polymerization. The scheme is reproduced with permission from ref²⁴.

2.2 Thermoresponsiveness

Thermoresponsiveness is in general related to LCST behavior, which means with exceeding a certain temperature a miscibility gap occurs in water. It is believed to be an entropic effect caused by hydrophobic domains, which are surrounded by a water cage below LCST, and which are aggregating above LCST. Neither commercially available NVF nor NVA nor NMVA reveal such a behavior in water till 100 °C due to their hydrophilicity. However, the addition of salt leads to a salt-out effect for PNVA with a liquid-liquid separation above the LCST. For example the LCST of PNVA is decreased to 18 ± 1 °C in a solution of $1.25 \text{ mol} \cdot \text{L}^{-1}$ (NH₄)₂SO₄. Representation above the LCST of PNVA is decreased to 18 ± 1 °C in a solution of

Several strategies have been established to introduce thermoresponsive behavior in water including

- 1. Co-polymerization with commercially available thermoresponsive monomer
- 2. Synthesis of a thermoresponsive monomer for (co-)polymerization
- 3. Post-functionalization of the (Co-)polymer.

In this section at first the synthesis of thermoresponsive *N*-vinylamide monomers is described as they are not commercially available. Furthermore, homopolymers by post-modification are considered and the LCST of the resulting homopolymers is discussed. Afterwards copolymers and, in particular, thermoresponsive copolymers are presented.

2.2.1 Thermoresponsive *N*-vinylamide monomers and polymers

The majority of literature is based on the modification of commercially available NVF, which can lead to structures shown in Figure 2.1. A hydrophobic modification decreases the LCST, which is for example for PNVIBA in the range of 39-41 °C.³⁰ Modifications like Figure. 2.1a were reviewed by Panarin in 2015 and include for example Michael adducts of esters, ketones, and nitrils or alkylations.³¹ Recently, 1-bromo alkyl ethers was used for the synthesis of NVF

derivatives with an oligo ethylene glycol chain. While methoxy-terminated chains do not reveal LCST behavior, it is found for ethoxy-terminated chains, namely *N*-vinyl-*N*-ethoxyethylformamide (EOENVF) and *N*-vinyl-*N*-ethoxyethoxyethylformamide (2EOENVF), which have an LCST of 48 °C and 77 °C, respectively (Table 1).³²

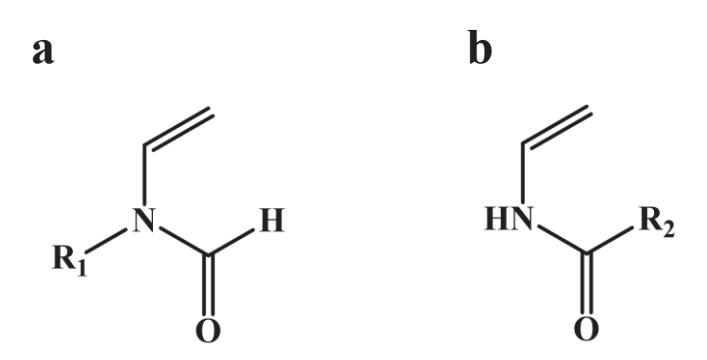


Figure 2.1. Modifications of NVF at the *N*-position (a) or the aldehyde position (b)

Reactions, which lead to structures shown in Figure 2.1b are more complex to synthesize. The original synthesis of NVIBA involves a two-step reaction. The first step was formation of N-(α -alkoxyethyl)alkylamide by coupling of acetaldehyde, alcohol, and the respective alkylamide. N-(α -alkoxyethyl)alkylamide was subsequently pyrolyzed (alcohol elimination). An alternative route was suggested in 2015 using acyl-chloride (iso-butyryl chloride). The amide structure is kept after hydrolysis with good yield (89 %). The reaction leads also to good yields for formation of N-vinylbenzamide (80%) and isobutyl-N-vinylcarbamate (80%). A direct synthesis of various N-vinylamides was realized using an ester or aldehyde, which is coupled with 1-azido-2-iodo ethane. The formed N-vinylazide underwent a [3+2] cycloaddition with subsequent rearrangement and nitrogen extrusion. The esters led to α , β -unsaturated N-vinylamides and aldehydes to N-vinylamides, e.g. iso-butyraldehyde yields in NVIBA (72%).

2.2.2 Post-functionalization of PVAm

As shown in Scheme 2.1 primary amine groups offer a variety of modification techniques. Commonly used for hydrophobic modification are condensation reactions with acid chlorides³⁵, alkyl bromides³⁶, carboxy-acids³⁷, and acryl amides.³⁸ For example a series of alkylated PVAms was prepared using acid chlorides as kinetic hydrate inhibitors. While poly(*N*-vinyl-isopentanamide) was not soluble in water, butyl- and propylamides showed LCST behavior (44 and 83 °C, respectively). Ethylamide was soluble in the complete temperature range.³⁵ The LCST of the resulting homopolymers are summarized in Table 1.

Table 1. The molecular weight and LCST of N-Vinylamide homopolymers.

Structure	Mn	$M_{\rm w}$	PDI	LCST	Ref.
R_1 R_2 R_2	[g·mol ⁻¹]	[g·mol ⁻¹]		[°C]	
PNVA	1.3·10 ⁵	#NA	#NA	> 100	28
$R_1 = -H$					
$R_2 = -CH_3$					
PNMVA	$\sim 1.0 \cdot 10^4$	#NA	#NA	> 100	29
$R_1 = -CH_3$					
$R_2 = -CH_3$					
PNVIBA	1.1·10 ⁴	1.5·10 ⁴	1.4	39-41	30
$R_1 = -H$					
$R_2 = -CH(CH_3)_2$					

poly(N-vinyl butyramide)	#NA	1.5-	#NA	44	35
PNVBA	77111	$1.9 \cdot 10^4$	771121		
$R_1 = -H$					
$R_2 = -CH_2CH_2CH_3$					
poly(N-vinyl propylamide)	#NA	$13.8 - 17.2 \cdot 10^4$	#NA	83	35
PNVPrA		17.2 10			
$R_1 = -H$					
$R_2 = -CH_2CH_3$					
poly(N-vinyl-N-n-propyl formamide)	0.3·10 ⁴	#NA	2.52	20	39
PNVNPrF					
$R_1 = -CH_2CH_2CH_3$					
$R_2 = -H$					
poly(N-vinyl-N-iso-propyl formamide)	0.3·10 ⁴	#NA	2.54	38	39
PNVNiPrF					
$R_1 = -CH(CH_3)_2$					
$R_2 = -H$					
poly(N-vinyl-N-n-propyl acetamide)	~ 1.0·10 ⁴	#NA	#NA	39-40	29
PNVNPrA					
$R_1 = -CH_2CH_2CH_3$					
$R_2 = -CH_3$					
EOENVF	1.2·10 ⁴		3.6	48	32
$R_1 = -CH_2CH_2OCH_2CH_3$					
$R_2 = -H$					
2EOENVF	$1.1 \cdot 10^4$		2.3	77	32
$R_1 = -CH_2CH_2OCH_2CH_2$ OCH_2CH_3					
$R_2 = -H$					

The LCST-values should be considered cautious since several factors have an influence such as molecular weight, heating rate, pH-value, etc.⁴⁰ However, based on Table 1 it can be concluded:

- The alkylation of the amine-position (R₁) has a stronger influence than respective alkylation of the aldehyde position (R₂), *e.g.*, modification with n-propyl at R₁ leads to a LCST of 20 °C, while a modification at R₂ leads to a LCST of 44 °C. This effect is less pronounced for the isopropyl homologues (38 °C vs. 39-41 °C). The comparison between the isomers PNVIBA (39-41 °C) and PNIPAm (32 °C) underlines this hypothesis.
- The results, whether n-propyl modification is more effective than iso-propyl modification, are not conclusive. At R_2 the LCST is increased for using n-propyl (44 °C) compared to iso-propyl (39-41 °C), while for R_1 the trend is inverted (20 °C compared to 38 °C). The latter one follows also the trend of PNIPAm (32 °C) and P(N-n-propylacrylamide) (25 °C).
- The longer the alkyl-chain the lower is the LCST. While homopolymers of iso-butyl-NVF or n-butyl-NVF are not water-soluble, propyl modifications yield in a LCST in the range of 20-44 °C and ethyl modifications give a LCST above 80 °C.

2.3 Copolymerization

PVAm are highly versatile polymers due to the presence of amine functionality which makes the polymer pH and ion sensitive. This opens new avenues of high-end applications. To explore further the possibility to introduce another functionality like thermoresponsiveness NVF is often copolymerized with a second monomer. ^{11,21,42,44} Due to its structural similarity and the narrow copolymerization parameters (Table 2) NVF can be copolymerized with NVA to obtain a statistical copolymer as shown in Chapter 3. ⁴² Therein, the formamide group is selectively hydrolyzed and consequently the amine:amide ratio defines the amine density. Similarly, but under controlled conditions the group of Debuigne copolymerized NVA in presence of NMVA using a [Co(acac)₂] complex to obtain a low PDI (1.1 – 1.2), while the copolymerization

parameters show preferential incorporation of NVA (Table 2).^{21,22} NVA was afterwards hydrolyzed to the amine. Copolymerization parameters which are not covered by the review of Pinschmidt (Vinyl acetate, sodium acrylate, n-butyl acrylate, acrylamide, maleic anhydride)⁵ and Panarin (acrylamide, sodium acrylate, acrylic acid, acrylonitrile, methyl acrylate, n-butyl acrylate, vinyl acetate, NVP, 2-hydroxyethyl methacrylate, methacrylic acid)³¹ are summarized in Table 2.

Table 2. Copolymerization parameters for different comonomers.

Monomer pair		Fineman- Ross	Mayo- Lewis	Kelen- Tudos	Non- linear	Reference
NVF- NVA	r _{NVF}	0.92 ± 0.04	1.04 ± 0.12	-	-	42
1111	r _{NVA}	0.97 ± 0.04	1.05 ± 0.10	-	-	Chapter 3
NVF- NIPAm	r _{NVF}	0.081±0.004	-	0.092±0.037	-	43
above LCST	T NIPAm	0.85±0.083	-	1.11±0.147	-	_
NVF- NIPAm	r _{NVF}	1.07	0.91	-	-	45
below LCST	T NIPAm	1.22	1.13	-	-	Chapter 5
NVA- NMVA	rnva	2.19	-	2.39	2.00	21
11111 1 1 1	r _{NMVA}	0.70	-	0.76	0.56	
NVF- NVIBA	r _{NVF}	-	-	-	1.08	11
I V I I I	rnviba	-	-	-	0.92	
NVA- NVIBA	rnva	-	-	-	0.99	46
IVIDA	r _{NVIBA}	-	-	-	0.94	

2.3.1 Thermoresponsive Copolymers

Synthesized or commercially available thermoresponsive monomers can be copolymerized with NVF and subsequently hydrolyzed yielding in thermo- and pH responsive copolymers.

Even in 1997 the group of Akashi presented a NVIBA-NVF copolymer.³⁰ The structure of

NVIBA in comparison to commercially available NIPAm is shown in Figure 2.2. Due to the structural similarity, the copolymerization parameters show only slight preferential incorporation of NVF compared to NVIBA (Table 2). The lower critical solution temperature (LCST) could be tuned with the NVF content in the range of 40 °C (0 mol% NVF) to 70 °C (40 mol% NVF) (Figure 2.3). Upon hydrolysis of the formamide group the LCST is shifted to higher temperature because of the more hydrophilic nature of the vinylamine (VAm). Furthermore with increasing hydrolysis degree, that means with a VAm content of 2.4 mol% and above, the LCST was not reached in terms of a transmittance lower than 50 % as claimed by the authors.¹¹

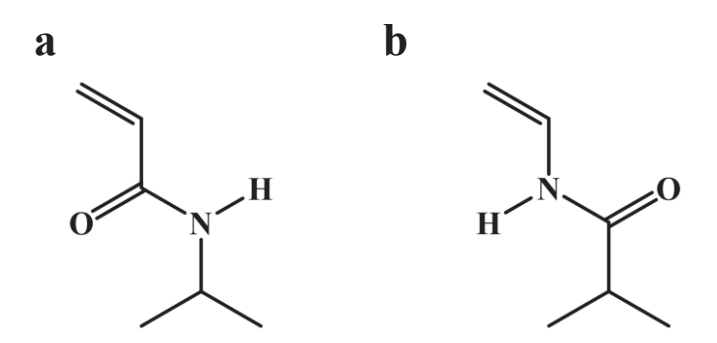


Figure 2.2. The structure of a) NIPAm and b) NVIBA

Thermoresponsive copolymers of NVF and NVF derivatives were prepared (EOENVF and 2EOENVF), where the *N*-position was functionalized either with an oligo ethylene glycol chain or by an azobenzene. Depending on the chain length of the oligo ethylene glycol the LCST could be tuned between 55 and 90 °C, while a functionalization with the azobenzene could only lead to a 10 % transmittance loss in UV-Vis spectroscopy on raising the temperature from 20 to 90 °C. 32,47

Maybe the best investigated commercially available thermoresponsive monomer is NIPAm. NVF:NIPAm copolymers/microgels were prepared by free radical reaction. However, since the polymerization was carried out at 50 °C which is above the LCST of NIPAm the copolymerization parameters differ widely by a factor around 10 indicating the formation of

block-like copolymers (Table 2).⁴³ As will be shown in Chapter 5 the synthesis of copolymers at reaction temperature of 35 °C lead to statistical copolymers (Table 2). Consequently, the LCST could be tuned with the VAm:NIPAm ratio from ~40 °C to 50 °C (VAm:NIPAm ratio of 1:5 to 1:3) (Chapter 5 and Figure 2.3).⁴⁵

The LCST in dependence on the NVF/VAm content is shown in Figure 2.3. In the considered range the increase of the LCST with NVF or VAm content is approximately linear. One might conclude that the slope, that means the increase of the LCST with NVF content, is lower for nalkyl derivatives (NVF-co-NVBA: 0.42 °C·mol%-¹, NVF-co-NVNPrF: 0.48 °C·mol%-¹) than for iso-alkyl derivatives (NVF-co-NVIBA: 0.77 °C·mol%-¹, NVF-co-NVNiPrF: 0.69 °C·mol%-¹), but there is not enough data for a detailed analysis and more work is necessary – especially in the case of thermoresponsive VAm-copolymers.

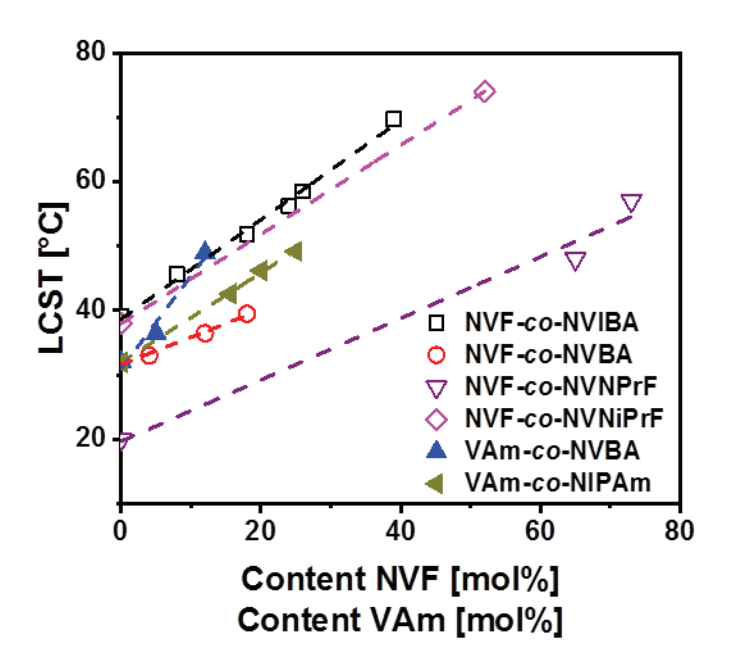


Figure 2.3. The LCST in dependence on the NVF (open symbols) or VAm (closed symbols) content for the copolymers NVF-*co*-NVIBA (black squares)⁴⁸, NVF-*co*-NVBA (red circles)⁴⁹, NVF-*co*-NVNPrF (purple triangles) ³⁹, NVF-*co*-NVNiPrF (pink diamonds) ³⁹, VAm-*co*-NVBA (blue triangles)⁴⁹, and VAm-co-NIPAm (green triangles)⁴⁵. The dashed line is a linear fit of the data points.

3. Hydrogels and microgels

Gels are three-dimensional crosslinked structures. These structures can be realized for instance by the polymerization of a monomer in presence of a bifunctional crosslinker or by crosslinking already prepared pre-polymers. The first route which is the most common route for the preparation of hydrogels is challenging in the case of PVAm based hydrogels, because the harsh hydrolysis conditions of the formamide can also lead to the hydrolysis of the crosslinker. Several strategies were introduced to overcome this drawback (Figure 2.4). NVF can be copolymerized with a crosslinker, which is either stable under hydrolysis conditions or is replaced with another crosslinker after hydrolysis. Furthermore the (partially) hydrolyzed (Co-)polymers of VAm can be crosslinked exploiting either the free amine groups for crosslinking reactions or using the free amine group as chain transfer agent (CTA) and grafting a (crosslinked) polymer network onto PVAm. The chemical crosslinkers are summarized at the end of this section in Table 3.

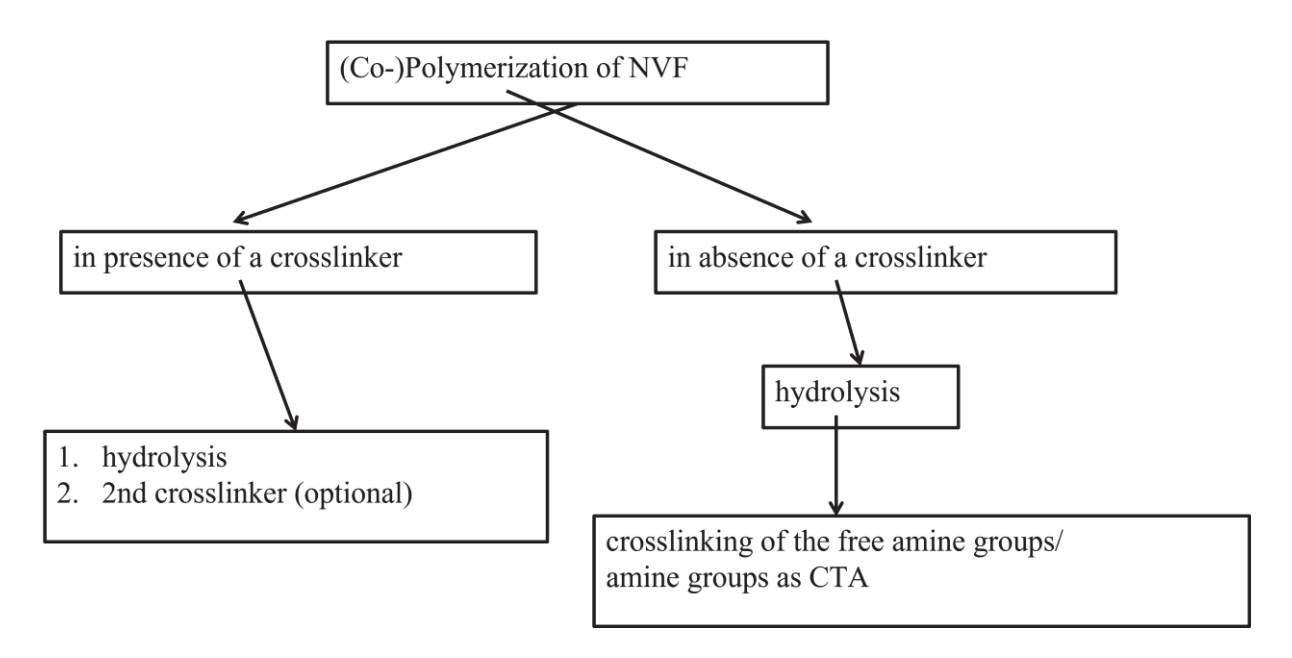


Figure. 2.4. Strategies for the gelation of PVAm.

3.1 Copolymerization with crosslinker

Hollow hydrogel capsules were prepared via the first method by polymerization of NVF with *N*, *N*'-methylene bisacrylamide (MBAA) as crosslinker and poly(2-ethyl-2-oxazoline) as emulsion stabilizer using azo-bis(isobutyronitril) (AIBN) as initiator. The gels were subsequently hydrolyzed, which also led to the hydrolysis of MBAA. With the addition of glutaraldehyde (GA), the amine groups were preferentially crosslinked at the periphery resulting in hollow hydrogel capsules. ⁵¹⁻⁵³ Confocal laser scanning microscopy and scanning electron microscopy reveal the uniform shape (Figure 2.5). These capsules were exploited for the loading and release of a probe molecule (Chromatrope 2R). This probe molecule could bind to the primary amine groups by electrostatic interaction depending on the pH. ⁵¹

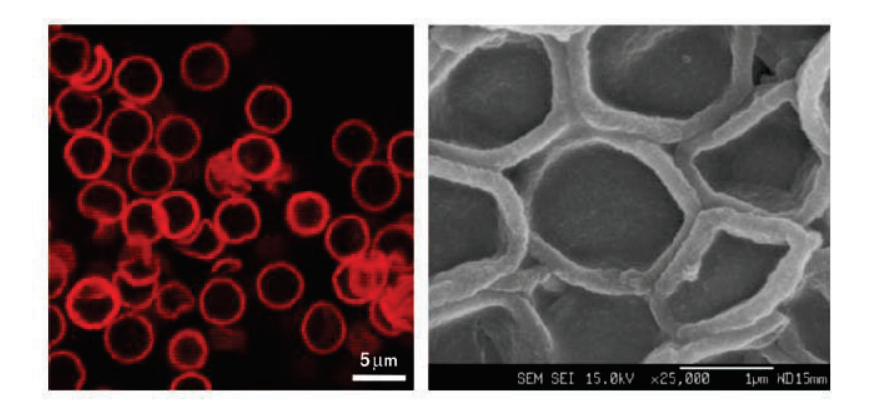
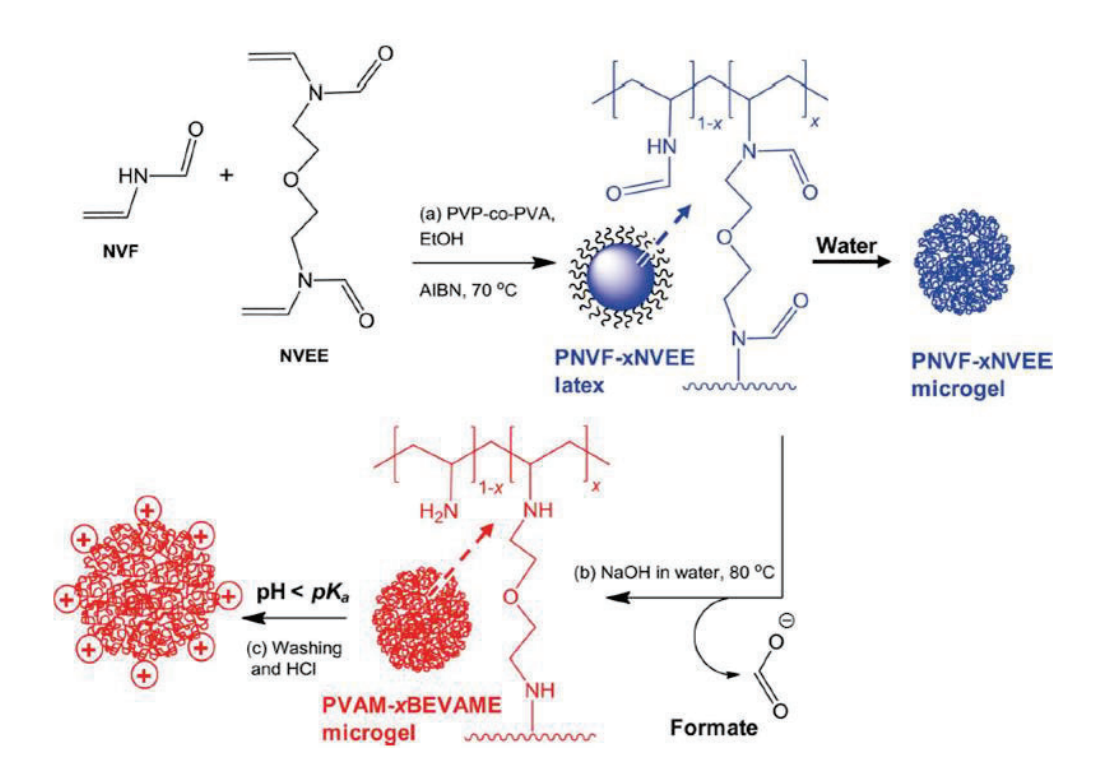


Figure 2.5. Hollow hydrogel capsules crosslinked with GA. a) Confocal laser scanning microscopy image of the capsules stained with rhodamine B isothiocyanate. b) Scanning electron image of the dried capsules. Reproduced with permission from ref.⁵¹

These hollow capsules were further used for the formation of gold nanoparticles (NP), where the size of the NP could be controlled by the crosslinking density (the GA concentration) of the hollow capsules. Depending on the NP size the NP showed vibrant colors due to the surface plasmon resonance. On irradiation with intensive laser light the NP generated heat leading to the rupture of the hollow capsules.⁵² Moreover it was found that the hollow capsules have only little cytotoxicity and enhanced cell adhesion.⁵³ PVAm microgels were prepared to improve the

adhesion force on wet cellulose. For this NVF was copolymerized with 1,3-divinylimidazolid-2-one as crosslinker and subsequent basic hydrolysis (5 wt% NaOH, 70 °C, 100 h) resulted in PVAm microgels. 1,3-divinylimidazolid-2-one was chosen because of its acid hydrolysis stability (formic acid will be released from the crosslinker, but the crosslinks are retained). Compared to linear PVAm the microgels showed a better adhesion on wet cellulose.⁵⁴ In other approaches 2-(*N*-vinylformamido)ethyl ether (NVEE) was synthesized as a crosslinker which was also stable under the hydrolysis conditions of NVF.⁵⁵⁻⁵⁷ NVEE was copolymerized with NVF in presence of poly(vinylpyrrolidin) (PVP)-*co*-poly(vinyl alcohol) (PVA) and AIBN as initiator. On NVF hydrolysis to the corresponding amine resulted in pH-responsive microgels with high amine content and a cluster like morphology. The reaction is summarized in Scheme 2.3.⁵⁵



Scheme 2.3. Reaction scheme for the fabrication of microgels by the group of Saunders. Reproduced with permission from ref.⁵⁵

This system was further extended with the incorporation of glycidylmethacrylate (GMA). Upon hydrolysis, it was found that along with hydrolysis of formamide epoxy-groups of the GMA were hydrolyzed resulting in polyampholyte microgels. However, NVF in the core was not accessible for neither basic nor acidic hydrolysis and remained intact. This was explained by the electrostatic repulsion from the hydrolyzed NVF moieties in the case of the acidic hydrolysis and the hydrolyzed GMA moieties in the case of the basic hydrolysis.⁵⁶ In another study, the PVAm microgels were post-functionalized with GMA obtaining microgels with amine groups and a free double bond at the periphery. Above a critical concentration, these microgels aggregate to form a physical hydrogel, which was afterward covalently fixated via free radical reaction of the double bonds using ammonium peroxodisulfate (APS) giving rise to a double crosslinked gel (DN). Compared to the single network, gels with the double network had 5-fold increase of the storage modulus G' (7.4 kPa for the DN gel compared to 1.35 kPa for the PVAm and 1.77 kPa for the GMA functionalized single network microgels). These microgels were further used as injectable gels when used together with an APS/N,N,N',N'-Tetramethylethane-1,2-diamine (TEMED) solution. TEMED lowered the initiation temperature of the APS, which initiated successful crosslinking at 37 °C.⁵⁷ To increase the ductility of the hydrogel PVAm-NVEE microgels were crosslinked by partially oxidized dextran obtaining a microgel composite hydrogel (MCH). The resulting acid labile imine bond allowed reversibility of the reaction. Depending on the respective mass ratios the MCH had a G' of 54 kPa with a yield strain of 125 %. On adjusting the pH-value to 3.3 cleavage of the imine bond was induced which resulted in reduction of G' to approximately 10 % of its original value.⁵⁸ Further, interpenetrating polyion complexes of PVAm hydrogels and poly(acrylic acid) (PAA) are extensively investigated. The hydrogels were prepared by copolymerization of NVF, NVA, and N,N-5-Oxanonamethylene-bis-N-vinylacetamide as crosslinker. NVF was subsequently partially hydrolyzed to obtain a tailored pH-responsivity (2 M NaOH, 60 °C). DN hydrogels were obtained by swelling the gels in a solution containing acrylic acid (AAc), MBAA, and

APS. The resulting DN hydrogels showed pH-responsive behavior which was dependent on the degree of hydrolysis and the AAc content.⁵⁹ In a subsequent study, AAc was polymerized on the surface of the partially hydrolyzed P(NVF-*co*-NVA) gels (hydrolysis: 5 wt% KOH in isopropanol, 80 °C). The thickness of the polyion complex layer was controllable by the hydrolysis time. Due to the pH-responsiveness, a pH-dependent release of model compounds (FITC-dextrane), monovalent anionic (Allura Red), cationic (methylene blue), and multivalent anionic (1,3,6-naphthalenetrisulfonate) were demonstrated.^{60,61} In further work, AAc was replaced by vinyl phosophonic acid without a crosslinker. The swelling ratio was pH-dependent and could be decreased from 14-25 to 2-5, while at pH = 2 a sustained release of the anionic model drug (Allura Red) was shown.⁶¹

Similar method was followed to obtain thermoresponsive gels.⁴³ ⁴⁴ NVF was copolymerized with NIPAm in presence of MBAA as crosslinker, 2,2'-azobis(2-methylpropionamidine) dihydrochloride (V-50) as a radical initiator, and cetyltrimethyl ammonium bromide as an emulsion stabilizer. The NVF groups were subsequently selectively hydrolyzed under acidic conditions (pH = 1.5, 70 °C, 24 h) to obtain thermoresponsive microgels with free amine groups. The degree of hydrolysis was found to be between 30 and 40%. However, hydrolysis of the MBAA groups was not reported. The swelling of the microgels was pH-dependent and increased with decreasing pH because of the free amine groups. Furthermore, the microgels revealed a volume phase transition temperature (VPTT) at around 32 °C due to the presence of the NIPAm moieties. 43 These microgels were used for the reversible absorption of CO₂. In contrast to previous results complete hydrolysis of the NVF under strongly acidic conditions (2 mol·L⁻¹ HCl or 1 mol·L⁻¹ H₂SO₄ at 60 °C for 24 h) was reported, whereas under medium acidic conditions or basic conditions the degree of hydrolysis ranges from 43% to 74% (2 mol·L⁻¹ trifluoroacetic acid, KOH, or sodium methanolat at 60 °C for 24 h). Also, in this case a degradation of the MBAA was not reported. The high affinity of primary amine groups to CO₂ together with the thermoresponsiveness of NIPAm was exploited for the reversible

absorption/desorption of CO_2 . The absorption/desorption was monitored by measuring the conductivity, which was increased by the absorption of CO_2 from 30 to 95 μ S·cm⁻¹. However, complete desorption was not achieved as the conductivity remained at 40 μ S·cm⁻¹ even on heating to 70 °C under N_2 flow. This was explained by the reaction of amine with CO_2 resulting in carbamate moieties.

3.2 Crosslinking of prepolymers

The first reported gels from PVAm prepolymer were prepared by crosslinking the polymer with nonaethylene glycol diglycidylether. Swelling ratios of 2,000 % were observed for these gels at a pH of 3, while the gels contract at lower or higher pH value, while addition of salt (KCl or CuCl₂) led to a (reversible) shrinkage of the gel.⁶² In a follow up work, the applicability of the Donnan theory was used to predict the swelling behavior of the gels as function of the ionic composition of the solvent. It was found that the experimental results matches with the theoretical prediction for the addition of KCl.⁶³

In another approach obtaining thermoresponsive block-copolymers of NIPAm and N-vinylphtalimid (NVI) were prepared from NIPAm and PVPI as macro-CTA in dimethyl formamide with AIBN as initiator. PVPI was subsequently hydrozinolyzed to obtain PVAm-b-NIPAm. The prepolymer was used for the synthesis of nanogels by subsequent crosslinking with naphthalene-1,8:4,5-tetracarboxylic dianhydride or perylene-3,4:9,10-tetracarboxylic dianhydride, respectively to achieve imide-bonded nanogels with an optoelectronic core. While the nanogels collapsed with increasing temperature, the optical properties were not affected. The latter ones were tunable by changing the solvent. To obtain optoelectronic properties together with thermoresponsiveness the nature of the crosslinker was changed: With chemically crosslinked fixed cores using either 2,5-thiophenedicarboxaldehyde or anthracene-9,10-dicarboxaldehyde and with self-assembled cores using monofunctional crosslinker (2-thiophenecarboxaldehyde and 9-anthracenecarboxaldehyde). Without chemical crosslinking

the polymers existed as unimers in organic solvents, while they form micelles in aqueous solution due to the hydrophobic interaction. As the resulting imine bonds were acid labile (pH < 5.2), the nanogels disintegrates under acidic conditions as shown in Figure. 2.6. On exceeding the LCST the optical properties were changed.⁶⁵

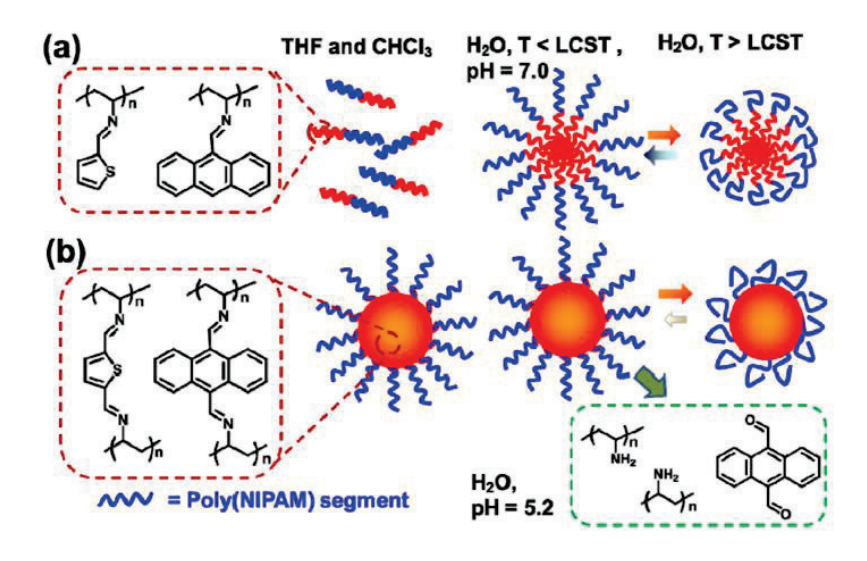
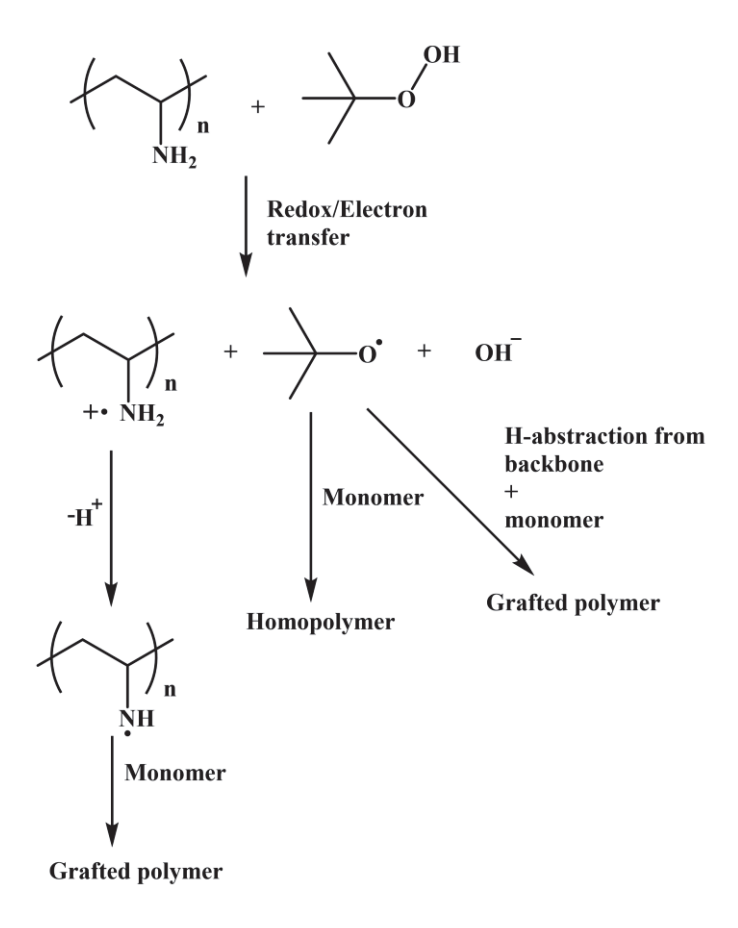


Figure 2.6. The optical properties arising from the thiophene or anthracene moieties could be tuned by the solvent and the temperature. Reproduced with permission from ref.⁶⁵

As previously shown for poly(ethylene imine) (PEI) free primary amino groups can be used as CTA.⁶⁶⁻⁷² For example in the preparation of core-shell particles PVAm was used as macro-CTA. For this NVF was polymerized via free radical reaction in water and the formamide groups were hydrolyzed under acidic conditions (3 mol·L⁻¹ HCl, 100 °C, 48 h) resulting into PVAm. Using tert-butyl hydroperoxide (TBHP) vinyl monomers can be grafted onto PVAm. The mechanism of the reaction is shown in Scheme 2.4. TBHP and PVAm form a redox pair. Subsequent electron transfer generates two radicals – an amine radical and an oxy radical. The amine radical as well as the H-abstraction of the backbone by the oxyl radical can initiate graft polymerization. As side reaction the oxyl radical can also initiate the homopolymerization of the vinyl-monomer. Recombination can lead to a chemical crosslinking.



Scheme 2.4. Mechanism of PVAm as macro-CTA with TBHP. The scheme is reproduced and modified with permission of ref.⁷²

In particular, methyl methacrylate (MMA), styrene, and mixtures of MMA and n-butylacrylate were grafted from PVAm and polymerized to obtain particles with narrow size distribution. ⁶⁶ The kinetics of this reaction was enhanced with a lower TBHP/PVAm molar ratio as well as a lower molecular weight of the PVAm. ⁶⁷ Increasing molecular weight of PVAm led to an increase of the particle diameter with PVAm was located on the surface of the gel particles. ⁶⁷ Similarly, AAc was grafted from PVAm using TBHP. Microgels are formed by electrostatic interaction between AAc and VAm. In a second step the microgels were swollen in a AAm/TBHP solution. Reaction with TBHP generated radicals on the surface of the microgels inducing the polymerization of AAm forming an MCH. The obtained hydrogels were transparent under basic conditions (pH = 12) and became opaque and shrunk sligthly under acidic conditions (pH = 3). ⁶⁸

This method was further used for the fabrication of thermoresponsive microgels. 69-71 NIPAm was grafted from PVAm together with MBAA as crosslinker leading to the formation of microgels with a VPTT of 32 °C. These microgels had a crosslinked PNIPAm core and a PVAm shell, which was confirmed by TEM imaging and Zeta-potential measurements.⁷¹ In addition acrylamide (AAm) was grafted from the microgels resulting in MCH. The MCH were thermoreponsive in the range between 25 °C and 45 °C and show improved mechanical properties compared to conventional AAm gels. During compression these gels could withstand a force of up to 21.9 MPa at a strain of 96 % with an elastic modulus of up to 40.49 kPa, compared to a maximum force of 0.13 MPa at a strain of 73.1 %. The elastic modulus of AAm gels was not determined.⁶⁹ Potassium peroxodisulfate was also used to graft AAc, acryloyloxyethyl trimethyl ammonium chloride (DAC), and AAm on to obtain pH- and thermoresponsive MCH. The pH-responsiveness was shown by different swelling ratios in dependence on pH – a minimum of the swelling ratio was found at neutral pH, whereas in acidic (pH < 5) and basic (pH > 8) regime swelling increased due to less electrostatic interaction of AAc and DAC. Also, these MCH showed enhanced mechanical properties such as a compressive strength of up to 30 MPa at 84% strain. Furthermore, the gels could recover after compression test due to self-healing behavior of physically bound AAc/DAC moieties.⁷⁰

3.3 Other methods

Due to the presence of free amine groups PVAm and its derivatives can also form gels by non-covalent interactions, such as composite gels with silica particles or ionic interaction. The interaction of PVAm with inorganic oxide particles such as silica was comprehensively reviewed by Spange et al. in 2004.⁷³ Recent studies show the interaction of silica with PVAm to obtain micro- and nanogel capsules.⁷⁴ For this 3-methacryloxypropyltrimethoxysilane functionalized silica particles were dispersed in ethanol with NVF, 2-Bis[2,2'-di(*N*-vinylformamido)-ethoxy]propane as acid-labile crosslinker, PVP, and AIBN as initiator. After

gelation silica was etched and PNVF hydrolyzed with 1 M NaOH under sonication at room temperature. The thickness of the PVAm shell could be controlled by the polymerization time and the overall diameter by the silica particle size. Since an acid-labile crosslinker was used, kinetics of degradation under acidic conditions were investigated in dependence on the pH. The half-life of a capsule ranged from 42 min at pH = 4.0 to > 3 days at pH = 7.4. As expected the capsule size and zeta potential decreased with increasing pH-value.⁷⁴ This method was also patented in 2011.⁷⁵

PVAm can complex with Cu²⁺, which was also investigated as catalyst for the polymerization of vinyl monomers.^{76,77} Also, a hydrogel was prepared by complexation of PVAm with Cu²⁺, which was applied as water sensor. The hydrogel had a fast electrical response to water/humidity changes and thus showed good capability to detect leakages in long water pipelines.⁷⁸

The structure of the crosslinkers and their properties are summarized in Table 3. Although the number of studies about PVAm-based hydro- and microgels is limited, some conclusions can be made:

- 1. The copolymerization with a crosslinker and subsequent hydrolysis is in general used for the fabrication of microgels. The instability of MBAA during the hydrolysis should be considered and can be exploited for the formation of hollow capsules. These microgels can be crosslinked to obtain MCH giving raise to improved mechanical properties
- 2. Chemical crosslinking of the prepolymers leads to highly swellable hydrogels, which are generally weak.
- 3. Using PVAm as macro-CTA generates microgels. Core-shell microgels are easily accessible via this method. MCH with an AAm network had improved mechanical properties compared to an AAm SN gel.

Table 3. Structure of the crosslinkers and their properties

Structure of the crosslinker	Comment	Ref.
MBAA N N N N N N N N N N N N N N N N N N	degrades partially under hydrolysis conditions for NVF	43,44,51- 53
GA o	crosslinking of prepolymers, acid labile	51-53
1,3-Divinylimidazolid-2-one	stable under hydrolysis conditions, releases formic acid	54
NVEE ON NOON NOO	stable under hydrolysis conditions, releases formic acid	55-58
N,N-5-oxanonamethylene-bis- N -vinylacetamide	stable under hydrolysis conditions	59-61,79
Nonaethylene glycol diglycidylether	crosslinking of pre- polymers by amine-bond	62,63
Phenylcarbonate-telechelic PEG	crosslinking of pre- polymers by carbamate- bond, releases phenol, physical gels also possible	42,45,80 Chapter 3, 4 and 5
Naphthalene-1,8:4,5-tetracarboxylic dianhydride	crosslinking of pre- polymers by imide-bond	64

4. References

- Pelton, R. Polyvinylamine: A Tool for Engineering Interfaces. *Langmuir* **30**, 15373-15382, doi:10.1021/la5017214 (2014).
- 2 Badesso, R. J., Pinschmidt, R. K. & Sagl, D. J. *Proc. Am. Chem. Soc. Div. Polym. Mat. Sci. Eng.* **69**, 251-252 (1993).
- Trommler, K. et al. The Reaction of Poly(Vinyl Amine) with Acetone in Water. *Macromol. Chem. Phys.* **220**, doi:10.1002/macp.201800444 (2018).
- Jones, G. D., Zomleffer, J. & Hawkins, K. Attempted Preparation of Polyvinylamine. *J. Org. Chem.* **09**, 500-512 (1944).

5 Pinschmidt, R. K. J. Poly(vinylamine) at Last. *J. Polym. Sci. A: Polym. Chem.* **48**, 2257-2283, doi:10.1002/pola.23992

10.1002/POLA (2010).

- Maki, Y., Mori, H. & Endo, T. Controlled RAFT Polymerization of *N*-Vinylphthalimide and its Hydrazinolysis to Poly(vinyl amine). *Macromol. Chem. Phys.* **208**, 2589-2599, doi:10.1002/macp.200700330 (2007).
- Badesso, R. J., Nordquist, A. F., Pinschmidt, R. K. & Sagl, D. J. in *Hydrophilic Polymers* Ch. 25, 489-504 (American Chemical Society, 1996).
- 8 Mullier, M. & Smets, G. Polymers and Group Interaction. IV. Hofmann Reaction on Polyvinylamides. *J. Polym. Sci.* **23**, 915-930 (1957).
- 9 Gu, L., Zhu, S. & Hrymak, A. N. Acidic and Basic Hydrolysis of Poly(*N*-vinylformamide). *J. Appl. Polym. Sci.* **86**, 3412-3419, doi:10.1002/app.11364 (2002).
- 10 Witek, E., Pazdro, M. & Bortel, E. Mechanism for Base Hydrolysis of Poly(*N*-vinylformamide). *J. Macromol. Sci. A* **44**, 503-507, doi:10.1080/10601320701235461 (2007).
- Yamamoto, K., Serizawa, T., Muraoka, Y. & Akashi, M. Synthesis and Functionalities of Poly(*N*-Vinylalkylamide). XII. Synthesis and Thermosensitive Property of Poly(vinylamine) Copolymer Prepared from Poly(*N*-vinylformamide-*co-N*-vinylisobutyramide). *J. Polym. Sci. A* **38**, 3674-3681 (2000).
- Dréan, M., Guégan, P., Jérôme, C., Rieger, J. & Debuigne, A. Far Beyond Primary Poly(vinylamine)s through Free Radical Copolymerization and Amide Hydrolysis. *Polym. Chem.* 7, 69-78, doi:10.1039/c5py01325a (2016).
- Okatova, O. V., Gavrilova, I. I., Ul'yanova, N. N., Panarin, E. F. & Pavlov, G. M. Hydrodynamic, Molecular, and Conformational Characteristics of Macromolecules of a Random Copolymer of *N*-Methyl-*N*-Vinylacetamide and *N*-Methyl-*N*-Vinylamine Hydrochloride. *Russ. J. Appl. Chem.* **85**, 1239-1246, doi:10.1134/S1070427212080174 (2012).
- Gavrilova, I. I., Panarin, E. F. & Nesterova, N. A. Homopolymerization of *N*-Vinylamides in the Presence of Water-Soluble Initiators and Preparation of Polyelectrolytes from the Polymerization Products. *Russ. J. Appl. Chem.* **85**, 413-416, doi:10.1134/s1070427212030160 (2012).
- Roy, D., Brooks, W. L. & Sumerlin, B. S. New Directions in Thermoresponsive Polymers. *Chem. Soc. Rev.* **42**, 7214-7243, doi:10.1039/c3cs35499g (2013).
- Klouda, L. & Mikos, A. G. Thermoresponsive Hydrogels in Biomedical Applications. *Eur. J. Pharm. Biopharm.* **68**, 34-45, doi:10.1016/j.ejpb.2007.02.025 (2008).
- Liu, R., Fraylich, M. & Saunders, B. R. Thermoresponsive Copolymers: From Fundamental Studies to Applications. *Colloid Polym. Sci.* **287**, 627-643, doi:10.1007/s00396-009-2028-x (2009).
- 18 Kröner, M., Dupuis, J. & Winter, M. *N*-Vinylformamide Synthesis and Chemistry of a Multifunctional Monomer. *J. Prakt. Chem.* **342**, 115-131 (2000).
- Nakabayashi, K. & Mori, H. Recent Progress in Controlled Radical Polymerization of *N*-Vinyl Monomers. *Eur. Polym. J.* **49**, 2808-2838, doi:10.1016/j.eurpolymj.2013.07.006 (2013).
- Fan, W. & Yamago, S. Synthesis of Poly(*N*-vinylamide)s and Poly(vinylamine)s and Their Block Copolymers by Organotellurium-Mediated Radical Polymerization. *Angew. Chem. Int. Ed. Engl.* **58**, 7113-7116, doi:10.1002/anie.201902940 (2019).
- Dréan, M. *et al.* Controlled Synthesis of Poly(vinylamine)-Based Copolymers by Organometallic-Mediated Radical Polymerization. *Macromolecules* **49**, 4817-4827, doi:10.1021/acs.macromol.6b00992 (2016).

- Stiernet, P. *et al.* Tailor-Made Poly(vinylamine)s via Thermal or Photochemical Organometallic Mediated Radical Polymerization. *ACS Symp. Ser.* **1284**, 349-363 (2018).
- Stiernet, P., Jérôme, C. & Debuigne, A. Precision Design of Vinyl Amine and Vinyl Alcohol-Based Copolymers via Cobalt-Mediated Radical Polymerization. *Polym. Chem.* **10**, 3055-3065, doi:10.1039/c9py00020h (2019).
- Debuigne, A. *et al.* Key Role of Intramolecular Metal Chelation and Hydrogen Bonding in the Cobalt-Mediated Radical Polymerization of *N*-Vinyl Amides. *Chem. Eur. J.* **18**, 12834-12844, doi:10.1002/chem.201201456 (2012).
- 25 Matyjaszewski, K. in *Controlled Radical Polymerization ACS Symposium Series* 258-283 (1998).
- Demarteau, J., Debuigne, A. & Detrembleur, C. Organocobalt Complexes as Sources of Carbon-Centered Radicals for Organic and Polymer Chemistries. *Chem. Rev.* **119**, 6906-6955, doi:10.1021/acs.chemrev.8b00715 (2019).
- Debuigne, A., Champouret, Y., Jerome, R., Poli, R. & Detrembleur, C. Mechanistic Insights into the Cobalt-Mediated Radical Polymerization (CMRP) of Vinyl Acetate with Cobalt(III) Adducts as Initiators. *Chem. Eur. J.* **14**, 4046-4059, doi:10.1002/chem.200701867 (2008).
- Hong, J. S. *et al.* Cloud Points and Phase Separation of Aqueous Poly(*N*-vinylacetamide) Solutions in the Presence of Salts. *Colloid Polym. Sci.* **274**, 1013-1019 (1996).
- Ajiro, H., Takemoto, Y., Akashi, M., Chua, P. C. & Kelland, M. A. Study of the Kinetic Hydrate Inhibitor Performance of a Series of Poly(*N*-alkyl-*N*-vinylacetamide)s. *Energ. Fuel* **24**, 6400-6410, doi:10.1021/ef101107r (2010).
- 30 Suwa, K. *et al.* Synthesis and Functionalities of Poly(*N*-vinylalkylamide). IV. Synthesis and Free Radical Polymerization of *N*-vinylisobutyramide and Thermosensitive Properties of the Polymer. *J. Polym. Sci. Part A. Polym. Chem.* **35**, 1763-1768 (1997).
- Panarin, E. F. *N*-Vinylamides and Related Polymers as Delivery Agents of Biologically Active Compounds. *Russ. Chem. Bull.* **64**, 15-23 (2015).
- Kawatani, R., Kawata, Y., Yusa, S.-i., Kelland, M. A. & Ajiro, H. Synthesis of Thermosensitive Poly(*N*-vinylamide) Derivatives Bearing Oligo Ethylene Glycol Chain for Kinetic Hydrate Inhibitor. *Macromolecules* **51**, 7845-7852, doi:10.1021/acs.macromol.8b01573 (2018).
- Tu, S. & Zhang, C. Facile Preparation of *N*-Vinylisobutyramide and *N*-Vinyl-2-pyrrolidinone. *Org. Process. Res. Dev.* **19**, 2045-2049, doi:10.1021/acs.oprd.5b00303 (2015).
- Choi, H., Shirley, H. J., Hume, P. A., Brimble, M. A. & Furkert, D. P. Unexpected Direct Synthesis of *N*-Vinyl Amides through Vinyl Azide-Enolate [3+2] Cycloaddition. *Angew. Chem. Int. Ed. Engl.* **56**, 7420-7424, doi:10.1002/anie.201702727 (2017).
- Chua, P. C., Kelland, M. A., Ajiro, H., Sugihara, F. & Akashi, M. Poly(vinylalkanamide)s as Kinetic Hydrate Inhibitors: Comparison of Poly(*N*-vinylisobutyramide) with Poly(*N*-isopropylacrylamide). *Energ. Fuel* **27**, 183-188, doi:10.1021/ef301703w (2012).
- 36 Chen, X., Wang, Y. & Pelton, R. pH-Dependence of the Properties of Hydrophobically Modified Polyvinylamine. *Langmuir* **21** (2005).
- Yue, M., Imai, K., Yamashita, C., Miura, Y. & Hoshino, Y. Effects of Hydrophobic Modifications and Phase Transitions of Polyvinylamine Hydrogel Films on Reversible CO₂ Capture Behavior: Comparison between Copolymer Films and Blend Films for Temperature-Responsive CO₂ Absorption. *Macromol. Chem. Phys.* **218**, doi:10.1002/macp.201600570 (2017).

- Zelinskiy, S. N. *et al.* Poly(vinyl amine) as a matrix for a new class of polymers. *e-Polymers* **18**, 347-357, doi:10.1515/epoly-2018-0024 (2018).
- Kelland, M. A., Abrahamsen, E., Ajiro, H. & Akashi, M. Kinetic Hydrate Inhibition with *N*-Alkyl-*N*-vinylformamide Polymers: Comparison of Polymers to n-Propyl and Isopropyl Groups. *Energ. Fuel* **29**, 4941-4946, doi:10.1021/acs.energyfuels.5b01251 (2015).
- Halperin, A., Kroger, M. & Winnik, F. M. Poly(*N*-isopropylacrylamide) Phase Diagrams: Fifty Years of Research. *Angew. Chem. Int. Ed.* **54**, 15342-15367, doi:10.1002/anie.201506663 (2015).
- Cao, Y., Zhu, X. X., Luo, J. & Liu, H. Effects of Substitution Groups on the Raft Polymerziation of *N*-Alkylacrylamides in the Preparation of Thermosensitive Block Copolymers. *Macromolecules* **40**, 6481-6488 (2007).
- Fischer, T., Köhler, J., Keul, H., Singh, S. & Möller, M. Highly Swellable Hydrogels from Waterborne Poly(vinylamine-co-acetamide). *Macromol. Chem. Phys.* **219**, 1800399-1800408, doi:10.1002/macp.201800399 (2018).
- Xu, J., Barros Timmons, A. & Pelton, R. *N*-Vinylformamide as a Route to Amine-Containing Latexes and Microgels. *Colloid Polym. Sci.* **282**, 256-263, doi:10.1007/s00396-003-0901-6 (2004).
- 44 Yue, M., Imai, K., Miura, Y. & Hoshino, Y. Design and Preparation of Thermo-Responsive Vinylamine-Containing Micro-gel Particles for Reversible Absorption of Carbon Dioxide. *Polym. J.* **49**, 601-606, doi:10.1038/pj.2017.28 (2017).
- Fischer, T., Demco, D. E., Fechete, R., Moller, M. & Singh, S. Poly(vinylamine-co-N-isopropylacrylamide) linear polymer and hydrogels with tuned thermoresponsivity. *Soft Matter* **16**, 6549-6562, doi:10.1039/d0sm00408a (2020).
- Suwa, K., Morishita, K., Kishida, A. & Akashi, M. Syntheysis and Functionalities of Poly(*N*-vinylalkylamide). V. Control of a Lower Critical Solution Temperature of Poly(*N*-vinylalkylamide). *J. Polym. Sci. Part A. Polym. Chem.* **35**, 3087-3094 (1997).
- Kawatani, R., Nishiyama, Y., Kamikubo, H., Kakiuchi, K. & Ajiro, H. Aggregation Control by Multi-stimuli-Responsive Poly(*N*-vinylamide) Derivatives in Aqueous System. *Nanoscale Res. Lett.* **12**, 461, doi:10.1186/s11671-017-2221-7 (2017).
- Yamamoto, K., Serizawa, T., Muraoka, Y. & Akashi, M. Synthesis and Functionalities of Poly(*N*-vinylalkylamide). XII. Synthesis and Thermosensitive Property of Poly(vinylamine) Copolymer Prepared from Poly(*N*-vinylformamide-*co-N*-vinylisobutyramide). *J. Polym. Sci. Part A. Polym. Chem.* **38**, 3674-3681 (2000).
- Tachaboonyakiat, W., Ajiro, H. & Akashi, M. Synthesis of a Thermosensitive Polycation by Random Copolymerization of *N*-Vinylformamide and *N*-Vinylbutyramide. *Polym. J.* **45**, 971-978, doi:10.1038/pj.2013.12 (2013).
- Buwalda, S. J. *et al.* Hydrogels in a Historical Perspective: From Simple Networks to Smart Materials. *J. Control. Release* **190**, 254-273, doi:10.1016/j.jconrel.2014.03.052 (2014).
- Han, J. H., Koo, B. M., Kim, J. W. & Suh, K. D. A Facile Approach to Synthesize Uniform Hydrogel Shells with Controllable Loading and Releasing Properties. *Chem. Commun.*, 984-986, doi:10.1039/b715557c (2008).
- Kim, J. *et al.* Template-Free Uniform-Sized Hollow Hydrogel Capsules with Controlled Shell Permeation and Optical Responsiveness. *Langmuir* **28**, 11899-11905, doi:10.1021/la3017968 (2012).
- Han, J.-H. *et al.* Uniform hollow-structured poly(vinyl amine) hydrogel microparticles with controlled mesh property and enhanced cell adhesion. *Polymer* **55**, 1143-1149, doi:10.1016/j.polymer.2014.01.017 (2014).
- Miao, C., Chen, X. & Pelton, R. Adhesion of Poly(vinylamine) Microgels to Wet Cellulose. *Ind. Eng. Chem. Res.* **46** (2007).

- Thaiboonrod, S., Berkland, C., Milani, A. H., Ulijn, R. & Saunders, B. R. Poly(vinylamine) microgels: pH-responsive particles with high primary amine contents. *Soft Matter* **9**, doi:10.1039/c3sm27728c (2013).
- McCann, J., Thaiboonrod, S., Ulijn, R. V. & Saunders, B. R. Effects of crosslinker on the morphology and properties of microgels containing N-vinylformamide, glycidylmethacrylate and vinylamine. *J Colloid Interface Sci* **415**, 151-158, doi:10.1016/j.jcis.2013.09.030 (2014).
- Thaiboonrod, S., Milani, A. H. & Saunders, B. R. Doubly crosslinked poly(vinyl amine) microgels: hydrogels of covalently inter-linked cationic microgel particles. *J. Mater. Chem. B* **2**, 110-119, doi:10.1039/c3tb21579b (2014).
- McCann, J., Behrendt, J. M., Yan, J., Halacheva, S. & Saunders, B. R. Poly(vinylamine) microgel-dextran composite hydrogels: characterisation; properties and pH-triggered degradation. *J Colloid Interface Sci* **449**, 21-30, doi:10.1016/j.jcis.2014.09.041 (2015).
- Ajiro, H., Takemoto, Y., Asoh, T.-a. & Akashi, M. Novel polyion complex with interpenetrating polymer network of poly(acrylic acid) and partially protected poly(vinylamine) using N-vinylacetamide and N-vinylformamide. *Polymer* **50**, 3503-3507, doi:https://doi.org/10.1016/j.polymer.2009.06.016 (2009).
- Takemoto, Y., Ajiro, H., Asoh, T.-a. & Akashi, M. Fabrication of Surface-Modified Hydrogels with Polyion Complex for Controlled Release. *Chemistry of Materials* **22**, 2923-2929, doi:10.1021/cm1002302 (2010).
- 61 Ajiro, H., Takemura, K. & Akashi, M. Surface polyion complex gel with poly(vinylphosphonic acid) and poly(N-vinylamide)s. *Journal of Polymer Science Part A: Polymer Chemistry* **53**, 562-566, doi:10.1002/pola.27476 (2015).
- 62 Kobayashi, S., Suh, K.-D., Shirokura, Y. & Fujioka, T. Viscosity Behavior of Poly(vinylamine) and Swelling-Contraction Phenomen of Its Gel. *Polym. J.* **21**, 971-976 (1989).
- 63 Suh, K.-D., Bae, Y.-C., Kim, J.-W. & Kobayashi, S. Swelling of Poly(Vinyl Amine) Gels: Applicability of the Donnan Theory. *Journal of Macromolecular Science, Part A* **36**, 507-516, doi:10.1081/ma-100101545 (1999).
- Nakabayashi, K., Noda, D., Watanabe, Y. & Mori, H. Rylene bisimide-based nanoparticles with cross-linked core and thermoresponsive shell using poly(vinyl amine)-based block copolymers. *Polymer* **68**, 17-24, doi:10.1016/j.polymer.2015.04.075 (2015).
- Nakabayashi, K., Noda, D., Takahashi, T. & Mori, H. Design of stimuli-responsive nanoparticles with optoelectronic cores by post-assembly cross-linking and self-assembly of functionalized block copolymers. *Polymer* **86**, 56-68, doi:10.1016/j.polymer.2016.01.029 (2016).
- 66 Li, W. & Li, P. Synthesis of Well-Defined Amphiphilic Core-Shell Particles Containing Amine-Rich Shells. *Macromolecular Rapid Communications* **28**, 2267-2271, doi:10.1002/marc.200700449 (2007).
- Bonnefond, A., Pereira Gomes, C., de la Cal, J. C. & Leiza, J. R. Surfactant-free poly(methyl methacrylate)/poly(vinylamine) (PMMA/PVAm) amphiphilic core-shell polymer particles. *Colloid and Polymer Science* **295**, 135-144, doi:10.1007/s00396-016-3985-5 (2016).
- 68 Li, P. *et al.* The astonishing progress in performance of hydrogel triggered by the structure evolution of cross-linking junctions. *RSC Advances* **4**, doi:10.1039/c4ra07541b (2014).
- 69 Li, P. *et al.* A novel fabrication method of temperature-responsive poly(acrylamide) composite hydrogel with high mechanical strength. *Polymer* **54**, 5830-5838, doi:10.1016/j.polymer.2013.08.019 (2013).

- Xu, K. *et al.* A novel multi-responsive polyampholyte composite hydrogel with excellent mechanical strength and rapid shrinking rate. *J. Colloid Interf. Sci.* **345**, 360-368, doi:10.1016/j.jcis.2010.01.058 (2010).
- 71 Chen, Q., Xu, K., Zhang, W., Song, C. & Wang, P. Preparation and Characterization of Poly (*N*-isopropylacrylamide)/Polyvinylamine Core-Shell Microgels. *Colloid Polym. Sci.* **287**, 1339-1346, doi:10.1007/s00396-009-2095-z (2009).
- Li, P., Zhu, J., Sunintaboon, P. & Harris, F. W. New Route to Amphiphilic Core—Shell Polymer Nanospheres: Graft Copolymerization of Methyl Methacrylate from Water-Soluble Polymer Chains Containing Amino Groups. *Langmuir* **18**, 8641-8646 (2002).
- Spange, S. et al. in Polyelectrolytes with Defined Molecular Architecture I Advances in Polymer Science Ch. Chapter 0002, 43-78 (2004).
- Shi, L. & Berkland, C. Acid-Labile Polyvinylamine Micro-and Nanogel Capsules. *Macromolecules* **40**, 4635-4643 (2007).
- 75 Berkland, C. J. & Shi, L. Nanoparticles, Nanocapsules and Nanogels. US2011/287262 A1 (2011).
- Lu, J., Zhang, Z., Xia, X., Wang, L. & Zhu, X. Catalytic Function of Cross-Linked Polyvinylamine-Cu(II) Complexes for Polymerization of Methyl Methacrylate. *J. Mol. Catal. A Chem.* **207**, 205-214, doi:10.1016/S (2004).
- Lu, J., Zhang, Z., Xia, X. & Zhu, X. Complex of cross-linked polyvinylamine with Cu(II) as catalyst for vinyl polymerization. *Applied Catalysis A: General* **247**, 163-173, doi:10.1016/s0926-860x(03)00090-5 (2003).
- Mendoza-Payan, J. G., Flores-Gallardo, S. & Marquez-Lucero, A. Preparation and electrical characterization of poly(vinyl amine) hydrogels, crosslinked with Cu(II) ions, and evaluation of their potentiality as water sensor material. *J. Appl. Polym. Sci.* **115**, 790-801, doi:10.1002/app.31097 (2010).
- Ajiro, H., Takemoto, Y., Takemura, K., Asoh, T.-a. & Akashi, M. Releasing property from surface polyion complex gel. *Journal of Applied Polymer Science* **132**, n/a-n/a, doi:10.1002/app.42081 (2015).
- Fischer, T., Köhler, J., Möller, M. & Singh, S. Physical gels of poly(vinylamine) by thermal curing. *RSC Adv.* **10**, 21933-21939, doi:10.1039/d0ra01607a (2020).



1. Introduction

Poly(vinylamine) (PVAm), a polymer with a high density of primary amine groups, provides a versatile platform for multiple applications, such as water purification, paper additive, and dye fixation in applications such as textile processing,³ pigment dispersant,⁴ and so on. However, the instability of the corresponding monomer necessitates a two-step method for the formation of PVAm. Among the reported methods the polymerization of N-vinylformamide with a subsequent hydrolysis is the most reported and common one.⁵ Polymerization of Nvinylamides has been described in the literature previously using different solvents, different monomer concentrations, and temperatures. 6-10 Yamamoto et al. for example polymerized NVF in water at 60 °C at a concentration of 10 wt% for 24 h. 7 Further studies uses 70 °C, 2 h, and 6-15 wt% and 50-70 °C and 10-100 wt%, respectively. 8,9 Ajiro et al. prepared a P(VAmco-NVA) copolymer at 37 °C, 8 h with a concentration of 0.2 mol·L⁻¹ NVA and 0.8 mol·L⁻¹ NVF. 10 This method offers two options to tailor the resulting amine density: Incomplete hydrolysis or copolymerization with a second monomer, which is stable under the hydrolysis conditions. Both methods require knowledge about the hydrolysis kinetics. The hydrolysis can be catalyzed via an acidic or basic mechanism forming in case of PNVF either formic acid (acidic) or sodium formate (basic) as by-product (Scheme 3.1.).

acidic
$$+ HCl$$
 basic $+ NaOH$
 $+ NH_3 Cl$ $+ NaOH$
 $+ NH_3 Cl$ $+ NaOH$

Scheme 3.1. Acidic and basic hydrolysis of PNVF.

A systematic study about the kinetics of the acidic and basic hydrolysis of PNVF was published by Gu et al.¹¹ It was found that the basic hydrolysis results in higher reaction rates and equilibrium constants than the acidic one. Furthermore, an increase of the temperature leads to higher initial reaction rates. But, in the case of the basic hydrolysis there is no

influence on the final equilibrium amide conversion (~90 % at 60 °C, 70 °C, and 80 °C), while this greatly differs for the acidic hydrolysis (~40 % at 60 °C, 60 % at 70 °C, and 65 % at 80 °C). Additionally, only the basic hydrolysis leads to a complete hydrolysis requiring a base-to-amide ratio of at least 1. In the case of the acidic hydrolysis the already formed primary amine groups will be protonated. The electrostatic repulsion prevents the hydrolysis of adjacent formamide groups, which is known as polyelectrolyte effect, which is characterized by a broad titration curve.¹¹

In the case of copolymerization knowledge about the copolymerization parameters is crucial. Similar copolymerization parameters will lead to statistical polymers while a high difference in these parameters will lead to block-like copolymers. As rule of thumb structural similar monomers, that means a stereo-electronic similar environment of the double bond, have similar copolymerization parameters.¹² Thus, it is evident to use C=O-alkylated derivates of NVF as they have little impact on the stereo-electronic environment of the double bond and have an increased hydrolysis stability, which means under appropriate conditions a (nearly) selective hydrolysis is possible. In fact, studies show that a complete hydrolysis of PNVF was accomplished at 80 °C in 2 M NaOH, while no hydrolysis of PNVA was reported under these conditions.^{13,14}

The resulting free amine group can undergo numerous reactions and is consequently an excellent candidate for post-modification of the polymer. 15,16 Despite the reactivity of the amine, there is only little literature about the chemical gelation of prepolymers as summarized in Chapter 2. Kobayashi et al. used a bifunctional epoxide based crosslinker for the formation of a hydrogel investigating the pH-dependent swelling behavior with swelling ratios up to 2,500 %; nonetheless, the complete gelation process took 48 h and is not well investigated. 17 Furthermore Han et al. produced a hydrogel starting with PNVF. In a concerted reaction the formamide was hydrolyzed with sodium hydroxide solution and the formed amine groups crosslinked with glutaraldehyde. 18 As indicated by the research of Kobayashi PVAm-based gels are an attractive candidate for superabsorbent hydrogels due to their hydrophilicity. However, in all these papers the PVAm based polymers have not been exploited for synthesis of superabsorbent hydrogels (SHs). In general superabsorbent gels are loosely crosslinked three dimensional polymeric networks mainly of acrylic acid (AA) and/or acrylamide (AM) based monomers. 19 Typically, free radical polymerization is used for the synthesis of these gels. Depending on the type of crosslinker and crosslinking density a water uptake of 8,000 to 80,000 % was obtained.²⁰⁻²³ Addition of inorganic fillers or further introduction of physical crosslinks could enhance the water uptake to 280,000 %. 20,21,23 SHs used in commercial diapers show a water uptake of 23,800 %. Free radical polymerization is a very convenient and handy approach for preparing SHs. However, it is very difficult to control the formation of network structure and the products are inhomogeneous which leads to a decrease of the swelling ability. Crosslinking of pre-polymers might lead to a more homogeneous structure and therefore be advantageous in this case.

In this chapter the copolymerization of NVF with NVA is optimized and utilized to prepare SHs by polycondensation of the prepolymers with phenyl carbonate telechelic poly(ethylene glycol) (PEG-PC). This is a selective and straight-forward way by one step aminolysis of an alkyl-phenyl-carbonate in presence of a base.²⁴ NVA is used because of the structural similarity to NVF and to tailor the resulting amine density in the prepolymer after hydrolysis. PEG is chosen to increase the hydrophilicity of the network. Furthermore, the resulting carbamate linkage is stable under aqueous conditions. The copolymerization parameters and the hydrolysis efficiency as well as the hydrolysis stability of NVA are determined. Hydrolysis is performed under basic conditions aiming for a complete hydrolysis of the NVF. The crosslinking efficiency is monitored by high resolution ¹³C NMR. The structure-property relationship of the hydrogels is characterized by their swelling ratio and rheological properties. The crosslink density of the formed gels is tuned by the ratio of amine to carbonate (crosslinker) and by the pH value.

2. Experimental Part

2.1 Materials

N-Vinylformamide (NVF), phenyl chloroformate (PCF), triethylamine (TEA) and poly(ethylene glycol) (PEG) ($M_n = 400 \text{ g} \cdot \text{mol}^{-1}$) were purchased from Sigma Aldrich. N-Vinylacetamide (NVA) was purchased from ABCR. Pyridine was purchased from Roth. 2, 2'-Azobis[2-(2-imidazolin-2-yl)propane] dihydrochloride (VA044) was purchased from TCI. All chemicals were used as received without any purification.

2.2 Nomenclature:

The following nomenclature was used for polymers: **PNVF** for poly(*N*-vinylformamide), **PNVA** for poly(*N*-vinylacetamide), **PVAm** for poly(*N*-vinylamine), **P(NVF-co-NVA)** for poly(*N*-vinylformamide-*co-N*-vinylacetamide), **P(VAm-co-NVA)** for poly(*N*-vinylamine-*co-N*-vinylacetamide), **Copolymer A** for poly(*N*-vinylformamide-*co-N*-vinylacetamide)

NVF/NVA = 3/1 mol/mol, Copolymer B for poly(*N*-vinylformamide-*co-N*-vinylacetamide) NVF/NVA = 1/1 mol/mol, Copolymer C for poly(*N*-vinylformamide-*co-N*-vinylacetamide) NVF/NVA = 1/3 mol/mol. Copolymer 1 for poly(*N*-vinylamine-*co-N*-vinylacetamide) NVAm/NVA = 3/1 mol/mol, Copolymer 2 for poly(*N*-vinylamine-*co-N*-vinylacetamide) NVAm/NVA = 1/1 mol/mol, Copolymer 3 for poly(*N*-vinylamine-*co-N*-vinylacetamide) NVAm/NVA = 1/3 mol/mol. In the nomenclature of gels (Gx:y:z) the first number indicates the starting copolymer (Copolymer 1, Copolymer 2, Copolymer 3), the second number indicates the molar ratio of phenylcarbonate-to-amine groups (O-CO-OPh/NH₂) used for the synthesis, and the third number indicates the ratio triethylamine/amine groups Et₃N/NH₂ used for the synthesis.

2.3 Polymer and gel syntheses.

Copolymer B

NVF (3.64 g, 51.2 mmol), NVA (6.36 g, 51.2 mmol) and VA044 (331 mg, 1.02 mmol) were dissolved in water (90 mL). The reaction mixture was degased by three freeze-thaw cycles. After degasing the reaction mixture was heated up to 60 °C for 20 h under nitrogen. The resulting copolymer was precipitated in an excess of acetone, redissolved in water, and lyophilized obtaining a white solid (9.82 g, 98.2 wt%).

¹H NMR (400 MHz in D₂O, δ in ppm):1.35-1.75 (-CH₂ backbone), 1.75-1.95 (-CH₃), 3.0-4.0 (-CH backbone), 7.5-8 (-CHO)

GPC: $M_n = 5.6 \cdot 10^4 \text{ g} \cdot \text{mol}^{-1}$, $M_w = 1.2 \cdot 10^5 \text{ g} \cdot \text{mol}^{-1}$, PDI = 2.2

Copolymer A and C were prepared by the same procedure. Table 3.1 summarizes the amounts of reagents used.

Table 3.1 Amounts of reagents used for the synthesis of Copolymer A, B, and C in water (90 mL)

Formamide:Acetamide	NVF	NVA	VA044
ratio	[g] &	[g] &	[mg] &
	[mmol]	[mmol]	[mmol]
3:1 (Copolymer A)	6.32	3.68	383
	88.9	29.6	1.18
1:1 (Copolymer B)	3.64	6.36	331
	51.2	51.2	1.02

1:3 (Copolymer C)	1.60	8.40	292
	22.5	67.7	0.90

Copolymer 1

Copolymer A (10 g) was dissolved in 2 N sodium hydroxide solution (490 mL). The reaction mixture was heated up to 80 °C for 4 h. The mixture was neutralized with hydrochloric acid to pH = 7 and subsequently dialyzed (regenerated cellulose, SpectraPor®, molecular weight cutoff: 3.5 kDa) for 7 days. The water was removed by lyophilization obtaining a white solid (yield: 6.52 g, 65 wt%).

¹H NMR (400 MHz in D₂O, δ in ppm; Figure 3.1): 1.2-2.1 (-C*H*₂ backbone, -C*H*₃), 2.8-4.1 (-C*H* backbone), 8.3-8.4 (-NC*H*N-)

GPC: $M_n = 6.7 \cdot 10^4 \, \text{g} \cdot \text{mol}^{-1}$, $M_w = 1.5 \cdot 10^5 \, \text{g} \cdot \text{mol}^{-1}$, PDI = 2.2

Copolymer 2 and 3 were prepared by the same procedure using the same amount of polymer (10 g) and reagent (490 mL).

Phenyl carbonate telechelic poly(ethylene glycol) (PEG-PC)

To a solution of PEG (10 g, 25 mmol) in THF (100 mL) was added pyridine (2 eq, 3.96 g, 50 mmol). The reaction mixture was cooled with an ice bath. PCF (2 eq, 7.83 g, 50 mmol) was added dropwise without exceeding 5 °C in the reaction mixture. Afterwards the reaction was allowed to stir for further 16 h at room temperature. Pyridine hydrochloride was removed by filtration, the solution washed three times with water, and the solvent was removed by rotary evaporation. The product was obtained as colorless liquid (yield not determined).

¹H NMR (400 MHz in MeOD, δ in ppm): 3.3-3.5 (-C H_2 , backbone), 3.55-3.65 (-C H_2), 4.2-4.3 (-C H_2), 6.65-6.75 (unknown side product), 7.0-7.1 (-C H_2 , aryl, para), 7.1-7.2 (-C H_3 , aryl, para), 7.2-7.35 (-C H_4 , aryl, meta)

Preparation of the gel - G2:1:2.

To a solution of polymer 2 (50 mg) in methanol (520 μ L) was added triethylamine (79.7 mg, 788 μ mol). PEG-PC (252 mg, 394 μ mol) was dissolved in methanol (500 μ L) and added to the reaction mixture. The solutions were prepared for 5 wt% of the polymer with respect to the mass of TEA and MeOH, *i.e.*, the mass of methanol was calculated according to Equation

1 Further gel systems were prepared analogously; the respective amounts of reagents are summarized in Table 2.

$$m_{MeOH} = \frac{m_{Polymer}}{0.05} - m_{TEA} - m_{Polymer} \tag{1}$$

Table 2. Amounts of reagents used for synthesis of the gels.

Gel	Polymer [mg]	PEG-PC [mg]	Triethylamine	Methanol	Stability
	Amine groups	PhO-CO-O	[mg]	[mg]	
	[µmol]	groups [µmol]	[µmol]	[μL]	
G1:1:2	50	455	144	806	+
	711	711	1422	1020	
G1:1:1	50	455	71.9	878	+
	711	711	711	1111	
G1:1:0.5	50	455	36.0	914	+
	711	711	356	1157	
G1:0.5:2	50	227	144	806	+
	711	355	1422	1020	
G1:0.5:1	50	227	71.9	878	+
	711	355	711	1111	
G1:0.5:0.5	50	227	36.0	914	+
	711	355	356	1157	
G1:0.25:2	50	114	144	806	+
	711	178	1422	1020	
G1:0.25:1	50	114	71.9	878	+
	711	178	711	1111	
G1:0.25:0.5	50	114	36.0	914	+
	711	178	355	1157	
G2:1:2	50	252	79.7	870	+

	394	394	788	1102	
G2:1:1	50	252	39.8	910	+
	394	394	394	1152	
G2:1:0.5	50	252	19.9	930	+
	394	394	197	1177	
G2:0.5:2	50	126	79.7	870	+
	394	197	788	1102	
G2:0.5:1	50	126	39.8	910	+
	394	197	394	1152	
G2:0.5:0.5	50	126	19.9	930	+
	394	197	197	1177	
G2:0.25:2	50	63.0	79.7	870	+
	394	98.4	788	1102	
G2:0.25:1	50	63.0	39.8	910	+
	394	98.4	394	1152	
G2:0.25:0.5	50	63.0	19.9	930	+
	394	98.4	197	1177	
G3:1:2	50	108	34.1	916	-
	168	168	336	1159	
G3:1:1	50	108	17.0	933	-
	168	168	168	1181	
G3:1:0.5	50	108	8.52	941	-
	168	168	84.0	1181	
G3:0.5:2	50	53.9	34.1	916	-
	168	84.0	336	1159	
G3:0.5:1	50	53.9	17.0	933	-

	168	84.0	168	1181	
G3:0.5:0.5	50	53.9	8.52	941	-
	168	84.0	84.0	1192	
G3:0.25:2	50	26.9	34.1	1159	-
	168	42.0	336	1020	
G3:0.25:1	50	26.9	17.0	933	-
	168	42.0	168	1181	
G3:0.25:0.5	50	26.9	8.52	941	-
	168	42.0	84.0	1192	

^{*} green tables show data incorporated in the publication while the grey tables are omitted

2.4 Measurements

NMR spectra

Proton-NMR spectra were recorded on a Bruker Avance III-400 FT-NMR (Bruker Corporation, Billerica, MA, USA) spectrometer at 400 MHz. ¹³C NMR spectra as well as the kinetic measurement were recorded on a Bruker Avance II-600 FT-NMR spectrometer (Bruker Corporation, Billerica, MA, USA) at 150 MHz. Deuterated methanol (CD₃OD) and deuterium oxide (D₂O) were used as solvents. Trioxane was used as internal standard for the hydrolyzed copolymers 1-3.

Reaction Kinetics

To determine the reaction rate a 1:1 molar ratio of NVF:NVA were copolymerized at 35 °C for 120 min recording ¹H NMR spectra every 5 min. The copolymerization parameters were determined by the method of Fineman-Ross and Mayo-Lewis using 5 different NVF:NVA ratios (3:1; 1:1; 1:3; 1:5; 1:10) in the feed. The ratio of NVF:NVA was determined at conversions below 10 %.

Size exclusion chromatography (SEC) analyses

Molecular weights ($M_{n,SEC}$ and $M_{w,SEC}$) and molecular weight distributions (PDI = $M_w \cdot M_n^{-1}$) were determined by SEC. SEC analyses were carried out using water (HiPerSolv

CHROMANORM® HPLC grade, VWR) as the eluent containing 10 % acetonitrile, $0.1 \text{ mol} \cdot L^{-1}$ sodium chloride, 0.1 wt% triflouroacetic acid and 0.01 wt% sodium azide. The machine was equipped with an HPLC pump (1200, Agilent), a refractive index detector (RI) (1200, Agilent), and an UV-detector (VWD, 1200, Agilent). The samples contained $0.5 \, \mu L \cdot m L^{-1}$ ethylene glycol (99.5 %, Fluka analytical) as internal standard. One pre-column (8 × 50 mm) and three Novema Max gel columns (8 × 300 mm, Polymer Standards Service) were applied at a flow rate of $1.0 \, m L \cdot min^{-1}$ at 25 °C. The diameter of the gel particles measured 5 μm , the nominal pore widths were 30, 100, and 1000 Å. Calibration was performed using narrowly distributed poly(ethylene oxide) standards (Polymer Standards Service). Results were evaluated using the PSS WinGPC UniChrom software (Version 8.3.2).

Swelling behavior

The as-prepared hydrogels were weighed and immersed in a large amount of deionized water at ambient temperature. To determine the swelling ratio the excess water was removed, and the hydrogel carefully blotted. The swelling ratio was calculated with Equation 2.

Swelling ratio [%] =
$$\frac{m_2 - m_1}{m_1} \cdot 100\%$$
 (2)

where m_2 and m_1 are the mass of the swollen and as-prepared sample, respectively. The swelling ratio with respect to the dry weight hydrogels, which are swollen to equilibrium, were lyophilized and weighed.

Rheology

Measurements were conducted with a Discovery Hybrid Rheometer HR 3 (TA Instruments, USA) and a 40 mm parallel plate. Unless otherwise noted a frequency of 1 Hz and an oscillation strain of 1 % were used. The reagents were mixed directly before the measurement and 1 mL of the solution were placed on the plate. The gap was adjusted to $800 \, \mu m$ and solvent evaporation prevented by a solvent trap.

Potentiometric Titration

The copolymers were dissolved in 0.5 M HCl solution and the volatiles were removed in vacuo. The residue was dissolved in 1 M KCl solution in degassed water and titrated against 0.1 M NaOH solution measuring the pH-value. The degree of ionization (DOI) was calculated neglecting any interionic interactions with Equation 3:²⁵

$$DOI = \frac{[-NH_3]^+}{[-NH_2] + [-NH_3]^+} = \frac{10^{-pH}}{10^{-pH} + 10^{-pK_A}}$$
(3)

3. Results and Discussion

Free radical copolymerization of NVF with NVA was performed water using different monomer ratios and VA044 as initiator (Scheme 3.2a). The resulting copolymers were then subjected to a selective hydrolysis of the NVF repeating units yielding copolymers with free amine groups. These hydrolyzed prepolymers were crosslinked with PEG-PC in the presence of triethylamine (TEA) forming a hydrogel (Scheme 3.2b). The swelling properties and the rheological behaviour of the polymer networks were determined.

Scheme 3.2. Copolymerization of *N*-vinylformamide with *N*-vinylacetamide in different molar ratios leading to copolymers A, B, and C and their selective hydrolysis to copolymers 1, 2, and 3 (a), and schematic representation of the polymer networks prepared from P(VAm-co-NVA) and bis phenylcarbonate telechelic poly(ethylene glycol) (b)

3.1 Polymer synthesis

Optimization of the reaction parameters was done by SEC varying the reaction temperature and monomer concentration. A monomer ratio of NVF:NVA = 1:1 was chosen and the composition confirmed by ¹H NMR.

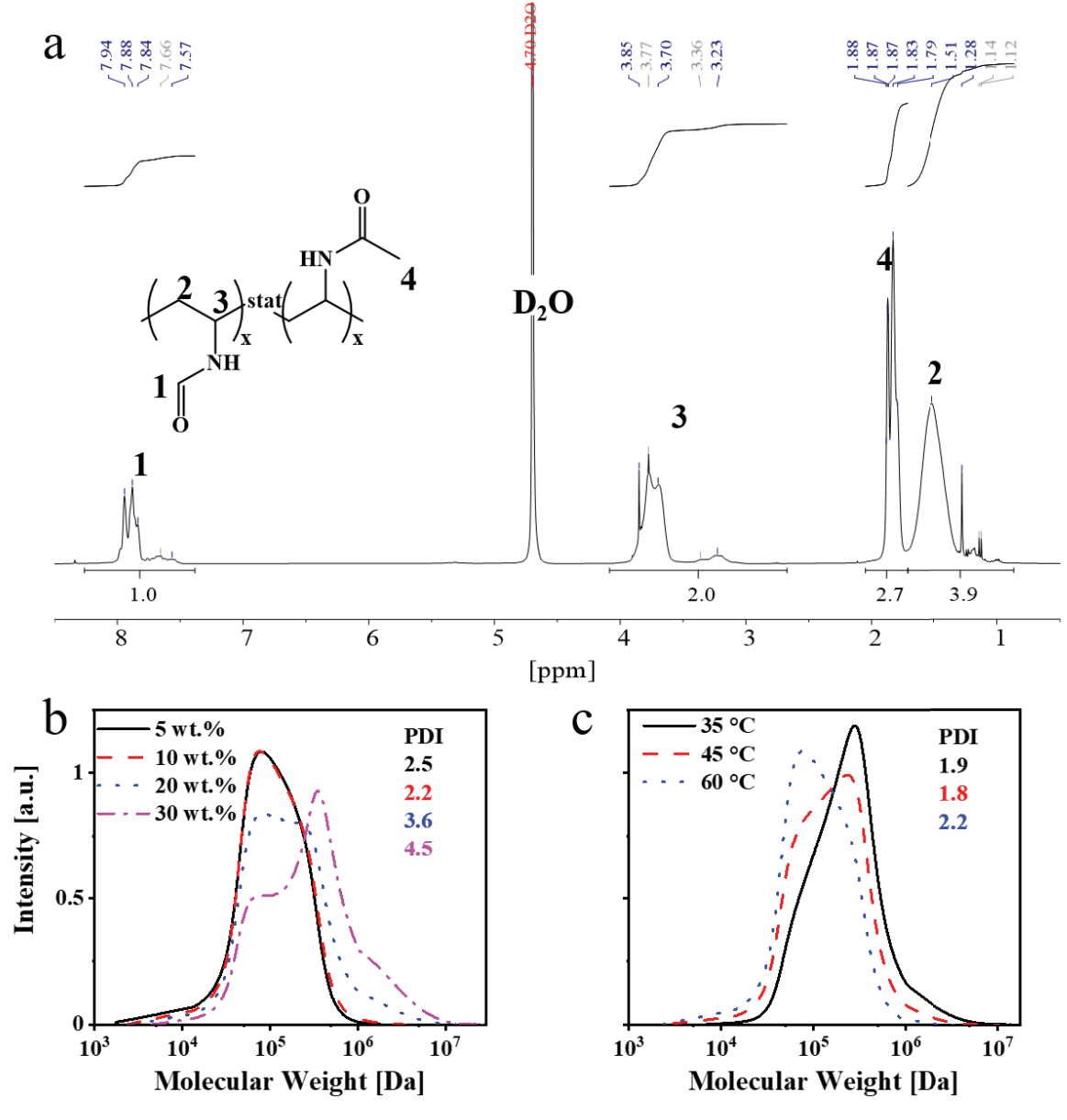


Figure 3.1. a) Proton NMR of Copolymer B in D_2O and molecular weight distribution in variation of the monomer concentration at constant temperature (T = 60 °C) (b), and in variation of the reaction temperature at a constant monomer concentration (c = 10 wt.%) (c) determined by SEC.

The variation of the monomer concentration (T = 60 °C, $c_{Monomer} = 5$, 10, 20, and 30 wt.%) is shown in Figure 3.1b revealing that the molecular weight distribution broadens exceeding a

concentration of 10 wt% as indicated by an increase of the PDI from 2.5 ($c_{Monomer} = 5$ wt.%) to 4.5 ($c_{Monomer} = 30$ wt.%). This is caused by the so-called "gel- or Trommsdorff-effect", which is in agreement with literature data.⁸ The gel-effect is caused by an increase of the viscosity, whereby termination reactions which are diffusion controlled become less likely. Furthermore, polymerizations of equimolar amounts of NVF and NVA were performed at 10 wt% and different temperatures (T = 35, 45 and 60 °C). SEC analysis of these polymers show that with decreasing temperature the molecular weight increases and the PDI decreases slightly from 2.2 at 60 °C to 1.9 at 35 °C. (Figure 3.1c). Based on these preliminary results copolymers of NVF and NVA were prepared in different molar ratios at T = 60 °C in aqueous solution using a monomer concentration of 10 wt% and VA044 as initiator. The structural similarity of NVF and NVA suggests similar reactivity while polymerization. This reactivity can be expressed by the copolymerization parameters. Herein, the methods of Fineman-Ross and Mayo-Lewis were used to quantify the copolymerization parameters. The Fineman-Ross method uses a linearization of the copolymerization equation (4).

$$\frac{d[A]}{d[B]} = \frac{1 + r_A \frac{[A]}{[B]}}{1 + r_B \frac{[B]}{[A]}} = \frac{[A]}{[B]} \cdot \frac{r_A[A] + [B]}{[A] + r_B[B]} \tag{4}$$

With [A] and [B] being the concentration of the monomers and r_A and r_B the respective copolymerization parameters. The linearization of equation (4) suggested by Fineman and Ross leads to equation (5)

$$y \cdot \frac{x-1}{x} = \frac{y^2 r_A}{x} - r_B \tag{5}$$

With $x = n_A \cdot n_B^{-1}$ and $y = [A] \cdot [B]^{-1}$, where n_A and n_B is the amount of monomer A and B, respectively. The copolymerization parameters can be determined with the slope (r_A) and the y-intercept (r_B) plotting $y \cdot (x^{-1})$ x-1 against y^2 x⁻¹. Five different NVF:NVA ratios (3:1; 1:1; 1:3; 1:5; 1:10) were used in the feed and the ratio of NVF:NVA was determined at conversions below 10 % by ¹H-NMR. As shown in Figure 3.2a and b the values of the copolymerization parameters are close to unity proving the formation of a statistical copolymer (Fineman-Ross: $r_{NVF} = 0.92 \pm 0.04$, $r_{NVA} = 0.97 \pm 0.04$; Mayo-Lewis: $r_{NVF} = 1.04 \pm 0.12$, $r_{NVA} = 1.05 \pm 0.10$). For further investigation three different NVF:NVA molar ratios were used for polymerization.

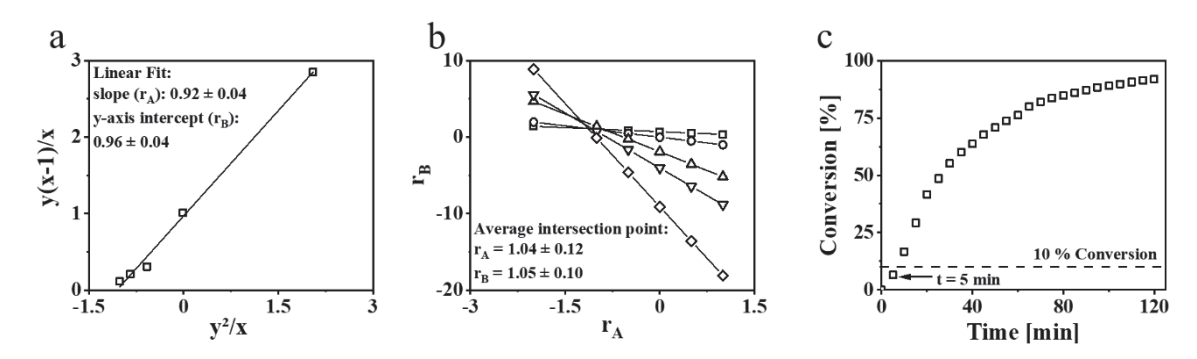


Figure 3.2. The copolymerization parameters determined by the methods of Fineman-Ross (a) and Mayo-Lewis (b). (c) shows the conversion in dependence on the time calculated by ¹H NMR at 35 °C, 10 wt% monomer concentration and 1 mol% initiator concentration.

As evident from Figure 3.2c the conversion is below 10 % after 5 min (highlighted by the arrow in Figure 3.2c) indicating that the methods of Fineman-Ross and Mayo-Lewis are applicable. Furthermore, as already shown in Figure 3.1c, there is no Gel-effect visible at these reaction parameters, which would be characterized by an increase of the reaction rate at a high conversion (35 °C, 10 wt% monomer concentration, 1 mol% initiator concentration).

To validate the kinetic results, three different NVF:NVA ratios (3:1, 1:1, and 1:3) were polymerized and analyzed by ¹H NMR spectroscopy (Figure 3.3). Taking the formamide-signal (-CHO) arising from NVF as standard the relative ratio of the methyl group caused by the NVA can be determined and compared to the theoretical ratio as shown in Table 3. While for the ratios NVF:NVA 3:1 and 1:1 the respective integrals are matching, there is a deviation for the ratio 1:3 indicating that less NVA being in the prepolymer. However, this may be caused by the intrinsic error of the measurement method as the integral intensity of the formamide group is very low in this case.

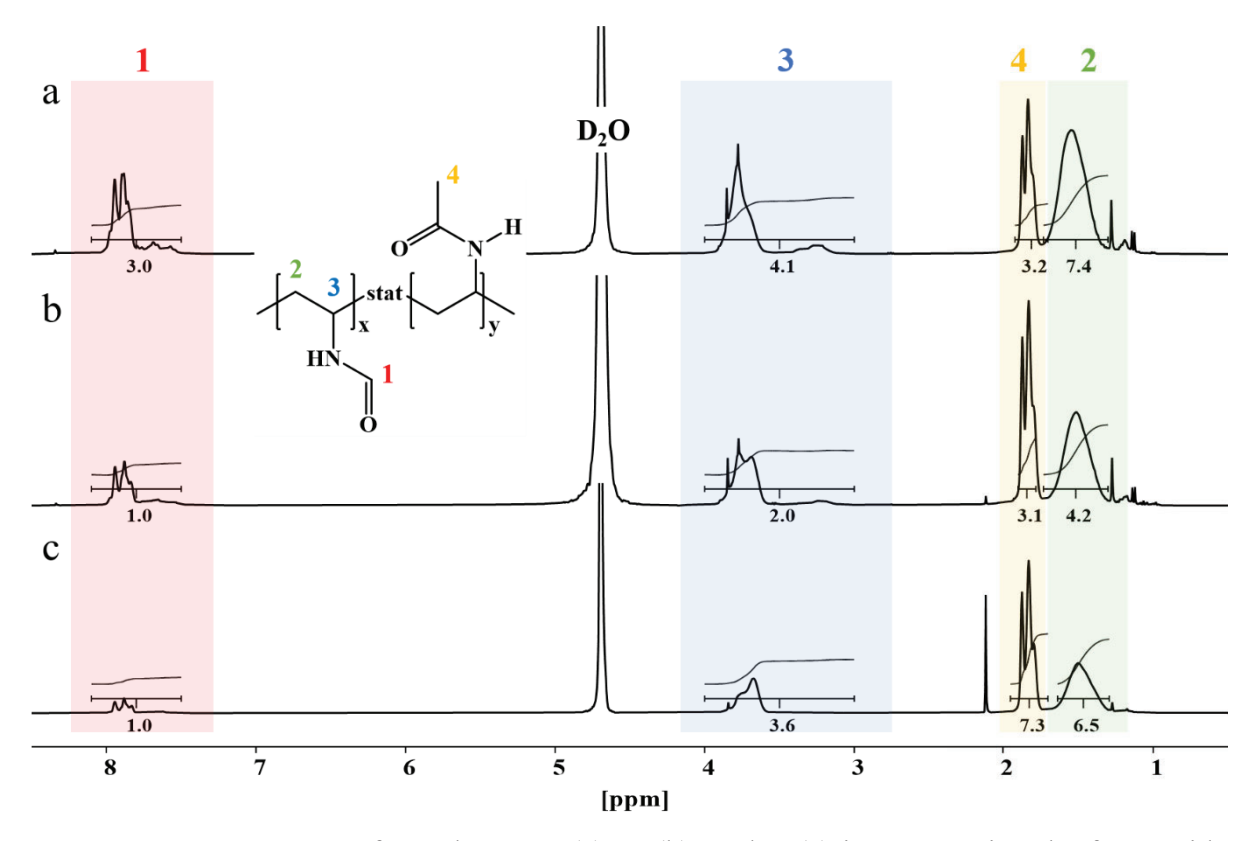


Figure 3.3. Proton NMR of copolymer A (a), B (b), and C (c) in D₂O. Using the formamide signal as standard it can be seen, that the theoretical ratios were obtained.

Table 3. Theoretical and experimental integral ratios of the formamide and acetamide group

Copolymer	Ratio NVF:NVA	Integral CHO (NVF)	Integral CH ₃ (NVA)
		I_1	I ₄ / ₃
Copolymer A	3:1	3	1.07
Copolymer B	1:1	1	1.03
Copolymer C	1:3	1	2.43

The copolymers with a molar ratio of NVF:NVA = 3:1, 1:1, and 1:3 in the feed were named copolymer A, copolymer B, and copolymer C. (Scheme 3.2)

The prepolymers were subsequently hydrolyzed under basic conditions (2 M NaOH, 8 h, 80 °C). From ¹H spectroscopy it is visible that the formamide signal disappears completely (Figure 3.4). Furthermore, signal 2 and 4 become indistinguishable and are combined.

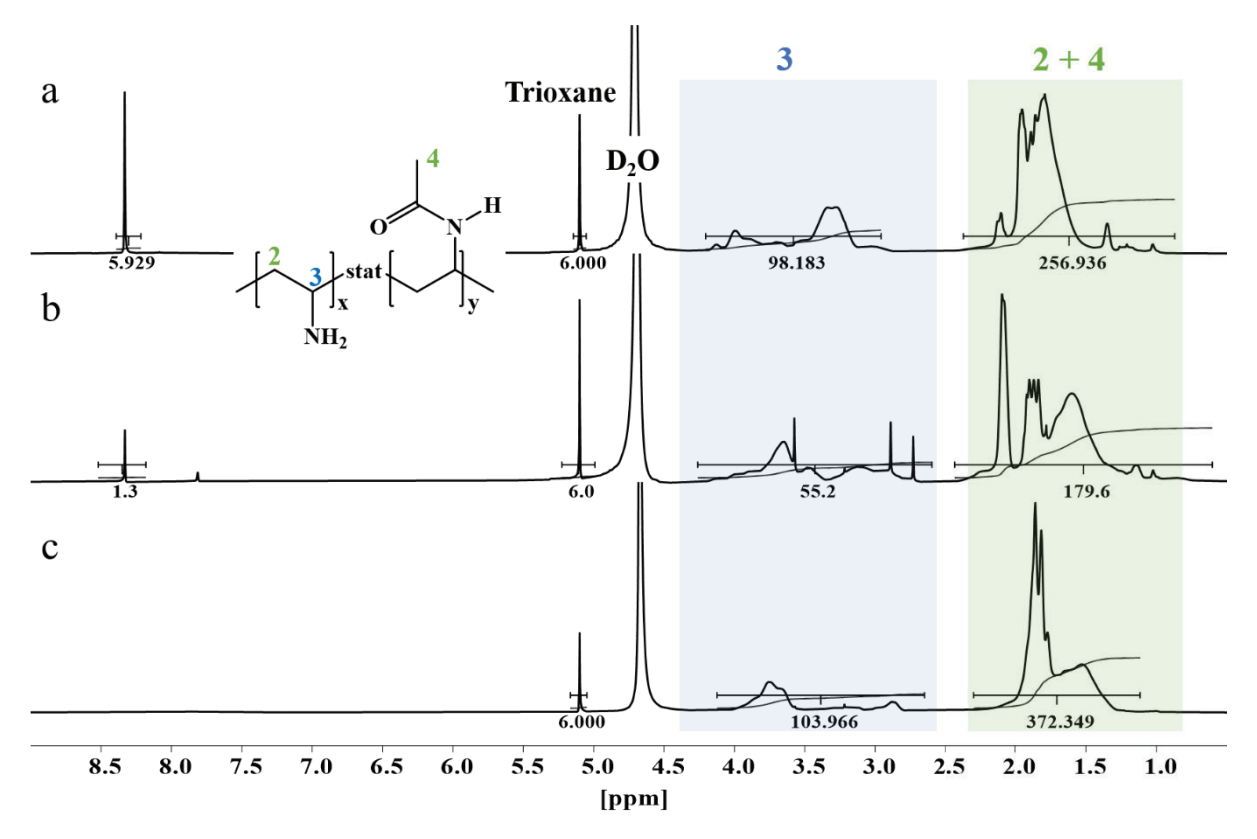


Figure 3.4. Proton NMR of copolymer 1 (a), 2 (b), and 3 (c) using trioxane as standard. From the integrals it is evident, that NVF was selectively hydrolyzed.

Using trioxane as internal standard the relative integrals of the backbone hydrogens and the methyl hydrogens give the VAm:NVA ratio via equation (6) and (7).

$$[VAm] = \frac{I_3}{I_{total}} \cdot \frac{n_{total}}{n_3} \cdot \chi \tag{6}$$

$$[NVA] = \frac{I_{2+4}}{I_{total}} \cdot \frac{n_{total}}{n_{2+4}} \cdot y \tag{7}$$

With [VAm] and [NVA] being the respective experimental content in the polymer, I the respective integral as indicated in Figure 3.4, n the number of protons of the respective integral and x and y the theoretical content of VAm and NVA in the feed. The results are shown in Table 4.

Table 4. Experimental integral ratios of the amine and acetamide

Copolymer	[VAm:NVA] _{theoretical}	[VAm]	[NVA]
Copolymer 1	3:1	3.11	0.99
Copolymer 2	1:1	1.06	0.98
Copolymer 3	1:3	1.15	2.90

Under the experimental conditions for the hydrolysis of copolymers A, B, and C it is visible that the ratio of NVF to NVA repeating units before hydrolysis corresponds to the ratio of NVAm to NVA repeating units after hydrolysis (Figure 3.4 and Table 3), that means the acetamide group of the NVA was not affected by the hydrolysis, while the formamide was completely hydrolyzed. Consequently, the used experimental conditions (2 M NaOH, 80 °C, 8 h) allow a selective hydrolysis of the formamide group.

The signal around 8.3-8.4 ppm suggests the occurrence of a side reaction. It is discussed in literature that this signal is caused by a cyclization reaction of adjacent VAm-NVF moieties forming a 1,4,5,6 tetrahydropyrimidine structure. However, it is also possible that this signal refers to the ammonium-chlorid salt (-NH₃+Cl⁻). The strong hydrogen bonding between the ammonium and the chloride ion prevents on the one hand the exchange with deuterium making the protons visible in H-NMR and on the other it will not be removed by dialysis. In our experiments this side reaction is observed and occurs in the range of 8 % for copolymer 1 and 4.5% for copolymer 2. In copolymer 3 no signal for the side product is observed (Figure 3.4).

The statistical monomer distribution in the copolymers 1, 2, and 3 can be qualitatively supported by a potentiometric titration (Figure 5a) giving also the degree of ionization (DOI) (Figure 5b). From the DOI it is evident, that still around 40 % (copolymer 3) to 80 % (copolymer 1) of the amine groups are charged at a pH value of 7. The statistical distribution of the monomers is visible by the development from two discrete equivalent points (copolymer 3) to a broad spreading caused by the polyelectrolyte effect (copolymer 1) (Figure 3.5a). A block-like copolymer would show the polyelectrolyte effect even at low amine to amide ratio. From the first equivalence point (transition from structure 1 to 2 in Figure 3.5c).

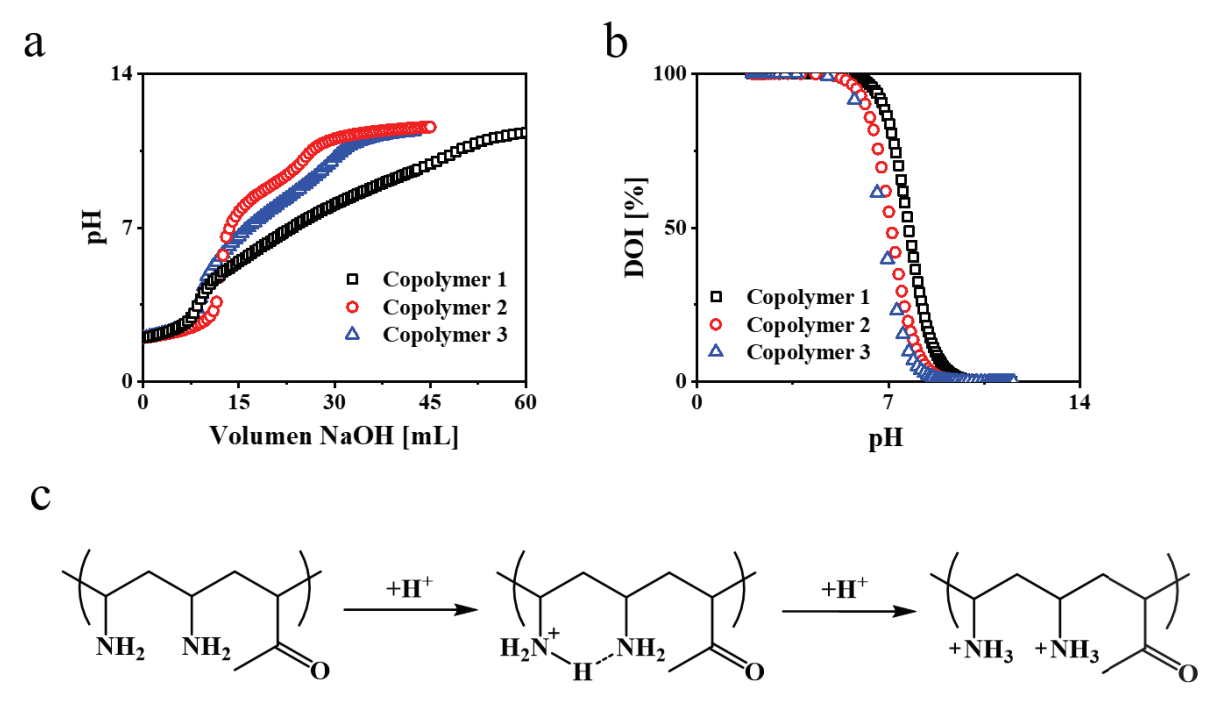


Figure 3.5. The titration curve of copolymer 1 (black squares), copolymer 2 (red circles), and copolymer 3 (blue triangles) against 0.1 M NaOH (a). The corresponding DOI calculated by equation 3 is shown in (b). The origin of the two discrete equivalent points in the titration curve can be explained by the scheme shown in (c).

3.2 Chemical Gelation

Post polymerization condensation reaction in which amine groups are reacted with alkylphenyl-carbonates with formation of carbamate (urethane) groups and elimination of phenol are known. 24,26 In our experiments we reacted copolymers 1, 2, and 3 (decreasing amine content from copolymer 1-3) with PEG-PC (M_n of PEG 400 g mol⁻¹) to obtain gels of decreasing crosslinking density. Due to the insolubility of PEG-PC in water crosslinking was performed in methanol. For copolymer 1 and 2 a concentration of 5 wt% did not lead to the formation of a gel by addition of the crosslinker. However, increasing the concentration to 10 wt.% addition of the crosslinker led to spontaneous precipitation of a physical gel. The physical gel will be discussed in Chapter 4. As seen from the potentiometric titration, at pH = 7 still 40 – 80 % of the amine groups are protonated (charged) depending on the amine: amide ratio (Figure 3.5) of the polymer backbone. To have only (exclusively) free amine which undergo nucleophilic reaction with the carbonates groups a base (triethylamine, (TEA)) was added to the reaction mixture. This way, we obtained in the formation of a transparent hydrogel. Performing the gelation in deuterated solvents 1 H-NMR shows the formation of phenol (Figure 3.6). The formation of phenol proves the condensation reaction between the

phenylcarbonate groups, and the amine groups as suggested in Scheme 3.2 leading to carbamate crosslinks.

To explore the efficiency of the reaction, swelling behavior, and mechanical properties hydrogels were prepared using three different copolymers reacted with three different amounts of crosslinker obtaining three different carbonate-to-amine ratios. In addition, three different base concentrations were applied yielding 27 gel samples (see Table 2). The nomenclature of the gel samples is Gx:y:z, where x is the corresponding copolymer (1-3), y the carbonate-to-amine ratio (1, 0.5, or 0.25) and z the equivalents of TEA with respect to the amine groups (0.5, 1, or 2), i.e. G1:0.5:1 means that one equivalent of copolymer 1 (amine:amide ratio of 3:1) was reacted with 0.5 equivalents PC-groups (a carbonate-to-amine ratio of 0.5:1) and 1 equivalent TEA per amine group.

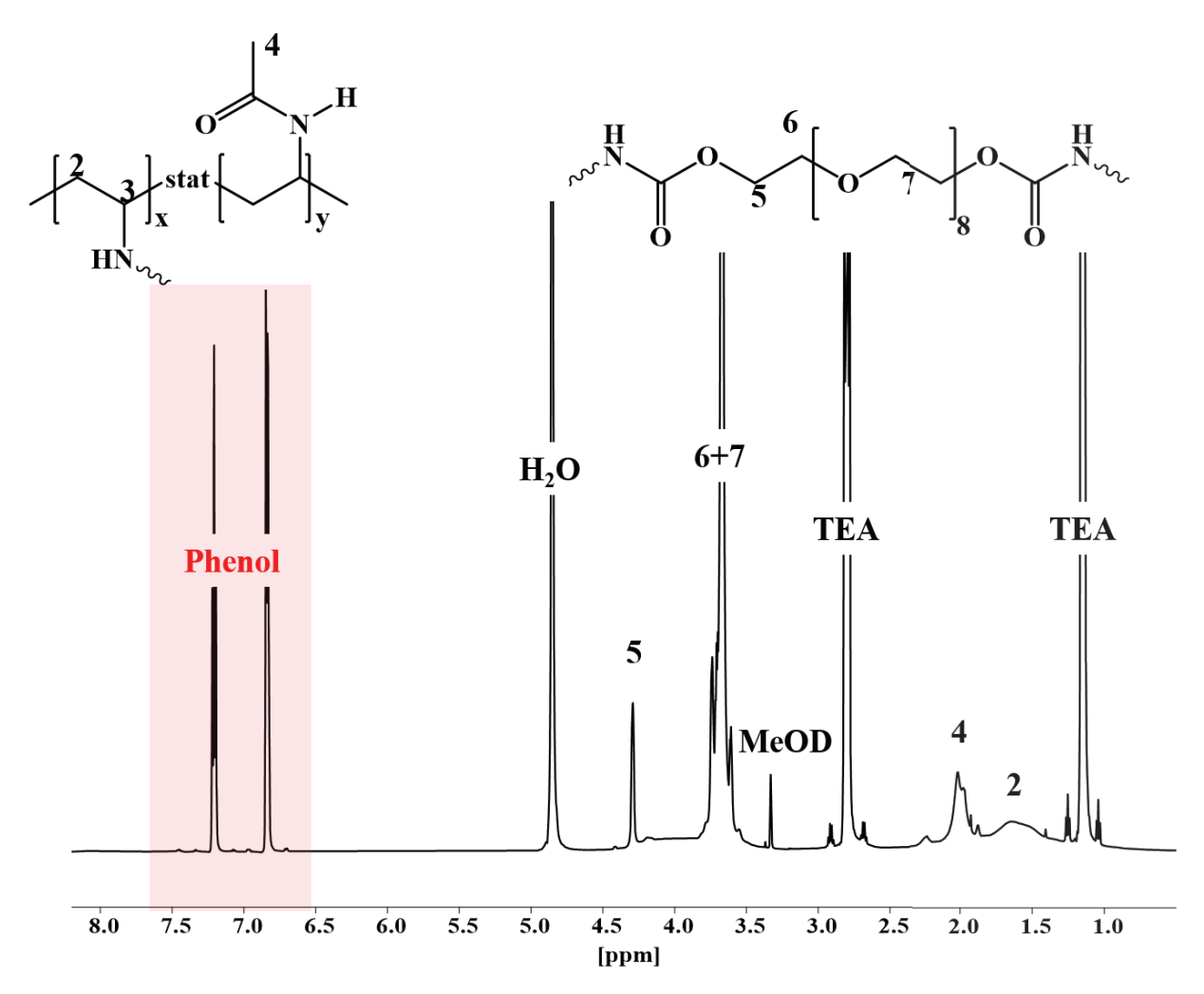


Figure 3.6. Proton NMR of the as-prepared hydrogel in MeOD. The presence of phenol indicates a successful reaction.

The completeness of the reaction was monitored by high resolution ¹³C NMR (150 MHz, 20,000 scans). In Figure 3.7 an exemplary ¹³C NMR of G2:1:2 is shown. The conversion was calculated by dividing the unreacted aromatic phenylcarbonat-carbons (b-d) by the total aromatic carbons, that means the aromatic phenylcarbonat carbons (b-d) and the phenol carbons (f-h). It is noteworthy that PEG-PC might also react with the solvent (methanol). The resulting methylcarbonate group might be referred to signal 7 (H₃COCOOC-), but the overall intensity is low. Therefore, it is neglected. Furthermore, the copolymer is not visible due to its restricted mobility.

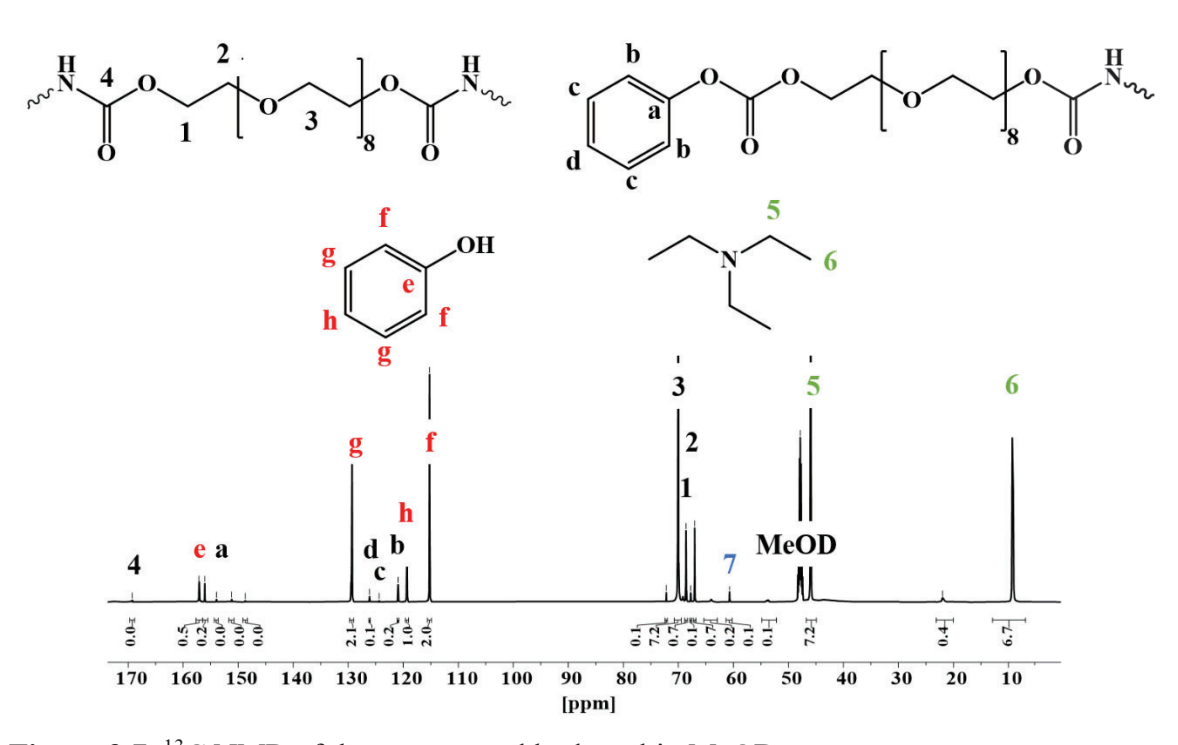


Figure 3.7. ¹³C NMR of the as-prepared hydrogel in MeOD.

It was found, that G2:1:2, which has a high crosslinking density, shows, that 8.8 % phenylcarbonate groups remain unreacted, whereas in case of G2:0.5:2 no unreacted carbonate groups were found (Table 4). It is very likely that the high crosslinking density and fast gelation restricts the motion of the crosslinker leading to inhomogenities like backbiting, *i.e.* an intramolecular crosslinking reaction, in the network. With decreasing the amount of crosslinker the reaction proceeds to complete conversion.

Table 4. Calculated amount of unreacted carbonate groups from ¹³C NMR

Gel	% [PhO-CO-O-]
G2:1:2	8.8
G2:0.5:2	0
G2:1:0.5	40.2

3.3 Swelling Behavior

In the following section the structure property relationship, in the particular case, the effect of the amine concentration in P(VAm-co-NVA) upon crosslinking with PEG-PC and a carbonate-to-amine ratio of 1:1 in presence of TEA with an amine-to-TEA ratio of 1:2 is investigated (Gx:1:2). Furthermore, the effect of the carbonate-to-amine ratio on the crosslinking density is studied for copolymer 2 and a amine-to-TEA ratio of 1:2 (G2:y:2). Finally, the effect of the amine-to-TEA ratio on the swelling behavior of copolymer 2 crosslinked with PEG-PC with a carbonate-to-amine ratio of 1:1 is studied (G2:1:z). Figure 3.8 shows the swelling ratio of G1:1:2, G2:1:2, and G3:1:2 in water in dependence on time, i.e. for the copolymers 1, 2, and 3 with an carbonate-to-amine ratio of 1:1 and 2 equivalents of TEA. It is visible that the polymer with the lowest amine content, i.e. copolymer 3, does not show a stable structure as the swelling ratio decreases after two hours, which means that the structure disintegrates. The hydrogels made of copolymer 1 and 2 show a stable structure with swelling ratios up to 2,000 % for copolymer 2 and 1,000 % for copolymer 1. This is an intuitive result since copolymer 1 possesses a higher amine density and therefore a higher crosslinking density which results in a lower swelling ratio. The swelling curve for G1:1:2 and G2:1:2 exhibits a sigmoidal shape, which is more prominent for G2:1:2. Due to the higher swelling ratio of G2:1:2 copolymer 2 was further investigated.

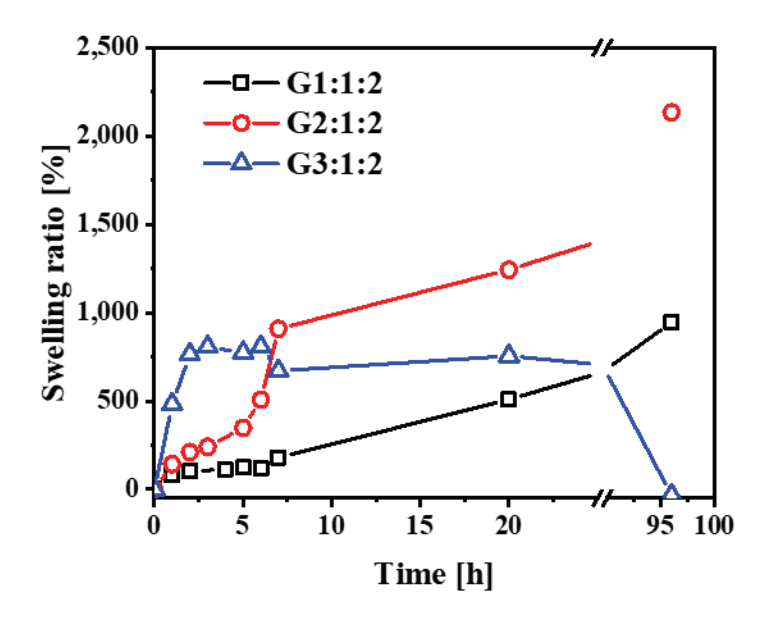


Figure 3.8. Swelling ratio of G1:1:2, G2:1:2, and G3:1:2 in water in dependence on the time

The swelling ratio of the gels in dependence on the carbonate-to-amine ratio (G2:1:2, G2:0.5:2, G2:025:2) are shown in Figure 3.9. Therein, three different swelling regimes can be identified as indicated by the dashed line: The first regime is characterized by a low slope. Since the gels are prepared in methanol, first a solvent exchange takes place on swelling the gel in water, this is due to a co-nonsolvency effect known for methanol-water mixtures.²⁷ This means, that the gels can swell either in pure methanol or in pure water, but in mixtures of both the structure first collapses. Due to this, swelling is hindered and is diffusion controlled. This effect can be seen visually as the transparent hydrogel prepared from methanol turns whitish after having contact with water. The second state is reached after methanol is completely replaced by water, so the co-nonsolvency is overcome and the structure opens again facilitating further water uptake. Visually the gel is transparent again. In the last state the gel is swollen to equilibrium and no further change is visible. Varying the crosslinking density, i.e. the ratio of carbonate-to-amine, it is visible that the slope of the first state is very similar for all three crosslinking densities, i.e. in the collapsed state. However, the water uptake is highest for the lowest crosslinking density. This is an expected result as a lower crosslinking density results in a greater pore size providing more space for swelling

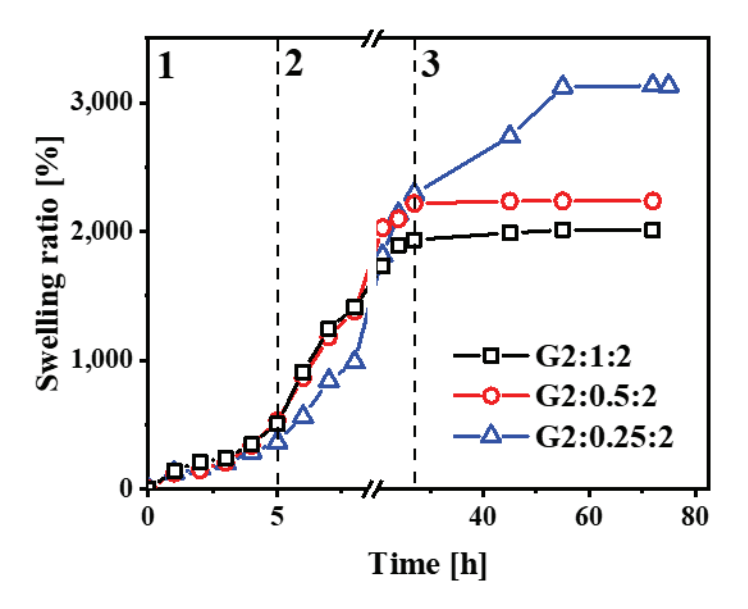


Figure 3.9. Swelling ratio in dependence on the time for G2:1:2, G2:0.5:2, and G2:0.25:2

It is noteworthy that these swelling ratios are calculated with respect to the as-prepared weight in methanol. Lyophilized gels, which are swollen to equilibrium, give the swelling ratio with respect to the dry gel, these values are presented in Table 5. It can be seen that G2:0.25:2 has a swelling ratio of 96,900 %, which means that 1 g gel has a water uptake of \sim 1 kg, which is beyond the single network acrylate based SHs synthesized via free radical polymerization (8,000 to 80,000 %). The swelling of this gel is homogeneous and the outstanding swelling ability is visualized in Figure 3.10.

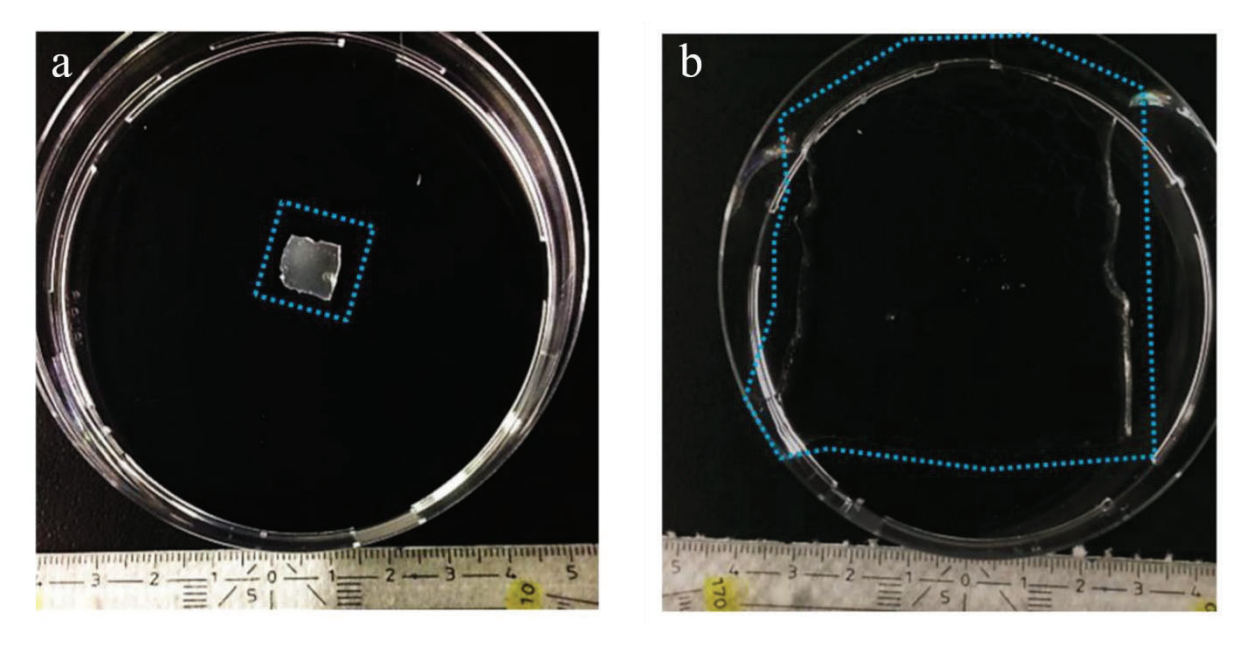


Figure 3.10. Image of the as-prepared G2:0.25:2 (a) and swollen in water (b). The dotted blue line highlights the hydrogel boundary.

This swelling behavior of the hydrogels can further be controlled with respect to the ratios of amine, carbonate, and the base. Furthermore, the flexibility of tailoring the amine to amide ratio in the polymer backbone provides an added advantage to tune the swelling behavior of the hydrogel.

Table 5. Swelling ratio of G2:1:2, G2:0.5:2, and G2:0.25:2 at equilibrium with respect to the dried gel

Gel	Swelling ratio [%]
G2:1:2	39,300
G2:0.5:2	45,900
G2:0.25:2	96,900

The swelling ratio as a function of the added base for G2:1:z (z = 2, 1, 0.5) is shown in Figure 11. It is visible that the swelling ratio depends strongly on the ratio of added base to the amine groups in the pre-polymer. The high swelling ratios of gels produced with 1 eq and 0.5 eq of TEA indicates a very loose structure with a low crosslinking density. This is also in accordance with 13 C NMR measurements. It was found that for G2:1:0.5 40.2 % of the carbonate groups remain unreacted (Table 4).

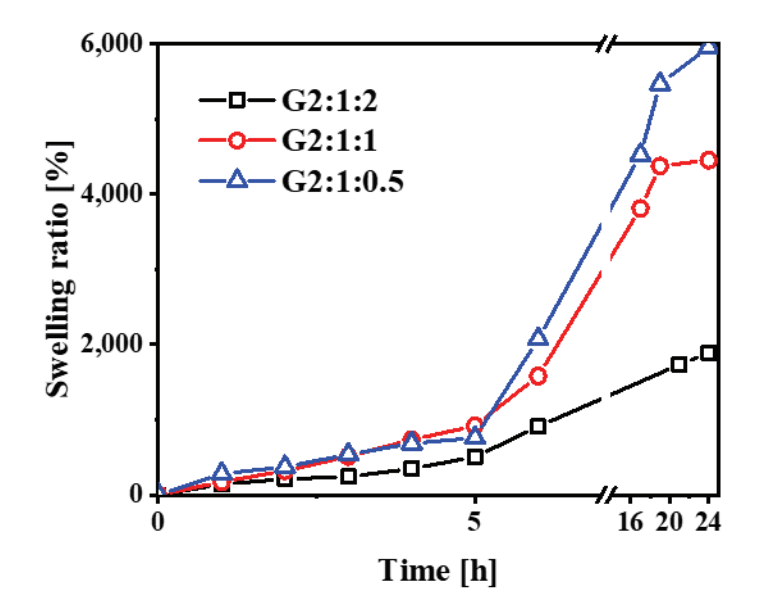


Figure 3.11. Swelling ratio in dependence on the amount of TEA added for G2:1:2, G2:1:1, and G2:1:0.5.

3.4 Rheological Behavior

In this section the structure property relationship with respect to the rheological properties is investigated. In general, the viscoelastic behavior of gels can be described in terms of rheology with the storage modulus G' representing the elastic response and the loss modulus G" representing the viscous response. The ratio between G" and G' is defined as the dissipation factor $\tan \delta$. If $\tan \delta$ is lower than one, the G' exceeds the G", so the elastic response is dominating, whereas in case of a $\tan \delta$ above one the gel is more liquid-like. To determine G', the force was measured at a constant strain of 1 % and a constant frequency of 1 Hz. Since the gelation with copolymer 1 containing the highest amine density is very fast and copolymer 3 gave only a loosely crosslinked structure, copolymer 2 was used for this investigation. The effect of the carbonate-to-amine ratio on the rheological properties is studied (G2:y:2).

The evolution of G' and G" in dependence of the time is shown in Figure 3.12a-c. The strong increase of G' in the beginning indicates a fast gelation. On calculation it is evident that $\tan \delta$ drops down to nearly to (G2:1:2) or less than 0.01 (G2:0.5:2, G2:0.25:2) which shows the gel is very elastic.

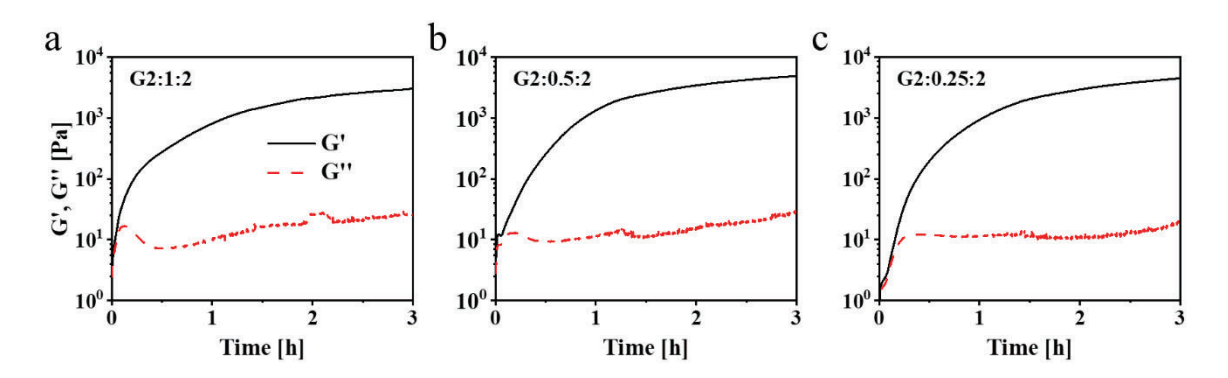


Figure 3.12. G', G", and $\tan \delta$ of a) G2:1:2, b) G2:0.5:2, and G2:0.25:2 in dependence of the time with a frequency of 1 Hz and an oscillation strain of 1 %; d) G' of G2:y:2 after the time sweep; e) G' of 2:y:2 in dependence on the oscillation strain with 1 Hz, and f) G' of G2:1:z after the time sweep.

Figure 3.13a shows the G' for G2:y:2 (y = 1, 0.5, 0.25). It is visible that carbonate-to-amine ratio of 0.5 has the highest modulus. This is an indication that the crosslinking at this ratio is more efficient than for the higher crosslinking density, which is already indicated by 13 C NMR and the swelling experiments. The gels exhibit no frequency dependence in the

measured range between 1 and 100 Hz with a strain of 1 %, which is expectable for chemical gels (Figure 3.13b).

However, the amplitude sweep which determines the deformability of hydrogels does not show a dependence of the crosslinking density on the yield strain (Figure 3.13c). This shows that mechanical properties do not vary significantly between the three sets of hydrogels considered here, since it appears that the apparent crosslinking density is similar for all gels. The apparent crosslinking density is the sum of chemical crosslinks and entanglements (topological crosslinks). Thus, the gels with higher amine to carbonate ratio show predominantly chemical crosslinking while the gels with low ratio are dominated by polymer chain entanglements. Furthermore, it is visible that the linear viscoelastic region (LVE), *i.e.* where the G' is independent on the applied strain, is up to 20 % strain, which confirms that the measurements at 1% strain were performed within the LVE.

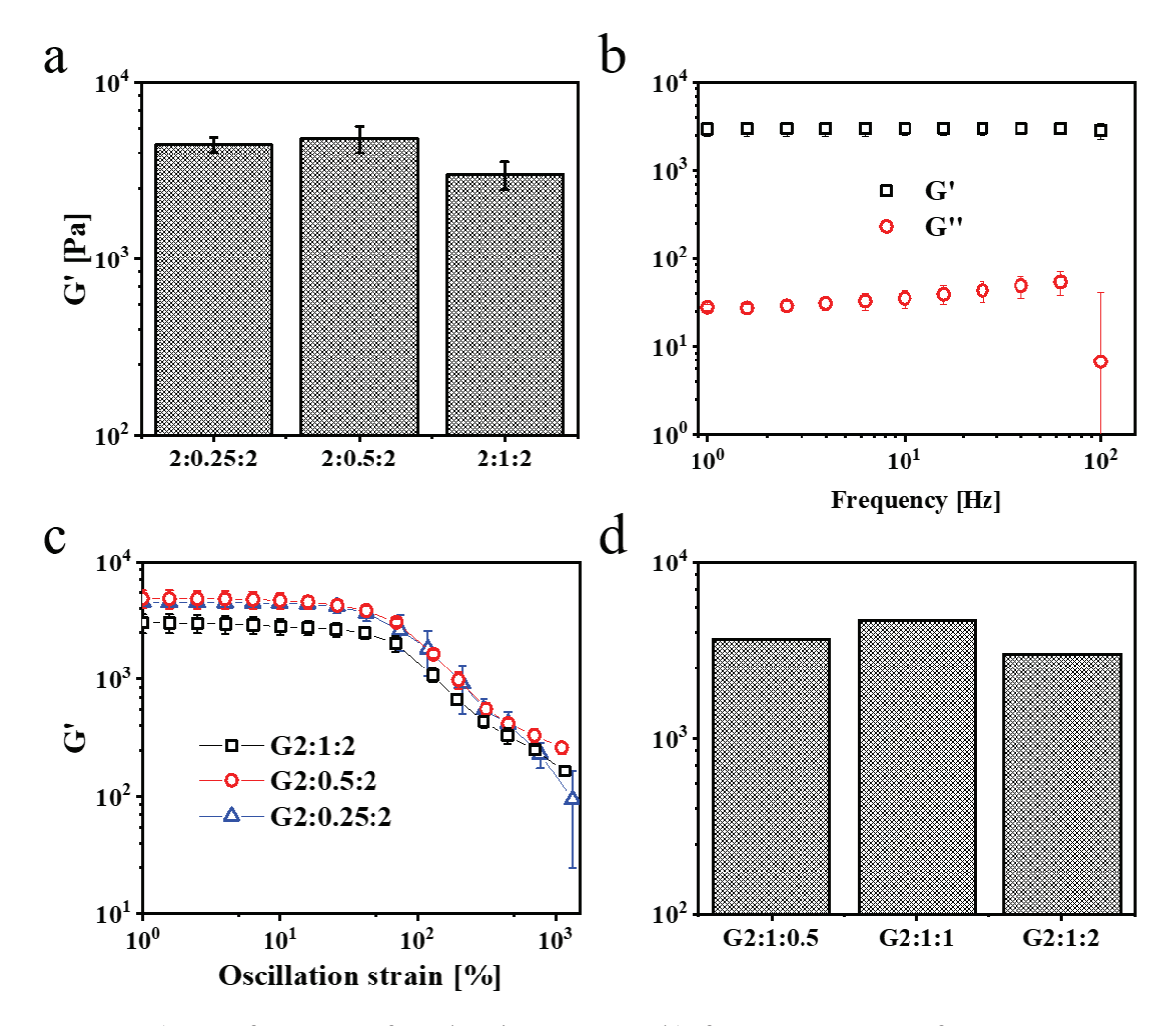


Figure 3.13. a) G' of G2:y:2 after the time sweep; b) frequency sweep for G2:1:2 at 1 % strain, c) G' of 2:y:2 in dependence on the oscillation strain with 1 Hz, and d) G' of G2:1:z after the time sweep.

Figure 3.12f shows G' in dependence on the amine-to-TEA ratio (G2:1:z). It is visible that there is a plateau for G2:1:1, whereas G' is lower for G2:1:0.5 and G2:1:2. It is very likely that this is caused either by incomplete crosslinking (G2:1:0.5), as measured by ¹³C NMR (Table 4) and swelling experiments (Figure 3.11), or by inhomogenities due to the fast gelation (2:1:2) as shown in Figure 3.12a-c and ¹³C NMR (Table 4).

4. Conclusion

In this chapter it was demonstrated by measuring and calculating the copolymerization parameters, that copolymerization of NVF and NVA leads to statistical copolymers. Under certain hydrolysis conditions NVF can be selectively hydrolyzed, while NVA remained intact. Crosslinking P(VAm-co-NVA) with PEG-PC via carbonate-amine coupling in presence of a base leads to hydrogels with superabsorbent properties. The swelling ratio and mechanical properties can be tuned by the ratio of repeat units (ratio of monomer in the initial polymerization), the carbonate-to-amine ratio, and the triethylamine-to-amine ratio. A swelling ratio up to 97000 % was achieved, which is higher than the ones of established superabsorbent hydrogels based on AA/AM. The gel has limited mechanical properties. This is because of single networks formed by chemical crosslinks; however, this can be overcome by exploiting the unreacted free amine groups the gel offers for physically crosslinking or by introduction of an interpenetrating second network.

5. References

- 1 Chen, Q. & Zhu, L. PVA/PVAm Hydrogel Membranes for Removal of Metal Ions from Aqueous Solution. *Appl. Mech. Mater.* **130-134**, 1507-1510, doi:10.4028/www.scientific.net/AMM.130-134.1507 (2011).
- Wang, S. W., Min; Chen, Fushan. Synthesis of poly(vinylamine-co-(sodium acrylate)) and its application as a paper strength additive. *Bioresources* **10**, 750-759 (2015).
- Ma, W., Zhang, S., Tang, B. & Yang, J. Pretreatment of cotton with poly(vinylamine chloride) for salt-free dyeing with reactive dyes. *Color. Technol.* **121**, 193-197 (2005).
- 4 Kou, H. & Liu, Y. Polyamine-polyacrylate dispersant. United States patent (2013).
- Badesso, R. J., Nordquist, A. F., Pinschmidt, R. K. & Sagl, D. J. in *Hydrophilic Polymers* Ch. 25, 489-504 (American Chemical Society, 1996).
- Nakabayashi, K. & Mori, H. Recent Progress in Controlled Radical Polymerization of *N*-Vinyl Monomers. *Eur. Polym. J.* **49**, 2808-2838, doi:10.1016/j.eurpolymj.2013.07.006 (2013).

- Yamamoto, K., Serizawa, T., Muraoka, Y. & Akashi, M. Synthesis and Functionalities of Poly(*N*-Vinylalkylamide). XII. Synthesis and Thermosensitive Property of Poly(vinylamine) Copolymer Prepared from Poly(*N*-vinylformamide-*co-N*-vinylisobutyramide). *J. Polym. Sci. A* **38**, 3674-3681 (2000).
- 8 Gu, L., Zhu, S., Hrymak, A. N. & Pelton, R. H. Kinetics and modeling of free radical polymerization of N-vinylformamide. *Polymer* **42**, 3077-3086 (2001).
- Zataray, J. *et al.* Characterization of poly(N-vinyl formamide) by size exclusion chromatography-multiangle light scattering and asymmetric-flow field-flow fractionation-multiangle light scattering. *J. Appl. Polym. Sci.*, 42434-42434, doi:10.1002/app.42434

10.1002/APP.42434 (2015).

- Ajiro, H., Takemoto, Y., Asoh, T.-A. & Akashi, M. Novel polyion complex with interpenetrating polymer network of poly(acrylic acid) and partially protected poly(vinylamine) using N-vinylacetamide and N-vinylformamide. *Polymer* **50**, 3503-3507, doi:10.1016/j.polymer.2009.06.016 (2009).
- Gu, L., Zhu, S. & Hrymak, A. N. Acidic and Basic Hydrolysis of Poly(*N*-vinylformamide). *J. Appl. Polym. Sci.* **86**, 3412-3419, doi:10.1002/app.11364 (2002).
- 12 Elias, H.-G. *Makromoleküle*. (Hüthig & Wepf Verlag, 1990).
- Kazuya, Y. *et al.* Synthesis and functionalities of poly(N-vinylalkylamide). XIV. Polyvinylamine produced by hydrolysis of poly(N-vinylformamide) and its functionalization. *J. Appl. Polym. Sci.* **89**, 1277-1283, doi:doi:10.1002/app.12230 (2003).
- 14 Pinschmidt, R. K. *et al.* N-Vinylformamide Building Block for Novel Polymer Structures. *J. Macromol. Sci. A* **34**, 1885-1905, doi:10.1080/10601329708010315 (1997).
- 15 Badesso, R. J., Pinschmidt, R. K. & Sagl, D. J. *Proc. Am. Chem. Soc. Div. Polym. Mat. Sci. Eng.* **69**, 251-252 (1993).
- Pelton, R. Polyvinylamine: A Tool for Engineering Interfaces. *Langmuir* **30**, 15373-15382, doi:10.1021/la5017214 (2014).
- 17 Kobayashi, S., Suh, K.-D., Shirokura, Y. & Fujioka, T. Viscosity behavior of poly(vinylamine) and swelling-contraction phenomen of its gel. *Polym. J.* **21**, 971-976 (1989).
- Han, J. H., Koo, B. M., Kim, J. W. & Suh, K. D. A Facile Approach to Synthesize Uniform Hydrogel Shells with Controllable Loading and Releasing Properties. *Chem. Commun.*, 984-986, doi:10.1039/b715557c (2008).
- Zohuriaan-Mehr, M. J. & Kabiri, K. Superabsorbent Polymer Materials: A Review. *Iran Polym. J.* **17**, 451-477 (2008).
- Zhong, M. *et al.* Dually cross-linked single network poly(acrylic acid) hydrogels with superior mechanical properties and water absorbency. *Soft Matter* **12**, 5420-5428, doi:10.1039/c6sm00242k (2016).
- Zhang, Y., Liu, Y., Liu, J., Guo, P. & Heng, L. Super water absorbency OMMT/PAA hydrogel materials with excellent mechanical properties. *RSC Advances* **7**, 14504-14510, doi:10.1039/c7ra00372b (2017).
- Dehbari, N., Tavakoli, J., Singh Khatrao, S. & Tang, Y. In situ polymerized hyperbranched polymer reinforced poly(acrylic acid) hydrogels. *Mater. Chem. Front.* 1, 1995-2004, doi:10.1039/c7qm00028f (2017).
- Huang, Y. *et al.* Preparation and swelling properties of graphene oxide/poly(acrylic acid-co-acrylamide) super-absorbent hydrogel nanocomposites. *Colloid Surfaces A* **401**, 97-106, doi:10.1016/j.colsurfa.2012.03.031 (2012).

- He, Y., Goel, V., Keul, H. & Möller, M. Synthesis, Characterization, and Selectivity of Bifunctional Couplers. *Macromol. Chem. Phys.* **211**, 2366-2381, doi:10.1002/macp.201000340 (2010).
- Mendoza-Payan, J. G., Flores-Gallardo, S. & Marquez-Lucero, A. Preparation and electrical characterization of poly(vinyl amine) hydrogels, crosslinked with Cu(II) ions, and evaluation of their potentiality as water sensor material. *J. Appl. Polym. Sci.* **115**, 790-801, doi:10.1002/app.31097 (2010).
- Pittelkow, M., Lewinsky, R. & Christensen, J. B. Selective Synthesis of Carbamate Protected Polyamines Using Alkyl Phenyl Carbonates. *Synthesis* **15**, 2195-2202 (2002).
- Mukherji, D., Marques, C. M. & Kremer, K. Polymer Collapse in Miscible Good Solvents is a Generic Phenomenon Driven by Preferential Adsorption. *Nat. Commun.* **5**, 4882-4887, doi:10.1038/ncomms5882 (2014).

Chapter 4.

Physical gels of P(VAm-co-VAA) by thermal curing

This chapter is reproduced from RSC Adv., 2020, 10, 21933, which is under a Creative Commons Attribution-NonCommercial 3.0 Unported Licence.

All experiments and data analysis were done by T.F.

1. Introduction

Physically crosslinked hydrogels have unique self-healing properties and present therefore a powerful material class with a wide range of applications. The variety of non-covalent bonds including ionic interactions, hydrogen bonding, 2,3 π - π -stacking, host-guest interaction, and the hydrophobic effect provides an ideal platform for the fabrication of physical gels with tailored strength and properties. Due to the associative and transient nature, they have inherently unique features. The properties are properties and present therefore a powerful material class with a wide range of applications. The variety of non-covalent bonds including ionic interactions, hydrogen bonding, and are recovered to the properties are recovered to the properties and present the properties are recovered to the associative and transient nature, they have inherently unique features.

The variety and versatility of the interactions are also reflected by the variety of manufacturing methods.^{9,10} Gelation induced by mixing two components in a good solvent is in this context a simple and straightforward pathway. In this case, the attraction of the first component to the second component must be higher than the solvent. Among the different physical interactions, hydrogen bonding is one of the best investigated.^{2,3,11}-¹³ In this context poly(vinylamine) (PVAm), a waterborne polymer is an attractive candidate for formation of physical gels as it can facilitate hydrogen bonding with its high density of primary amines. 14,15 Few papers published in the last decade focused on the use of PVAm for chemically crosslinked microgels, ¹⁶⁻¹⁹ or hydrogel capsules. ²⁰ While very few literatures report on the fabrication of a physical gel based on PVAm, this is only by exploiting its cationic behavior, for example with carboxymethyl cellulose or copper.^{21,22} (see also Chapter 2). Alternative to ionic interaction for the formation of physical gel, PVAm can be easily formulated exploiting hydrogen bonding interaction. Since PVAm can, if protonated, act as a hydrogen donor, addition of a second component acting as hydrogen acceptor will facilitate gel formation. Organic carbonates have shown to be strong hydrogen bond acceptors.²³ To the best of our knowledge, there are no physical gels reported using organic carbonate compounds.

However, physical gels including those which are formed by hydrogen bonds can be kinetically trapped in a meta-stable state during gelation. Thermal curing, which is composed of a heating and a cooling step, can drive towards the thermodynamical equilibrium state. In principle on heating hydrogen bonds are disrupted at high temperature, while on cooling the bonds will be reformed due to their transient nature without affecting the mechanical properties. Nevertheless, the effect of thermal equilibration is not well investigated. Recently, Fuentes-Caparrós et al. investigated the effect of thermal curing on low molecular weight gelator peptide gels. They found out, that their gels are kinetically trapped and that thermal curing can change the

microstructure of the gels leading to significantly different properties compared to the as-prepared gels.²⁴

Taking this into account, in this chapter the formation of physically crosslinked hydrogels using PVAm and phenylcarbonate-telechelic-poly(ethylene glycol) (PEG-PC) is reported and the effect of thermal curing on the mechanical properties of the gel is shown. Proton NMR, rheology, and UV-Vis spectroscopy was used to analyze the predominant physical interaction responsible for the formation of the gel. ^{25,26} The critical gelation concentration for the formation of the gel was determined by measuring the storage modulus G' and the loss modulus G" in dependence on the time, with different wt% of p(VAm-co-VAA). The frequency response of G' and G" of the physical gel was measured by small-amplitude oscillation shear (SAOS) experiments to investigate, whether the bonds have a transient physical or permanent chemical nature. To show the effect of thermal curing on the change in the mechanical properties of the gels, the gels were subjected to repeated heating-cooling cycles. The versatility of the system also comes from the fact that these hydrogels could be further chemically crosslinked via carbamate linkages by the reaction of phenylcarbonate and primary amine in the presence of a base.²⁷

2. Materials and Methods

2.1 Materials

N-Vinylformamide (NVF), phenylchloroformat (PCF), and poly(ethylene glycol) (PEG) (Mn = 400 Da) were purchased from Sigma Aldrich. N-Vinylacetamide (NVA) was purchased from ABCR. 2, 2'-Azobis[2-(2-imidazolin-2-yl)propane] dihydrochloride was from TCI. Methanol (MeOH) and triethylamine (TEA) were purchased from Sigma Aldrich. Deuterated methanol and water were purchased from Deutero. All chemicals were used as received without any purification.

2.2 Methods

Nuclear magnetic resonance (NMR)

Proton NMR spectra were recorded on a Bruker Avance III-400 (Bruker Corporation, Billerica, MA, USA). Deuterated methanol (CD₃OD) and deuterium oxide (D₂O) were used as solvents. The residual solvent signal of methanol or deuterium oxide was used as the internal standard unless otherwise noted.

Size Exclusion Chromatography (SEC)

Molecular weights (M_{n,SEC} and M_{w,SEC}) and molecular weight distributions (PDI = Mw·Mn⁻¹) were determined by SEC. SEC analyses were carried out using water (HiPerSolv CHROMANORM® HPLC grade, VWR) as the eluent containing 10 % acetonitrile, 0.1 mol·L⁻¹ sodium chloride, 0.1 wt% triflouroacetic acid and 0.01 wt% sodium azide The machine was equipped with an HPLC pump (1200, Agilent), a refractive index detector (RI) (1200, Agilent), and an UV-detector (VWD, 1200, Agilent). The samples contained 0.5 μL·mL⁻¹ ethylene glycol (99.5 %, Fluka analytical) as internal standard. One pre-column (8·50 mm) and three Novema Max gel columns (8·300 mm, Polymer Standards Service) were applied at a flow rate of 1.0 mL·min⁻¹ at 25 °C. The diameter of the gel particles measured 5 μm, the nominal pore widths were 30, 100, and 1000 Å. Calibration was performed using narrowly distributed PEG standards (Polymer Standards Service). Results were evaluated using the PSS WinGPC UniChrom software (Version 8.3.2).

Rheology

Rheological measurements were conducted with a Discovery Hybrid Rheometer HR 3 (TA Instruments, USA) and a 40 mm parallel plate with a solvent trap. Unless otherwise stated time-dependent measurements were conducted at a frequency of 1 Hz and an amplitude of 1 % strain. Frequency sweeps were performed either at an amplitude of 0.1 % for small amplitude oscillation shear SAOS experiments (0.01 – 100 Hz) or at an amplitude of 1 % (1-100 Hz). Temperature dependent rheological measurements were performed between 20 °C-55 °C, with a heating rate of 5 °C·min⁻¹ at a frequency of 1 Hz and an amplitude of 1 %. Amplitude sweeps were performed with a frequency of 1 Hz (1-1000 %).

A typical set of breakage-thermal curing cycles consists of 5 heating cooling cycles, a frequency sweep, and a subsequent amplitude sweep as shown in Figure 4.1.

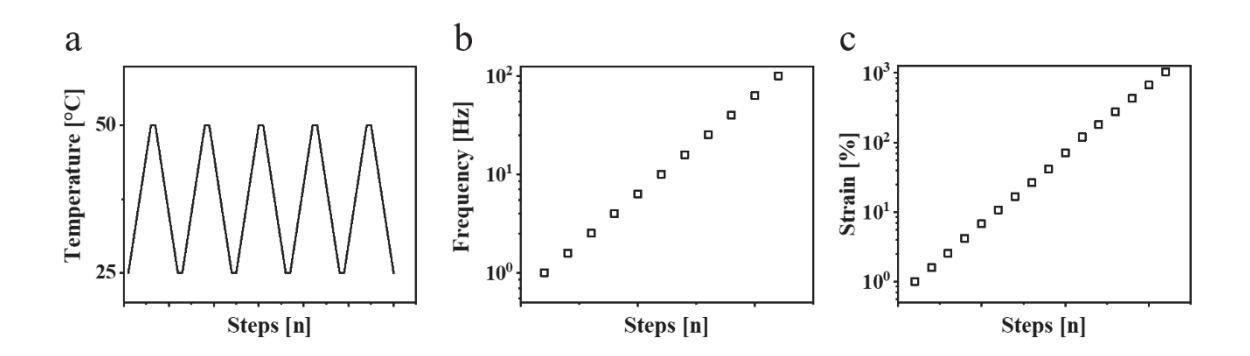


Figure 4.1. a) Temperature progression during the heating-cooling cycles, b) frequency sweep, and c) oscillation sweep.

UV-Vis spectroscopy

UV-Vis spectroscopy was performed with a Jasco V780 spectrophotometer (Jasco, Tokio, Japan) from 200 to 600 nm at 10 to 50 °C with a decrement of 5 °C. The respective concentrations for the measurements are mentioned in Table 1.

Dynamic light scattering (DLS)

DLS measurements were performed using an ALV/CGS-3 Compact Goniometer System with an ALV/LSE 5004 Tau Digital Correlator and a JDS Uniphase laser operating at 632.8 nm. The experiments were carried out at a fixed scattering angle θ = 90 °. All samples were filtered through a 0.45 µm PET-filter before the measurements. The temperature was set either to 20 °C or to 50 °C.

Differential scanning calorimetry (DSC)

Thermal analysis was performed with a DSC-7 from Perkin Elmer (Waltham, USA) in sealed stainless steel crucibles to prevent any solvent evaporation. 10 heating cooling cycles were performed between 25 °C and 60 °C with a heating rate of 5 °C·min⁻¹.

Table 1. Concentrations and combinations used for temperature dependent UV-Vis spectroscopy. The molar ratio of amine to carbonate are kept constant to 1:1.

С	ompound 1	wt%	Compound 2	wt%	Formation of
					physical gel
a	PEG-PC	34	-	-	-
b	p(VAm-co-	10	-	-	-
	VAA)				
c	p(VAm-co-	5	PEG-PC	20	-
	VAA)				
d	p(VAm-co-	10	PEG-PC	34	+
	VAA)				

2.3 Synthesis

p(NVF-co-VAA)

NVF (3.64 g, 51.2 mmol), NVA (6.36 g, 51.2 mmol) and VA044 (331 mg, 1.02 mmol) were dissolved in water (90 mL). The on mixture was degased by three freeze-thaw cycles. After degasing the reaction mixture was heated up to 60 °C for 20 h under nitrogen. The resulting copolymer was precipitated in an excess of acetone, redissolved in water, and lyophilized obtaining a white solid (9.82 g, 98.2 wt%).

Proton NMR (400 MHz in D₂O, δ in ppm): 1.35-1.75 (-CH₂ backbone), 1.75-1.95 (-CH₃), 3.0-4.0 (-CH backbone), 7.5-8 (-CHO)

SEC: $M_n = 5.6 \cdot 10^4 \text{ g} \cdot \text{mol}^{-1}, M_w = 1.2 \cdot 10^5 \text{ g} \cdot \text{mol}^{-1}, PDI = 2.2$

Hydrolysis of p(NVF-co-NVA)

p(NVF-co-NVA) (10 g) was dissolved in sodium hydroxide solution (2 mol·L⁻¹, 490 mL). The reaction mixture was heated up to 80 °C for 4 h. The mixture was neutralized with hydrochloric acid to pH = 7 and subsequently dialyzed (regenerated cellulose, SpectraPor®, molecular weight cut-off: 3.5 kDa) for 7 days. The water was removed by lyophilization obtaining a white solid (yield: 6.52 g, 65 wt%).

Proton NMR (400 MHz in D₂O, δ in ppm): 1.2-2.1 (-CH₂ backbone, -CH₃), 2.8-4.1 (-CH backbone)

SEC:
$$M_n = 5.1 \cdot 10^4 \text{ g} \cdot \text{mol}^{-1}$$
, $M_w = 1.1 \cdot 10^5 \text{ g} \cdot \text{mol}^{-1}$, $PDI = 2.1$, $DP = 700$

Phenylcarbonate telechelic poly(ethyleneglycol (PEG-PC)

To a solution of PEG (10 g, 25 mmol) in THF (100 mL) was added pyridine (2 eq, 3.96 g, 50 mmol). The reaction mixture was cooled with an ice bath. PCF (2 eq, 7.83 g, 50 mmol) was added dropwise without exceeding 5 °C in the reaction mixture. Afterwards the reaction was allowed to stir for further 16 h at room temperature. Pyridine hydrochloride was removed by filtration, the solution washed three times with water and the solvent was removed by rotary evaporation. The product was obtained as colorless liquid (yield not determined).

¹H NMR (400 MHz in MeOD, δ in ppm): 3.3-3.5 (-CH2, backbone), 3.55-3.65 (-CH2), 4.2-4.3 (-CH2), 6.65-6.75 (unknown side product), 7.0-7.1 (-CH, aryl, para), 7.1-7.2 (-CH, aryl, para), 7.2-7.35 (-CH, aryl, meta), DP = 9

Physical gelation of p(VAm-co-VAA) with an amine-to-carbonate ratio of 1:1 p(VAm-co-VAA) (50 mg, 394 μmol amine groups) was dissolved in methanol (450 mg, 570 μL) and PEG-PC (252 mg, 394 μmol phenylcarbonate groups) was added.

3. Results and Discussion

The physical gels were obtained by dissolving 10 wt% of p(VAm-co-VAA) in methanol (with subsequent addition of PEG-PC (Table 1). This leads to a phase separation with precipitation of a colourless to yellowish gel (Figure 4.2). The methanol content of the physical gel was determined by removing the supernatant and subsequent drying of the gel fraction and found to be $45.5\% \pm 1.5\%$. Attempts to swell the gel, either in methanol or in water, failed as the gel dissolves in an excess of solvent suggesting physical crosslinks.

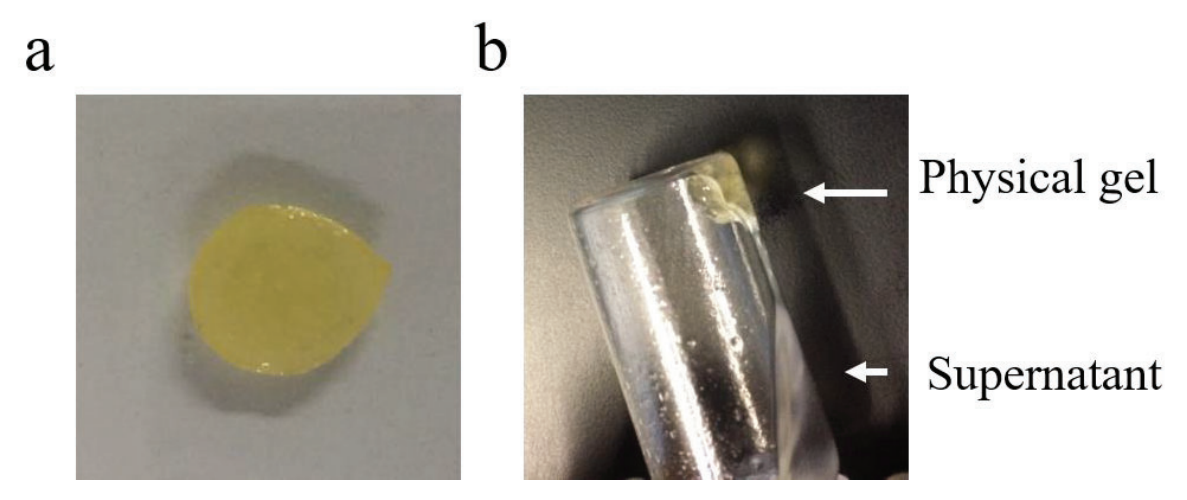


Figure 4.2. a) A piece of the physical gel, b) just prepared physical gel with supernatant.

In order to estimate the critical concentration at which gelation occurs, rheological measurements were performed. Three samples of p(VAm-co-VAA) (5 wt%, 7 wt%, and 10 wt%) in methanol were mixed with PEG-PC (amine-to-carbonate molar ratio 1:1). G' and G" were monitored (1 Hz, 1 %) in dependence on the time. From these values the dissipation factor $\tan \delta$ was calculated (G"·G'-1) and plotted against the time (Figure 4.3a).

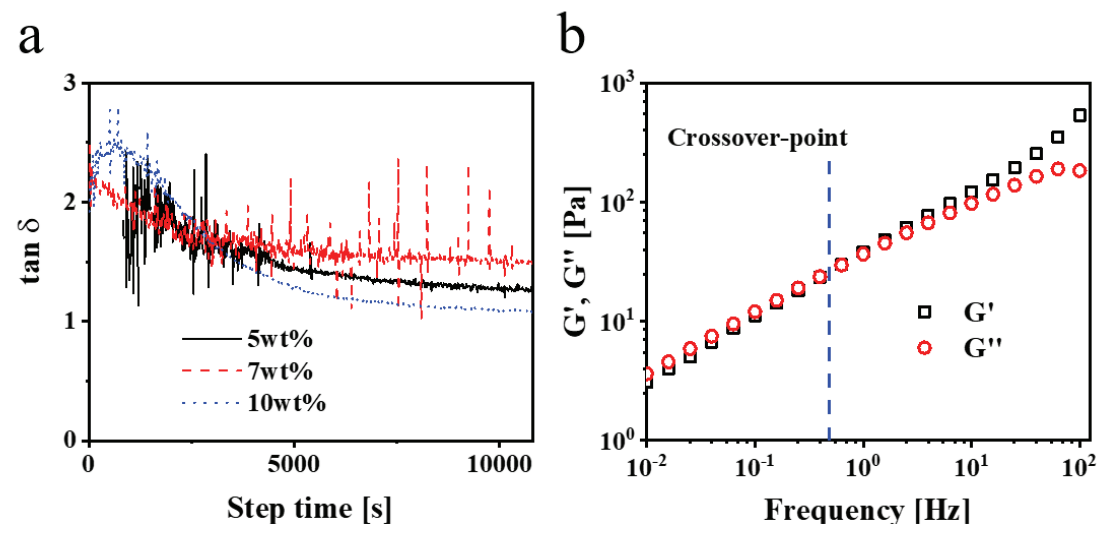


Figure 4.3. a) Dissipation factor tan δ for 5, 7, and 10 wt% of p(VAm-coVAA) and b) SAOS for 10 wt% p(VAm-co-VAA) revealing a crossover-point.

The lower the tan δ value the more elastic is the response, *i.e.*, at a tan δ of 1 and/or lower, the elastic response is dominating. At 10 wt%, the tan δ approximates 1 (Figure 4.3a); this corresponds to the critical gel concentration. To validate the transient nature of the bonds the gels were measured with a SAOS experiment measuring G' and G'' (pre-

conditioning time: 3 h, amplitude: 0.1 %). As can be seen in Figure 4.3b G' and G" increases linearly with the frequency, which is common for physical gels.²⁸ Furthermore, there is a crossover point, where G' exceeds G", at around 0.5 Hz, which is related to the average lifetime of the bond.²⁹ From these observations, it can be concluded that the gel is physically crosslinked. This hypothesis is supported by concentration dependent ¹H NMR. It is visible that with increasing concentration the overall proton signals are broadened, the relative intensity of the signals of p(VAm-co-VAA) decreases (peak 1-3), and the water signal around 4.7 ppm shifts and sharpens. Furthermore, there is a gradual downfield shift of the aromatic protons (peak a) and an upfield shift of peak 5 (inlet Figure 4.4a). The overall peak broadening and the decrease of the intensity of peak 1-3 are caused by a restricted mobility. Polymeric signals in general are broadened because their chains are less mobile than small molecules.³⁰ This shows, that there is a strong interaction between p(VAm-co-VAA) and PEG-PC, which become more prominent with increasing concentration. The mobility is further restricted, and the signal becomes even less visible, which affects not only the backbone signals (peak 1-2) but also the methyl-group of the acetamide (peak 3). The presence of H₂O as an impurity in MeOD can be seen by the broadening of the water signal, which is caused by an intermolecular exchange of deuterium with the deuterated methanol. So, there is a co-existence of H₂O and HDO, which leads to a broad signal. However, the sharpening of this peak with increasing concentration suggests that this exchange is to some extent inhibited by the gel structure. The slight downfield shift of signal 'a' and upfield shift of signal 5 are caused by intermolecular interaction. In general electron-withdrawing groups affect hydrogen bonding leading to a downfield shift in the spectrum. Furthermore, the absence of phenol in the spectrum rules out any chemical crosslinking (Chapter 3). 27

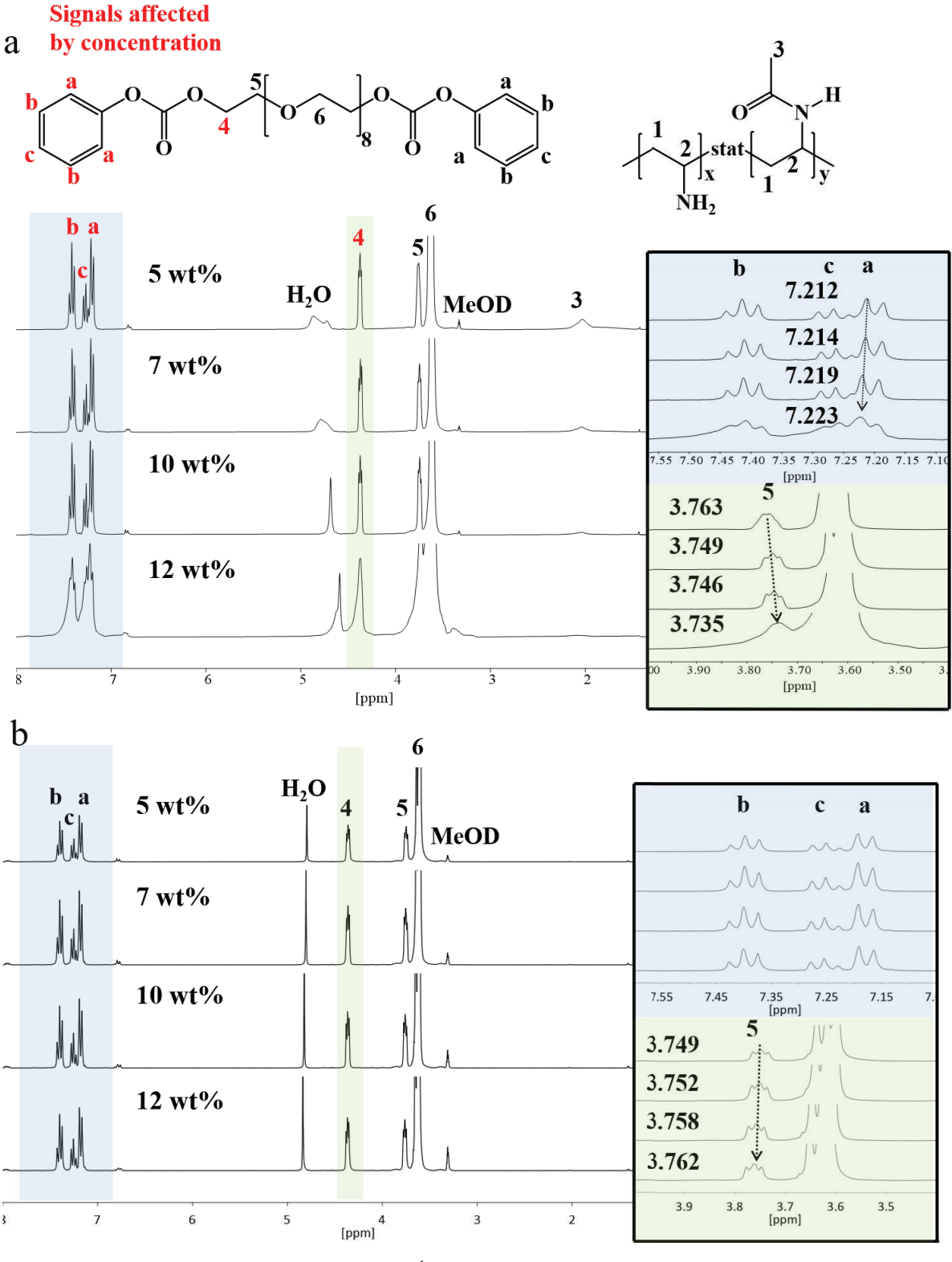


Figure 4.4. a) Concentration dependent ¹H-NMR of the physical gels with different wt% in MeOD. Peak 1 and 2 are not visible due to their short relaxation time. b) concentration dependent ¹H-NMR of pure PEG-PC without p(VAm-co-VAA) with the respective wt%.

The ¹H NMR spectrum of the supernatant reveals, that it consists mainly of PEG-PC, although the presence of p(VAm-co-VAA) cannot be ruled out because of its weak signals (Figure 4.5).

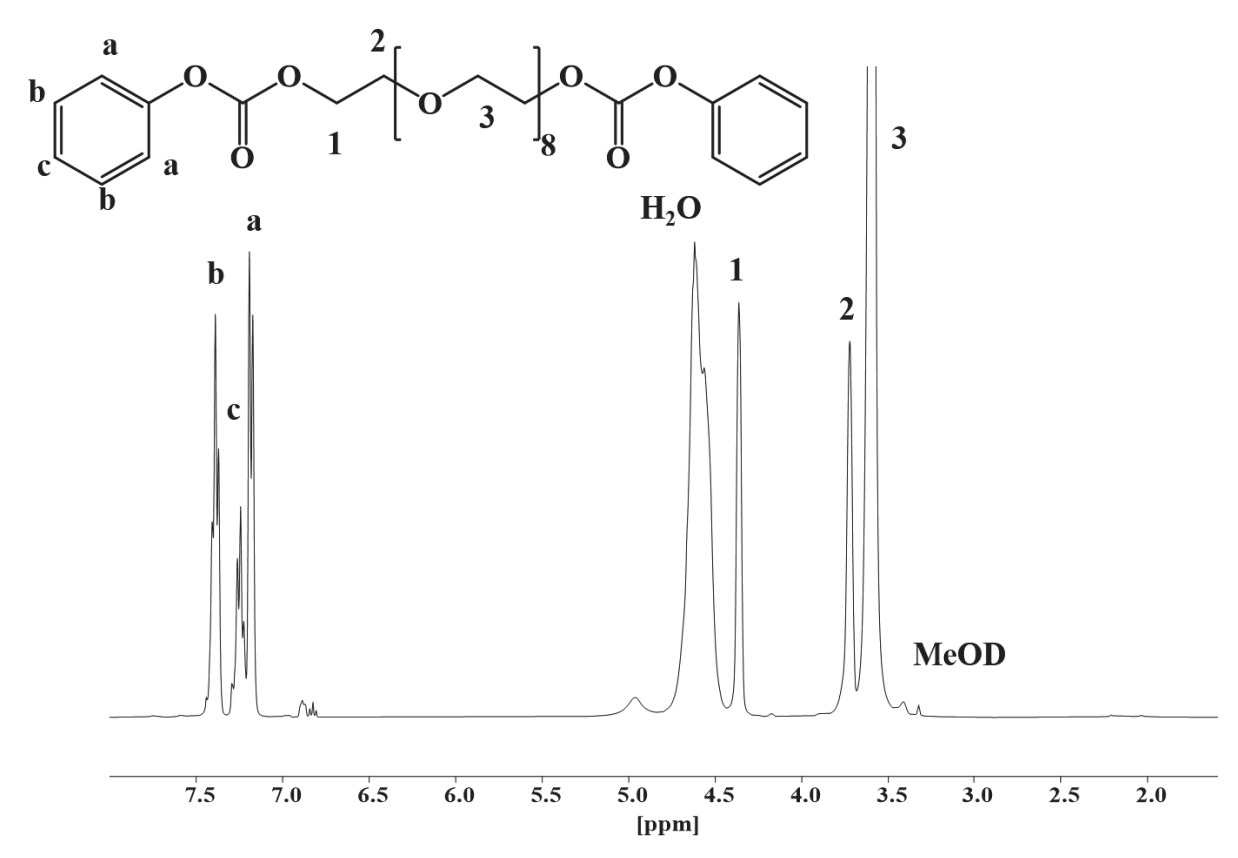


Figure 4.5. ¹H-NMR of the supernatant in MeOD.

To further investigate the nature of the physical crosslinks like hydrogen bonding and π - π -stacking, which can be affected by the change in temperature, temperature dependent UV-Vis spectroscopy was performed. The UV-vis spectra were recorded from 250 nm to 450 nm. The temperature range was kept between 50 °C to 10 °C with a step of 5 °C, keeping the temperature constant during each measurement (Figure 4.6). Four sets of measurements were done using (a) only PEG-PC and (b) only p(VAm-co-VAA) in the concentrations which resulted into the formation of physical gels and a combination of PEG-PC and (p(VAm-co-VAA) which did not (c) and did (d) resulted into the corresponding physical gel. The respective wt% is mentioned in Table 1. On decreasing the temperature, UV spectrum of PEG-PC (Figure 4.6a) reveals two effects. The main maximum at 290 nm, which is due to the $\pi \rightarrow \pi^*$ transition of the carbonyl-group³¹, experiences a hypochromic shift and a shoulder appears at ~ 310 nm, which is due to the $\pi \rightarrow \pi^*$ transition of the phenyl-group.

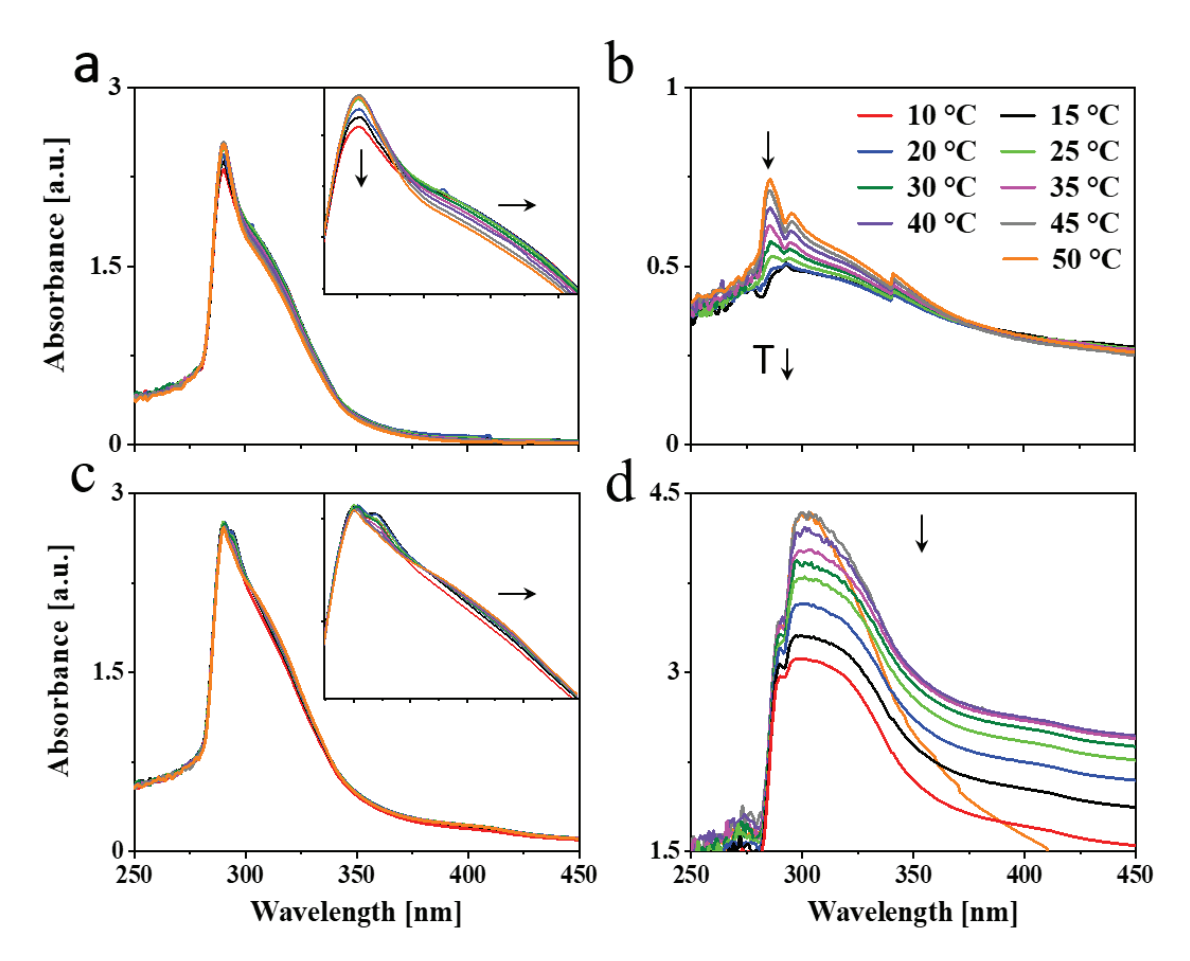


Figure 4.6. UV-vis spectrum of (a) PEG-PC in methanol, (b) p(VAm-co-VAA) in methanol, (c) PEG-PC + 5 wt% p(VAm-co-VAA) in methanol, and (d) PEG-PC + 10 wt% p(VAm-co-VAA) in methanol in dependence on the temperature. The arrows indicate the shift of the absorbance with decreasing temperature. PEG-PC exhibits due to π - π stacking a bathochromic shift upon decreasing temperature, which is also visible in a combination with 5 wt% of p(VAm-co-VAA). The hypochromic shifts in (a, b, and d) are caused by aggregation.

The shoulder at 310 nm indicates π - π -stacking.³² With decreasing temperature, the π - π -stacking is enhanced because the energy gap between the π and the π^* orbital is
decreased. Therefore, less energy is needed for the transition, this results in a
bathochromic towards a longer wavelength. The hypochromic shift of the carbonylgroup, which appears along with the bathochromic shift of the phenyl-group, supports
this hypothesis (Figure 4a). Generally, hypochromic shifts are associated with
conformational changes in proteins and DNA. The unstacking of the bases in case of
DNA at elevated temperature induces a conformational change in the structure, which
in turn increases the number of exposed chromophores and consequently the

absorbance.³³ Taking this into account, the UV-Vis spectrum of PEG-PC suggests the presence of aggregates at room temperature, which is stabilized by π -stacking. The spectrum of p(VAm-co-VAA) (Figure 4.6b) is dominated by a hypochromic shift of the main maximum at 285 nm, which is due to the $n \rightarrow \pi^*$ transition of the acetamide group.³⁴ This shift also indicates the presence of aggregates verified by DLS (Figure 4.7). Aggregation is caused by either hydrogen bonding of the amine and carbonylgroup, or by hydrophobic interaction of the acetamide. Furthermore, the UV-Vis spectrum shows a gradual hypsochromic shift of the maximum. This shift is related to hydrogen bonding either with the solvent or the polymer itself.³³

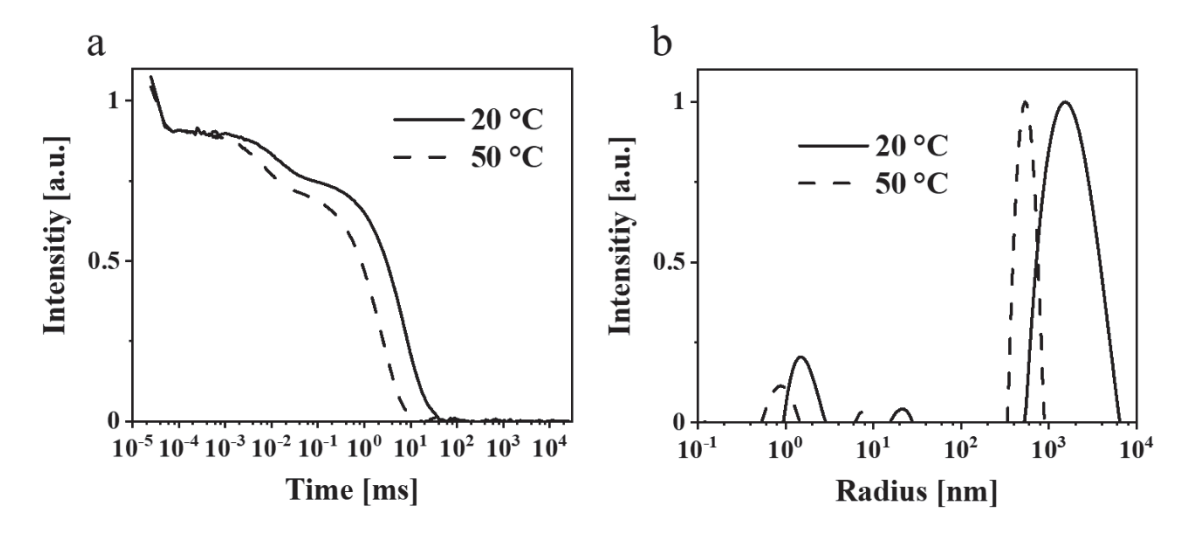


Figure 4.7. Autocorrelation function (a) and the respective calculated hydrodynamic radii (b) obtained by DLS for p(VAm-co-VAA) at 20 and 50 °C.

However, mixing 5 wt.% of p(VAm-co-VAA) with PEG-PC (no gelation), the UV-VIS spectrum is dominated by the absorption of PEG-PC (Figure 4.6c). The bathochromic shift is still visible indicating π - π -stacking. Furthermore, there is a hypsochromic shift of the maximum indicating hydrogen bonding. Since this was not visible without the p(VAm-co-VAA), it is caused by hydrogen bonding between protonated amine groups of p(VAm-co-VAA) and the carbonate groups of the PEG-PC. With increasing the concentration to 10 wt% the spectrum changes dramatically (Figure 4.6d).

The absorption between 280-310 nm decreases showing a predominant hypochromic shift with decreasing temperature, while there is no bathochromic shift visible anymore. This indicates that the hydrogen bonds are dominating the formation of the hydrogel implying that the carbonate groups of the PEG-PC are strongly hydrogen-bonded to the protonated amine groups of p(VAm-co-VAA) restricting the mobility of the

phenylcarbonate groups. Based on these results, we postulate a physical crosslinked structure as shown in Scheme 4.1.

Scheme 4.1. Postulated structure of the physical crosslinked gel. The arrows indicate secondary attractive forces. π - π -stacking is not shown.

The strong intermolecular interaction resulting in the formation of physical gels is likely due to the formation of hydrogen bonds between the carbonate group of PEG-PC as a strong hydrogen acceptor and protonated amines of p(VAm-co-VAA) as hydrogen donor, although the possibility of π - π -stacking between the phenyl-groups of PEG-PC cannot be ruled out. From titration curves of p(VAm-VAA) in water²⁷ and due to the fact that the p(VAm-co-VAA) was neutralized to pH = 7 after hydrolysis it can be estimated that around 50 % of the amine groups were protonated and available for hydrogen bonding (Chapter 3). Due to the transient nature of the hydrogen bonds, the gel should exhibit a temperature sensitive behaviour. As it is well known from literature hydrogen bonds can break with increasing temperature.³⁵ To investigate the temperature responsive behaviour of the gels rheological measurements were conducted with a temperature ramp. The temperature was increased to 50 °C with subsequent cooling to 25 °C (1 Hz, 1 %, 5 °C min⁻¹, Figure 4.8. In total 5 of these heating/cooling cycles were performed subsequently. It can be seen from Figure 4.8, that instead of an expected decrease in G', the values drastically increases from ~50 Pa to ~7 kPa.

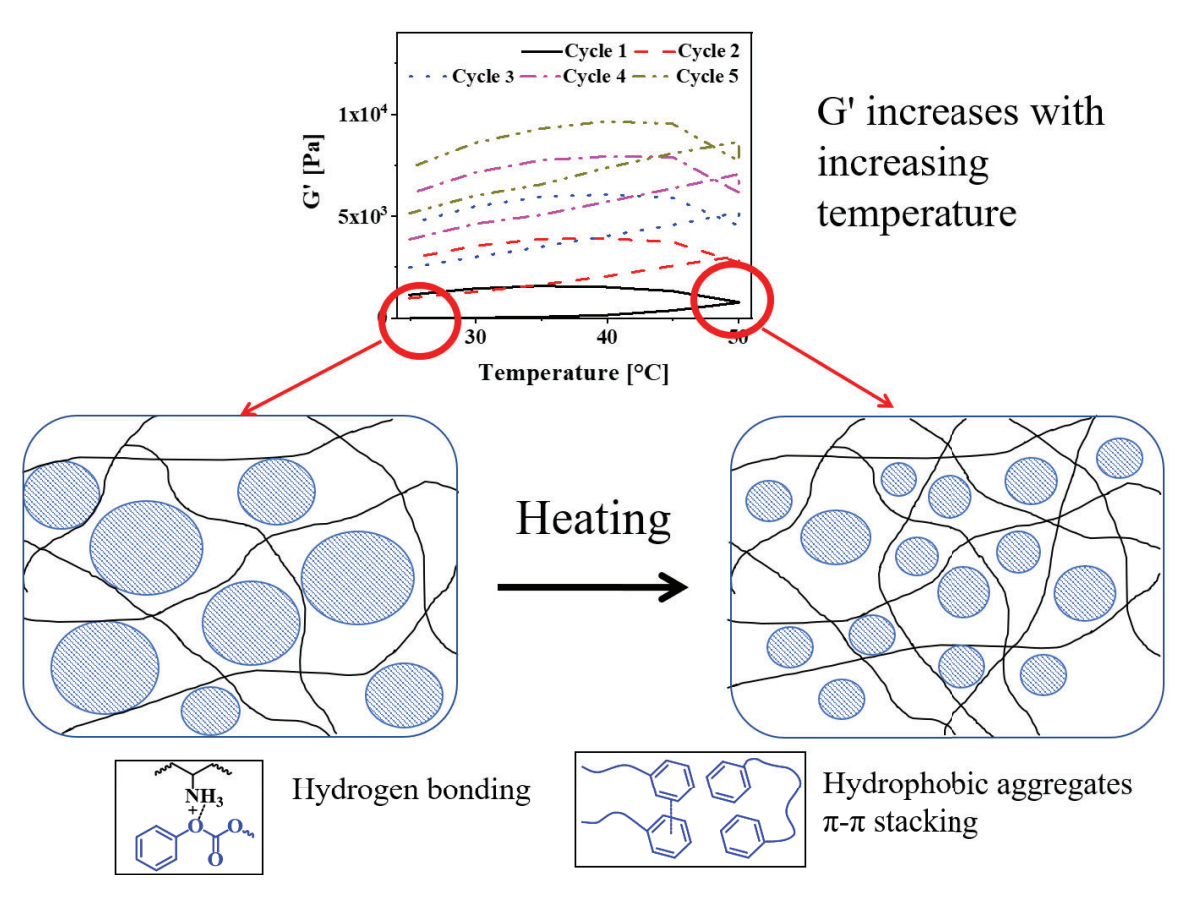


Figure 4.8. Evolution of G' during heating-cooling cycles and the schematical explanation for the increase of G' while heating

We postulate that this increase in modulus is caused by thermal annealing of the gel resulting in a change in gel microstructure. This means that the increase of the temperature reduces the aggregates formed due to fast gelation and leads to better mixing of the gel (schematic illustration Figure 4.8). Polymer mixing is an enthalpic (endothermic) process that can be monitored by differential scanning calorimetry (DSC). DSC was performed in sealed stainless-steel crucibles to ensure that no solvent evaporations happen and for at least 10 heating/cooling cycles with 5 °C·min⁻¹. p(VAm-co-VAA), PEG-PC and the physical gel were measured. In the latter case, the gel and the supernatant were analyzed. For p(VAm-co-VAA) and PEG-PC no signal was observed (Figure 4.9a and b). The supernatant (Figure 4.9c) reveals a prominent endothermic signal at 40 °C, whereas the physical gel (Figure 4.9d) has a weak signal at 55 °C.

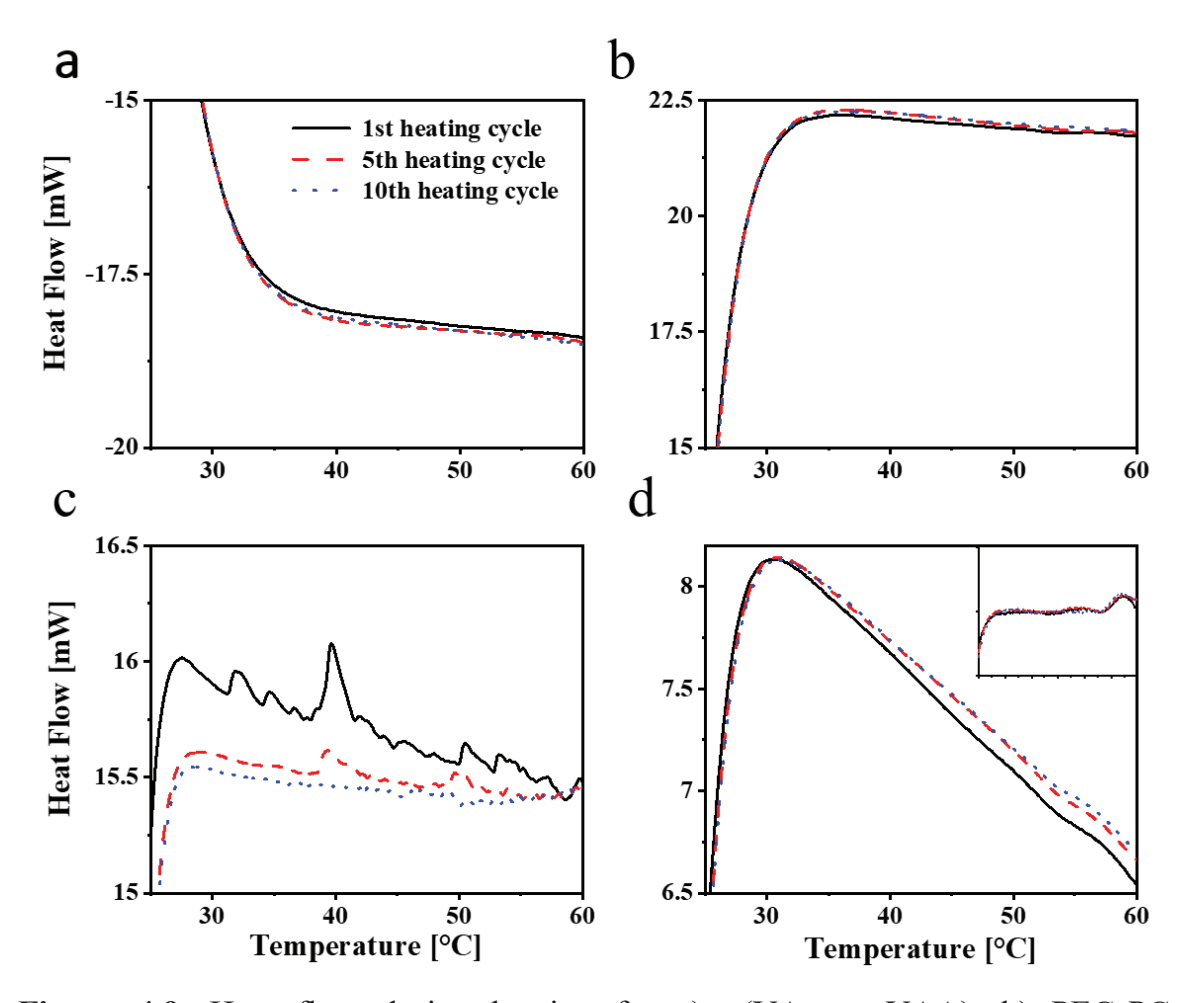


Figure 4.9. Heat flow during heating for a) p(VAm-co-VAA), b) PEG-PC, c) supernatant of the physical gel, and d) the physical gel.

These signals are attributed to mixing, which means the homogenization process mentioned above. This homogenization temperature is decreased for the supernatant. The supernatant is in a liquid state, so it is more mobile and the energy barrier to break the hydrogen bonds is decreased. Furthermore, the signal is more prominent than in the strongly bound physical gel and anneals after the 10 heating/cooling cycles.

To verify that the gel is still only physically bound after temperature treatment, the gelation in the NMR tube was performed. The tubes were heated up to 50 °C and 80 °C respectively for 4 h (Figure 4.10a). Even after the treatment at 80 °C, no phenol formation was observed.²⁷

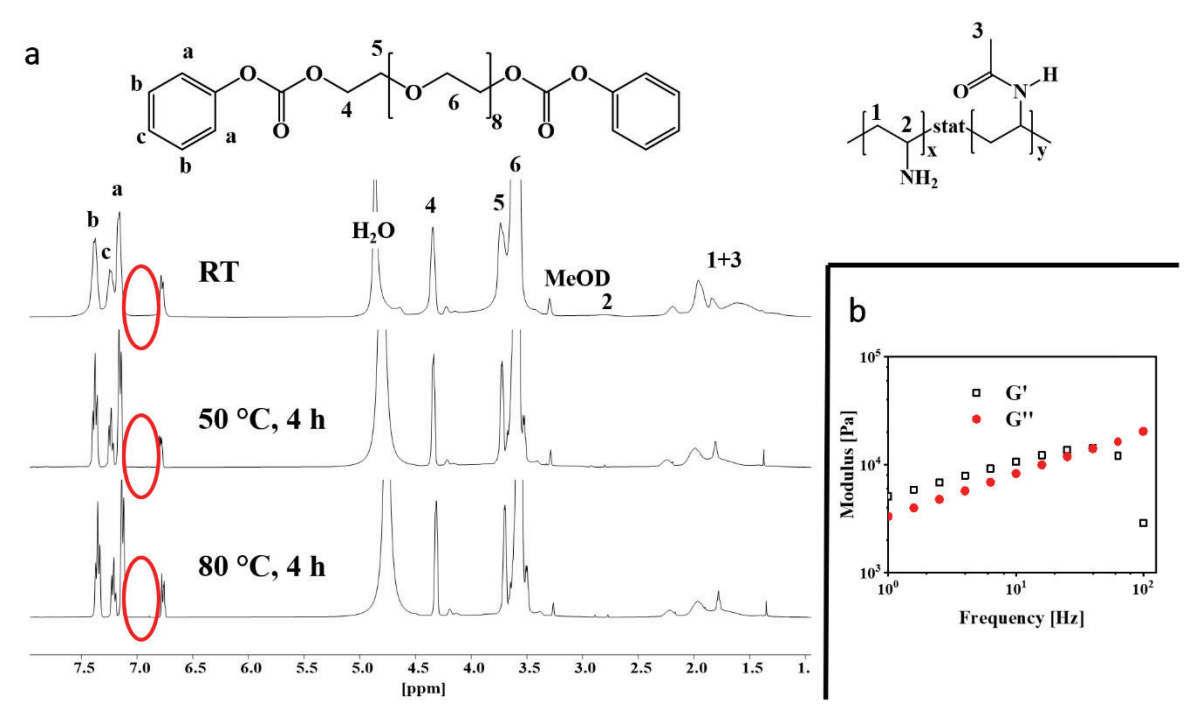


Figure 4.10. a) Proton-NMR of physical gels treated at RT, 50 °C, and 80 °C. The red circle indicates, where phenol signals would appear in MeOD. b) SAOS experiment after heating-cooling cycles.

In accordance with these results, a subsequent SAOS measurement after the heating/cooling cycle exhibited a dependency of G' and G" on the frequency, confirming the physical nature of crosslinks. (Figure 4.10b). Thus, these heating/cooling cycles induce a thermo-curing of the gel with an increase of G' by more than two orders of magnitude. To the best of my knowledge, this behaviour has not been reported so far. In general, physical gels have an inherent self-healing behaviour due to the transient nature of the bonds. To investigate whether the gel shows this kind of behaviour and can return to the enhanced modulus, the gel was broken in an amplitude sweep, *i.e.*, the amplitude was subsequently increased to 1,000 % (1 Hz, Figure 4.11a). Consequently, G' drops down to ~ 200 Pa. Immediately after the amplitude sweep, the gel was subjected to another five heating/cooling cycles. G' recovers after these 5 cycles (G' ~ 7 kPa, not shown). This explains the transient nature of the physical bonds as they are re-formed after breakage.

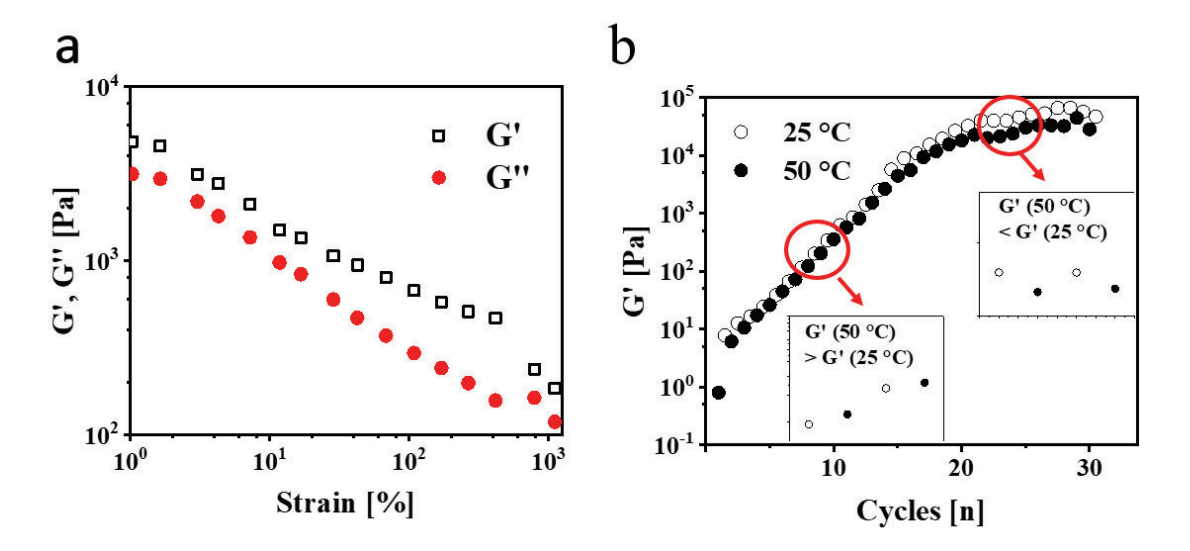


Figure 4.11. a) Oscillations sweep to break the physical gel. b) evolution of G' for a physical gel which was subjected to 30 heating/cooling cycles.

Repeating this breakage and thermal curing sets a further increase of G' was observed, which was recorded up to 20 kPa. We deduce this increase in modulus to further homogenization. In order to decouple the increase of the modulus from the amplitude sweep, another gel sample was subjected to 30 heating/cooling cycles (Figure 4.11b). It is visible that after 20 cycles a plateau is reached with a G' of 50 kPa confirming the previous results. Moreover, it is visible from Figure 11b that after reaching the plateau the G' at 25 °C is always higher than 50 °C.

This shows that higher temperature leads to a breakage of the hydrogen bonds but only after complete homogenization we see the effect. However, in the stage of homogenization (most prominent between cycles 5 and 15), there is a linear increase on the logarithmic scale. To understand this behaviour the single sets of the breakage-thermal curing cycles were analyzed further (Figure 4.8 and 4.12). It is visible that the "shape", which means the slope of G' during heating and cooling, of the temperature cycles changes: At the first two sets G' increases with increasing temperature (Figure 4.8 and 4.12a), whereas this is not the case for the 3rd and the following sets (Figure 4.12b).

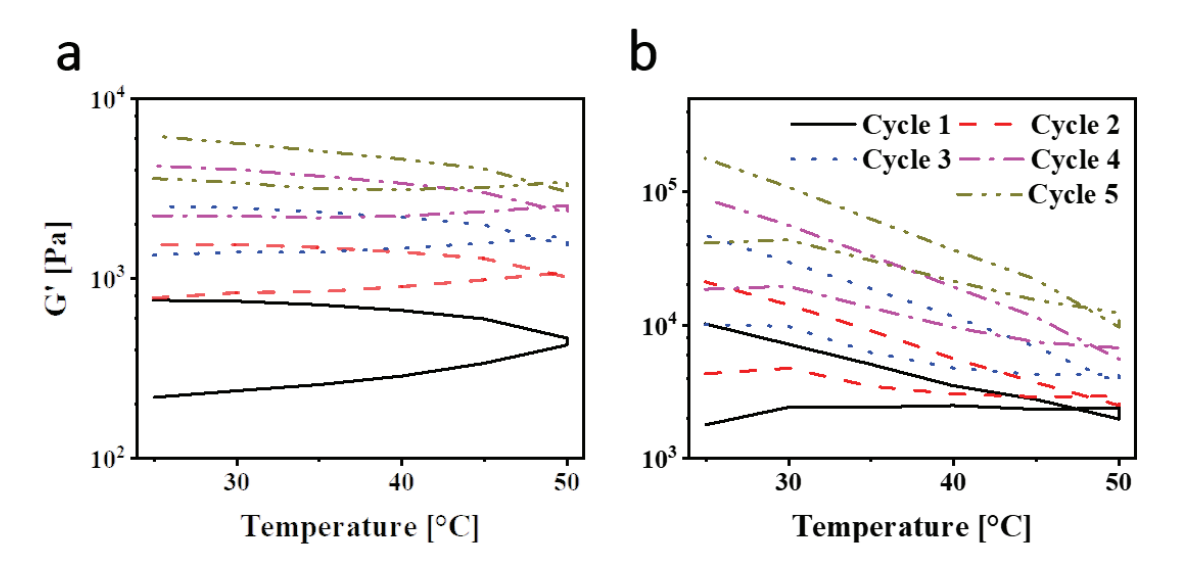


Figure 4.12. Evolution of G' during the 2nd (a) and 3rd (b) set of heating/cooling cycles

The increase of the temperature leads to a breakage of the hydrogen bonds on the one hand, but on the other also results in homogenization, which overcompensates the reduction of G' due to breakage of comparably few hydrogen bonds. However, in the 3rd set the gel is homogenized (which is also visible by the increase of G' from 7 kPa after the 2nd set to 20 kPa after the 3rd set) to an extent that further homogenization does not overcompensate the breakage of the hydrogen bonds leading therefore to a decrease of G' with increasing temperature.

4. Conclusions

In conclusion, physical gels were successfully prepared from p(VAm-co-VAA) and PEG-PC. Rheology, NMR, and UV-Vis spectroscopy were used to determine the structure of the gel revealing the formation of aggregates. Heating/Cooling cycles within the rheometer can homogenize the structure resulting in a tough physical gel with storage moduli above 50 kPa. Furthermore, the gel is fully self-healable. These experiments highlight the possibility to tune the modulus and to anneal inhomogeneities in physical gels.

5. References

Sun, T. L. *et al.* Physical hydrogels composed of polyampholytes demonstrate high toughness and viscolelasticity. *Nat. Mater.* **12**, 932-937, doi:10.1038/nmat3713

10.1038/NMAT3713 (2013).

- Dai, X. *et al.* A Mechanically Strong, Highly Stable, Thermoplastic, and Self-Healable Supramolecular Polymer Hydrogel. *Adv. Mater.* **27**, 3566-3571, doi:10.1002/adma.201500534 (2015).
- Guo, M. *et al.* Tough stimuli-responsive supramolecular hydrogels with hydrogen-bonding network junctions. *J Am. Chem. Soc.* **136**, 6969-6977, doi:10.1021/ja500205v (2014).
- 4 Li, L., Yan, B., Yang, J., Chen, L. & Zeng, H. Novel mussel-inspired injectable self-healing hydrogel with anti-biofouling property. *Adv. Mater.* **27**, 1294-1299, doi:10.1002/adma.201405166 (2015).
- Nakahata, M., Takashima, Y. & Harada, A. Highly Flexible, Tough, and Self-Healing Supramolecular Polymeric Materials Using Host-Guest Interaction. *Macromol. Rapid Comm.*, doi:10.1002/marc.201500473 (2015).
- Tuncaboylu, D. C., Sari, M., Oppermann, W. & Okay, O. Tough and Self-Healing Hydrogels Formed via Hydrophobic Interactions. *Macromolecules* **44**, 4997-5005, doi:10.1021/ma200579v (2011).
- 7 Appel, E. A., del Barrio, J., Loh, X. J. & Scherman, O. A. Supramolecular polymeric hydrogels. *Chem Soc Rev* **41**, 6195-6214, doi:10.1039/c2cs35264h (2012).
- 8 Voorhaar, L. & Hoogenboom, R. Supramolecular polymer networks: hydrogels and bulk materials. *Chem Soc Rev* **45**, 4013-4031, doi:10.1039/c6cs00130k (2016).
- 9 Mantooth, S. M., Munoz-Robles, B. G. & Webber, M. J. Dynamic Hydrogels from Host-Guest Supramolecular Interactions. *Macromol. Biosci.*, e1800281, doi:10.1002/mabi.201800281 (2018).
- Draper, E. R. & Adams, D. J. Low-Molecular-Weight Gels: The State of the Art. *Chem* **3**, 390-410, doi:10.1016/j.chempr.2017.07.012 (2017).
- Noro, A., Hayashi, M., Ohshika, A. & Matsushita, Y. Simple preparation of supramolecular polymer gels via hydrogen bonding by blending two liquid polymers. *Soft Matter* 7, doi:10.1039/c0sm01334j (2011).
- Edwards, W. & Smith, D. K. Dynamic evolving two-component supramolecular gelshierarchical control over component selection in complex mixtures. *J. Am. Chem. Soc.* **135**, 5911-5920, doi:10.1021/ja4017107 (2013).
- Hu, X., Vatankhah-Varnoosfaderani, M., Zhou, J., Li, Q. & Sheiko, S. S. Weak Hydrogen Bonding Enables Hard, Strong, Tough, and Elastic Hydrogels. *Adv Mater* **27**, 6899-6905, doi:10.1002/adma.201503724 (2015).
- 14 Pinschmidt, R. K. J. Poly(vinylamine) at Last. *J. Polym. Sci. A: Polym. Chem.* **48**, 2257-2283, doi:10.1002/pola.23992

10.1002/POLA (2010).

- Pelton, R. Polyvinylamine: A Tool for Engineering Interfaces. *Langmuir* **30**, 15373-15382, doi:10.1021/la5017214 (2014).
- 16 Chen, Q., Xu, K., Zhang, W., Song, C. & Wang, P. Preparation and Characterization of Poly (*N*-isopropylacrylamide)/Polyvinylamine Core-Shell Microgels. *Colloid Polym. Sci.* **287**, 1339-1346, doi:10.1007/s00396-009-2095-z (2009).
- Xu, J., Barros Timmons, A. & Pelton, R. *N*-Vinylformamide as a Route to Amine-Containing Latexes and Microgels. *Colloid Polym. Sci.* **282**, 256-263, doi:10.1007/s00396-003-0901-6 (2004).

- Xu, K. *et al.* A novel multi-responsive polyampholyte composite hydrogel with excellent mechanical strength and rapid shrinking rate. *J. Colloid Interf. Sci.* **345**, 360-368, doi:10.1016/j.jcis.2010.01.058 (2010).
- Yue, M., Imai, K., Miura, Y. & Hoshino, Y. Design and Preparation of Thermo-Responsive Vinylamine-Containing Micro-gel Particles for Reversible Absorption of Carbon Dioxide. *Polym. J.* **49**, 601-606, doi:10.1038/pj.2017.28 (2017).
- 20 Kim, J. *et al.* Template-Free Uniform-Sized Hollow Hydrogel Capsules with Controlled Shell Permeation and Optical Responsiveness. *Langmuir* **28**, 11899-11905, doi:10.1021/la3017968 (2012).
- Feng, X. P., Robert. Carboxymethyl cellulose: Polyvinylamine complex hydrogel swelling. *Macromolecules* **40**, 1624-1630 (2007).
- Mendoza-Payan, J. G., Flores-Gallardo, S. & Marquez-Lucero, A. Preparation and electrical characterization of poly(vinyl amine) hydrogels, crosslinked with Cu(II) ions, and evaluation of their potentiality as water sensor material. *J. Appl. Polym. Sci.* **115**, 790-801, doi:10.1002/app.31097 (2010).
- Alcalde, R., Atilhan, M., Trenzado, J. L. & Aparicio, S. Physicochemical Insights on Alkylcarbonate-Alkanol Solutions. *J Phys Chem B* **120**, 5015-5028, doi:10.1021/acs.jpcb.6b02961 (2016).
- Fuentes-Caparros, A. M. *et al.* Annealing multicomponent supramolecular gels. *Nanoscale* **11**, 3275-3280, doi:10.1039/c8nr09423c (2019).
- Volkov, S. N. Some aspects of the DNA hypochromic effect theory. *Int. J. Quantum Chem.* **16**, 119-132 (1979).
- Rest, C. *et al.* Self-assembly and (hydro)gelation triggered by cooperative pi-pi and unconventional C-H...X hydrogen bonding interactions. *Angew. Chem. Int. Ed.* **53**, 700-705, doi:10.1002/anie.201307806 (2014).
- Fischer, T., Köhler, J., Keul, H., Singh, S. & Möller, M. Highly Swellable Hydrogels from Waterborne Poly(vinylamine-co-acetamide). *Macromol. Chem. Phys.* **219**, 1800399-1800408, doi:10.1002/macp.201800399 (2018).
- Zhao, J., Mayumi, K., Creton, C. & Narita, T. Rheological properties of tough hydrogels based on an associating polymer with permanent and transient crosslinks: Effects of crosslinking density. *J. Rheol.* **61**, 1371-1383, doi:10.1122/1.4997589 (2017).
- Indei, T. & Takimoto, J. Linear viscoelastic properties of transient networks formed by associating polymers with multiple stickers. *J. Chem. Phys.* **133**, 194902, doi:10.1063/1.3498779 (2010).
- 30 (!!! INVALID CITATION !!! {}).
- Zidan, H. M. Electron Spin Resonance and Ultraviolet Spectral Analysis of UV-Irridiated PVA Films Filled with MnCl2 and CrF3. *J. Appl. Polym. Sci.* **88**, 104-111 (2003).
- Wang, K.-Y. *et al.* Novel multifunctional organic semiconductor materials based on 4,8-substituted 1,5-naphthyridine: Synthesis, single crystal structures, opto-electrical properties and quantum chemistry calculation. *Organic & biomolecular chemistry* **10**, 6693-6704, doi:10.1039/c2ob25926e (2012).
- Nicola, N. A. & Leach, S. J. Interpretation and Application of Thermal Difference Spectra of Proteins. *Int. J. Peptide Protein Res.* **8**, 393-415 (1976).
- Robin, M. B. *Higher Excited States of Polyatomic Molecules*. Vol. 2 (Academic Press, 1975).
- Kuo, S.-W. Hydrogen-bonding in polymer blends. J. Polym. Res. 15, 459-486 (2008).

Chapter 5 Thermoresponsive P(VAm-co-NIPAm) hydrogels

This chapter is reproduced from Soft Matter 2020,16, 6549-6562 with permission from the Royal Society of Chemistry.

HRMAS NMR data analysis and application to the two-state model and Boltzmann model were performed by D. Demco and R. Fachete.

All other experiments and data analysis is performed by T.Fischer

1. Introduction

Thermoresponsive systems experience rising attention in the past decades. The most prominent and best investigated example in the class of thermo-responsive polymers and their related hydrogels is poly(*N*-isopropylacrylamide) P(NIPAm). P(NIPAm) is characterized by a steep phase transition exceeding the so-called lower critical solution temperature (LCST). Below the LCST P(NIPAm) has a good water-solubility due to the hydrophilic amide group and hydrogen bonds to the surrounding water molecules resulting in a random coil formation. An increase of the temperature breaks these hydrogen bonds leading to a hydrophobic aggregation of the isopropylgroups and consequently a (meso)-globule structure. Its phase diagram is comprehensively reviewed by Halperin et al. concluding that the LCST of pure P(NIPAm) depends on the molecular weight and polydispersity, the tacticity, and, in case of low molecular weights (> 50 kDa), the end groups. A great potential of tailoring the LCST arises from the possibility to introduce a second monomer tuning the hydrophilicity of the resulting copolymer, which is already extensively exploited, especially in case of acrylic acid (AAc). A comprehensive study in dependence on the content of acrylic acid was performed by Lue et al. The LCST of the copolymers increases with increasing AAc content due to the additional osmotic pressure created by the carboxy-group.

Preferably, this co-monomer should contain functional group which offers the possibility for crosslinking or attachment of a drug or a bioactive molecule. Maybe the most versatile functional group is the primary amine due to its nucleophilicity and reactivity. In this context N-vinylformamid (NVF) is a promising candidate as it can be hydrolyzed to the corresponding amine. (Chapter 3) However, there is few literature about this system for synthesis of microgels. 6-8 (Chapter 2) In the study by Xu et al. microgel particles were prepared by free radical polymerization of NVF, NIPAm, and N,N'-methylenebis(acrylamide) (MBAA) as crosslinker. The microgels were subsequently hydrolyzed under acidic conditions (70 °C, 24 h, pH = 1.5). It was found that the degree of swelling increases with increasing hydrophilicity, i.e., with increasing formamide content and increasing degree of hydrolysis of this formamide group to the even more hydrophilic amine group. Furthermore the electrophoretic mobility is increased after hydrolysis.⁶ Similarly, Yue et al. prepared microgel particles for the reversible absorption of carbon dioxide. Gelation was obtained by thermo-initiated free radical polymerization of NVF and NIPAm in water in presence of MBAA as crosslinker. The formamide group was subsequently hydrolyzed in methanol in presence of an acid or a base. The volume phase transition temperature (VPTT) of the resulting gels is around 65 °C (Ratio NVF:NIPAm = 3:5). In these studies the reported copolymerization parameters of $r_{NVF} = 0.09$ and r_{NIPAm} = 0.9 differs widely indicating the formation of block copolymers. More detailed information can be found in Chapter 2.

In this Chapter a pathway to synthesize amine-functional NIPAm copolymers is illustrated. Therefore, NVF is copolymerized with NIPAm with different monomer ratios and subsequently hydrolyzed to obtain free amine groups. The amine groups are crosslinked with phenylcarbonate telechelic ethylene glycol (EG-PC) to form a hydrogel exploiting amine-carbonate chemistry. Crosslinking from a copolymer exploiting the free amine groups is an attractive alternative. In Chapter 3 it was shown that a P(VAm-co-acetamide) copolymer can be crosslinked via carbamate formation with a phenylcarbonate telechelic poly(ethylene glycol) resulting in highly swellable hydrogels. The thermoresponsive properties are comprehensively investigated in terms of UV-Vis spectroscopy, rheology, differential scanning calorimetry (DSC) and NMR spectroscopy.

The first part of this chapter deals with the characterization of the free polymer determining the copolymerization parameters and the hydrolysis kinetics. Furthermore, the phase transition of the free polymers as well as the hydrogels is investigated by rheology and UV-Vis spectroscopy. In the second part, NMR method represented by the proton transverse magnetization relaxation (T₂) NMR is extensively applied for characterization of side chains dynamics of hydrogel network and the state of water in hydrogel pores as a function of crosslink density induced by different monomer ratios. Moreover, ¹H NMR diffusometry of water molecules is investigated to characterize the pore network properties and hydrogel morphology in the swollen and collapsed states.

For this a recently developed two state model¹⁰⁻¹² is applied to describe the temperature induced phase transition of linear polymers and hydrogels with tuned hydrophilicity detected by ¹H HRMAS NMR spectroscopy. The coil-to-globule and swollen-to-collapsed phase transitions for linear polymers and hydrogels are described by specific thermodynamic quantities like transition temperature, transition entropy, and width of the phase transition. This statistical model was previously applied to the case of temperature-responsive linear homopolymers and polymer brushes onto nanoparticles with hydrophilic and hydrophobic end groups.^{10,13,14} The investigation was made using the spectral integral intensity of ¹H HRMAS NMR spectra edited by the spin echo. This NMR method is based upon the changes of polymer side-chains dynamics that occurs in the hydrophilic-to-hydrophobic phase transition and is reflected in the transverse magnetization relaxation.

2. Experimental section

2.1 Materials

N-Vinylformamide (NVF), *N*-isopropylacrylamide (NIPAm), phenyl chloroformate (PCF), triethylamine (TEA), chloroform, sodium hydroxide (NaOH) and ethylene glycol were purchased from Sigma Aldrich (Merck, Darmstadt, Germany). 2, 2'-Azobis[2-(2-imidazolin-2-yl)propane] dihydrochloride (VA044) was purchased from TCI (TCI Deutschland GmbH, Eschborn, Germany). Hydrochloride acid was purchased from VWR (VWR International GmbH, Darmstadt, Germany). NIPAm was recrystallized and filtered in hot hexane (50 °C). All other chemicals were used as received without any purification.

2.2 Polymer Synthesis for NVF-to-NIPAm Ratio of 1 to 5

NVF (0.87 g, 12.2 mmol), NIPAm (4.13 g, 36.5 mmol), and VA044 (0.16 g, 0.49 mmol) were dissolved in water (95 mL). The reaction mixture was degased by three freeze-thaw cycles. After degasing the reaction mixture was heated up to 35 °C for 20 h under nitrogen. The resulting copolymer was precipitated in an excess of acetone, redissolved in water, and lyophilized obtaining a white solid. The monomer ratios 1:3 and 1:4 were prepared following the same procedure with the amounts mentioned in Table 1.

Table 1. Amounts of reagents used for the copolymers

Formamide:NIPAm	NVF	NIPAm	VA044
ratio	[g] &	[g] &	[mg] &
	[mmol]	[mmol]	[mmol]
1:3	0.866	4.13	157
	12.2	36.5	0.487
1:4	0.679	4.32	154
	9.55	38.2	0.477
1:5	0.558	4.44	152
	7.85	39.3	0.471

¹H NMR (400 MHz in MeOD): δ 0.9-1.2 (br, 3H), 1.2-2.2 (br, 4H), 3.4-4.0 (br, 2H), 7.5-8.1 (br, 1H) SEC: $M_n = 1.07 \cdot 10^5 \text{ g} \cdot \text{mol}^{-1}$, $M_w = 2.88 \cdot 10^5 \text{ g} \cdot \text{mol}^{-1}$, PDI = 2.68 (1:5)

2.3 Copolymerization parameters

To determine the reaction rate a 1:1 molar ratio of NVF:NIPAm were copolymerized at 35 °C for 120 min recording ¹H NMR spectra every 5 min. The copolymerization parameters were determined by the method of Fineman-Ross and Mayo-Lewis using 5 different NVF:NIPAm ratios (10:1, 5:1 1:1; 1:5; 1:10) in the feed (details about these methods can be found in Chapter 2). The ratio of NVF:NIPAm was determined at conversions below 10 %.

2.4 Hydrolysis

The polymer (5 g) was dissolved in HCl (2 mol·L⁻¹, 250 mL). The reaction mixture was heated up to 80 °C for 8 h. The mixture was neutralized with NaOH (2 mol·L⁻¹) to pH = 7 and subsequently dialyzed (regenerated cellulose, SpectraPor®, molecular weight cut-off: 3.5 kDa) for 7 days. The water was removed by lyophilization obtaining a white solid.

¹H NMR (400 MHz in MeOD): δ 0.9-1.2 (br, 3H), 1.2-2.2 (br, 4H), 3.4-4.0 (br, 2H)

2.5 Hydrolysis Kinetics

In order to determine the hydrolysis kinetics three different conditions were applied (Table 2). The polymer (2 g) was dissolved in HCl (100 mL). Samples were taken after 1, 2, and 4 h, neutralized with NaOH (2 mol·L⁻¹) to pH = 7 and subsequently lyophilized. The 1 H NMR peak integral of the formamide group (CHO) was used to calculate the conversion.

Table 2. Reaction conditions for the selective hydrolysis of the formamide group.

Sample	c (HCl)	Temperature	
Number	[mol·L ⁻¹]	[°C]	
1	2	40	
2	4	40	
3	2	80	

2.6 Synthesis of Phenylcarbonate Telechelic Ethylene Glycol (EG-PC)

Ethylene glycol (1 g, 16.1 mmol) was dissolved in THF (50 mL) and pyridine added (2 eq, 2.6 mL, 32.2 mmol). The reaction mixture was cooled with an ice bath. Phenylchloroformate (2 eq, 4.1 mL, 32.2 mmol) was added dropwise without exceeding 5 °C. Afterwards the reaction was allowed to stir for further 16 h at room temperature. Pyridine hydrochloride was removed by filtration, the solution washed three times with water and the solvent was removed.

¹H NMR (400 MHz in CDCl₃): δ 4.45 (s, 2H), 7.09-7.14 (d, 2H, J = 7.6 Hz), 7.14-7.20 (t, 1H, J = 7.5 Hz), 7.27-7.34 (t, 2H, J = 7.9 Hz)

2.7 Gelation

To a solution of polymer (1:3) (50 mg, 131 μ mol amine groups) in methanol (1.0 mL), triethylamine (44.4 μ L, 2 eq per amine group) was added. The crosslinker EG-PC (38.3 mg, 65.5 μ mol, 0.5 eq, *i.e.* 1 eq carbonate per amine group) in chloroform (100 μ L) was added to the solution. The amounts for the ratios 1:4 and 1:5 are summarized in Table 3.

Due to the solubility of the crosslinker and the polymer the gels were prepared in a mixture of methanol and chloroform. After preparation the gels can be precipitated in water due to the co-nonsolvency effect.¹⁵ Afterwards they were swollen in water.

Table 3. Amounts for the preparation of the hydrogels.

Amine:NIPAm ratio	Amount	Amount EG-	Amount TEA
	[mg] &	PC [mg] &	[µL] &
	[µmol] amine	[µmol]	[µmol]
	groups		
1:3	50	38.3	33.6
	131	65.5	162
1:4	50	29.6	25.9
	101	50.5	202
1:5	50	23.2	20.4
	79.6	39.8	159

2.8 UV-Vis spectroscopy

UV/Vis-spectra were recorded using 1 mg·mL⁻¹ solutions of p(NVF-co-NIPAm) in H₂O on a Varian Cary 100 Bio. The absorbance was measured in the temperature range from 25 to 80 °C with a heating rate of 0.5 °C·min⁻¹.

2.9 Differential Scanning Calorimetry (DSC)

DSC spectra were recorded using 15 % of the copolymer in water on a DSC-7 (Perkin Elmer, Waltham, USA) in the range of 20 to 70 °C with a heating rate of 10 °C·min⁻¹ in aluminum crucibles.

2.10 Size-exclusion chromatography

Molecular weights (M_{n,SEC} and M_{w,SEC}) and molecular weight distributions (M_w·M_n⁻¹) were determined by size-exclusion chromatography (SEC). SEC analyses were carried out using water (HiPerSolv CHROMANORM® HPLC grade, VWR) as the eluent containing 0.1 mol·L⁻¹ sodium chloride, 0.3 wt% triflouroacetic acid and 0.01 wt% sodium azide The machine was equipped with an HPLC pump (1200, Agilent), a refractive index detector (RI) (1200, Agilent), and an UV-detector (VWD, 1200, Agilent). The samples contained 0.5 μL·mL⁻¹ ethylene glycol (99.5 %, Fluka analytical) as internal standard. One precolumn (8·50 mm) and three Novema Max gel columns (8·300 mm, Polymer Standards Service) were applied at a flow rate of 1.0 mL·min⁻¹ at 25 °C. The diameter of the gel particles measured 5 μm, the nominal pore widths were 30, 100, and 1000 Å. Calibration was performed using narrowly distributed poly(ethylene oxide) standards (Polymer Standards Service). Results were evaluated using the PSS WinGPC UniChrom software (Version 8.3.2).

2.11 Rheology

Measurements were conducted with a Discovery Hybrid Rheometer HR 3 (TA Instruments, USA) and a 40 mm parallel plate. The gelation time as well as G' and G" of the as-prepared gels were measured with a frequency of 1 Hz and an oscillation strain of 1 %. The reagents were mixed directly before the measurement and 1 mL of the solution were placed on the plate. The gap was adjusted to $800 \, \mu m$ and solvent evaporation prevented by a solvent trap.

The phase transition of the linear polymer (10 wt% in water) and the gel (5 wt% in water) was studied monitoring G' and G" at a temperature ramp from 25 °C to 70 °C at a rate of 0.5 °C·min⁻¹ with a frequency

of 1 Hz and an amplitude of 20 % strain. A frequency sweep was performed from 0.01 Hz to 100 Hz with 20 % strain at 25 °C and 70 °C.

To measure the gelation time the crosslinker was mixed with the copolymer directly before the measurement. G' and G" were measured in dependence on the time at 1 Hz and 1 % strain for at least 3 h.

2.12 NMR

Proton high-resolution NMR spectra were recorded on a Bruker Avance III-400 FT-NMR spectrometer at 400 MHz. The kinetic measurement was performed with a Bruker Avance II-600 FT-NMR spectrometer (Bruker Corporation, Billerica, MA, USA) at 600 MHz. Deuterium oxide was used as solvent.

Proton high-resolution magic-angle sample spinning (HRMAS) NMR on P(VAm-co-NIPAm) linear polymers and hydrogels were recorded on a wide bore AV700 Bruker NMR spectrometer operating at frequency of 700.2378 MHz, equipped with a cross-polarization MAS (CPMAS) probehead with a 3.2 mm rotor. The rotor frequency was set at 5 kHz. All the 1 H HRMAS spectra were externally referenced to tetramethylsilane (TMS). For all measurements the recycle delay was 10 s, the radio-frequency pulse length was 1.9 μ s, while the dwell time was 10 μ s, and the number of scans was 64. The time domain data were 4 k and the zero filling was done with 16 k.

The NMR resonances of VAm and NIPAm monomers are difficult to be separated by spectral deconvolution. Therefore, the total integral spectral region in the aliphatic region of 0 ppm - 4.6 ppm was considered for all spectra as reflecting the process of temperature-induced phase transition. This quantity is informative even if only NIPAm is a thermosensitive monomer.

The effect of temperature-induced transition on polymer chain conformations is enhanced by the method of transverse magnetization relaxation (T_2) spin-echo editing of the 1 H HRMAS NMR spectrum ($c > c^*$). The radio-frequency pulse sequence used is 90 0 x- τ -180 0 y- τ -180 0 -y- τ -acquisition, where 2 τ is the spin-echo time, 90 0 and 180 0 are the pulse flip angles with the phases x, y, and –y, for the first step of CYCLOPS phase cycling. The value of τ used in this work was τ =20 μ s. For short spin-echo times the transverse magnetization relaxation described by the effective rate T_2^{-1} can be considered to be monoexponential and the decay of the normalized integral intensity $I(T) \cdot I_0^{-1}$ of the HRMAS NMR spectrum at temperature T is given by

$$\frac{I(T)}{I_0} \cong 1 - \frac{3\tau}{T_2},\tag{1}$$

where $3\tau \ll T_2$. The effect of coil-to-globule and swollen-to-collapsed states in the process of phase transition is encoded in polymer backbone and side-chain dynamics and is detected by the effective transverse relaxation rate T_2^{-1} , that is multiplied by the time interval 3τ . This last quantity can be made bigger compared with the spectrometer dead time and therefore, enhances the sensitivity to the temperature-induced phase transition. The integral intensity of NMR resonances for a fixed echo time 3τ will reflect the T_2 changes in the process of phase transition. For CPMAS NMR probehead the dead time is of the order of 2 μ s and hence, the solid-like signals that occurred for globule linear polymers or collapsed hydrogels are only to a small degree filtered out.

The transverse magnetization relaxation (T_2) is measured using spin-echo decay by the pulse sequence: 90 0 x- τ -180 0 y- τ -spin-echo acquisition, where 2 τ is the spin-echo time. 17,18 It is assumed that for T_2 measurements the static magnetic field is homogenous enough such that the effect of water self-diffusion can be neglected in the first approximation.

The apparent diffusivity D of water in polymer dispersions and hydrogels were measured using the AV700 Bruker NMR wide bore spectrometer with a Diff50 Bruker unit by pulsed-field-gradient stimulated echo (PFGSE) sequence of Stejskal-Tanner.¹⁹ The experiment is two-dimensional, by recording the dependence of the NMR peak integral intensity upon the applied field gradient strength. The apparent diffusivity was obtained by fitting the normalized stimulated spin echo decay as a function of gradient strength g given by Stejskal-Tanner equation¹⁹

$$\frac{I(g)}{I_0} = e^{-q^2 D\left(\Delta - \frac{\delta}{3}\right)},\tag{2}$$

where the convention $q = \gamma \delta g$, for the diffusion wave vector is employed.^{17,18} In the above equation I(g) is the integral intensity of the aliphatic spectral region obtained by the Fourier transform of the half decay of stimulated echo at a given value of magnetic field gradient g, and I_0 is the integral intensity for small values of field gradient value compared to the maximum of the gradient strength g_{max} . Equation 2 can be rewritten as

$$\frac{I(g)}{I_0} = e^{-bD},\tag{3}$$

where the quantity b is defined as

$$b = \gamma^2 g^2 \delta^2 \left(\Delta - \frac{\delta}{3} \right), \tag{4}$$

and magnetogyric ratio γ has the units of rad·s⁻¹·T⁻¹. The duration of the gradient pulse is denoted by δ and Δ is the diffusion time defined as the time interval between the gradient pulses. In all the ¹H high-resolution

NMR diffusometry experiments reported in this study the delays were set to $\delta = 2$ ms and $\Delta = 20$ ms. The field gradient g was applied in the z direction and incremented in 16 steps with a linear ramp from 2 % to 95 % of maximum field gradient in the range of $g_{max} = (1 \div 10) \text{ T} \cdot \text{m}^{-1}$. The stimulated echo decay was collected into 16 k data points and Fourier transformed by applying zero-filling to 32 k data points and an exponential window function with a line broadening factor of 5 Hz. A relaxation delay of 10 s was used with a spectral window of 6 kHz. The NMR measurements were made in deuterated aqueous solutions of 5 or 10 wt% concentration of linear polymer. For both CPMAS 3.2 and Diff 50 NMR probe heads, the temperature calibration was made using neat ethylene glycol chemical shift resonances.

The intensity of the NMR free-induction decay is proportional to the Curie factor and therefore, depends on the inverse of temperature. In the following this dependence is neglected in the limited range of temperatures $15 \, ^{\circ}\text{C} - 65 \, ^{\circ}\text{C}$ used in the NMR measurements.

The effective values of ${}^{1}H$ longitudinal relaxation time T_{I} for linear copolymers and hydrogels in the temperature ranges of measurements by HRMAS NMR spectroscopy and diffusometry must be smaller compared to the employed recycle delay of 10 s in order not to interfere with phase transition changes of NMR resonances. This condition is fulfilled for the samples as for instance, for p(VAm-co-NIPAm) hydrogel with the monomer ratio 1:5 by saturation-recovery pulse sequence the value are measured: $T_{I}(23 \, {}^{\circ}\text{C}) = 1.23 \pm 0.3 \, \text{s}$ and $T_{I}(65 \, {}^{\circ}\text{C}) = 3.58 \pm 0.2 \, \text{s}$. Hence, all NMR experiments were made with recovery time of 10 s, which is longer than the proton T_{I} of our samples. These results are in agreement with those reported in Ref. 20 for 1H HRMAS NMR study of temperature-induced phase transition of PNIPAm hydrogels.

For variable-temperature NMR experiments, kinetic of swelling or deswelling of hydrogels have to be taken into account.^{21,22} The duration of thermodynamic equilibrium in the process of heating in 2 °C or 3 °C increments depends on the crosslink density of hydrogels and the value as well as the region of the temperature jump. Therefore, the NMR spectra were recorded after 30 min dwell time^{21,22} in order to observe the quantitative variation of resonance integral intensity.

3. Results and Discussion

3.1 Synthesis of the Polymer

P(NVF-*co*-NIPAm) was prepared by free radical polymerization in water with 2,2'-azobis[2-(2-imidazolin-2-yl)propane] dihydrochloride (VA044) as initiator (Scheme 1).

Scheme 5.1. Polymerization scheme of NVF and NIPAm in different ratios.

The copolymerization parameters determined by the method of Mayo-Lewis and Fineman-Ross reveal that NIPAm polymerizes slightly faster than NVF (Mayo-Lewis: $r_{NIPAM} = 1.13$ and $r_{NVF} = 0.91$; Fineman-Ross: $r_{NIPAM} = 1.22$ and $r_{NVF} = 1.07$) (Figure 5.1), which is contrary to reported copolymerization parameters of $r_{NIPAm} = 1.0$ and $r_{NVF} = 0.09$.

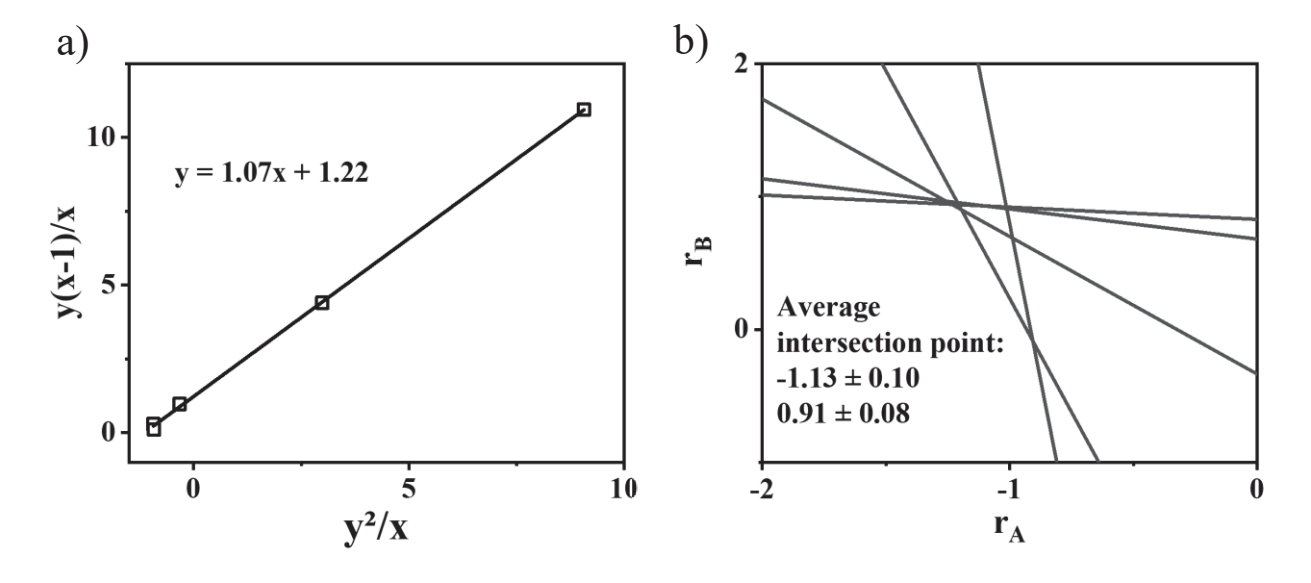


Figure 5.1. Copolymerization parameters by the methods of Fineman-Ross (a) and Mayo-Lewis (b)

The difference is deduced to the decreased polymerization temperature (35 °C compared to 50 °C, as in the reference⁶) which is below the LCST of the copolymer. ¹H NMR of the different NVF to NIPAm ratios show that the desired ratios could be obtained with minor deviations (Figure 5.2 and Table 4) using the isopropyl-group as reference.

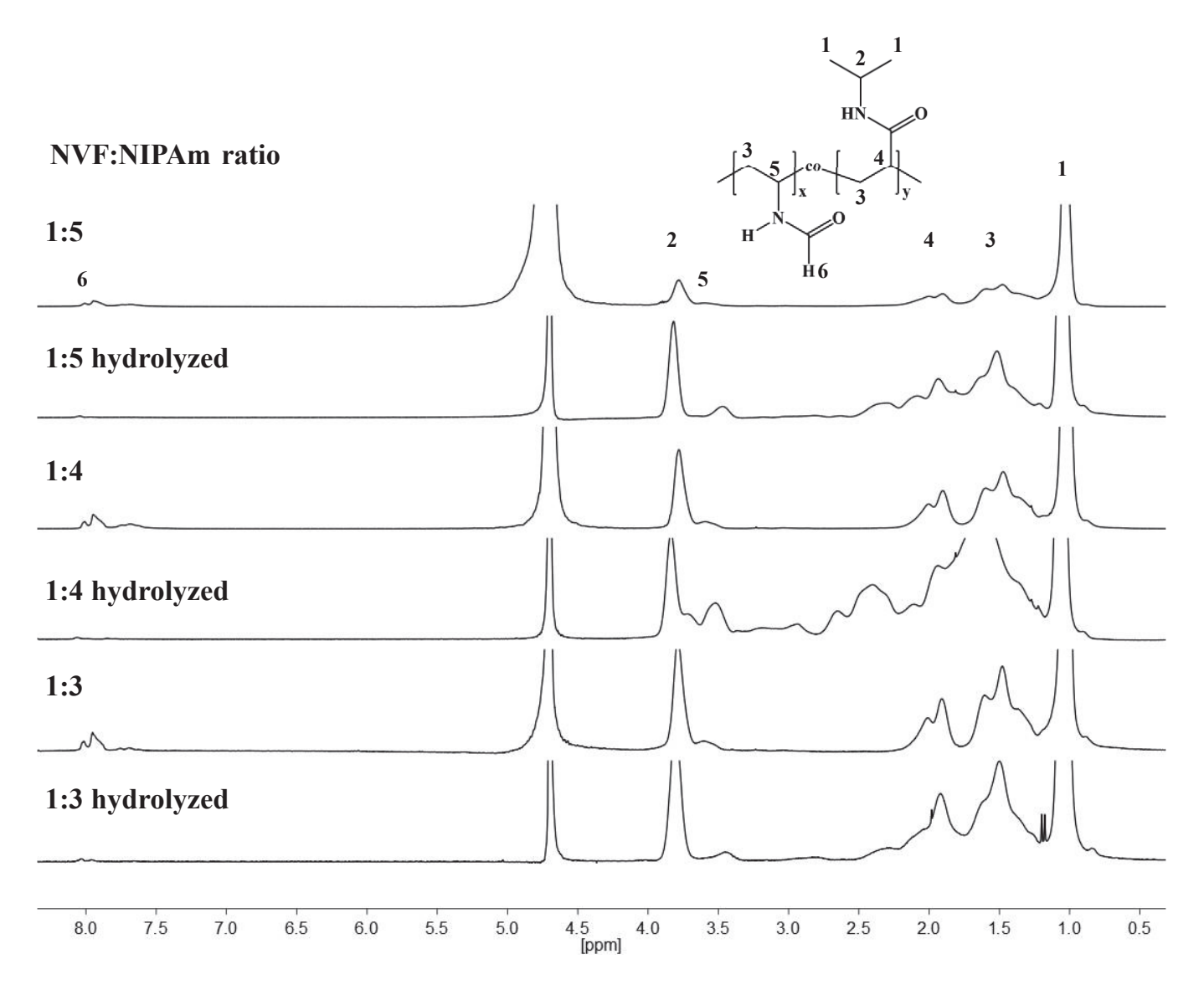


Figure 5.2. Proton NMR spectra of P(NVF-*co*-NIPAm) before and after hydrolysis. It is visible that the signal of the formamide proton nearly disappears after hydrolysis.

Table 4. Theoretical and experimental integral ratios 1:5, 1:4, and 1:3. The integral of the iso-propylgroup was taken as reference.

VAm:NIPAm ratio	Integral iso-propyl group I1/6	Integral formamide goup I6
1:5	5	0.99
1:4	4	1.29
1:3	3	1.01

To obtain a functional group the NVF was subsequently selectively hydrolyzed as visible in Scheme 5.1. Despite the numerous literatures about NVF hydrolysis of the free polymer^{9,23,24}, there is none with a

thermoresponsive co-monomer present. Therefore, a common method of acidic hydrolysis, which is above the LCST (80 °C, 2 N HCl) is compared with two different concentrations below the LCST (40 °C, 2 N HCl and 40 °C, 4 N HCl). After 1, 2, and 4 h samples were taken, and the hydrolysis degree calculated comparing the proton of the formamide (-CHO) to the methyl-groups (-CH₃) of NIPAm as reference. Hydrolysis was more efficient at the higher temperature above LCST, *i.e.*, if the polymer precipitates. Extrapolation indicates that a degree of hydrolysis over 90 % is obtained after 8 h. In fact, the experimental degree of hydrolysis was confirmed by ¹H NMR to be > 90 % (91.5 % for 1:5, 90.2 % for 1:4, and 93.3 % for 1:3 ratios). (Figure 5.2, Figure 5.3, and Table 5)

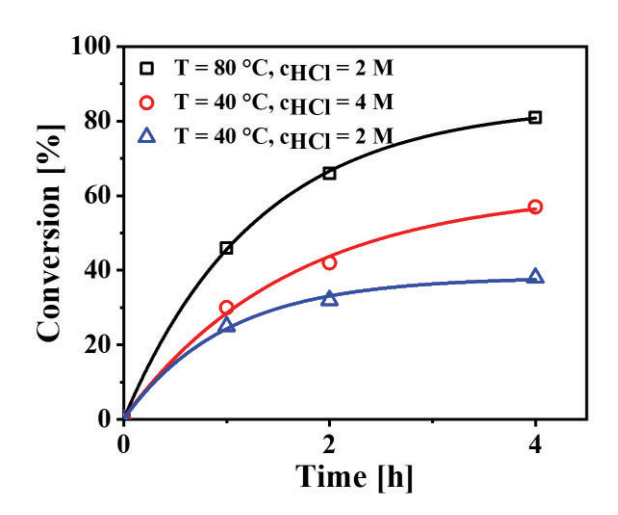


Figure 5.3. Degree of hydrolysis calculated by ¹H NMR after 1, 2 and 4 h. The continuous line represents an exponential fit $(y = A_1 e^{-\frac{x}{t_1}} + y_0)$ with being A₁, t₁, and y₀ fitting parameters.

Table 5. Degree of hydrolysis of the formamide group for the VAm:NIPAm ratios 1:5, 1:4, and 1:3.

VAm:NIPAm ratio	Degree of hydrolysis [%]
1:5	91.5
1:4	90.2
1:3	93.3

3.2 Temperature-Induced Phase Transition of p(VAm-co-NIPAm)

NIPAm-based polymers have shown to undergo a phase transition in aqueous solution above LCST. Exceeding the LCST the hydrophobic iso-propyl groups of the NIPAm aggregates and the polymer precipitates (cloud point). The cloud point and the LCST are determined by UV-Vis and DSC, respectively.

The results of the UV-Vis measurement (1 mg·mL⁻¹, 0.5 °C·min⁻¹, 260 nm, pH = 7) is shown in Figure 5.4a. The onset of the attenuation in the spectrum increases with decreasing NIPAm content from 42.6 °C (1:5) to 46.2 °C (1:4) and 49.2 °C (1:3), which is attributed to the introduction of a hydrophilic group. This is in agreement with results of Stile et al., who observed an increase of the LCST while introducing acrylic acid groups.²⁵ Demixing ca be observed als by an endothermic transition in DSC. Comparably the onset of the endothermic DSC (15 wt% in H₂O, 10 °C·min⁻¹) peak increases with decreasing NIPAm content from 39.7 °C (1:5) to 40.0 °C (1:4) and 44.2 °C (1:3) as seen in Figure 5.4b. The results are summarized in Table 6.

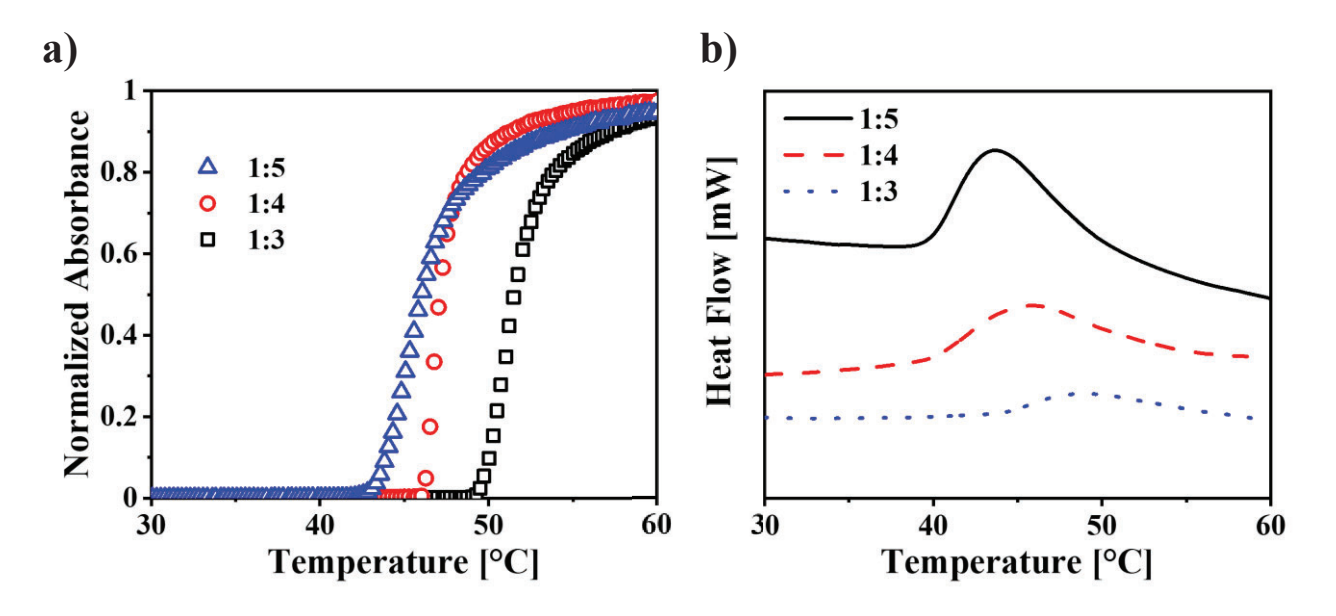


Figure 5.4. (a) Absorbance of the copolymers with the VAm:NIPAm ratio 1:3, 1:4, and 1:5 (260 nm, 1 mg· mL⁻¹, pH = 7) The cloud point increases with decreasing NIPAm content from 49.2 °C for the ratio 1:3 to 42.6 °C for the ratio 1:5. (b) DSC curve of the copolymers (endo up) with a heating rate of 10 °C·min⁻¹ and a concentration of 15 wt%. The signal intensity decreases with decreasing NIPAm content and the LCST is shifted to higher temperatures (Table 6).

Table 6. Cloud point and LCST values of the different VAm:NIPAm copolymer ratios (1:5, 1:4, 1:3) by DSC and UV-Vis.

VAm:NIPAm	Tonset	Tpeak	Tonset
ratio	(DSC)	(DSC)	(UV-Vis)
	[°C]	[°C]	[°C]
1:5	39.7	43.6	42.6
1:4	40.0	45.6	46.2
1:3	44.2	48.6	49.2

The coil collapse, which can lead to aggregation, can be monitored by rheology. The storage modulus G' and the loss modulus G" are measured in dependence on the temperature. The hydrophobic aggregates participate in the storage of the elastic energy. The results are shown in Figure 5.5a and b (10 wt% in water, 0.5 °C·min⁻¹, 1 Hz, 20 % strain). In Figure 5.5a, three stages are differentiated. Stage I shows a decrease of G' and G" which is common for a fluid and attributed to the increased mobility caused by the increased temperature. Stage II reveals a steep decrease of G", which is not found for G'. In general, a decrease of G" means, that less energy is dissipated during one oscillation.

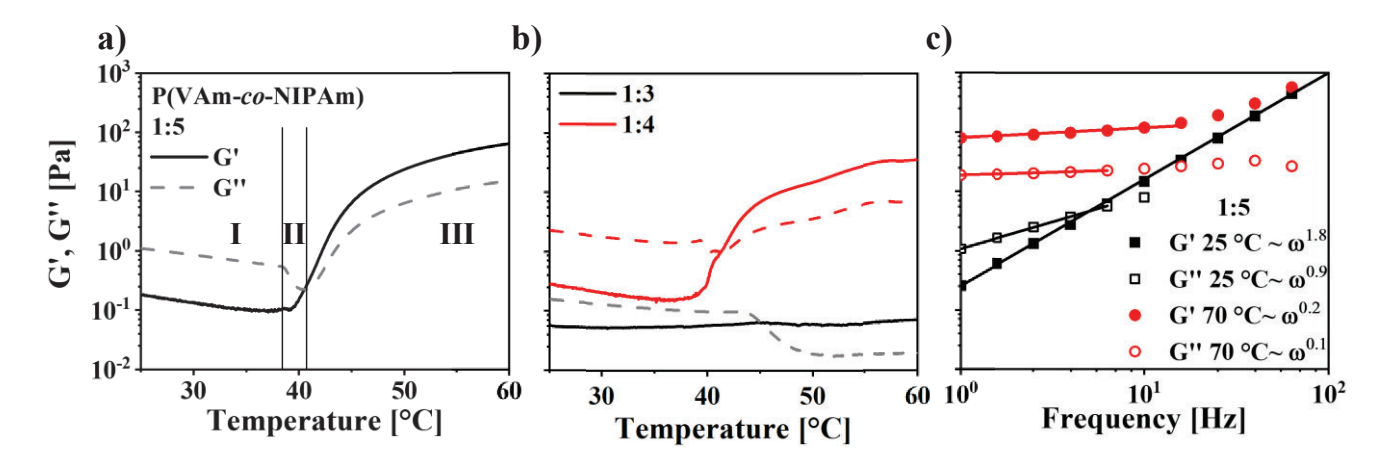


Figure 5.5. G' and G" in dependence on the temperature for the VAm:NIPAm ratios of 1:5 (a), 1:4, and 1:3 (b). For the ratios 1:5 and 1:4 G" is characterized by a decrease around the LCST (stage II) followed up by an increase, whereas G' shows only an increase. (c) shows the frequency dependence of the VAm:NIPAm ratio 1:5 on G' and G" at 25 °C and 70 °C. Below the LCST the moduli obey a power law according to the Maxwell model, whereas above the LCST the copolymer shows collapsed aggregated behavior.

However, this stage is not seen for NIPAm homopolymers. We speculate that this is caused by hydrogen bonding between the primary amine group of the vinylamine monomer and the carbonylgroup of the NIPAm monomer. FTIR studies by Maeda et al. reveal that around 13 % of the carbonyl groups are in hydrogen bonding to the secondary amine of the NIPAm monomer. ²⁶ It is likely that an interaction with the primary amine is favored. Though, there seem to be an optimum amine-to-NIPAm ratio for this phenomenon, as it is most prominent for the ratio 1:5 and becomes less visible for the ratio 1:4 and nearly invisible for the ratio 1:3.

Stage III is characterized by the hydrophobic aggregation, which means both – G' and G" increases with increasing temperature and G' exceeds G". This means that more energy is required to obtain the desired strain, and the elastic response, so the energy, which is stored and not dissipated, is dominating. This behavior is also most prominent for the ratio 1:5, because the NIPAm content and consequently the groups which facilitate the hydrophobic aggregation is the highest. It is less visible for the ratio 1:4; in case of 1:3 there is no increase of G' (Figure 5.5b). This can be explained by the fact the aggregation is the lowest and the system remains in the meso-globule state.

Further evidence of this behavior is obtained by measuring the frequency dependence below and above the LCST (25 °C and 70 °C, 1 – 100 Hz, 20 % strain). The intrinsic lifetime of a physical interaction τ determines whether this interaction can participate in the elastic response or not. Below the LCST the dominating interactions are chain entanglements and hydrogen bonding. There is a strong frequency dependence and a transition of G' over G". For a quantitative discussion of rheometry results the mass concentration c of polymer solution has to be considered, which is in this case $c \approx 100 \text{ mg} \cdot \text{mL}^{-1}$. When the whole volume of the solution is packed with polymer coils of gyration radius R_g it is possible to define the overlap concentration c^* . The quantitative definition of c^* is given by equation (5)²⁷

$$c^* = \frac{1}{\left(\sqrt{2}R_g\right)^3} \frac{M}{N_A},\tag{5}$$

where M is the molecular weight and N_A is the Avogadro's number. For a solution of linear P(VAm-co-NIPAm) having the monomer ratio of 1:5, the average molecular mass is $M \approx 2.36 \cdot 10^5 \, \mathrm{g \cdot mol^{-1}}$, and $R_g \approx 13 \, \mathrm{nm}$ at 20 °C. On putting these values in Equation (5) we yield an overlap concentration of $c^* \approx 3.5 \, \mathrm{mg \cdot mL^{-1}}$. This shows that the polymer solutions with concentration c is in semi-dilute or entangled regime, i.e., $c > c^*$. The results of Figure 5.5c be interpreted on a molecular level of investigated linear statistical polymers. The frequency dependence of the linear viscoelastic response in oscillatory shear of monodisperse linear polymer dispersion can be explained using Maxwell model, consisting of an elastic component connected in series with a viscous component.²⁸⁻³¹

This simple model describes well $G'(\omega)$ and $G''(\omega)$ for solutions of linear polymers in the coil regime and the corresponding equations are given by

$$G'(\omega) = \frac{J_{eq}\eta^2\omega^2}{1 + J_{eq}^2\eta^2\omega^2},\tag{6}$$

$$G''(\omega) = \frac{\eta \omega}{1 + J_{eq}^2 \eta^2 \omega^2},\tag{7}$$

where η is viscosity of polymer solution and J_{eq} is the steady state compliance.²⁸ From the above equations it is deduced that at low shear frequency ω , $G'(\omega) \ll G''(\omega)$ as it is shown in Figure 5.5c. Furthermore, for low shear frequency domain and Equations (6) and (7) the following relations can be written²⁸ as

$$\eta = \lim_{\omega \to 0} \frac{G''(\omega)}{\omega},\tag{8}$$

$$J_{eq} = \frac{1}{\eta^2} \lim_{\omega \to 0} \frac{G'(\omega)}{\omega^2}.$$
 (9)

Hence, the frequency power laws of s G' and G" are derived from above equations:

$$G'(\omega) = J_{eq}\eta^2\omega^2,\tag{10}$$

$$G''(\omega) = \eta \omega, \tag{11}$$

in the regime of low shear frequency. These relationships can be also obtained from Equations (6) and (7) for $J_{eq}^2\eta^2\omega^2\ll 1$. The frequency dependence of G' and G" shown in Figure 5.5c for linear P(VAm-co-NIPAm) with monomer ratios 1:5 measured at 25 °C, are in good agreement with the powers of shear frequency derived above, *i.e.*, $G'(\omega)\sim\omega^{1.8}$ and $G''(\omega)\sim\omega^{0.9}$. The same power law with slightly different exponents were obtained from the rheometer data at temperature of 25 °C, for linear P(VAm-co-NIPAm) with monomer ratios 1:4 ($G'(\omega)\sim\omega^{1.5}$ and $G''(\omega)\sim\omega^{0.98}$) and 1:3 ($G'(\omega)\sim\omega^{1.9}$ and $G''(\omega)\sim\omega^{0.96}$) (Figure 5.6a and b).

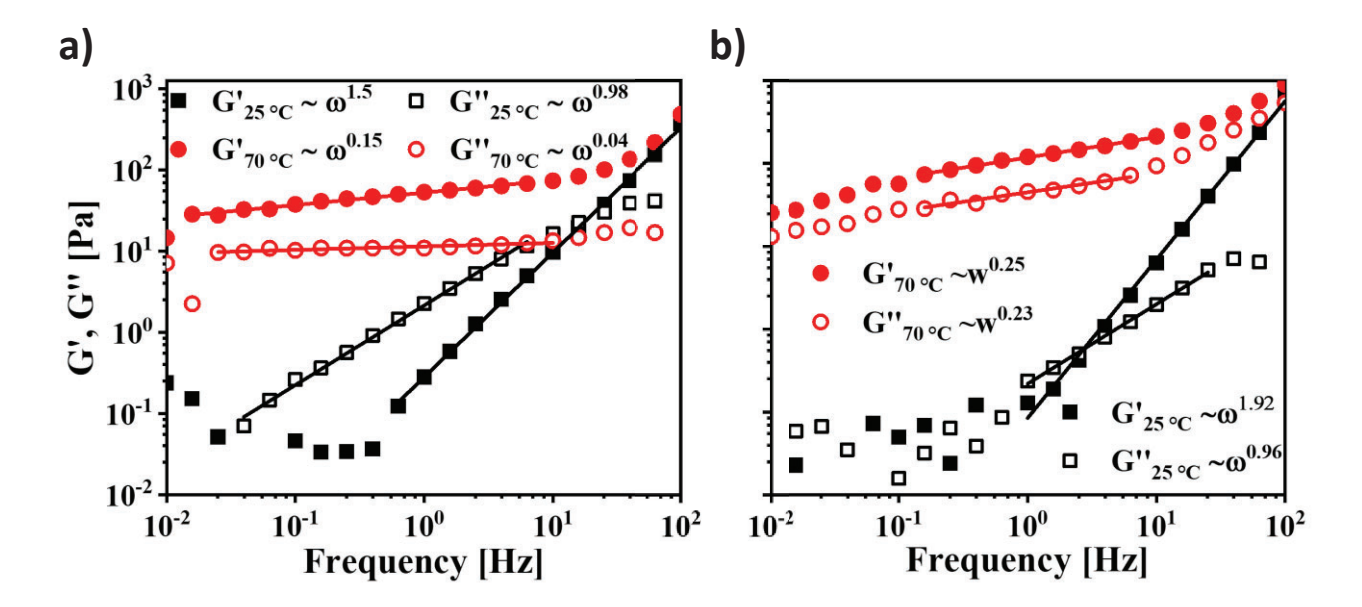


Figure 5.6. Frequency dependence of storage modulus (G') and loss modulus (G") for P(VAm-co-NIPAm) linear polymers with VAm:NIPAm monomer ratios of 1:3 (a) and 1:4 (b). The rheometry measurements were made at temperature of 25 °C (squares) and 70 °C (circles). The frequency dependence power law exponents are shown in the figure legend and obtained from a linear fit.

From equations (6) and (7) we evaluate the crossing shear frequency ω_0 where $G'(\omega_0) = G''(\omega_0)$, that is given by $\omega_0 = (\eta J_{eq})^{-1}$ (Figure 5.5c). The frequency ω_0 is the reciprocal of the polymer average stress relaxation time $\tau = \eta J_{eq}$ that characterize the polymer stress dynamics.²⁸ This quantity was evaluated from the dependences depicted in Figure 5.5c and Figure 5.6 and is given for linear P(VAm-*co*-NIPAm) with monomer ratios 1:5 and 1:3 to be $\tau = 17$ ms and $\tau = 88$ ms, respectively, *i.e.* the average lifetime is higher in case of the more hydrophobic monomer ratio, which is an intuitive result.

Above the LCST the linear polymer P(VAm-co-NIPAm) is in the globule state. The rheometry data shown in Figure 5.5c at temperature of 70 °C, which means above the LCST, are characterized by G' > G" being in a good approximation independent of frequency. This behavior can be compared to that of hydrogels where viscoelastic moduli are predominantly elastic and frequency independent for a wide frequency range. It can be concluded that at this temperature the P(VAm-co-NIPAm) globule forms aggregates.

A statistical description of the temperature - induced phase transition of a polymer network can be developed similar to that of ensembles of linear polymer chains or brushes in interaction with a solvent. This approach is based on the two-state model represented by swollen and collapsed hydrogel states and described the system behavior in the region of phase transition.

Here the argumentation presented in Reference ¹⁰ is followed. The statistical ensemble of the polymer network in the presence of a solvent is composed of two sub-ensembles or states, *i.e.*, hydrophilic and hydrophobic in thermodynamic equilibrium between them and with thermal bath. The distribution of these statistical sub-ensembles depends upon thermodynamic potentials of the network/solvent system. The assumed model is similar to that of monomers of the polymer chain that can exist into two distinct and interconverting states of hydrophilic and hydrophobic nature.³²⁻³⁵

The statistical average of a thermodynamic quantity designed as "observable" $\langle O(T) \rangle$, measured at temperature T, can be written as³⁶

$$\langle O(T) \rangle = \frac{\sum_{i=1,2} e^{(-\beta G_i)} o_i(T)}{\sum_{i=1,2} e^{(-\beta G_i)}},$$
 (12)

where Gibbs free energy for the *i*-state is $G_i = H_i - TS_i$. The enthalpy and entropy thermodynamic potentials are denoted by H_i and S_i , respectively. The quantity β is given by $\beta = (k_B \cdot T)^{-1}$, where T is the temperature and k_B is the Boltzmann constant. Equation (12) is written based on the first principles and in the temperature regime of volume phase transition has the general form,

$$\langle O(t) \rangle = \frac{\langle O_{swollen} \rangle}{1 + e^{\frac{(T_t - T)\Delta S}{k_B T_t}}} + \frac{\langle O_{collapsed} \rangle}{1 + e^{\frac{(T_t - T)\Delta S}{k_B T_t}}}$$
(13)

where the statistic quantities $< O_{\text{swollen}} >$ and $< O_{\text{collapsed}} >$ described swollen and collapsed sub-ensembles of polymer network. The phase transition temperature is denoted by T_{t} and in the narrow temperature region of phase transition $\Delta H \approx T_{\text{t}} \Delta S$, where ΔS is the change in the entropy and $\beta \approx (k_{\text{B}} T_{\text{t}})^{-1}$.

Equation (13) is applied to describe the evolution of the integral intensity I(T) of the ¹H NMR spectra in the process of temperature – induced phase transition for a responsive linear polymer and hydrogel and was applied previously for thermoresponsive linear polymer dispersions and brushes. ^{10,12,13} The corresponding relationship is given by

$$I(T) = \frac{I_{swollen}}{1 + e^{\frac{(T - T_t)|\Delta S|}{k_B T_t}}} + \frac{I_{collapsed}}{1 + e^{-\frac{(T - T_t)|\Delta S|}{k_B T_t}}},$$
(14)

where $|\Delta S|$ is the absolute value of the change in entropy, the quantities I_{swollen} and $I_{\text{collapsed}}$ are the NMR spectral integral intensities in the temperature region of swollen and collapsed hydrogel, respectively. In the case of responsive linear polymers in the region of coil-to-globule transition the quantities I_{swollen} and $I_{\text{collapsed}}$, must be replaced by I_{coil} and I_{globule} . All the important features of the hydrogel like for instance, heterogeneity and polymer - solvent interaction are implicitly included in the values of statistical observables around phase transition and in the thermodynamic potentials of the system.

A phenomenological equation of states used for description of the temperature - induced phase transition is given by the Boltzmann sigmoidal function, ¹⁰

$$I(T) = \frac{A_1}{1 + e^{\frac{(T - T_t)}{\Delta T_t}}} + A_2, \tag{15}$$

where A_1 and A_2 are fit parameters related to the statistical observables for swollen and collapsed hydrogel or linear polymers and ΔT_t is the full width of the phase transition. From Equation (15), in the swollen regime for $T < T_t$ we get $I_{swollen} = A_1 + A_2$, and in the plateau region of the collapsed state when $T > T_t$ we can write $I_{collapsed} = A_2$. Therefore, $I_{swollen} - I_{collapsed} = A_1$. It is worth mentioning that two-state model and Boltzmann sigmoidal function lead to the same value of NMR observable at $T = T_t$, i.e., $I(T_t) = (I_{swollen} + I_{collapsed})/2$. Furthermore, if we assume that the first order derivative as a function of temperature of Equations (14) and (15) are identical for $T = T_t$, we yield $\Delta T_t = T_t(|\Delta S| \cdot k_B^{-1})^{-1}$. Hence, the width of the temperature-induced phase transition that can be correlated with the duration of phase transition depends upon the transition temperature and the absolute change in the entropy at the transition.

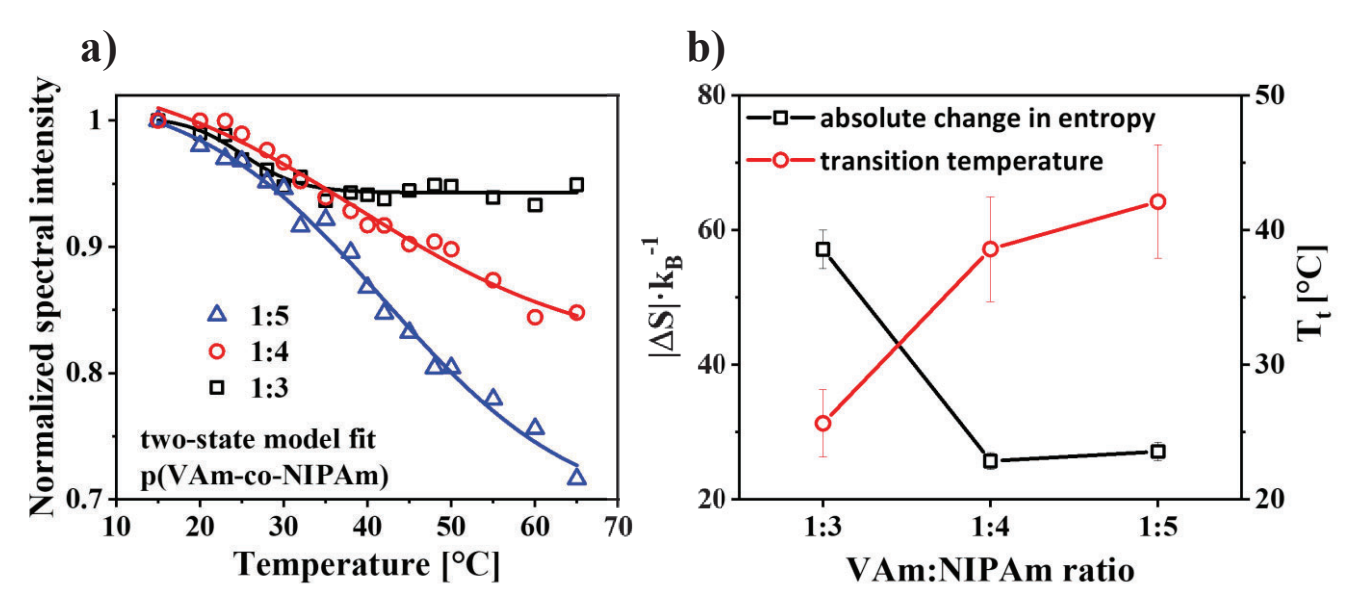


Figure 5.7. (a) Normalized integral intensity in the aliphatic region of ¹H HRMAS spectra for p(VAm-co-NIPAM) linear polymers with VAm:NIPAm ratios of 1:3 (squares), 1:4 (circles), and 1:5 (triangles) (5 wt% in D₂O). The fits with the two-state model are shown by the continuous lines. (b) Coil-to-globule transition temperatures T_t and normalized absolute change in the entropy $|\Delta S| \cdot k_B^{-1}$ at phase transition as a function of VAm:NIPAm ratio. These thermodynamic parameters were obtained by the fits with the two-state model Equation (14).

The temperature-induced coil –to –globule transition in P(VAm-co-NIPAM) linear polymers with different monomer ratios where detected from integral intensity of the ¹H HRMAS NMR spectra. These dependences are shown in Figure 5.7a.

The data fits were made using Equation (14) for coil-to-globule transition and the thermodynamic parameters are shown in Figure 5.7. Coil-to-globule transition temperature T_t increases by the increase in the monomer ratio, *i.e.*, to the increase in the content of thermoresposive NIPAm (Figure 5.7b). Moreover, the absolute change in the entropy $|\Delta S| \cdot k_B^{-1}$ at the coil-to-globule transition decreases by the increase in the NIPAm content (Figure 5.7b). The cooperative disruption of the polymer-water network that leads to coil-to-globule transition depends on the number of isopropyl group in the statistical linear polymer P(VAm-co-NIPAM).

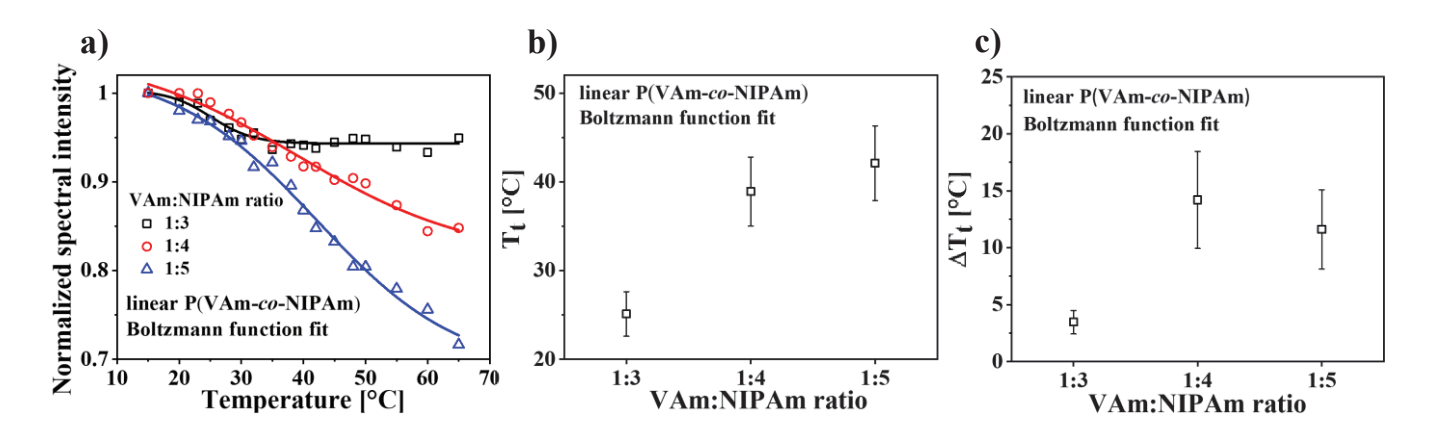


Figure 5.8. (a) Temperature-induced coil-globule transition curves of P(VAm-co-NIPAm) linear polymers with different VAm:NIPAm monomer ratios. The data were fitted with Boltzmann functions (continuous lines). (b) Transition temperatures Tt obtained from the fits with Boltzmann function and shown as a function of monomer ratios. (c) Width of transition temperatures Δ Tt obtained from the fits with Boltzmann function as a function of monomer ratios.

The phenomenological Boltzmann sigmoidal equation (15) can be also used for the fits of the coil-to-globule transition sigmoidal curves of Figure 5.7a. The results are shown in Figure 5.8. The transition temperatures T_t (Figure 5.8b) are very close to the values obtained by the two-state model (Figure 5.7b). Moreover, the widths of the phase transition ΔT_t (Figure 5.8c) show an increase with increasing NIPAm content. This is in the agreement with the coil-to-globule transition curve shapes of Figure 5.7a.

3.3 Temperature-Induced Phase Transition of the Hydrogels

The free amine groups can be crosslinked by a telechelic phenylcarbonate crosslinker as shown in Chapter 3. During this reaction phenol is released, which can be detected by NMR (Figure 5.9).

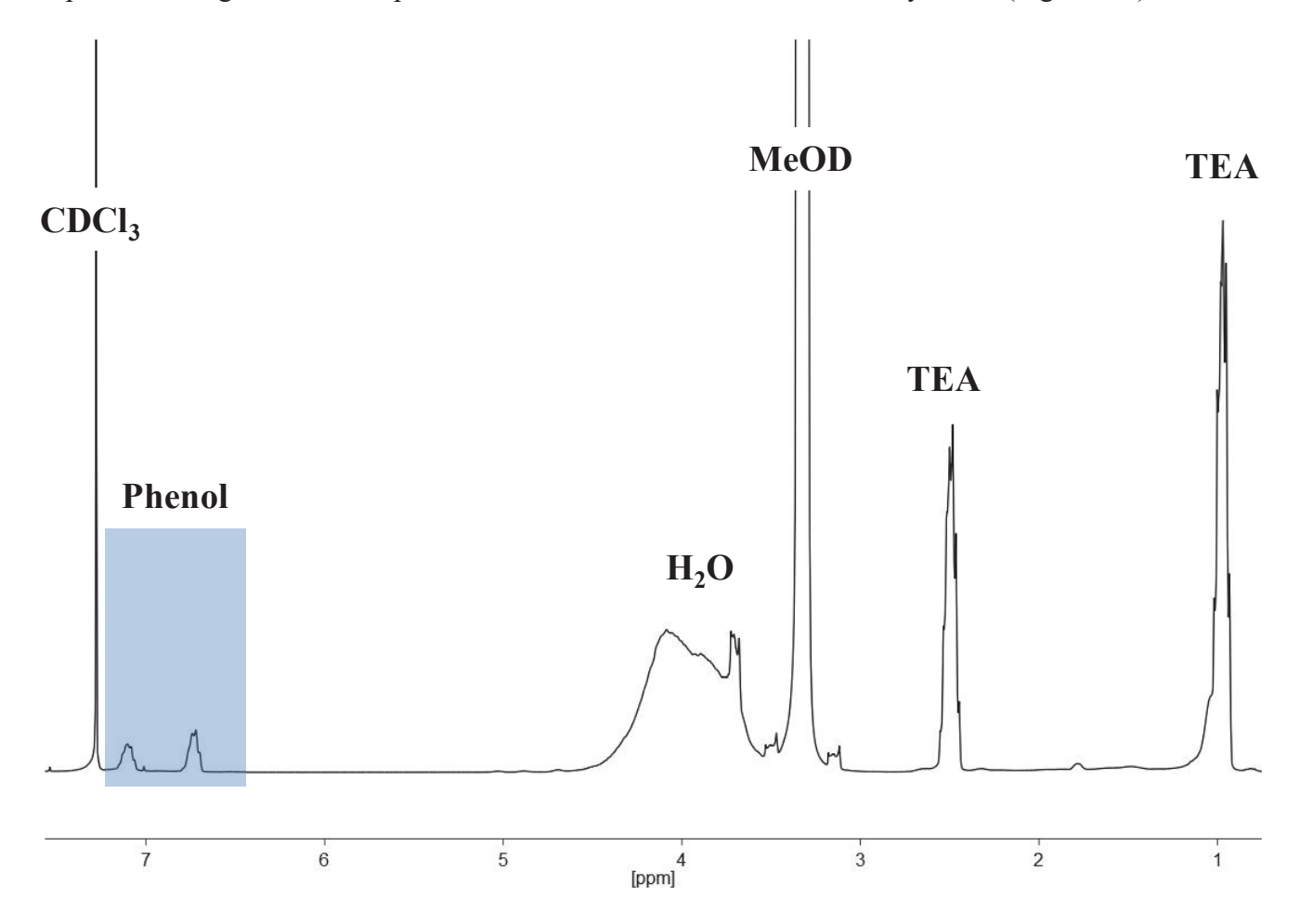


Figure 5.9. Proton NMR spectrum of the gel prepared inside the NMR tube in CDCl₃ and MeOD in presence of triethyl amine (TEA). The presence of phenol marked in blue shows the successful conversion of the crosslinker.

The phenol was subsequently washed out to obtain the gels. The ¹H NMR of the washed gels in D₂O shows the absence of phenol (blue area inFigure 5.10). Furthermore, the gelation can be detected by rheology (Figure 5.11a). The plateau moduli (G') increase with decreasing NIPAm content (29 kPa for 1:5, 43 kPa for 1:4, and 63 kPa for 1:3). This is an intuitive result as the number of free amine groups, which are available for crosslinking, increases with decreasing NIPAm content.

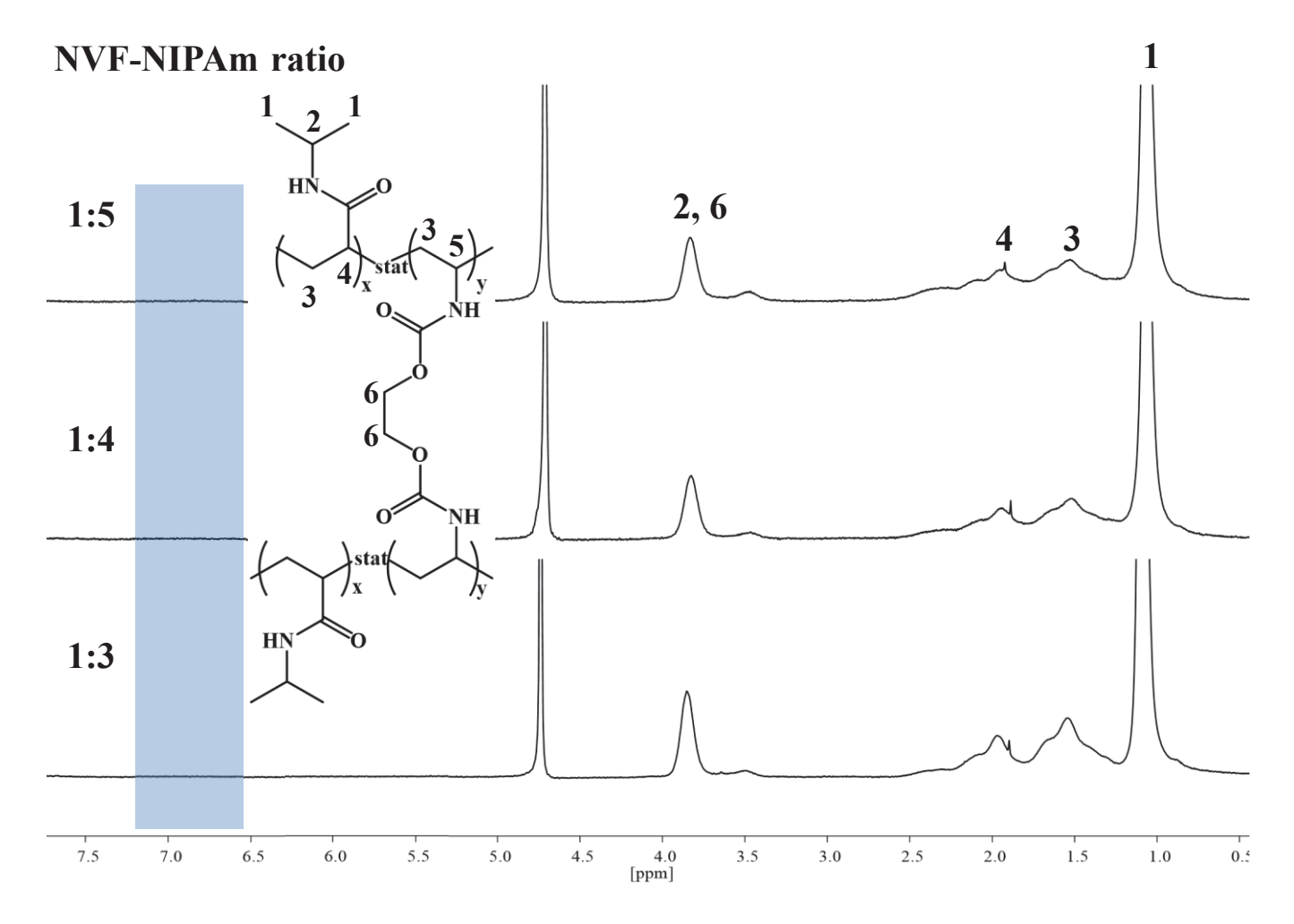


Figure 5.10. Proton NMR spectra of the washed hydrogels in D_2O . It is visible that there is no phenol present (area marked in blue).

The influence of crosslinking on the transition temperature compared to the LCST, measured by UV-Vis is shown in Figure 5.11b for the swollen gels. The transition temperature was found to be 39.4 °C for the ratio 1:5, 40.3 °C for 1:4, and 43.3 °C for 1:3 which is significantly lower compared to the free copolymers (1:5 -43.9°C, 1:4 -46.4 °C, and 1:3 -50.0 °C).

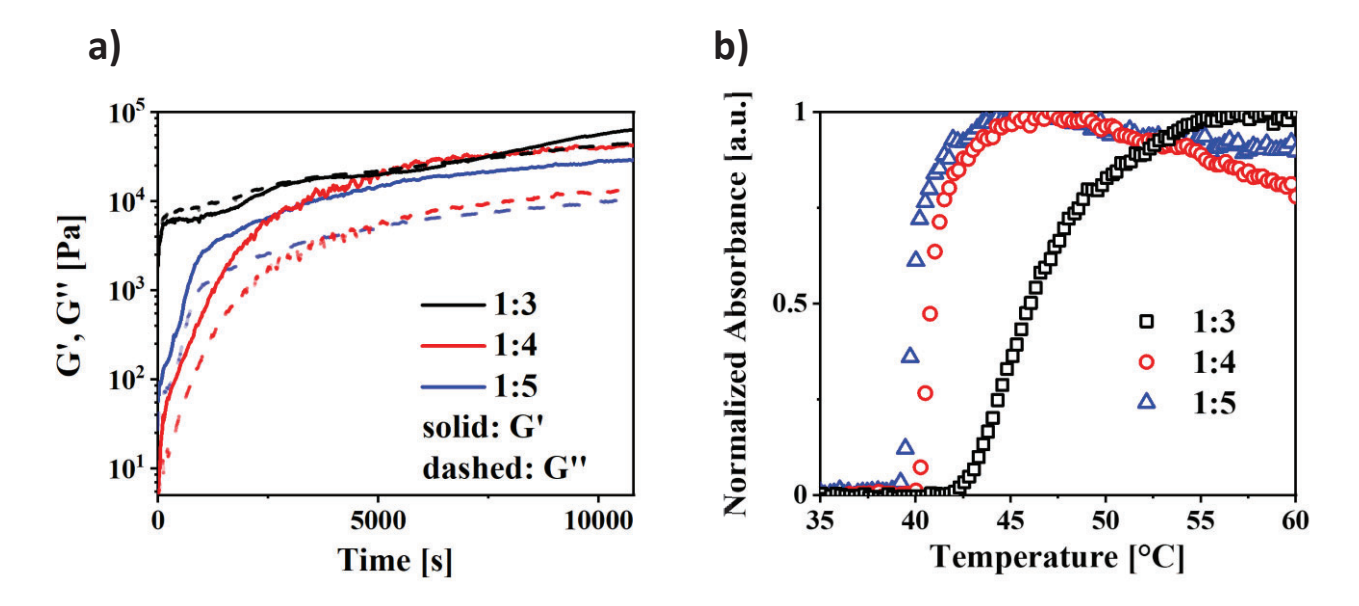


Figure 5.11. (a) The storage modulus G' and loss modulus G" in dependence of the time for the gelation of different VAm:NIPAm ratios inside the rheometer. (b) UV-Vis spectra of the swollen gels with different VAm:NIPAm ratio in dependence of the temperature (260 nm, pH = 7, 0.5 °C·min⁻¹).

This is attributed to the decrease of the hydrophilicity from the crosslinking as visible in Scheme 2. Consequently, it is also visible that the decrease of the transition temperature is strongest for the ratio 1:3. This is the ratio with the highest crosslinking density suggesting, that the hydrophobic nature of the crosslinker also imparts in the hydrophobic aggregation. Furthermore, the increase of the absorbance is much steeper for the VPTT of the gel than for the cloud point of the polymer solution, which is broadened by the broad PDI.³

Scheme 5.2. Gelation of P(VAm-co-NIPAm) with phenylcarbonate telechelic ethylene glycol.

The rheological investigation of the swollen gels is shown in Figure 5.13a. Compared to the free copolymer the transition is slightly shifted to lower temperatures, which agrees with the UV-Vis data.

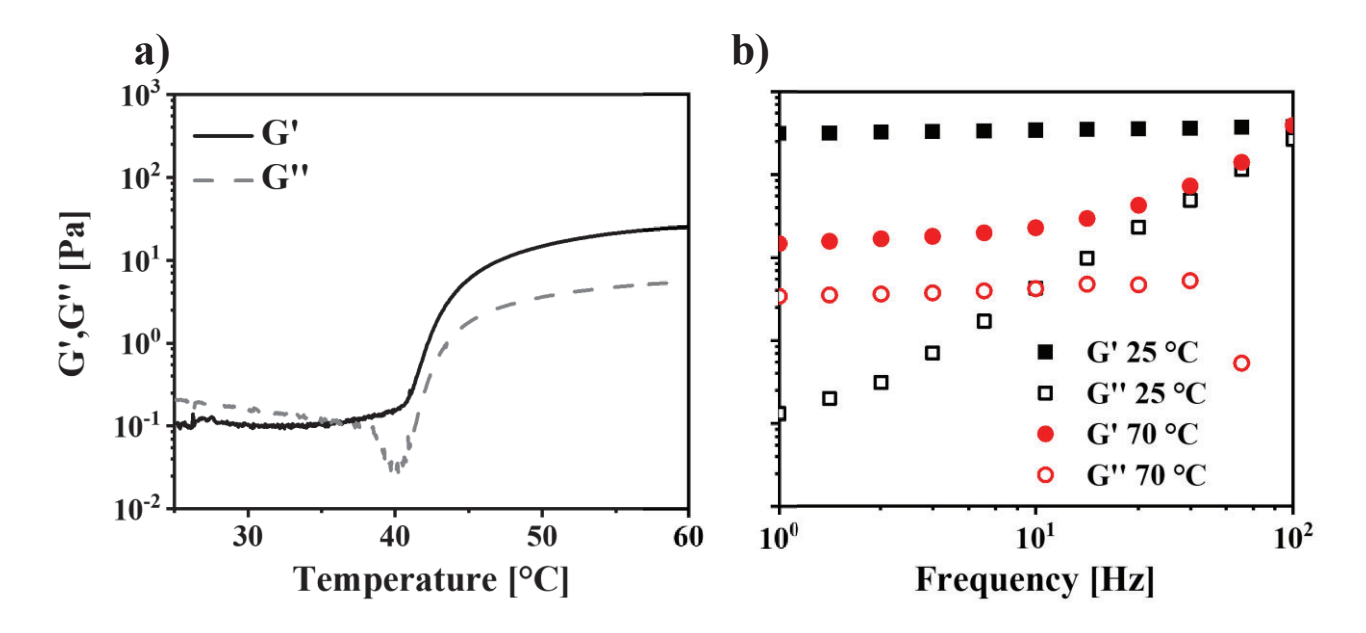


Figure 5.13. (a) G' and G" in dependence on the temperature for the hydrogel with the VAm:NIPAm ratio of 1:5. (b) shows the frequency dependence of corresponding hydrogel on G' and G" at 25 °C and 70 °C.

The frequency sweep reveals that the frequency dependence drastically decreases (from $G' \sim \omega^{1.8}$ for the copolymer to $G' \sim \omega^{0.04}$ for the hydrogel; Figure 5.5c and Figure 5.13b). This shows successful crosslinking as covalent bonds have an infinite lifetime and therefore no frequency dependence.

Proton HRMAS NMR spectra of P(VAm-co-NIPAm) hydrogels with monomer ratio of 1:5 at 20 °C (swollen state) and 65 °C (collapsed state) are shown in Figure 5.14a and 5.14b, respectively. The aliphatic spectral region is shown and peaks assignments to both monomers are made by the inset scheme of Figure 5.15a. For P(NIPAm) in the aliphatic region four peaks were detected and correspond to methyl protons of N-isopropyl (δ_{CH3} 1.2 ppm), CH protons of the same group (δ_{CH} 3.9 ppm), methylene protons (δ_{CH2} 1.6 ppm), and methane protons (δ_{CH2} 1.7 ppm). The proton peak at δ_{HDO} 4.8 ppm corresponds to protonated D₂O.

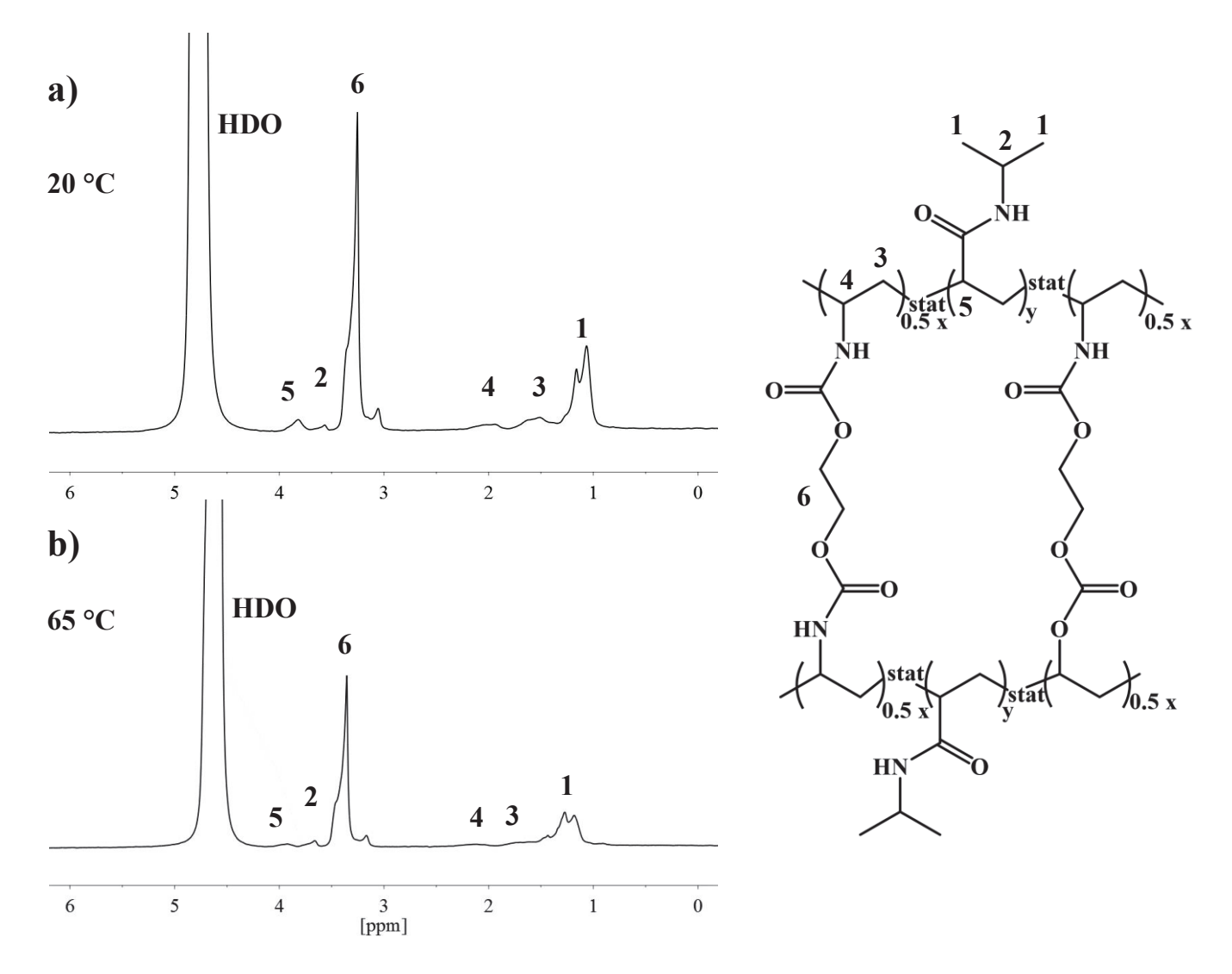


Figure 5.14. Proton HRMAS NMR spectra of P(VAm-co-NIPAm) hydrogel with monomer ratio of 1:5 measured at (a) 20 °C, and (b) 65 °C. The resonances corresponding to the VAm and NIPAm monomers are designed by numbers in the legend inset of Figure 5a and in the two polymer networks spectra.

The thermoresponsive isopropylgroup of NIPAm changes the integral intensity in the process of temperature induced phase transition as evident in Figure 5.14. Moreover, the integral intensity of VAm monomer and the crosslinker that is not thermoresponsive, is indirectly affected by the hindrance in chains and side chains dynamics of polymer backbone in the process of NIPAm collapse (compare Figure 5.14a to Figure 5b).

The volume phase transition of hydrogels is encoded in the change of the NMR spectral integral intensity that was taken for the full aliphatic region. This spectral region is dominated by the resonances of thermoresponsive NIPAm monomers. The restriction of side-chain dynamics due to hydrogel collapse broadens the NMR peaks such that at the end of phase transition these resonances are reduced in intensity

(Figure 5.15a). Temperature-induced phase transition was investigated by ¹H HRMAS NMR spectroscopy for P(VAm-*co*-NIPAm) hydrogels with the same values of VAm:NIPAm monomer ratios as those of the linear polymers (Figure 5.7a). Comparing the temperature-induced phase transition sigmoidal curves for linear polymers and hydrogels (Figure 5.7a and Figure 5.15a) we can note that differences exist in the dependences upon monomer ratios. The fits of good quality by the two - state model (Equation 14) of phase transition curves for P(VAm-*co*-NIPAM) hydrogels are shown in Figure 5.15a with continuous lines.

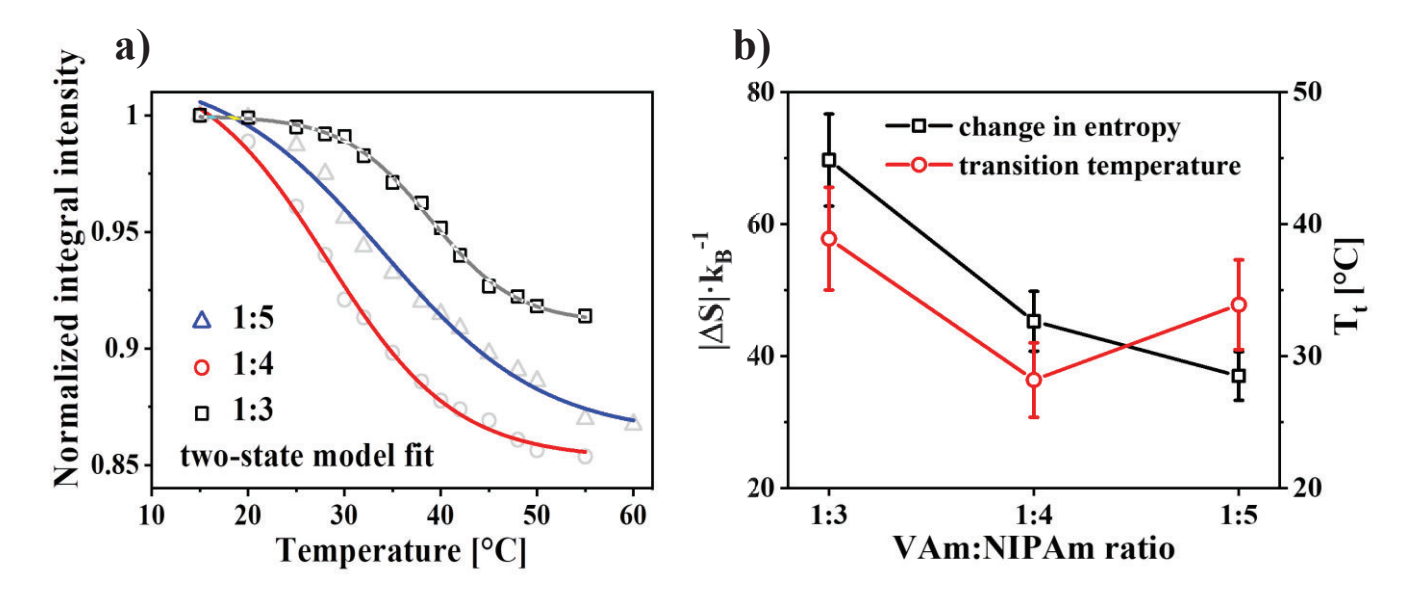


Figure 5.15. (a) Normalized integral intensity of the 1 H HRMAS spectra for P(VAm-co-NIPAM) side chains within hydrogels with monomer ratios of 1:3 (circles), 1:4 (squares), and 1:5 (triangles). The fits with the two-state model (Equation 14) are shown by continuous lines. (b) Transition temperatures T_{t} and normalized absolute change in the entropy $|\Delta S| \cdot k_{B}^{-1}$ in the process of temperature-induced phase transition as a function of monomer ratio of P(VAm-co-NIPAM) hydrogels. These thermodynamic parameters were obtained by the fits of data shown in (a) with the two-state model (Equation (14)).

The data fits with the two-state model lead to the values of the transition temperature T_t and normalized absolute value of entropy $|\Delta S| \cdot k_B^{-1}$ as shown in Figure 5.15b. The value of T_t decreases slightly with increasing NIPAm content that means with decrease in crosslink density revealing, that less thermal energy is needed to break the cooperative water molecule interactions with the polymer network. Furthermore, the change of $|\Delta S| \cdot k_B^{-1}$ as a function of the monomer ratio Figure 5.15b for the networks shows that the hydrogel collapsed state has a polymer network more disordered for the monomer ratio of 1:5 compared to that of 1:3. Moreover, the change in the entropy is also affected by the existence of heterogeneous collapsed network, that is proved in the next sections by transverse magnetization relaxation (T_2) and self-diffusion coefficient (D) of water.

The volume phase transition curves of hydrogels (Figure 5.15a) were also fitted with Boltzmann sigmoidal functions and the results are depicted in Figure 5.16a. The transition temperature and width of volume phase transition obtained by the Boltzmann sigmoidal function fits are shown in Figure 5.16b and Figure 5.16c, respectively. In agreement with the transition temperatures obtained by two-state model (Figure 5.15b) a small decrease in the values of T_t was revealed (Figure 5.15b). Moreover, the width of the phase transition ΔT_t (Figure 5.16c) shows an increase with the increase of NIPAm monomer content. The quantity ΔT_t is related to the equilibration time of the network along the volume phase transition and shows that with increase of the NIPAM content in the statistical polymer backbone the achievement of thermodynamic equilibrium becomes longer. 37,38

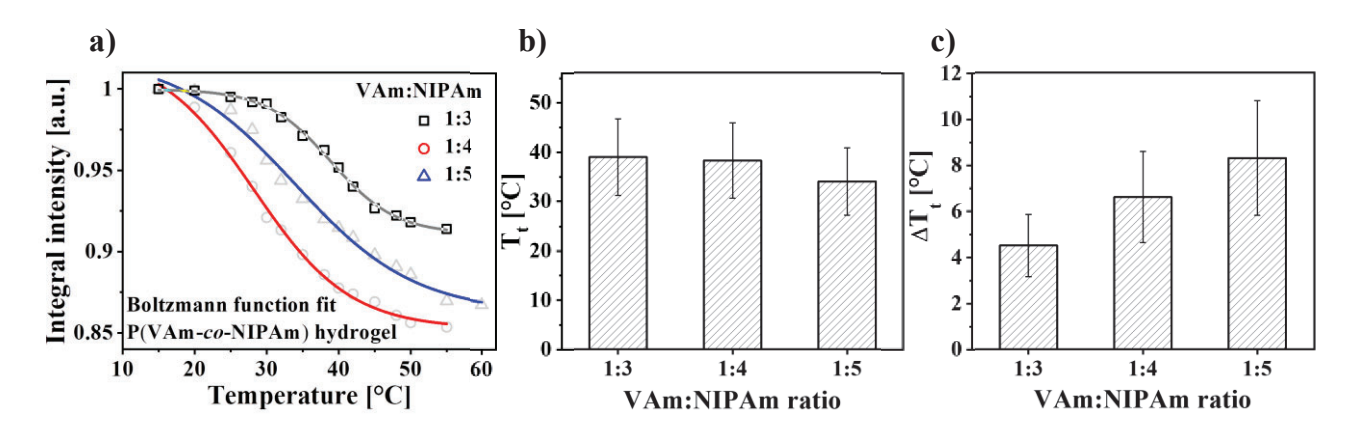


Figure 5.16. (a) Temperature-induced phase transition curves of P(VAm-co-NIPAm) hydrogels with different VAm:NIPAm monomer ratios. The data were fitted with Boltzmann functions and shown with continuous lines. (b) Transition temperatures Tt, and (c) width of transition temperatures Δ Tt as a function of monomer ratios obtained from the fits with Boltzmann functions.

3.4 Water States and Side – Chain Dynamics by ¹H HRMAS

Proton HRMAS NMR spectroscopy in combination with spin-echo approach offer the possibility to measure separately the transverse magnetization relaxation (T_2) of ¹HDO complex as well as that of polymer side chains. Proton T_2 decays of protonated deuterated water within p(VAm-co-NIPAm) hydrogels with the monomer ratios 1:3, 1:4, and 1:5 are shown in Figure 5.17a.

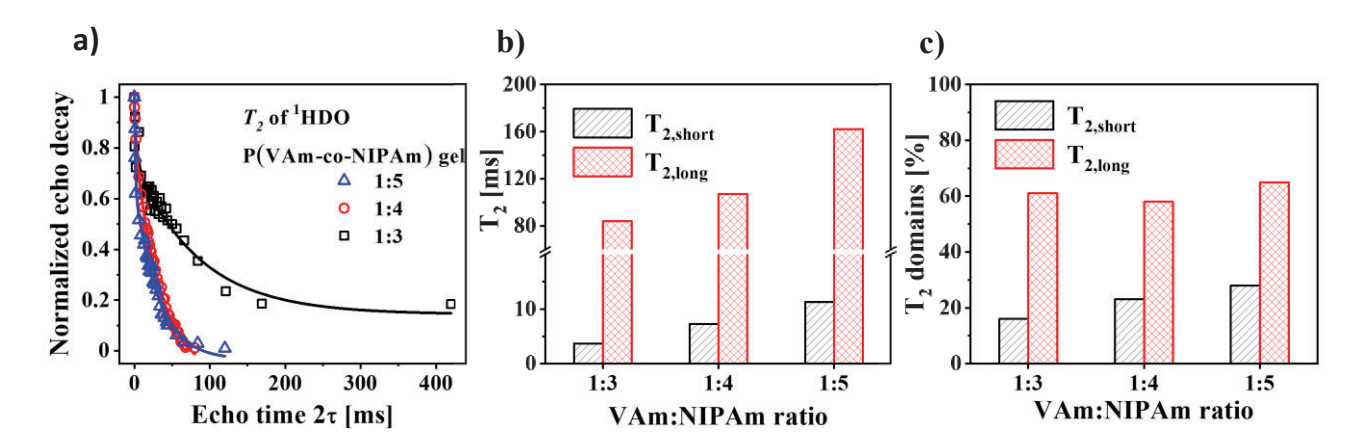


Figure 5.17. (a) Proton transverse magnetization decays of ¹HDO within P(VAm-*co*-NIPAm) hydrogels with monomer ratios of 1:3 (squares), 1:4 (circles), and 1:5 (triangles). The HRMAS NMR measurements were made at 23 °C under sample rotation at the magic angle with the frequency of 5 kHz. The normalized echo decays were fitted with a biexponential functions Equation 16 (continuous lines) (b) The dependence of T_{2,short} and T_{2,long} for ¹HDO water molecules upon monomer ratios within P(VAm-*co*-NIPAm) hydrogels measured at 23 °C. (c) The T₂ fractions of ¹HDO complex in hydrogel pores function of monomer ratios. Estimated errors in the transverse relaxation values are of the order of 5 %.

The proton magnetization relaxation data are given by the integral spectrum of 1 HDO and depicted in Figure 5.17a as a function of the spin - echo time 2τ . The best fits of these decays were given by a biexponential function, *i.e.*,

$$\frac{I(2\tau)}{I(0)} = A_0 + A_1 e^{-\frac{2\tau}{T_{2,short}}} + A_2 e^{-\frac{2\tau}{T_{2,long}}},\tag{16}$$

where the exponential amplitudes $A_{1,2}$ are related to the proton fractions characterized by $T_{2,short}$ and $T_{2,long}$, respectively. The T_2 relaxation times of ¹HDO and their distributions within hydrogel are shown in Figure 5.17b and Figure 5.17c, respectively, as a function of VAm:NIPAm ratio of the hydrogel in the swollen state at 23 °C. The water molecules moving inside the hydrogel pores have a distribution of the correlation times that can be approximated by a bimodal distribution. ^{17,39} The bound water have a hindered dynamics due to the interactions with polymer segments and therefore, a stronger proton dipolar interactions that leads to short values of T_2 (hereafter denoted by $T_{2,short}$). The free or bulk water present in the main volume of the network pores are characterized by fast modulation of dipolar interactions by the rotation and translation of the molecules leading to long values of T_2 relaxation times (hereafter denoted by $T_{2,long}$). With increasing NIPAm content the crosslinking density is lower and hence the pore size is increased. Therefore, the hindering effect of the polymer network upon the water molecules dynamics is reduced and $T_{2,long}$

increased (Figure 5.17b). The amplitude and frequency of polymer chains and side-chains dynamics become bigger when the hydrogel pores increase in size leading to a $T_{2,\text{short}}$ increase (Figure 5.17b). For the reasons discussed above the T_2 fractions follow the same trend as that of transverse relaxation times (Figure 5.17c). Proton transverse magnetization decays of p(VAm-co-NIPAm) hydrogel side chains in the swollen state with VAm:NIPAm ratio of 1:3, 1:4, and 1:5 are shown in Figure 5.18a. The measurements were made by a combination of spin echo and HRMAS NMR spectra taking the integral intensities of the aliphatic spectral region. Proton transverse magnetization decays can be best fitted with biexponential functions (Equation (16)) having the decay rates of $T_{2,\text{short}}^{-1}$ and $T_{2,\text{long}}^{-1}$. Along the polymer chains segmental dynamics heterogeneity is present similar to that reported for thermosensitive native α -elastin biohybrid microgel. Hence, the $T_{2,\text{short}}$, can be assigned to the protons in the crosslink domains of VAm monomer and $T_{2,\text{long}}$ to the hydrophilic network domains of NIPAm. The transverse magnetization times ($T_{2,\text{short}}$) are function of the crosslink density, *i.e.*, VAm content of the hydrogel network. These dependences are shown in Figure 5.18b. Both T_2 components increase with increasing NIPAm content due to the bigger pores and therefore, larger chain flexibility (Figure 5.18b). The most sensitive to the increase in monomer ratios is $T_{2,\text{short}}$ of side chains as depicted in Figure 5.18c.

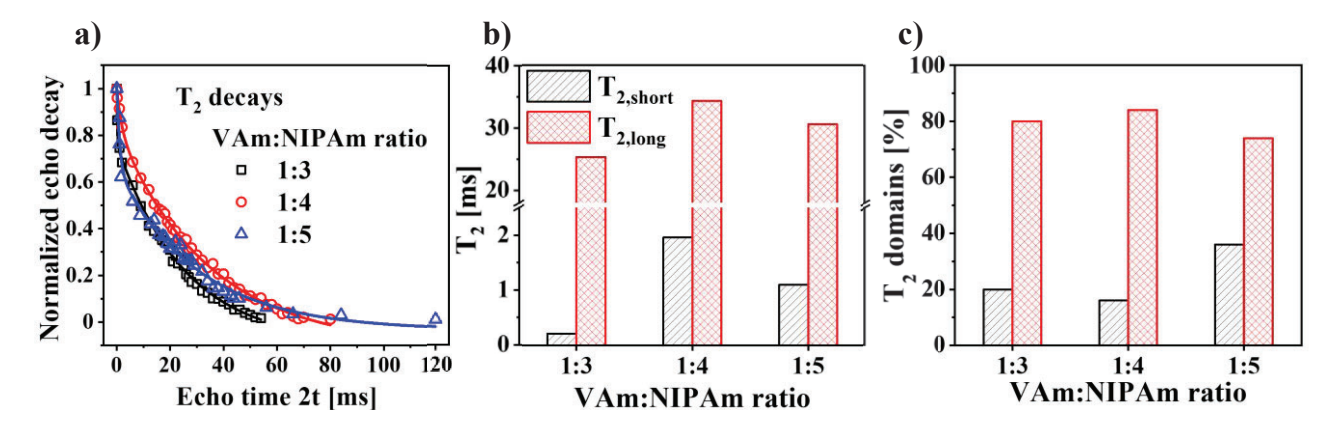


Figure 5.18. (a) Proton transverse magnetization decays of P(VAm-co-NIPAm) hydrogel side chains in the swollen state with VAm:NIPAm ratios of 1:3 (squares), 1:4 (circles), and 1:5 (triangles). The HRNMR measurements were made at 23 °C under sample rotation at the magic angle with the frequency of 5 kHz. The normalized echo decays were fitted with a biexponential functions (continuous lines). (b) The dependence of proton $T_{2,\text{short}}$ and $T_{2,\text{long}}$ of polymer chains and side chains upon monomer ratios for P(VAm-co-NIPAm) hydrogel in the swollen state measured at 23 °C. (c) The T_2 fractions along the polymer chains are shown as a function of monomer ratios. Estimated errors in the transverse relaxation values are of the order of 5 %.

3.5 Polymer Diffusometry by ¹H HRNMR.

Mass transport of linear P(VAm-co-NIPAm) with tuned hydrophilicity of polymer chains in deuterated water can be investigated by ¹H HRNMR diffusometry. ^{17,18,43,44} The dependence of integral intensity I(q) of NMR peaks in the aliphatic region of linear P(VAm-co-NIPAm) upon the diffusion wave vector q, is given by Equation (2)¹⁹

For a polymer dispersion with a bimodal distribution of fast (D_{fast}) and slow (D_{slow}) diffusivities the corresponding diffusion decay is given by

$$\frac{I(q)}{I(0)} = A_0 + A_1 e^{-q^2 \left(\Delta - \frac{\delta}{3}\right) D_{fast}} + A_2 e^{-q^2 \left(\Delta - \frac{\delta}{3}\right) D_{slow}},\tag{17}$$

where A_0 is the baseline and the fractions of polymer diffusivity are denoted by $A_{1,2}$.

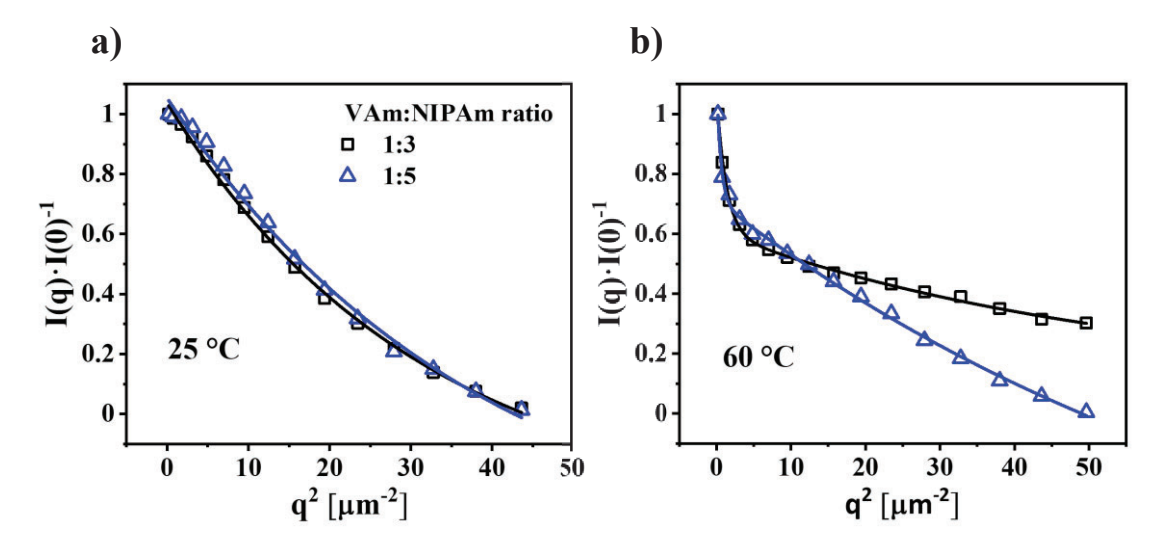


Figure 5.19. Diffusivity decays for linear P(VAm-co-NIPAM) with VAm:NIPAm ratios of 1:3 and 1:5 measured at temperature of 25 °C (a) and 60 °C (b). The continuous lines are fits by Equation (2) in (a) and Equation (17) in (b)

The experimental measured dependences of $I(q) \cdot I(0)^{-1}$ ratios upon q^2 are shown in Figure 5.19 for linear P(VAm-co-NIPAm) with monomer ratios of 1:3 and 1:5 measured at 25 °C and 60 °C, respectively. The diffusivity decays measured at 25 °C are fitted in a good approximation by a single exponential function (Equation (2)). The semidilute polymers are in the coil states below LCST with the diffusivities D that are given in Table 5. The linear polymers collapsed into globule states that aggregate at temperature of 60 °C. A bimodal distribution of aggregates was detected with small aggregates or single-globules characterized by D_{fast} and swollen domains with smaller diffusivity D_{slow} (Table 5).

Table 5. Diffusivity of linear P(VAm-co-NIPAm) with monomer ratios of 1:3 and 1:5 measured at 25 °C and 60 °C. Equation (2) and Equation (17) where used for single exponential and biexponential fits, respectively (Figure 9).

VAm:NIPAm ratio	Diffusivity	Diffusivity	
	at 25 °C [m ² ·s ⁻¹] a	at 60 °C [m ² ·s ⁻¹] a	
1:3	$D = 1.60 \cdot 10^{-12}$	$D_{\text{fast}} = 3.87 \cdot 10^{-11}$	
		$D_{\rm slow} = 9.30 \cdot 10^{-13}$	
1:5	$D = 1.29 \cdot 10^{-12}$	$D_{\rm fast} = 9.21 \cdot 10^{-11}$	
		$D_{\text{slow}} = 6.20 \cdot 10^{-13}$	

^aThe errors are of the order of 5 %.

From the data of Table 5 taken at 25 °C we conclude that in the semidilute concentration regime of linear p(VAm-co-NIPAm) the mass transport is described by a normal diffusion with a mean square displacement of $\langle r^2 \rangle = 6D\Delta$. ^{17,18,43,44} The Einstein relationship $D = k_B T \cdot \xi^{-1}$, shows that diffusivity D is correlated with ξ that is the frictional coefficient between polymer and solvent. Hence, the polymer with monomer ratio of 1:5 has a larger frictional coefficient compared to that of polymer with 1:3 due to bigger number of hydrophilic NIPAm monomers. Furthermore, it is mentioned that diffusional kurtosis^{43,44} that is related to softer restrictions of polymer in the regime where the concentration is close to that of concentrated solutions was not detected in these experiments at temperatures below or above the LCST.

3.6 Hydrogel Morphology by Water Self-Diffusion.

In a homogeneous hydrogel without network defects two water reservoirs are assumed to exist, *i.e.* on the one hand the free water located within the hydrogel pores and on the other hand the bound water connected to the hydrophilic/hydrophobic groups of the copolymer. ⁴⁵⁻⁵⁰ The number of protons corresponding to free and bound water reservoirs are denoted by n_f and n_b , respectively. Furthermore, an exchange process with the rates k_f and k_b takes place between water reservoirs. At the thermodynamic equilibrium the detailed balance relationship: $k_f n_f = k_b n_b$, is fulfilled. Moreover, it is assumed that the effective diffusion coefficient of bound water in the swollen and collapsed states of the hydrogel is small, *i.e.*, $D_b \approx 0$, and this diffusion process is not detected due to the small values of magnetic field gradients used in our diffusion

experiments. In the approximation $T_{2b} \ll T_{2f}$ the normalized amplitude of stimulated echo in PGST experiment can be written as^{49,50}

$$\frac{I(q)}{I(0)} \approx \frac{M_f(q)}{M_f(0)},\tag{18}$$

where the amplitude of the stimulated echo is denoted by I(q), that is a function of the wave vector q. The normalized magnetization of the free water reservoir is given by 49,50

$$\frac{M_f(q)}{M_f(0)} = \begin{bmatrix} (a_+ - k_f - k_b - R_{1b}) exp(-a_+ \Delta) \\ -(a_- - k_f - k_b - R_{1b}) exp(-a_- \Delta) \end{bmatrix} (a_+ - a_-)^{-1},$$
(19)

where

$$a_{\pm} = \frac{1}{2} \left[q^2 D_f + k_f + k_b + R_{1f} + R_{1b} \right] \pm \frac{1}{2} \left[\left(q^2 D_f + k_f - k_b + R_{1f} - R_{1b} \right)^2 + 4k_f k_b \right]^{1/2}.$$
(20)

In the above equations the longitudinal magnetization relaxation rates for the proton reservoirs are given by R_{1f} and R_{1b} , and the diffusion time is denoted by Δ . The apparent diffusion coefficient for the proton fast reservoir is D_f and in the following it is denoted by D, and D_b are neglected $(D_f \gg D_b)$. In the fast water exchange limit and for small values of q it is given that $k_f + k_b \gg q^2 D$, and $k_f + k_b \gg R_{1f} + R_{1b}$, and hence from Equation (20) $a_+ \gg a_-$. In the limit of the above approximations the stimulated echo amplitude decay described by Equation (18), becomes single exponential with the exponent $a_- \approx q^2 D$, when $k_f < k_b$, as a result of the detailed balance relationship for $n_f > n_b$. Therefore, from the above equations it can be concluded that

$$ln\left(\frac{I(b)}{I(0)}\right) \cong -bD,$$
 (21)

where

$$b \equiv \gamma^2 \delta^2 \left(\Delta - \frac{\delta}{3} \right) g^2 \tag{22}$$

or in term of q wave vector

$$b \equiv q^2 \left(\Delta - \frac{\delta}{3} \right). \tag{23}$$

Equation (21) is valid for a homogenous hydrogel that is assumed to be present for the swollen state. It is shown below that for the collapsed state a heterogeneous hydrogel is detected with a bimodal distribution of pores that leads to biexponential diffusion decay. The water diffusivity

D is an effective diffusivity that means an average over length scales much longer than the correlation lengths of the pore spaces.⁴⁸

¹H HRNMR diffusion to measure the self-diffusion of the water molecules within hydrogels. The diffusion decays described by Equation (21) for water molecules within p(VAm-co-NIPAm) hydrogels with monomer ratio 1:5 are depicted in Figure 5.20. At temperature of 25 °C (Figure 5.20a) the thermoresponsive hydrogel is in the swollen

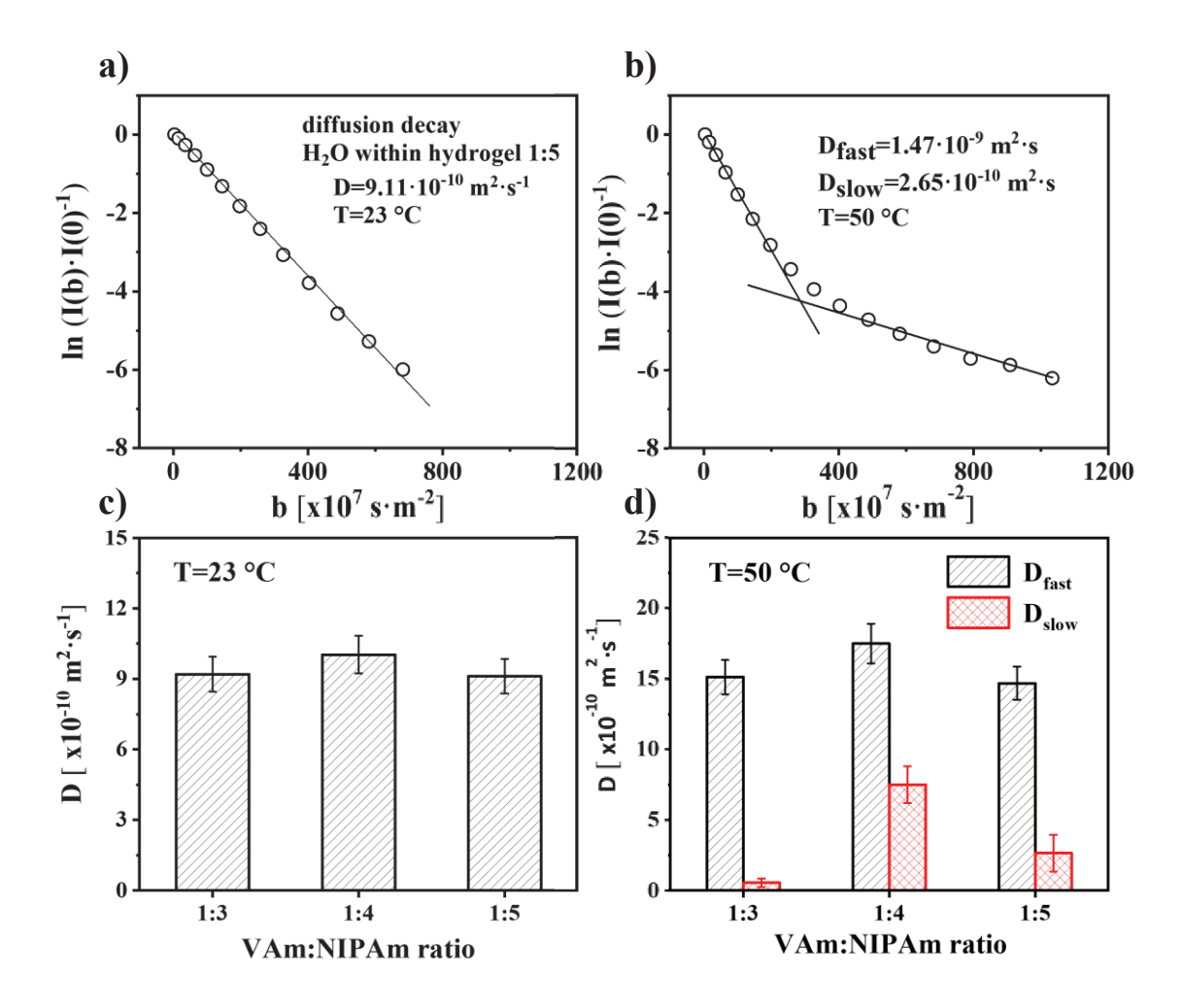


Figure 5.20. Water self-diffusion decays in the logarithmic scale within P(VAm-co-NIPAM) hydrogels with monomer ratio of 1:5 measured at two temperatures of 23 °C (a) and 50 °C (b). The continuous lines are linear fits by Equation (21) with the slopes being related to the H₂O diffusivity. (c) Water diffusivities for P(VAm-co-NIPAM) hydrogels versus VAm:NIPAm ratio measured at temperatures of 23 °C (swollen state) and 50 °C (d) (collapsed state).

state and only one diffusion coefficient was detected for the small range of b parameter as it is revealed by the linear fit. The hydrogel at 50 °C is in a collapsed state and two water diffusivities (D_{fast} and D_{slow}) were detected by NMR diffusometry (Figure 5.20b).

Using the result of the diffusion exchange model discussed above in the length regime explored by the water molecules diffusion the polymer network of swollen hydrogels is homogeneous with a uniform pore sizes. This is valid for all hydrogels investigated having VAm:NIPAm ratios of 1:3, 1:4, and 1:5.

This fact is revealed by the water diffusivities shown in Figure 5.20a. These diffusivities describe the Brownian motion of water molecules in network pores and show a weak dependence upon the monomer ratio. Moreover, we mention that D values reported in Figure 5.20a are smaller than that of free water at 20 °C of $D = 2.031 \cdot 10^{-9}$ m²·s⁻¹.

This is explained by the fact that polymer chains retard water molecules movement by reducing the average free volume, by increasing the hydrodynamic drag, and by acting as physical obstruction.⁵¹

In the case of hydrogel networks made of flexible polymer chains the most consistent solute diffusion model with data was that based on the hydrodynamic scaling. The corresponding relation is given by ^{51,52}

$$\frac{D}{D_0} = e^{-k_c R_S \varphi^{0.75}},\tag{24}$$

where D_0 is the diffusivity of the water at infinite dilution, *i.e.*, of bulk water, k_c is a constant for a given polymer network-solvent system, R_s is the radius of the solute, and φ is the volume fraction of the polymer in the hydrogel. From Equation (24) the diffusivity shown in Figure 5.20c reveals that the volume fraction of the polymer φ at 23 °C is not changing essentially with the increase in the monomer ratios, *i.e.*, with the decrease in the crosslink density. Furthermore, the following proportionalities are valid for the effective diffusivity D, *i.e.*, $D \propto \Pi$, and $D \propto \tau_{diff}^{-1}$ where Π is the hydrogel porosity and τ_{diff}^{-1} , is the inverse diffusive tortuosity, respectively.⁴⁸ Hence, the hydrogel porosity and inverse diffusive tortuosity follow the same trend as that of water diffusivity (Figure 5.20c).

At temperature of 50 °C the hydrogels are characterized by water molecules having fast and slow diffusivities as depicted in Figure 5.20d. The existence of a collapsed polymer network with a bimodal distribution of pores offers a plausible interpretation. In this case the water molecules diffusing in the small pores of collapsed network have a diffusivity D_{slow} of an order of magnitude smaller than that of bulk water $D = 3.935 \cdot 10^{-9} \,\text{m}^2 \cdot \text{s}^{-1}$ at 50 °C. For bigger pores at 50 °C the water diffusivity D_{fast} is larger but of the same order of magnitude compared to that of the water molecules into hydrogels at 23 °C (compare Figure 5.20c and Figure 5.20d).

In principle the microsegregation that can induces different pore size distribution can be realized for neutral hydrogels if the polymer chains have a pronounced amphiphilic character. The existence of multiple conformational transitions for poly(*N*-vinylcaprolactam) hydrogels were confirmed by high-sensitivity microcalorimetric measurements.⁵³ According to this investigation, the hydrogel undergoes two successive cooperative transitions that are associated with the microsegregation resulting in formation of hydrophobic domains whereas the high temperature transition is due to the hydrogel volume collapse. Furthermore, for poly(*N*-isopropyacrylamide) (PNIPAm) hydrogels only one volume phase transition was commonly detected by differential scanning calorimetry without any information about pore size distribution.⁵⁴⁻⁵⁶ The water diffusivity results of P(VAm-co-NIPAm) hydrogels having different monomer ratios reveal that pore size distribution *i.e.*, polymer network heterogeneity exists in a range of temperatures above the volume phase transition (Figure 5.20b).

The distribution of network heterogeneity of hydrogels is actually more complex and has important dynamic consequences.⁵⁷ To clarify this point it is stated that the thermodynamic state of an ergodic system after a long time is nearly independent of its initial state.⁵⁸ The presence of static inhomogeneity of gels which results from fluctuations during the gelation process can lead to differences between time averages and statistical ensemble averages. This non-ergodicity was shown to be present in dynamic light scattering (DLS) experiments when the light beam explores different gel regions.⁵² Moreover, a combination of macrorheology using traditional rheometers and optical approach of single-particle tracking was able to reveal the non-ergodicity of micrometer-sized traces diffusing in mucin gels.^{59,60} Furthermore, the nonergodicity of the polymer network is not revealed in the water self-diffusion measurements made by NMR. The NMR signal is detected from the entire hydrogel volume and hence, the ensemble average is made simultaneously with time average from all sample regions.

4. Conclusion

Thermoresponsive P(VAm-co-NIPAm) copolymers were successfully prepared by free radical polymerization. The copolymerization parameters indicate a statistical distribution of the monomers allowing the production of homogeneous water born hydrogels. The VPTT as well as the crosslinking density can be tuned by the VAm:NIPAm ratio. As shown by UV-Vis spectroscopy and rheology, crosslinking could decrease the VPTT to the physiological relevant region below 40 °C and render the hydrogels therefore attractive for biomedical application. Proton high-resolution MAS NMR spectroscopy was applied to obtain information related to

the temperature-induced phase transition of linear P(VAm-co-NIPAm) polymers and the corresponding hydrogels. The effect of tuned thermoresponsivity upon the phase transition temperature, change in the entropy and the width of the phase transition were obtained using the temperature dependence of spectral integral intensities of NMR peaks by fits with the novel two-state model and Boltzmann sigmoidal function. The dependences of transition temperature upon the VAm:NIPAm monomer ratios are different for linear polymer and hydrogels in the processes of coil-to-globule and swollen-to-collapse transitions, respectively. In case of the linear polymer the transition temperature is increased due to more extended hydrogen bond structure. While in case of the hydrogels the hydrophobic character of the crosslinker lowers the transition temperature. Furthermore, the larger contribution to elastic free energy of hydrogels shows, that the system is more ordered compared to the linear polymer as revealed by entropy changes.

The hydrogel morphology is related to the average pore size that is reflected in the water molecule diffusivities. The hydrogels in the swollen state can be considered in a good approximation to be homogeneous for the values of monomer ratio investigated. This is not the case for the hydrogels in the collapsed state where two water diffusivities were detected. Furthermore, free and bound states of water in hydrogel pores that change with the monomer ratio, were detected by T_2 measurements. The transverse magnetization relaxation was also used to reveal the network side chains dynamics. A bimodal heterogeneity was detected that we assume to be related to the free and bound water.

4. References

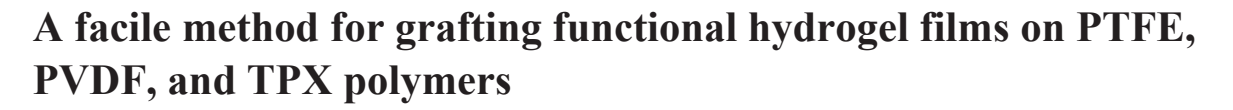
- 1 Pich, A. & Richtering, W. Chemical Design of Responsive Microgels. (Springer, 2010).
- Roy, D., Brooks, W. L. & Sumerlin, B. S. New Directions in Thermoresponsive Polymers. *Chem. Soc. Rev.* **42**, 7214-7243, doi:10.1039/c3cs35499g (2013).
- Halperin, A., Kroger, M. & Winnik, F. M. Poly(*N*-isopropylacrylamide) Phase Diagrams: Fifty Years of Research. *Angew. Chem. Int. Ed.* **54**, 15342-15367, doi:10.1002/anie.201506663 (2015).
- 4 Hertle, Y. & Hellweg, T. Thermoresponsive copolymer microgels. *J. Mater. Chem. B* 1, 5874-5885, doi:10.1039/c3tb21143f (2013).
- Lue, S. J., Chen, C.-H. & Shih, C.-M. Tuning of Lower Critical Solution Temperature (LCST) of Poly(N-Isopropylacrylamide-co-Acrylic acid) Hydrogels. *J. Macromol. Sci. B* **50**, 563-579, doi:10.1080/00222341003784550 (2011).
- Ku, J., Barros Timmons, A. & Pelton, R. N-Vinylformamide as a Route to Amine-Containing Latexes and Microgels. *Colloid Polym. Sci.* **282**, 256-263, doi:10.1007/s00396-003-0901-6 (2004).

- Yue, M., Imai, K., Miura, Y. & Hoshino, Y. Design and Preparation of Thermo-Responsive Vinylamine-Containing Micro-gel Particles for Reversible Absorption of Carbon Dioxide. *Polym. J.* **49**, 601-606, doi:10.1038/pj.2017.28 (2017).
- 8 Xu, K. *et al.* A novel multi-responsive polyampholyte composite hydrogel with excellent mechanical strength and rapid shrinking rate. *J. Colloid Interf. Sci.* **345**, 360-368, doi:10.1016/j.jcis.2010.01.058 (2010).
- Fischer, T., Köhler, J., Keul, H., Singh, S. & Möller, M. Highly Swellable Hydrogels from Waterborne Poly(vinylamine-co-acetamide). *Macromol. Chem. Phys.* **219**, 1800399-1800408, doi:10.1002/macp.201800399 (2018).
- Schweizerhof, S. *et al.* Temperature-Induced Phase Transition Characterization of Responsive Polymer Brushes Grafted onto Nanoparticles. *Macromol. Chem. Phys.* **218**, 1600495-1600506, doi:10.1002/macp.201600495 (2017).
- Schweizerhof, S., Demco, D. E., Mourran, A., Fechete, R. & Möller, M. Polymers Diffusivity Encoded by Stimuli-Induced Phase Transition: Theory and Application to Poly(*N*-Isopropylacrylamide) with Hydrophilic and Hydrophobic End Groups. *Macromol. Chem. Phys.* **219**, doi:10.1002/macp.201700587 (2018).
- Schweizerhof, S., Demco, D. E., Mourran, A., Fechete, R. & Moller, M. Diffusion of Gold Nanorods Functionalized with Thermoresponsive Polymer Brushes. *Langmuir* **34**, 8031-8041, doi:10.1021/acs.langmuir.8b01289 (2018).
- Schweizerhof, S. *et al.* Thermodynamic Parameters of Temperature-Induced Phase Transition for Brushes onto Nanoparticles: Hydrophilic versus Hydrophobic End-Groups Functionalization. *Macromol. Rapid Commun.* **38**, 1700362-1700368, doi:10.1002/marc.201700362 (2017).
- Singh, S. *et al.* Aggregation Behaviour of Biohybrid Microgels from Elastin-like Recombinamers. *Soft Matter* **12**, 6240-6252, doi:10.1039/c6sm00954a (2016).
- Mukherji, D., Marques, C. M. & Kremer, K. Polymer Collapse in Miscible Good Solvents is a Generic Phenomenon Driven by Preferential Adsorption. *Nat. Commun.* **5**, 4882-4887, doi:10.1038/ncomms5882 (2014).
- Schmidt-Rohr, K. & Spiess, H. *Multidimensional Solid-State NMR and Polymers*. (Academic Press, 1994).
- 17 Callaghan, P. T. *Translational Dynamics and Magnetic Resonance*. (Oxford University Press, 2011).
- 18 Kimmich, R. Tomography, Diffusometry, Relaxometry. (Springer-Verlag, 1997).
- Stejskal, E. O. & Tanner, J. E. Spin Diffusion Measurements: Spin Echoes in the Presence of a Time-Dependent Field Gradient. *J. Chem. Phys.* **42**, 288-292, doi:10.1063/1.1695690 (1965).
- Ru, G., Wang, N., Huang, S. & Feng, J. ¹H HRMAS NMR Study on Phase Transition of Poly(*N*-isopropylacrylamide) Gels with and without Grafted CombType Chains. *Macromolecules* **42**, 2074-2078 (2009).
- Li, Y. & Tanaka, T. Kinetics of swelling and shrinking of gels. *J. Chem. Phys.* **92**, 1365-1371, doi:10.1063/1.458148 (1990).
- Haraguchi, K., Takehisa, T. & Fan, S. Effects of Clay Content on the Properties of Nanocomposite Hydrogels Composed of Poly(*N*-isopropylacrylamide) and Clay. *Macromolecules* **35**, 10162-10171 (2002).
- Kazuya, Y. *et al.* Synthesis and functionalities of poly(N-vinylalkylamide). XIV. Polyvinylamine produced by hydrolysis of poly(N-vinylformamide) and its functionalization. *J. Appl. Polym. Sci.* **89**, 1277-1283, doi:doi:10.1002/app.12230 (2003).
- 24 Pinschmidt, R. K. *et al.* N-Vinylformamide Building Block for Novel Polymer Structures. *J. Macromol. Sci. A* **34**, 1885-1905, doi:10.1080/10601329708010315 (1997).

- Stile, R. A., Burghardt, W. R. & Healy, K. E. Synthesis and Characterization of Injectable Poly(*N*-isopropylacrylamide)-Based Hydrogels that Support Tissue Formation in Vitro. *Macromolecules* **32**, 7370-7379 (1999).
- Maeda, Y., Higuchi, T. & Ikeda, I. Change in Hydration State during the Coil-Gobule Transition of Aqueous Solutions of Poly(*N*-isopropylacrylamide) as Evidenced by FTIR Spectroscopy. *Langmuir* **16**, 7503-7509 (2000).
- Teraoka, I. *Polymer Solutions: An Introduction to Physical Properties*. (Wiley-Interscience, 2002).
- 28 Rubinstein, M. & Colby, R. H. *Polymer Physics*. (Oxford University Press, 2003).
- 29 Cowie, J. M. G. *Polymers: Chemistry and Physics of Modern Materials*. (Chapman and Hall, 1996).
- Young, R. J. & Lovell, P. A. *Introduction to Polymers*. (Chapman and Hall, 1991).
- Annable, T., Buscall, R., Ettelaie, R. & Whittlestone, D. The Rheology of Solutions of Associating Polymers: Comparison of Experimental Behavior with Transient Network Theory. *J. Rheol.* **37**, 695-726, doi:10.1122/1.550391 (1993).
- Karlström, G. A New Model for Upper and Lower Critical Solution Temperatures in Poly(ethylene oxide) solutions. *J. Phys. Chem.* **89**, 4962-4964 (1985).
- Matsuyama, A. & Tanaka, F. Theory of Solvation-Induced Reentrant Phase Separation in Polymer Solutions. *Phys. Rev. Lett.* **65**, 341-344, doi:10.1103/PhysRevLett.65.341 (1990).
- Bekiranov, S., Bruinsma, R. & Pincus, P. Solution Behavior of Poly(ethylene oxide) in Water as Function Temperature and Pressure. *Phys. Rev. E* **55**, 577-585 (1997).
- Baulin, V. A. & Halperin, A. Concentration Dependence of the Flory C Parameter within Two-State Models. *Macromolecules* **35**, 6432-6438 (2002).
- Landau, L. A. & Lifshitz, E. M. Statistical Physics. (Pergamon Press, 1963).
- 37 Shibayama, M. & Nagai, K. Shrinking Kinetics of Poly(*N*-isopropylacrylamide) Gels T-Jumped across Their Volume Phase Transition Temperatures. *Macromolecules* **32**, 7461-7468 (1999).
- Wang, J., Gan, D., Lyon, A. L. & El-Sayed, M. A. Temperature-Jump Investigations of the Kinetics of Hydrogel Nanoparticle Volume Phase Transitions. *J. Am. Chem. Soc.* **123**, 11284-11289 (2001).
- Shapiro, Y. E. Structure and Dynamics of Hydrogels and Organogels: An NMR Spectroscopy Approach. *Prog. Polym. Sci.* **36**, 1184-1253, doi:10.1016/j.progpolymsci.2011.04.002 (2011).
- Muiznieks, L. D., Weiss, A. S. & Keeley, F. W. Structural Disorder and Dynamics of Elastin. *Biochem. Cell Biol.* **88**, 239-250, doi:10.1139/o09-161 (2010).
- Kumashiro, K. K., Ho, J. P., Niemczura, W. P. & Keeley, F. W. Cooperativity Between the Hydrophobic and Cross-linking Domains of Elastin. *J. Biol. Chem.* **281**, 23757-23765, doi:10.1074/jbc.M510833200 (2006).
- Balaceanu, A., Singh, S., Demco, D. E. & Möller, M. Structural and Interaction Parameters of Thermosensitive Native α-Elastin Biohybrid Microgel. *Chem. Phys. Lett.* **612**, 182-189, doi:10.1016/j.cplett.2014.08.029 (2014).
- Demco, D. E., Filipoi, C., Zhu, X., Fechete, R. & Möller, M. Morphological Heterogeneity by Diffusional Kurtosis NMR Spectroscopy in Perfluorosulfonic Acid/SiO2Composite Proton-Exchange Membranes. *Macromol. Chem. Phys.* **214**, 1345-1355, doi:10.1002/macp.201300039 (2013).
- Casieri, C., Monaco, A. & De Luca, F. Evidence of Temperature-Induced Subdiffusion of Water on the Micrometer Scale in a Nafion Membrane. *Macromolecules* **43**, 638-642, doi:10.1021/ma902323t (2010).
- Edzes, H. T. & Samulski, E. T. Cross Relaxation and Spin Diffusion in the Proton NMR of Hydrated Collagen. *Nature* **265**, 521-523 (1977).

- Peschier, L. J. C., Bouwstra, J. A., de Bleyser, J., Junginger, H. E. & Leyte, J. C. Cross-Relaxation Effects in Pulsed-Field-Gradient Stimulate-Echo Measurements on Water in a Macromolecular Matrix. *J. Magn. Reson. B* **110**, 150-157 (1996).
- 47 Horstmann, M., Urbani, M. & Veeman, W. S. Self-Diffusion of Water in Block Copoly(ether–ester) Polymers: An NMR Study. *Macromolecules* **36**, 6797-6806, doi:10.1021/ma034633k (2003).
- 48 Kimmich, R. Principles of Soft-Matter Dynamics. (Springer, 2012).
- 49 Filipoi, C. *et al.* Channel Orientation Anisotropy in Perfluorosulfonic Acid/SiO2 Composite Proton Exchange Membranes: Water Self-Diffusion Study Using NMR. *Chem. Phys. Lett.* **513**, 251-255, doi:10.1016/j.cplett.2011.08.006 (2011).
- Filipoi, C. *et al.* Water Self-Diffusion Anisotropy and Electrical Conductivity of Perfluorosulfonic Acid/SiO2 Composite Proton Exchange Membranes. *Chem. Phys. Lett.* **554**, 143-149, doi:10.1016/j.cplett.2012.10.031 (2012).
- Amsden, B. Solute Diffusion within Hydrogels. Mechanism and Models. *Macromolecules* **31**, 8382-8395 (1998).
- 52 Cukier, R. I. Diffusion of Brownian Spheres in Semidilute Polymer Solutions. *Macromolecules* **17**, 252-255 (1984).
- Mikheeva, L. M. *et al.* Microcalorimetric Study of Thermal Cooperative Transitions in Poly(N-vinylcaprolactam) Hydrogels. *Macromolecules* **30**, 2693-2699, doi:10.1021/ma9615112 (1997).
- 54 Hirokawa, Y. & Tanaka, T. Volume Phase Transition in a Nonionic Gel. *J. Chem. Phys.* **81**, 6379-6380, doi:10.1063/1.447548 (1984).
- Kato, E. Volume-Phase Transition of *N*-Isopropylacrylamide Gels Induced by Hydrostatic Pressure. *J. Chem. Phys.* **106**, 3792-3797, doi:10.1063/1.473432 (1997).
- Otake, K., Inomata, H., Konno, M. & Saito, S. Thermal Analysis of the Volume Phase Transition with *N*-Isopropylacrylamide Gels. *Macromolecules* **23**, 283-289, doi:10.1021/ma00203a049 (1990).
- Xue, J. Z., Pine, D. J., Milner, S. T., Wu, X. I. & Chaikin, P. M. Nonergodicity and Light Scattering from Polymer Gels. *Phys. Rev. A* **46**, 6550-6563, doi:10.1103/PhysRevA.46.6550 (1992).
- Walters, P. An Introduction to Ergodic Theory. (Springer, 1982).
- Wagner, C. E., Turner, B. S., Rubinstein, M., McKinley, G. H. & Ribbeck, K. A Rheological Study of the Association and Dynamics of MUC5AC Gels. *Biomacromolecules* **18**, 3654-3664, doi:10.1021/acs.biomac.7b00809 (2017).
- 60 Cherstvy, A. G., Thapa, S., Wagner, C. E. & Metzler, R. Non-Gaussian, Non-Ergodic, and Non-Fickian Diffusion of Tracers in Mucin Hydrogels. *Soft Matter* **15**, 2526-2551, doi:10.1039/c8sm02096e (2019).

Chapter 6



This chapter is reproduced from Soft Matter, 2022,18, 4315-4324 with permission from the Royal Society of Chemistry.

Emulsification and gelation experiments and data analysis with Krytox® GPL101 was performed by J. Tenbusch.

All other experiments and data analysis is performed by T.Fischer

1. Introduction

Chemically inert and biocompatible polymers such as poly(ethylene) (PE), poly(4-methyl-1-pentene) (PMP or TPX), their fluorinated derivatives poly(tetrafluoroethylene) (PTFE), poly(vinylidene fluoride) (PVDF), are extensively used in biomedical devices. Their application comprises vascular grafts, prostheses, surgical sutures, and extracorporeal membrane oxygenators (ECMO). For instance, PTFE and its expanded form (ePTFE) is used for vascular grafts because of its limited thrombogenic potential. However, protein adsorption can still induce the coagulation cascade and thrombus formation, which limits its application for small diameter vascular grafts. TPX is used for the fabrication of hollow fiber membranes of ECMO devices. Despite great advancements, these membranes also suffer from protein adsorption and thrombus formation, which is one of the main causes of ECMO-related complications. 6-7

The examples highlight the imperative need to further modify the surface properties of such biomaterials, in particular for advanced blood compatibility. Ways to achieve this focus on rendering the surface hydrophilic (passive approach) and on endowing the surface with active molecules, which inhibit the coagulative response⁸⁻¹⁰ and eventually even promote reendothelization (active approach).¹¹ In order to combine both approaches, an ideal surface modification should consist of a biocompatible hydrogel, to which peptides and proteins do not bind by unspecific adsorption, which, however, can be equipped with specific biofunctional elements like cell-specific ligands, or cytokines and drugs which help to generate a functional natural interface to tissue or blood. Because hydrogels consist mainly of water, they can effectuate a certain stealth character and thus prevent unspecific interaction to enhance the selectivity of specific interactions.

Coating techniques applied so far involve plasma treatments,¹² radiation-induced surface grafting,¹³ and photochemical methods.¹⁴ They typically exploit surface oxidation to render the surfaces hydrophilic and to introduce reactive groups to which the coatings can be linked. However, these methods are tedious and require several steps. A powerful alternative is offered, if hydrophilic macromolecules can be grafted directly to the surface of the inert polymer to form a thin or even monomolecular coating. Such grafting of a hydrogel layer to hydrocarbon substrates has been realized based on C-H insertion crosslinking (CHic) described by J. Rühe.¹⁵ According to this method, a precursor polymer with photoactive groups like aromatic ketones, azides, or diazo groups is coated onto the substrate and irradiated with light. The photoactive groups form highly reactive species such as singlet nitrene or carbene radicals which undergo

insertion into C-H bonds. Most photoactive groups require irradiation with short wavelength UV light, which limits the application to rather flat surfaces and thin films. Thioxanthone groups are sensitive to longer wavelength ($\lambda \ge 360$ nm), but cannot solve the problem for complex surface structures, ¹⁷ while azides and azo groups can be activated by light as well as by thermal activation. ¹⁸⁻¹⁹ The latter is advantageous for systems where the coating is not accessible to the light source. Use of CHic has been reported for silicon wafers or glass substrates where a primer layer of functional silanes ensured tight binding to the substrate, ^{16, 19-23} direct grafting has been possible to polystyrene²⁴⁻²⁵ and poly(methylmethacrylate) surfaces. ²⁶ The reports demonstrate the versatility of the CHic technique to fabricate advanced bioanalytical devices e.g. immunoassays, ¹⁷ for anticoagulant surface modifications, ²³ and antimicrobial coatings. ²² All examples exploit the introduction of biofunctional molecules or groups within and by the CHic grafting/crosslinking step, i.e., simultaneous grafting, crosslinking, and functionalization. However, CHic has not yet been reported for inert materials like TPX, PVDF or PTFE.

Within this report, we demonstrate a facile method to generate thin hydrogel films on extremely inert polymer substrates such as TPX, PVDF and even PTFE binding. As the precursor polymer for the hydrophilic film, we chose poly(vinylacetamide-co-vinylamine) that was partially substituted by 4-azido-2,3,5,6-tetrafluorobenzoic acid by amidation of a fraction of the vinylamine comonomers. Poly(vinylacetamide) is a biocompatible very hydrophilic thermostable polymer that does not segregate from aqueous solution even at elevated temperatures up to the boiling point of water.²⁹ The amine functional polymer can be obtained by formamide-selective acid catalyzed hydrolysis of copolymers from vinylacetamide and vinylformamide. 30,31-32 Hence, amidation of only a part of the amine groups with 4-azido-2,3,5,6-tetrafluorobenzoic acid yields a polymer with two chemical functionalities, the CHinserting nitrene, and the primary amine groups, which can be further modified in aqueous solution, e.g. by peptide chemistry and Michael-type addition reactions. If this polymer is applied as an ultrathin or even monomolecular film, it can serve as a primer to enable wetting and further chemical modification. We chose the fluorinated phenyl azide because it can be safely handled below 100°C. The azide groups are activated by UV light at 302 nm and are insensitive against polar protic solvents and even oxygen. The nitrenes react only slowly with oxygen compared to the insertion into C-H bonds.³³ Furthermore, it allows selective prefunctionalization of the polymers by azide-alkyne cycloaddition or azide-thioacid amidation.³⁴ While the C-H insertion mechanism of nitrenes is broadly studied and successfully employed for C-H insertion crosslinking of polymers, we have been surprised that the precursor polymers could also be attached successfully to PTFE, where the grafting can only occur via attack to C-C and C-F bonds. We further investigated the wetting behavior of the hydrogel coating using dynamic contact angle measurements and show that the coating resembles a loosely crosslinked hydrogel where the polymer chains can re-orient once in contact with air or water.

2. Experimental Section

2.1 Materials

N-vinylformamide (NVF) and *N*-vinylacetamide (NVA) were purchased from TCI. Methyl pentafluorobenzoate was purchased from abcr. Sodium azide was from Roth. Magnesium sulfate, triethylamine, and *N*-hydroxysuccinimide (NHS) were purchased from Sigma Aldrich. 1-Ethyl-3-(3-dimethylaminopropyl)carbodiimide (EDC) was from Fluorochem. Rhodamine-B-isothiocyanate was from ChemCruz. All solvents, HCl, and NaOH were from VWR. All chemicals were used as received except *N*VF, which was distilled before usage. Poly(1-methylpenten) (TPX) and poly(vinylidene fluoride) (PVDF) were from Goodfellow. PTFE foil was from RCT. PVDF and PTFE were washed with CHCl₃, EtOH and water while TPX with EtOH and water before further modification.

2.2 Methods

Proton NMR spectra were recorded on a Bruker Avance III-400 FT-NMR spectrometer (Bruker Corporation, Billerica, MA, USA) at 400 MHz. UV-Vis measurements were performed with a Jasco V-780 spectrophotometer (Jasco Corporation, Tokyo, Japan) from 200 to 400 nm with a concentration of 1 mg·mL⁻¹ in water. Fourier transformation infrared spectroscopy (FT-IR) was performed with a Nexus 470 spectrometer (Thermo Nicolet, USA). X-ray photoelectron spectroscopy (XPS) was performed with a Kratos Ultra Axis (Kratos, United Kingdom). The samples were excited with monochromatic Al-K $_{\alpha 1,2}$ radiation (1486.6 eV). The resulting spectra were analyzed with CasaXPS software (Casa Software Ltd., United Kingdom). Confocal Laser Scanning Microscopy (CLSM) images were taken with a SP-8 (Leica GmbH, Wetzlar, Germany). Sessile drop contact angles (CA) were measured with a DSA 100 (Krüss, Germany). Drops of 10 μ L were placed on the sample surface with a rate of 200 μ L·s⁻¹. After an equilibration time of 60 s, the CA was determined using a Tangent-2 fitting mode.

Advancing and receding CAs θ were measured according to the Wilhelmy method³⁵ with a DCAT 25 (DataPhysics, Germany). For the measurement, polymer foil samples were cut to 3 cm x 3 cm. PTFE and TPX were pre-modified by static coating, i.e. forming a droplet on the

surface of the foil (see below) (2 mL of the functionalized polymer (2 mg·mL⁻¹ in water, 0.1 eq was carefully spread over the surface and the samples were treated afterward with UV at 302 nm for 20min.). The samples were spin-coated (see below, 750 μL of the functionalized polymer (5 mg·mL⁻¹ in MeOH, 0.025 eq) were added slowly on the surface while spinning at 3000 rpm with a subsequent UV treatment at 302 nm for 20min). Samples were thoroughly washed with water after each UV treatment and coated on both sides. The immersion depth was set to 8 mm with a motor speed of 0.5 mm·s⁻¹. Up to 5 cycles were performed in water, or to validate the amphiphilic behavior in n-hexadecane. The linear regime was fitted with a linear fit and the contact angle was calculated with the Wilhelmy equation (1).

$$\theta = \cos^{-1}(\frac{mg}{\sigma L})\tag{1}$$

With m being the mass extrapolated from the linear regime to zero immersion depth, g the gravity, σ the surface tension, and L the circumference of the sample.

Spin-Coating

Spin coating was performed with a Convac 1001s (Convac GmbH, Germany). Unless otherwise noted $300~\mu\text{L}$ of the functionalized polymer (5 mg·mL⁻¹ in MeOH, 0.025~eq) were added slowly on the surface while spinning at 3000~rpm. Afterward, the samples were UV treated in a CL-1000~Ultraviolet Crosslinker (UVP, Germany) for 20~min at 302~nm. Finally, the samples were washed thoroughly with water and EtOH for at least 30~s and dried in a filtered nitrogen stream.

Fluorescent Labeling

The samples were incubated with a solution of rhodamine-B-isothiocyanate in water (4 μ g·mL⁻¹, 1 h). Afterward, they were washed thoroughly with water and EtOH for at least 60 s and dried in a filtered nitrogen stream.

Synthesis of P(VAm-co-VAA)

The detailed synthesis is described elsewhere.³⁰ Briefly, *N*-Vinylformamide (NVF) (3.64 g, 51.2 mmol, 1 eq), *N*-vinylacetamide (NVA) (6.36 g, 51.2 mmol, 1 eq), and VA044 (331 mg, 0.51 mmol, 0.01 eq) were dissolved in water (90 mL) and degassed by at least three freezethaw cycles. The reaction mixture was stirred at 60 °C for 20 h. The product was precipitated in acetone, re-dissolved in water and lyophilized. The formamide group was selectively hydrolyzed by dissolving the polymer in NaOH (2 M, 500 mL) and refluxing at 80 °C for 4 h. The reaction mixture was neutralized and dialyzed for one week against water (SpectraPor,

MWCO 3.5 kDa). After dialysis, ion exchange was performed to remove residual chloride ions (Ampersep® 900). The product was obtained by lyophilization.

¹H NMR (400 MHz in D₂O, δ in ppm): 1.35-1.75 (-CH₂ backbone), 1.75-1.95 (-CH₃), 3.0-4.0 (-CH backbone), 7.5-8 (-CHO)

SEC:
$$M_n = 5.6 \cdot 10^4 \text{ g} \cdot \text{mol}^{-1}$$
, $M_w = 1.2 \cdot 10^5 \text{ g} \cdot \text{mol}^{-1}$, PDI = 2.2

Synthesis of 4-Azido-tetrafluorobenzoate

Methyl pentafluorobenzoate (4.02 g, 17.8 mmol, 1 eq) was dissolved in an acetone/water mixture (2:1, 45 mL). Sodium azide (1.5 g, 23.1 mmol, 1.3 eq) was added and the mixture refluxed at 85 °C for 6 h. After the reaction, the reaction mixture was cooled down to room temperature, diluted with water (75 mL), and extracted with Et_2O (3 x 75 mL). The combined organic phases were dried with anhydrous MgSO₄ and the solvent was removed in a vacuum. Yield: 3.4 g (=76.7 %)

¹H NMR (400 MHz in CDCl₃): δ 3.95 (s, 3H)

¹³C NMR (100.6 MHz in CDCl₃): δ 53.4, 107.67, 123.5, 139.2, 141.9, 144.2, 146.6, 159.9

¹⁹F NMR (376.5 MHz in CDCl₃): δ -151.1, -138.8

Synthesis of 4-Azido-tetrafluorobenzoic acid

4-Azido-tetrafluoromethylbenzoate (2 g, 8.03 mmol) was dissolved in NaOH (3.2 mL, 20 wt%) and Methanol (40 mL). The mixture was stirred overnight and subsequently acidified with HCl (2 M) to a pH lower than 1. The mixture was extracted with CHCl₃ (3 x 40 mL), the organic phases dried with anhydrous MgSO₄ and the solvent evaporated in vacuo.

Yield: 1.27 g (=67.2 %)

¹³C NMR (100.6 MHz in DMSO-d6): δ 108.5, 122.7, 138.9, 141.6, 143.1, 145.7, 160.2

 ^{19}F NMR (376.5 MHz in DMSO-d6): δ -151.7, -141.4

Synthesis of N-succinimidyl 4-azido-tetrafluorobenzoate

4-Azido-tetrafluorobenzoate (0.25 g, 1.06 mmol, 1 eq) was dissolved in DCM. NHS (230.15 mg, 1.06 mmol, 1 eq) and EDC (245 mg, 12.8 mmol, 1.2 eq) were added and the solution was allowed to stir overnight. This was followed by the addition of 35 mL DCM and

50 mL water and stirring for another 40 min. The organic phase was washed with water (5 x 50 mL) and brine (3 x 10 mL). The mixture was dried with MgSO₄ and the solvent was removed in vacuo.

Yield: 326.9 mg (92.8 %)

¹H NMR (400 MHz in CDCl₃): δ 2.85 (s, 4H)

¹⁹F NMR (376.5 MHz in CDCl₃): δ -149.9, -133.6

Functionalization of p(VAm-co-VAA) with $N\text{-}succinimidyl}$ 4-azido-tetrafluorobenzoate

P(VAm-co-VAA) (500 mg, 3.94 mmol amino groups) was dissolved in MeOH (25 mL). *N*-succinimidyl 4-azido-tetrafluorobenzoate (130.9 mg, 0.394 mmol, 0.1 eq/-NH₂) was dissolved in EtOH and added dropwise to the solution. TEA (250 μ L) was added and the solution was allowed to stir overnight. The product was precipitated in cold diethyl ether, re-dissolved in water, and lyophilized. The other prepolymers (azide/amine = 0.075, 0.05, and 0.025) were prepared in a similar manner.

Pre-Modification of PTFE and TPX

PTFE and TPX foils were cut in a square shape (2 cm x 2 cm). 800 μL of the functionalized polymer (2 mg·mL⁻¹ in water, 0.1 eq) were added to the surface and carefully spread. The samples were UV-treated in a CL-1000 Ultraviolet Crosslinker (UVP, Germany) for 20 min at 302 nm. The liquid phase was removed after UV treatment and the samples were washed with water and EtOH.

Crosslinking of PFPA_{0.025}-co-PVAm in Krytox GPL 101

P(VAm-co-VAA) with an azide/amine ratio of 0.025 (PFPA_{0.025}-co-PVAm) was dissolved in MilliQ® water and added to a 10-fold volume of Krytox® GPL101 oil (DuPont, USA). The mixture was subjected to ultrasonication using an ultrasonication finger (Sonifier W-250 D, 10% amplitude, 20 s, G. Heinemann) to form a stable emulsion. The emulsion was subjected to UV irradiation at 302 nm for 20 min as described above. Subsequently, the crosslinked gel-like structure was purified using a 0.1 μm PVDF filter to remove residual Krytox® oil and washed. The residue was taken up in the water, isolated after lyophilization as a brown solid, and analyzed *via* FT-IR spectroscopy.

3. Results and Discussion

Scheme 6.1 shows the polymer synthesis that was used to apply a hydrogel coating to substrates TPX, PVDF and PTFE. The polymer was prepared by free radical co-polymerization of *N*-vinylacetamide and *N*-vinylformamide. Subsequent selective acidic hydrolysis of the formamide groups yielded free amine groups. A fraction of those was reacted with *N*- succinimidyl 4-azido-tetrafluorobenzoate to yield the nitrene functionalized copolymer of vinylacetamide and vinylamine (Scheme 1).

Scheme 6.1. Reaction pathway to synthesize the prepolymer and representation of the proposed CHic reaction.

Table 6.1 gives an overview of the polymers, which were employed for the preparation of the coatings. They are all based on the same parent P(VAm-co-VAA) sample, which was prepared by free radical polymerization as described before.³⁰ The molecular weight of P(VAm-co-VAA) M_n (SEC) = $5.6 \cdot 10^4$ g·mol⁻¹ corresponds to an average degree of polymerization of DP = 670. Because of the nearly ideal co-polymerization kinetics of the two monomers, we assume homogeneous composition of all polymer chains.³⁰

Table 6.1. Theoretical average number of repeat units between two azides in one polymer (N_{RU}), theoretical average molecular weight between two azides (M_{aa}), the theoretical average number of azides (N_a) per polymer (based on the number average molecular weight of the polymer obtained by SEC) for the theoretical amine/azide ratios, and the experimentally determined azide/amine ratio by IR

Azide /Amine	N _{RU}	M _{aa} [g·mol ⁻¹]	Na	Experimentally ¹
0.1	~ 20	~ 1270	~ 47.2	0.11
0.075	~ 30	~ 1905	~ 31.5	0.075
0.05	~ 40	~ 2540	~ 23.6	0.044
0.025	~ 80	~ 5080	~ 11.8	0.028

The ratio between *N*-vinylformamide and *N*-vinlyacetamide was determined by ¹H-NMR in agreement with the monomer ratio employed (1:1). After hydrolysis of the *N*-vinylformamide units, the analysis of free amine groups corresponded to the original fraction of formamide groups. Substitution by azido tetrafluorobenzamide units was chosen to vary between 2.5 and 10 % of the amine groups corresponding to 20-80 monomer units between the crosslinking azide substituents (see Table 6.1). The number of azide groups per chain was a minimum of 10. Experimentally, the azide content was semi-quantitatively verified by the ratio of the IR intensities of the azide vibration (variable) and the amide vibration (Figure 6.1).

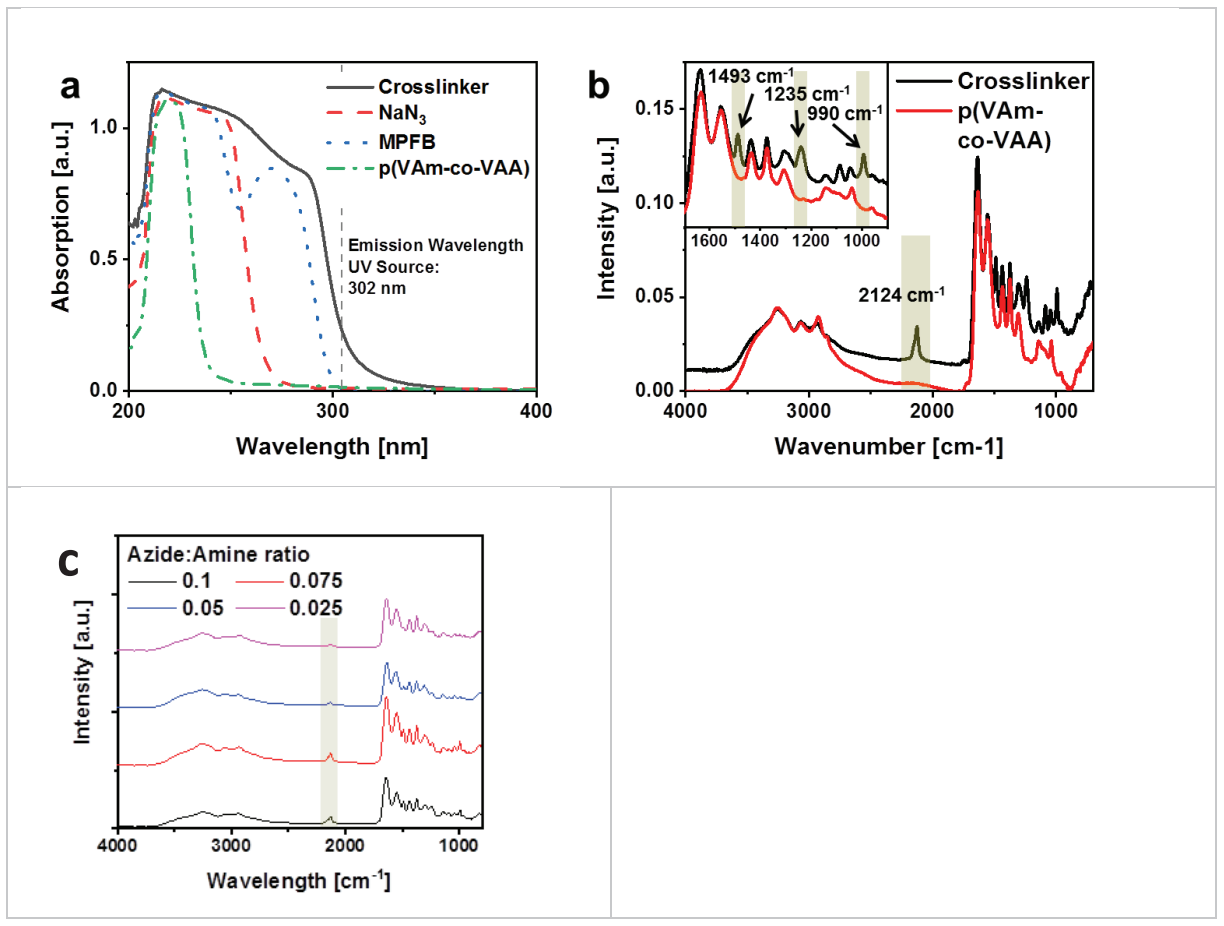


Figure 6.1. a) UV-Vis spectra of the starting materials and the crosslinker, b) IR spectra of P(VAm-co-VAA) and c) IR spectra of the crosslinker in different Azide:Amine ratio.

In the following, we refer to the azide-functionalized poly(vinylamide-co-vinylamine)s as prepolymers. For the preparation of a hydrophilic coating, we spin-coated TPX, PVDF and PTFE substrates by methanolic solutions of the polymer and immediately exposed to UV irradiation at 302 nm (the absorbance of the crosslinker is indicated in Figure 6.1a). This leads to the activation of azide to yield the highly reactive nitrenes. For all different substrates, we had to avoid dewetting during the deposition of the polymer when the solvent evaporated. To optimize the surface coating, PVDF was chosen as the substrate in the first instance. With 36 mN/m the surface energy of PVDF is the highest of the three polymers compared to $\gamma = 25 \text{ mN/m}$ nd $\gamma = 19 \text{ mN/m}$ for TPX and PTFE respectively. Spin coating was varied for solvent, rotation speed, concentration, volume added, and azide to amine ratio of the prepolymer (Figure. S3).

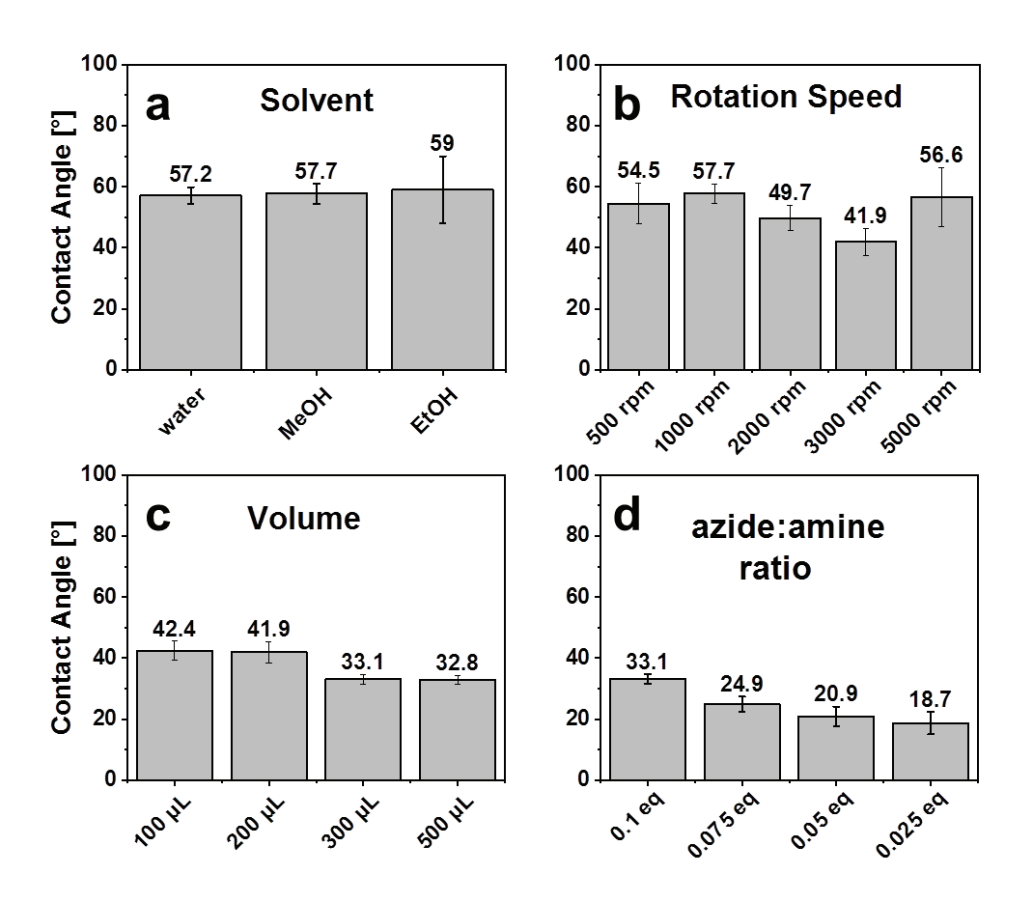


Figure 6.2. Sessile drop CA (H_2O , volume: 10 μ L, equilibration time: 60 s, n=5) of PVDF foils varying a) the solvent (rotation speed 1000 rpm, volume: 200 μ L, azide:amine ratio: 0.1), b) the rotation speed (solvent: MeOH, volume: 200 μ L, azide:amine ratio: 0.1), the volume (solvent: MeOH, rotation speed 3000 rpm, azide:amine ratio: 0.1), and the azide:amine ratio (solvent: MeOH, rotation speed 3000 rpm, volume: 300 μ L).

The coated PVDF samples were subsequently irradiated for 20 min with UV light at 302 nm and thoroughly washed with water and EtOH. Afterward, the hydrophilization was tested by the advancing contact angle against the water with the sessile drop method (Figure 6.2). A minimum contact angle of 19° was found for the prepolymer with an azide to amine ratio of 0.025 when applied in MeOH solution with a polymer concentration of 5 mg·mL⁻¹ by a volume of 75 µL·cm⁻² and a rotation speed of 3000 rpm. Such a low contact angle indicates the formation of a homogeneous, thin hydrogel layer that cannot be washed away by ethanol, which is a good solvent for the prepolymer.

When we used the same procedure to coat TPX and PTFE, we measured rather high contact angles of 108° and 115° against water, indicating either no or only very incomplete coverage by a hydrogel. In order to exclude the poor hydrophilization that was caused predominantly by

dewetting, we deposited the prepolymer in two steps. In the first step, a droplet of the prepolymer in water (azide to amine ratio: 0.1, concentration 2 mg·mL⁻¹) was applied to the sample and crosslinked by UV to form a pre-layer. Subsequently, a second layer of the prepolymer (azide to amine ratio: 0.025, concentration 5 mg·mL⁻¹) was applied by spin coating and irradiated by UV-light. The improvement of the wetting by water with contact angles of 15° and 45° against water for TPX and PTFE respectively indicates that the originally bad results must be assigned predominantly to dewetting during spin coating.

Figures 6.3 a) and b) depict optical micrographs of untreated and hydrophilized tiles of PVDF, TPX and PTFE. In all cases, the coating was colorless and invisible as expected for a very thin film. To visualize the coatings and demonstrate the accessibility of free -NH₂ groups, we labeled the coating by treatment with an aqueous solution of rhodamine-B-isothiocyanate. The fluorescent dye attaches readily to the free amine groups in the coating and the coating formation can be observed by confocal laser scanning microscopy (CLSM), with a voxel resolution of 300 nm (Figure. 6.3 c). As can be seen from Figure. 2c all the three substrates show prepolymer coating labeled with rhodamine (red). Of all the three substrates used, TPX which has a tertiary hydrogen atom in the side chain is the most suitable candidate for CHic insertion reaction. Coating PVDF is comparatively difficult because of the electronwithdrawing effect of the CF₂ groups which renders the C-H less nucleophilic, still, due to the high reactivity of nitrene, the insertion could be achieved. The image of the coating on PVDF shows lamellar scales of the semicrystalline PVDF which are covered by the red fluorescent hydrogel. The prepolymer attached predominantly to the edges of the lamellae, nevertheless, flat areas in between the edges, also show homogeneous coating as indicated by the even fluorescence intensity.

However, for PTFE which lacks C-H bonds, C-H insertion is considered not feasible. For the reaction to occur, the electrophilic nitrene must orient to the C-F insertion which, due to the electron-deficient carbon center is difficult. But in Figure 6.3 c), we see the rhodamine thio-isocyanate got bound to the surface rather evenly indicating homogeneous coating of the amine groups containing prepolymer. The image of the PTFE sample with fibrous type surface structure is typical for a surface of PTFE that was exposed to some shearing force.

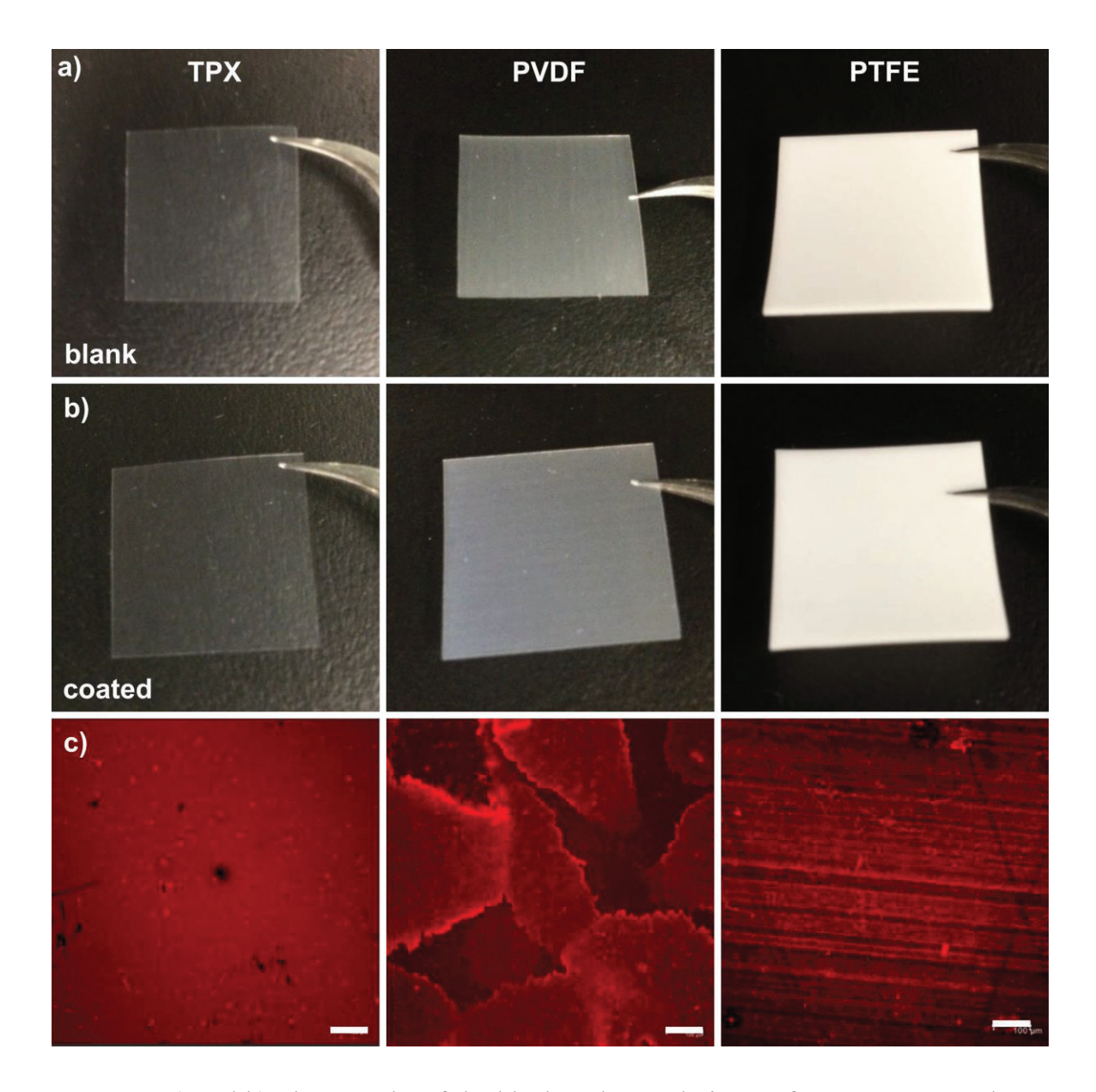


Figure 6.3. a) and b) Photographs of the blank and coated pieces of TPX, PVDF, and PTFE foil respectively, showing that the coating is nearly invisible, and c) Confocal laser scanning microscopy images of the respective coated samples stained with rhodamine revealing the accessibility of free primary amine groups. The scale bar indicates 100 μm.

To investigate the binding of the hydrophilic coating to the substrate we exposed the samples to a 4 h Soxhlet extraction with methanol. This is a rather rigorous extraction procedure during which non-covalently bound components get extracted about 50 times by hot freshly distilled methanol. For this, the samples were immersed into the hot methanol and rinsed off after about 5 min. After the extraction process, the samples were washed with water and fluorescently labeled with rhodamine-B-isothiocyanate.

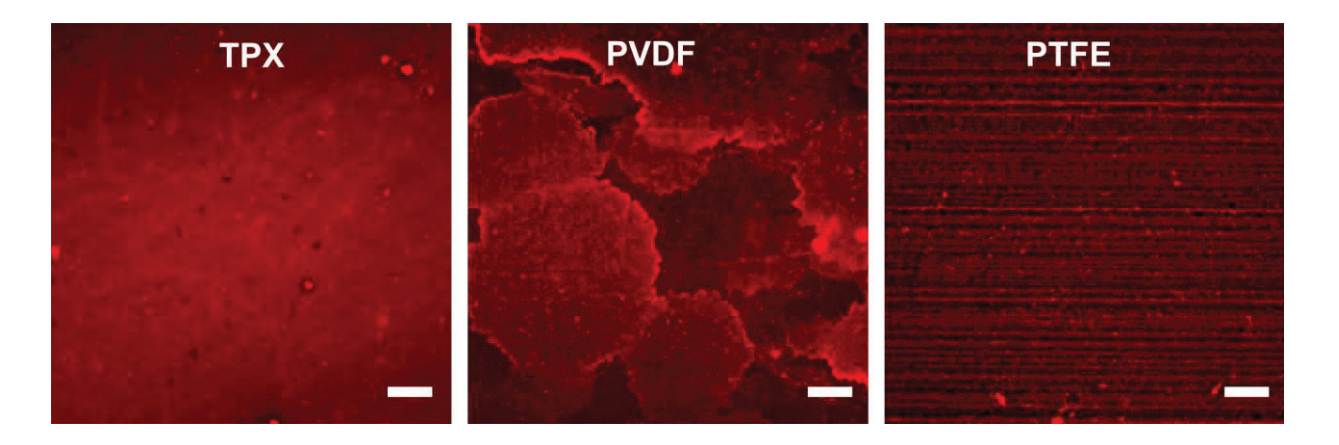


Figure 6.4. CLSM images of coated TPX, PVDF, and PTFE after treatment in a Soxhlet apparatus for 4 h in MeOH and staining with rhodamine-B-isothiocyanate. The coating is still intact and the amine groups are accessible. The scale bar represents 100 μm.

The confocal laser scanning microscopy images (CLSM) in Figure 6.4 a-c) depict the same staining effect of the surface as it is shown in Figure 6.3. For comparison, we show in Figure 6.5 images of the polymer surfaces which were exposed to the same extraction and fluorescence labeling processes, but not treated by the prepolymer before.

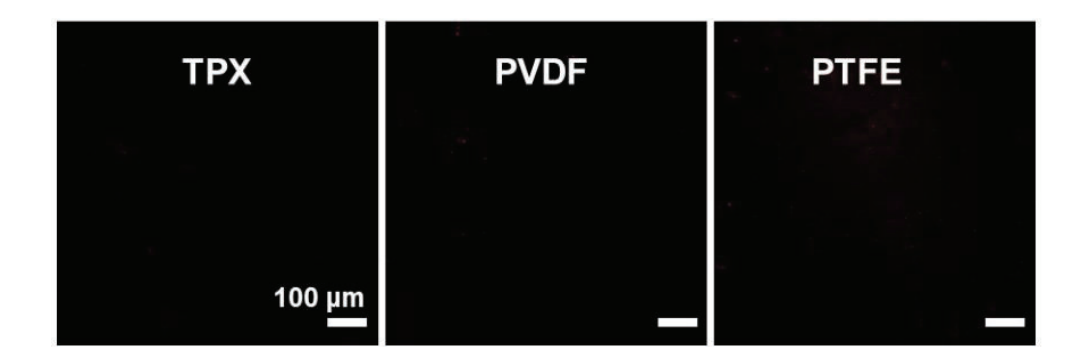


Figure 6.5. Confocal image of the polymer substrates after UV treating the surface with prepolymer devoid of azide functionality and staining with rhodamine-B-isothiocyanate. The scale bar represents $100 \ \mu m$

Since the fluorescence staining only demonstrates that the surfaces treated with prepolymer can be stained more efficiently than the blank polymer surfaces, it provides rather indirect evidence for the attachment of the hydrogel layer. Thus, we took additional efforts to investigate the grafting of a thin hydrogel layer and to analyze the chemical composition of the surface by X-ray photoelectron spectroscopy (XPS). XPS was performed after Soxhlet extraction in all cases. Figure 4 depicts the high-resolution C1s spectra of all the three coated foils that show characteristic C-N and C-O peaks arising from P(VAm-co-VAA). Further, on comparison of

high-resolution XPS spectra for TPX, PVDF and PTFE, we see the presence of C-F signal at 288 eV arising from prepolymer backbone in TPX showing the coating stability. While in the case of PVDF and PTFE the C-F signal is reduced by 16% and 48% respectively. The C-F signals in PVDF and PTFE are predominantly from the polymer substrate and reduction of the signal intensity again proves the presence of stable hydrogel coating on the substrate ((Figure 6.6 a-c), Table 1). The N/O ratio of the prepolymer on TPX, PTFE, and PVDF was calculated in the range of 0.8 to 1.2 (Table 6.2). In comparison to the native 'prepolymer,' the high oxygen content of the coatings can be due to its reaction with molecular oxygen.³⁷

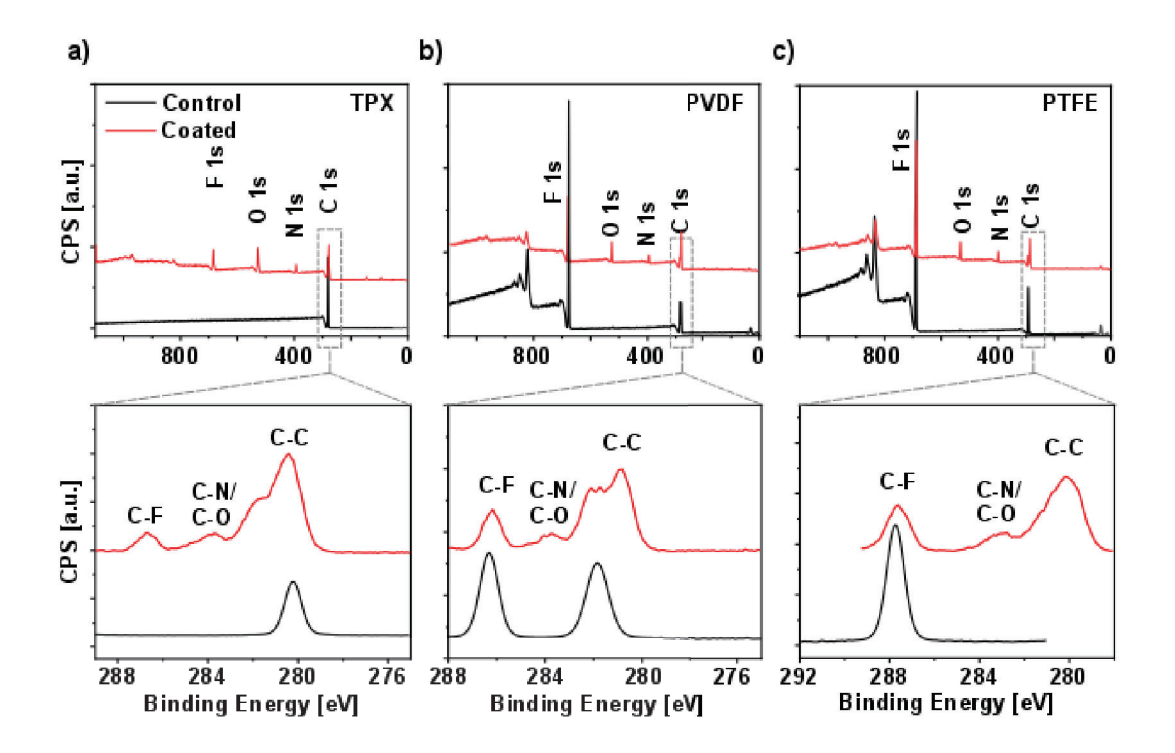


Figure 6.6. XPS survey and high-resolution C spectra of a) TPX, b) PVDF, and c) PTFE after soxhlet extraction

Table 6.2. Chemical composition of the blank and coated foils determined by XPS

Surface	C	N	O	F
	[atom%]	[atom%]	[atom%]	[atom%]
TPX control	100	0	0	0
TPX coated	66.8	5.5	9.4	18.4
PVDF control	53.1	0	0	46.9
PVDF coated	69.3	7.6	15.4	7.7
PTFE control	36.1	0	0	64

PTFE coated	53.3	6.8	8.8	31.1
Prepolymer ¹	65.5	21.1	11.3	2.1

Briefly, in the following paragraph are some possible side reactions in aqueous phase discussed and visualized in Figure 6.7: UV-treatment of the crosslinker in water leads to a color change from colorless to brownish. The color change indicates that to some extent the singlet nitrogen underwent ISC to the triplet nitrene which forms azo-compounds. The brownish liquid phase was further analyzed by UV-Vis and FT-IR spectroscopy. In UV-Vis a bathochromic shift is visible which is caused by the azocompounds. In FT-IR there is a small band at 1411 cm⁻¹, which is related to the N=N stretching of a trans-azo compound. At 1720 cm⁻¹ there is a new band, which has been reported by Meijer et al.³⁸: The intramolecular addition reaction of the singlet nitrene to the aromatic ring leads to the formation of a reactive ketenimine, which polymerizes to poly-1,2-azepines. The signal was deduced to simultaneous photo-oxidation of the polymer.³⁸ However, it is noteworthy that the substitution of an alkene with two amine groups can shift the absorbance to higher frequencies. Thus, also the C=C vibration might be responsible for the band.³⁹ Furthermore, there are two strong signals at 1510 and 1329 cm⁻¹. These are attributed to the asymmetric and symmetric stretching vibration of nitro-moieties. These are formed by the reaction of triplet nitrene with molecular oxygen as the water for the reaction was not degassed. ⁴⁰ Furthermore, the amide vibration is changed, i.e. the amide II band is shifted to lower frequencies. This might be attributed to hydrogen bonding.

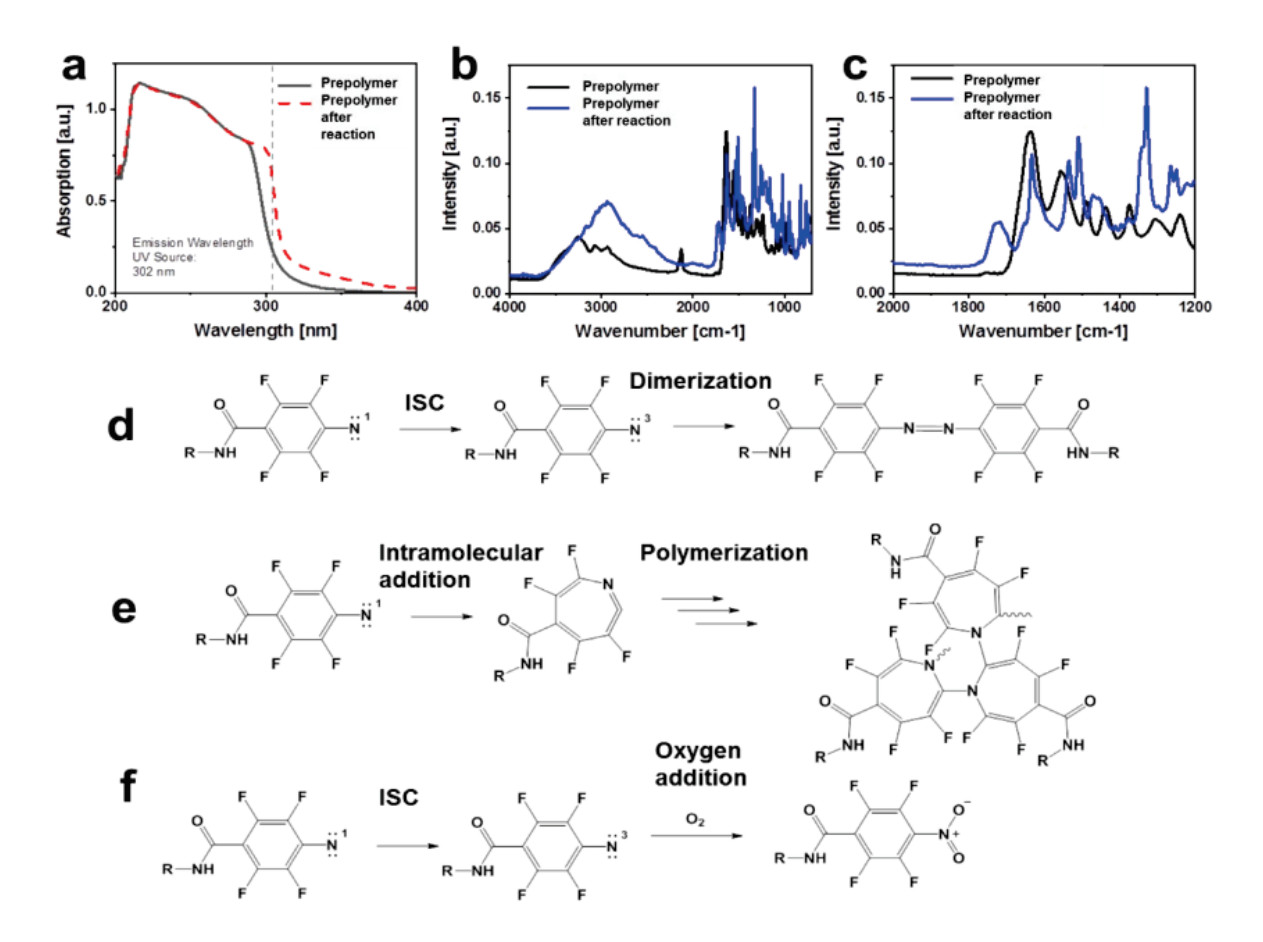


Figure 6.7. UV-Vis spectra (a) of the prepolymer and the prepolymer after reaction and their respective IR-spectra (b) and (c). The reaction scheme of ISC to the triplet nitrene with the following dimerization is shown in (d), an intramolecular addition to a ketenimine and the following polymerization is shown in (e), and ISC with subsequent oxygen addition is shown in (f).

To further ascertain the grafting of the prepolymer onto PTFE, we conducted a model experiment where a stable w/o emulsion of 5 wt% of PFPA_{0.025}-co-PVAm in water with a perfluorinated oil (Krytox® GPL101) was prepared at a ratio of 1:14 (Figure 6.8).

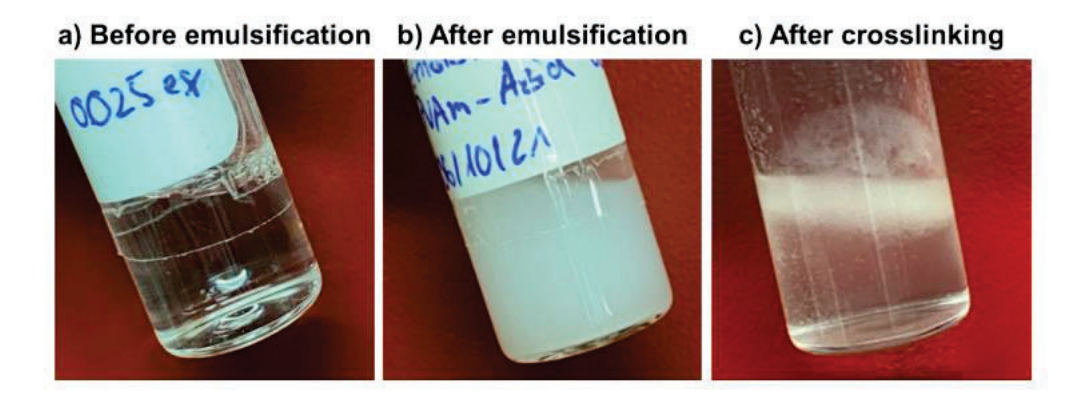


Figure 6.8. Photographs of a) 5 wt% of PFPA_{0.025}-co-PVAm in water added to Krytox® GPL101, b) after emulsification and c) after crosslinking procedure indicates the formation of a gel-like structure.

The rationale behind this experiment was to examine the grafting of the fluorinated oil on the polymer gel upon UV irradiation (Figure 6.9). After UV irradiation, the gel was purified and dried. Comparing the IR spectra of the dried network with the prepolymer and the fluorinated oil, we found that the absorption originating from the characteristic C=O stretching and N-H stretching at 1640-1550 cm⁻¹ of the *N*-vinylamides was still present in the emulsion crosslinked gel (Figure 6.9 b). However, the intensity of C-F stretching absorption at 1200-1000 cm⁻¹ increased significantly, indicating incorporation of the perfluorinated oil into the network. Due to the overlap with signals of C-F stretching, a distinct verification of the formation of N-F bonds is difficult, especially with the low molar ratio of theoretical N-F to C-F bonds present in both the oil and the prepolymer. Following our observation of the strong adhesion onto PTFE substrates as well as crosslinking within an emulsion with a perfluorinated oil and subsequent analysis, we hypothesize the formation of N-F bonds and due to the proximity of the electronic environment of the fluorine and the nitrene radical, an attractive electronic interaction cannot be ruled out.⁴¹ However, a more detailed molecular analysis will be necessary in the future with more simplistic model compounds.

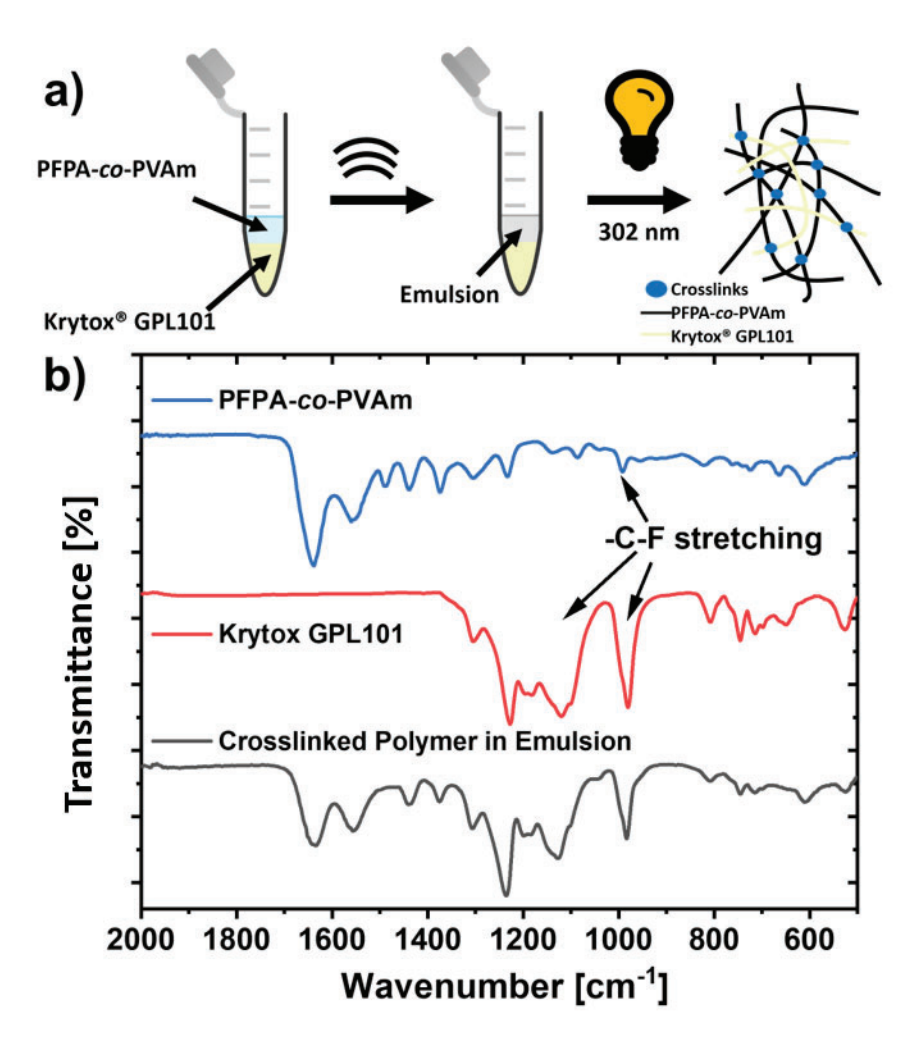


Figure 6.9. a) Schematic representation of the investigation of crosslinking of PFPA-co-PVAm within an emulsion with perfluorinated oil. b) FT-IR spectra of PFPA-co-PVAm, Krytox® GPL101 and crosslinked polymer in a water/perfluorinated oil emulsion indicate the integration of perfluorinated oil within the crosslinked hydrogel network.

The ability of the grafted hydrogel to prevent protein adsorption is associated with the steric repulsion caused by the perturbation that the protein molecules generate when in contact with the hydrogel layer. For effective prevention of protein adsorption surface density of the hydrogel layer is more critical than the thickness. As the surface coverage increases, loosely crosslinked polymeric chains start to repel each other and stretch out to avoid polymer-polymer repulsion and generate an entropic barrier which makes the adsorption of protein thermodynamically unfavorable.⁴²

To investigate the wetting behavior of the coatings Wilhelmy balance method was used (Figure. 6.10a). In this method, the force is measured which is needed to immerse (advancing CA) or

remove (receding CA) a sample from a liquid (Figure 6b). This force is related to the CA via the Wilhelmy equation (1). Unless otherwise stated water was used as the liquid phase.

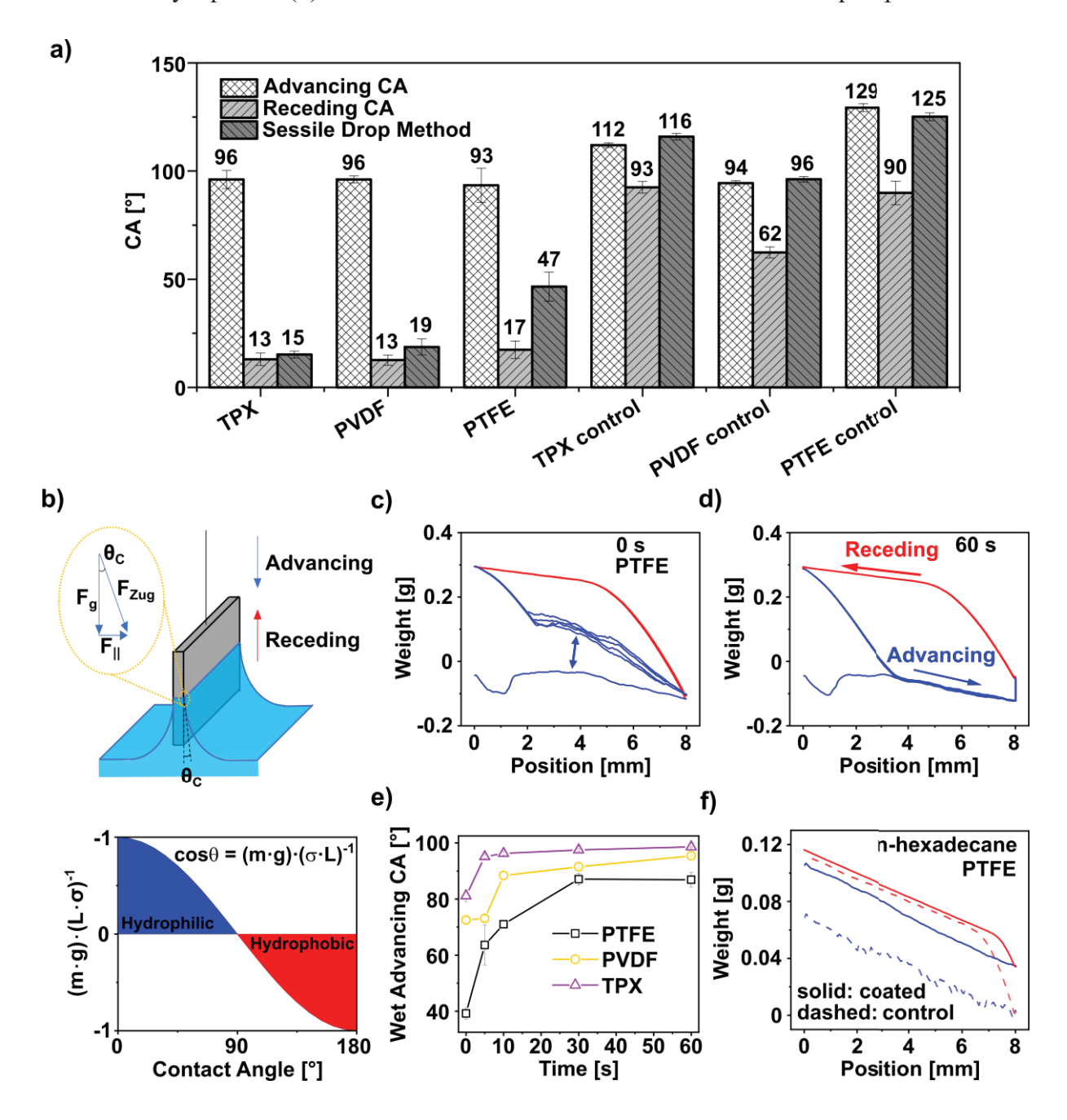


Figure 6.10. a) Advancing, receding, and sessile drop CA from blank and coated TPX, PVDF, and PTFE. It is visible that the functionalization hydrophilizes the surface. b) Schematic representation of the principle of the Wilhelmy balance and a graph showing that negative weights refer to hydrophobic CAs, while positive weights refer to hydrophilic CAs. c) and d) Exemplary graph of coated PTFE with multiple cycles performed using the Wilhelmy balance with changing the waiting time between the cycles from 0 s to 60 s. The graph shows the wet advancing CA. The arrow in c) indicates the difference between the dry and the wet advancing CA. e) The development of the wet advancing CA for the coated samples. With increasing

waiting time, a plateau is reached which is in the range of the dry advancing CA. f) proving the amphiphilicity of the coating by using n-hexadecane as a solvent for coated and blank PTFE.

As can be seen from Figure 6.10a, the coating altered the surface properties of the foils, and all coated samples tend to have the same values for the advancing CA ($\sim 95^{\circ}$) and receding CA (\sim 15°) resulting in a very high CA hysteresis of ~80° in comparison of the controls. This was also apparent when static CA measurements were performed using the sessile drop method. Interestingly, when the CAs obtained by the Wilhelmy balance method were compared with those determined by the sessile drop method, it was found that the sessile drop CA for the blank foils was close to the advancing CA and the one for the coated samples was close to the receding CA. Taking the hydrophilicity of P(VAm-co-VAA) into account the advancing CAs of the coated samples are unexpectedly high.^{30, 43} This leads us to conclude that the wetting behavior of the coating was influenced by the swelling and/or re-orientation of the polymer chains. This was ascertained by tracking the CA for the coated samples by the sessile drop method as a function of time (Figure 6.11). As can be visualized that although a decrease in contact angle was observed, this decrease was not instantaneous but rather in a timeframe of several seconds. To further analyze this, five subsequent cycles of CA measurements were performed with the Wilhelmy balance (as shown in Figure 6.10c). It is visible that for coated samples, the advancing CA decreases as soon as the surface is wetted (cycle 2). This means the CA hysteresis has a kinetic factor and the advancing CA depends on the wetting history of the sample. We refer to this as "wet advancing CA". However, the receding CA remained unaffected by the wetting history and the differences between the 2nd and the following cycles were negligible, which shows that once swollen the wetting behavior of the coating is not affected. In the dry state, because of low crosslink density (azide to amine ratio, 0.025:1), the hydrophobic backbone of P(VAm-co-VAA) is directed towards the air to reduce the surface tension, while when in contact with water there is a fast re-orientation of the functional hydrophilic groups of polymer chains rendering the surface more hydrophilic indicating formation of a loosely crosslinked hydrogel layer. This also confirms our previous observation that the lower the azide to amine ratio, the higher is the surface hydrophilicity which means a higher probability of rearrangement in the hydrogel layer, and a higher degree of swelling, indicating a scenario like the highly swollen open structure of a hydrogel film with diffused outer boundary and well solvated inner chain segments. Similar behavior has been reported for PMMA, 44-47 where the segmental motion of the polymer chains was observed at the water polymer interface. Upon

contact with water, the initial hydrophobic surfaces turn more hydrophilic due to the reorganization of the carbonyl-groups within seconds.⁴⁴ Additionally, this behavior was also shown for 2-hydroxy ethyl methacrylate/styrene block copolymers, where the CA hysteresis depended on the wetting history of the surface.⁴⁸

To quantify this re-orientation time a waiting time between each cycle was introduced ranging from 0-60 s which is in the timescale as previously shown for PMMA.⁴⁴ The measurement was halted when the sample was completely immersed or removed from the water phase (Figure. 6.10d). In Figure 6.10e) the wet advancing CA is plotted against the waiting time. As can be seen from the graph that the re-orientation time is related to the film material and decreases from TPX (fast transition) to PVDF and PTFE (slow transition). This can be already seen from the initial wet advancing CA (waiting time 0 s), which also decreases from TPX (81.1° \pm 2.1°) to PVDF (72.5° \pm 0.8°) and PTFE (39.2° \pm 2.0°). The re-orientation is related to the mobility of the polymer chains, which in turn depends on the crosslinking density and the texture of the surface (Figure 6.1c).

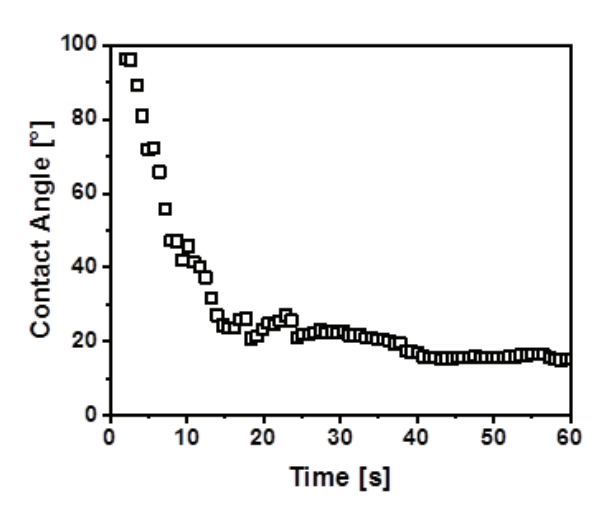


Figure 6.11. Sessile Drop Contact Angle development in dependence on time for a TXP foil.

The hypothesis of re-orientation can be verified by changing the medium from water to non-polar solvents such as n-hexadecane. If the hydrophobic polymer backbone is directed to the air, the sample will show a lipophilic behavior, which was tested for coated PTFE samples. In fact, due to the coating, the sample became more lipophilic than the blank PTFE as shown in Figure 6.10f (advancing CA $29.4^{\circ} \pm 5.0^{\circ}$ and receding CA $7.0^{\circ} \pm 0.7^{\circ}$ for the coated sample vs advancing CA $54.8^{\circ} \pm 0.8^{\circ}$ and receding CA $16.8^{\circ} \pm 3.4^{\circ}$ for the blank sample).

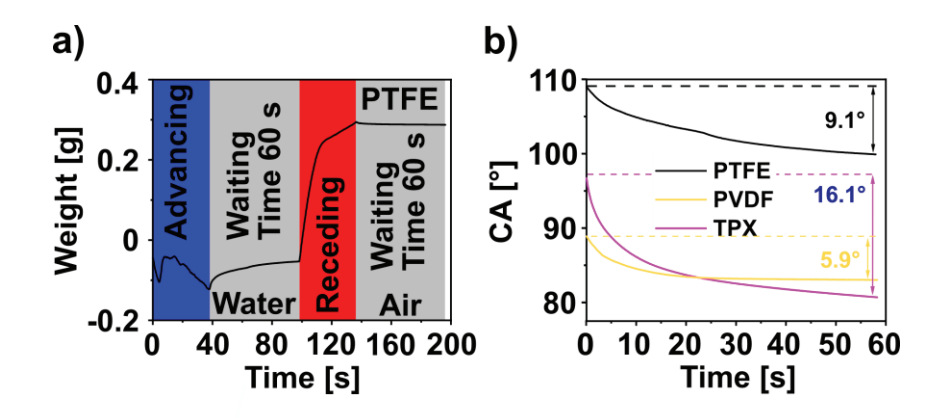


Figure 6.12. a) Time-dependent plot of the Wilhelmy balance for PTFE with a waiting time of 60 s. When immersed in the water phase the weight increases indicating swelling, while the weight only slightly decreased when removed from the water. b) The increase of the weight during the waiting time is transferred to the respective CA via equation 1. A higher decrease of the CA is correlated with a higher degree of swelling.

We further investigated the swelling behavior of the coating with respect to changes in waiting time in the water phase, between the advancing and receding CAs (Figure 6.12a). As can be seen from Figure 6.12a the weight was increased with a change of waiting time from 0 to 60s, indicating the swelling of the hydrogel film. The swelling gives an indirect trend for the thickness of the coating for a given crosslink density and the underlying layer material. In this case, the actual thickness is comparatively difficult to measure due to the surface structure of the foils. To correct differences, arising from the sample geometry the weight was transferred to the CA *via* equation 1 as shown in Figure 6.12b. The order of swelling obtained by the Wilhelmy balance shows TPX> PTFE> PVDF.

Conclusion

In this work, we show a fast and facile method to generate a stable, hydrophilic, and functional hydrogel coating onto PTFE, PVDF, and TPX under ambient conditions. The presence of accessible primary amine in the hydrogel allows flexible post-modification. While TPX is rich in C-H bonds, PVDF has less, and PTFE has none of it. Moreover, in none of the polymer substrates N-H or C=C bonds are present. The absence of C- H bonds in PTFE raises the question of whether the film is chemically or physically bound to the foil. A chemical bonding in PTFE would require the insertion of the nitrene in the C-F bond. In the case of PTFE since the abstraction of the hydrogen atoms is not possible a stable hydrogel coating on the surface

of these polymers can only result from N-F bond formation. Non-covalent hydrophobic interactions of the tetrafluoro phenyl group on the PTFE surface is ruled out as it can unlikely form a stable hydrogel coating in the context of our polymer composition. In such a case, the swelling of the hydrogel layer will lead to a strong increase in the volume of this coating, which will induce stress not only normal to the surface but also within the plane of the surface, eventually delaminating the complete layer or parts of it. To the best of our knowledge, there are no studies that explore the C-H insertion for fluorinated polymers.

By using dynamic contact angle measurements at the air-water interface, we showed that the coating resembles a loosely crosslinked hydrogel layer where the polymer chains can re-orient once in contact with air or water. In future works, the primary amine concentration of the coating will be tailored for bio-functionalization.

4. References

- 1. Ren, X.; Feng, Y.; Guo, J.; Wang, H.; Li, Q.; Yang, J.; Hao, X.; Lv, J.; Ma, N.; Li, W., Surface modification and endothelialization of biomaterials as potential scaffolds for vascular tissue engineering applications. *Chemical Society reviews* **2015**, *44* (15), 5680-742.
- 2. Jaganathan, S. K.; Supriyanto, E.; Murugesan, S.; Balaji, A.; Asokan, M. K., Biomaterials in cardiovascular research: applications and clinical implications. *BioMed research international* **2014**, *2014*, 459465.
- 3. Subramaniam, A.; Sethuraman, S., Biomedical Applications of Nondegradable Polymers. In *Natural and Synthetic Biomedical Polymers*, 2014; pp 301-308.
- 4. de Mel, A.; Cousins, B. G.; Seifalian, A. M., Surface modification of biomaterials: a quest for blood compatibility. *Int J Biomater* **2012**, *2012*, 707863.
- 5. Meinhart, J. G.; Deutsch, M.; Fischlein, T.; Howanietz, N.; Fröschl, A.; Zilla, P., Clinical autologous *in vitro* endothelialization of 153 infraingiunal ePTFE grafts. *Ann. Thorac. Surg.* **2001**, *71*, S327-S331.
- 6. Pflaum, M.; Kuhn-Kauffeldt, M.; Schmeckebier, S.; Dipresa, D.; Chauhan, K.; Wiegmann, B.; Haug, R. J.; Schein, J.; Haverich, A.; Korossis, S., Endothelialization and characterization of titanium dioxide-coated gas-exchange membranes for application in the bioartificial lung. *Acta biomaterialia* **2017**, *50*, 510-521.
- 7. Keeshan, B. C.; Rossano, J. W.; Beck, N.; Hammond, R.; Kreindler, J.; Spray, T. L.; Fuller, S.; Goldfarb, S., Lung transplant waitlist mortality: height as a predictor of poor outcomes. *Pediatr Transplant* **2015**, *19* (3), 294-300.

- 8. Hosseinnejad, A.; Fischer, T.; Jain, P.; Bleilevens, C.; Jakob, F.; Schwaneberg, U.; Rossaint, R.; Singh, S., Enzyme mimetic microgel coating for endogenous nitric oxide mediated inhibition of platelet activation. *Journal of Colloid and Interface Science* **2021**.
- 9. Hosseinnejad, A.; Ludwig, N.; Wienkamp, A. K.; Rimal, R.; Bleilevens, C.; Rossaint, R.; Rossaint, J.; Singh, S., DNase I functional microgels for neutrophil extracellular trap disruption. *Biomaterials science* **2021**, *10* (1), 85-99.
- 10. Winnersbach, P.; Hosseinnejad, A.; Breuer, T.; Fechter, T.; Jakob, F.; Schwaneberg, U.; Rossaint, R.; Bleilevens, C.; Singh, S., Endogenous Nitric Oxide-Releasing Microgel Coating Prevents Clot Formation on Oxygenator Fibers Exposed to In Vitro Blood Flow. *Membranes* **2022**, *12* (1).
- 11. Cassady, A. I.; Hidzir, N. M.; Grøndahl, L., Enhancing expanded poly(tetrafluoroethylene) (ePTFE) for biomaterials applications. *Journal of Applied Polymer Science* **2014**, *131* (15), 40533.
- 12. Crombez, M.; Chevallier, P.; Gaudreault, R. C.; Petitclerc, E.; Mantovani, D.; Laroche, G., Improving arterial prosthesis neo-endothelialization: application of a proactive VEGF construct onto PTFE surfaces. *Biomaterials* **2005**, *26* (35), 7402-9.
- 13. Mohd Hidzir, N.; Hill, D. J. T.; Taran, E.; Martin, D.; Grøndahl, L., Argon plasma treatment-induced grafting of acrylic acid onto expanded poly(tetrafluoroethylene) membranes. *Polymer* **2013**, *54* (24), 6536-6546.
- 14. Williams, S. K.; Kleinert, L. B.; Patula-Steinbrenner, V., Accelerated neovascularization and endothelialization of vascular grafts promoted by covalently bound laminin type 1. *Journal of biomedical materials research*. *Part A* **2011**, *99* (1), 67-73.
- 15. Prucker, O.; Naumann, C. A.; Rühe, R.; Knoll, W.; Frank, C. W., Photochemical Attachement of Polymer Films to Solid Surfaces via Monolayers of Benzophenone Derivatives. *J. Am. Chem. Soc.* **1999**, *121*, 8766-8770.
- 16. Kotrade, P. F.; Ruhe, J., Malonic Acid Diazoesters for C-H Insertion Crosslinking (CHic) Reactions: A Versatile Method for the Generation of Tailor-Made Surfaces. *Angew. Chem. Int. Ed. Engl.* **2017**, *56* (46), 14405-14410.
- 17. Zunker, S.; Rühe, J., Photo-Crosslinking of Thioxanthone Group Containing Copolymers for Surface Modification and Bioanalytics. *Macromolecules* **2020**, *53* (5), 1752-1759.
- 18. Breslow, D. S.; Sloan, M. F.; Newburg, N. R.; Renfrow, W. B., Thermal Reactions of Sulfonyl Azides. *J. Am. Chem. Soc.* **1969**, *91*, 2273-2279.

- 19. Schuh, K.; Prucker, O.; Rühe, J., Tailor-Made Polymer Multilayers. *Adv. Funct. Mater.* **2013**, *23* (48), 6019-6023.
- 20. Navarro, R.; Perez Perrino, M.; Prucker, O.; Ruhe, J., Preparation of surface-attached polymer layers by thermal or photochemical activation of alpha-diazoester moieties. *Langmuir* **2013**, *29* (34), 10932-9.
- 21. Pandiyarajan, C. K.; Prucker, O.; Zieger, B.; Ruhe, J., Influence of the molecular structure of surface-attached poly(N-alkyl acrylamide) coatings on the interaction of surfaces with proteins, cells and blood platelets. *Macromol Biosci* **2013**, *13* (7), 873-84.
- 22. Zou, P.; Laird, D.; Riga, E. K.; Deng, Z.; Dorner, F.; Perez-Hernandez, H. R.; Guevara-Solarte, D. L.; Steinberg, T.; Al-Ahmad, A.; Lienkamp, K., Antimicrobial and cell-compatible surface-attached polymer networks how the correlation of chemical structure to physical and biological data leads to a modified mechanism of action. *J. Mater. Chem. B* **2015**, *3* (30), 6224-6238.
- 23. Itagaki, N.; Oda, Y.; Hirata, T.; Nguyen, H. K.; Kawaguchi, D.; Matsuno, H.; Tanaka, K., Surface Characterization and Platelet Adhesion on Thin Hydrogel Films of Poly(vinyl ether). *Langmuir* **2017**, *33* (50), 14332-14339.
- 24. Moschallski, M.; Baader, J.; Prucker, O.; Ruhe, J., Printed protein microarrays on unmodified plastic substrates. *Anal Chim Acta* **2010**, *671* (1-2), 92-8.
- 25. Scherag, F. D.; Niestroj-Pahl, R.; Krusekopf, S.; Lucke, K.; Brandstetter, T.; Ruhe, J., Highly Selective Capture Surfaces on Medical Wires for Fishing Tumor Cells in Whole Blood. *Anal Chem* **2017**, *89* (3), 1846-1854.
- 26. Brandstetter, T.; Bohmer, S.; Prucker, O.; Bisse, E.; zur Hausen, A.; Alt-Morbe, J.; Ruhe, J., A polymer-based DNA biochip platform for human papilloma virus genotyping. *J Virol Methods* **2010**, *163* (1), 40-8.
- 27. Moschallski, M.; Evers, A.; Brandstetter, T.; Ruhe, J., Sensitivity of microarray based immunoassays using surface-attached hydrogels. *Anal Chim Acta* **2013**, *781*, 72-9.
- 28. Zinggeler, M.; Schonberg, J. N.; Fosso, P. L.; Brandstetter, T.; Ruhe, J., Functional Cryogel Microstructures Prepared by Light-Induced Cross-Linking of a Photoreactive Copolymer. *ACS Appl Mater Interfaces* **2017**, *9* (14), 12165-12170.
- 29. Hong, J. S.; Nakahara, T.; Maeda, H.; Kikunaga, Y.; Kishida, A.; Akashi, M., Cloud Points and Phase Separation of Aqueous Poly(*N*-vinylacetamide) Solutions in the Presence of Salts. *Colloid Polym. Sci.* **1996**, *274*, 1013-1019.

- 30. Fischer, T.; Köhler, J.; Keul, H.; Singh, S.; Möller, M., Highly Swellable Hydrogels from Waterborne Poly(vinylamine-co-acetamide). *Macromol. Chem. Phys.* **2018**, *219*, 1800399-1800408.
- 31. Pinschmidt, R. K. J., Poly(vinylamine) at Last. *J. Polym. Sci. A: Polym. Chem.* **2010**, 48, 2257-2283.
- 32. Pelton, R., Polyvinylamine: A Tool for Engineering Interfaces. *Langmuir* **2014**, *30* (51), 15373-82.
- 33. Schock, M.; Brase, S., Reactive & Efficient: Organic Azides as Cross-Linkers in Material Sciences. *Molecules* **2020**, *25* (4).
- 34. Noy, J.-M.; Li, Y.; Smolan, W.; Roth, P. J., Azide–para-Fluoro Substitution on Polymers: Multipurpose Precursors for Efficient Sequential Postpolymerization Modification. *Macromolecules* **2019**, *52* (8), 3083-3091.
- 35. Volpe, C. D.; Siboni, S., The Wilhelmy method: a critical and practical review. *Surface Innovations* **2018**, *6* (3), 120-132.
- 36. https://www.accudynetest.com/. (accessed 14.11.2021).
- 37. Mieres-Perez, J.; Mendez-Vega, E.; Velappan, K.; Sander, W., Reaction of Triplet Phenylnitrene with Molecular Oxygen. *J Org Chem* **2015**, *80* (24), 11926-31.
- 38. Meijer, E. W.; Nijhuis, S.; van Vroonhoven, F. C. B. M., Poly-1,2-azepines by the Photopolymerization of Phenyl Azides. Precursors for Conducting Polymer Films. *J. Am. Chem. Soc.* **1998**, *110*, 7209-7210.
- 39. Socrates, G., *Infrared and Raman Characteristic Group Frequencies: Tables and Charts*. Wiley: Chichester, New York, Weinheim, Toronto, Brisbane, Singapore, 2004.
- 40. Mieres-Perez, J.; Mendez-Vega, E.; Velappan, K.; Sander, W., Reaction of triplet phenylnitrene with molecular oxygen. *J. Org. Chem.* **2015**, *80* (24), 11926-31.
- 41. Setiawan, D.; Sethio, D.; Cremer, D.; Kraka, E., From strong to weak NF bonds: on the design of a new class of fluorinating agents. *Phys Chem Chem Phys* **2018**, *20* (37), 23913-23927.
- 42. Szleifer, l., Polymers and proteins: interactions at interfaces. *Curr. Opin. Solid State Mater. Sci.* **1997**, *2*, 337-344.
- 43. Illergard, J.; Wagberg, L.; Ek, M., Bacterial-growth inhibiting properties of multilayers formed with modified polyvinylamine. *Colloids and surfaces. B, Biointerfaces* **2011,** 88 (1), 115-20.

- 44. Horinouchi, A.; Atarashi, H.; Fujii, Y.; Tanaka, K., Dynamics of Water-Induced Surface Reorganization in Poly(methyl methacrylate) Films. *Macromolecules* **2012**, *45* (11), 4638-4642.
- 45. Zuo, B.; Liu, Y.; Wang, L.; Zhu, Y.; Wang, Y.; Wang, X., Depth profile of the segmental dynamics at a poly(methyl methacrylate) film surface. *Soft Matter* **2013**, *9* (39), 9376-9384
- 46. Horinouchi, A.; Fujii, Y.; Yamada, N. L.; Tanaka, K., Surface Reorganization of Thin Poly(methyl methacrylate) Films Induced by Water. *Chemistry Letters* **2010**, *39* (8), 810-811.
- 47. Myalitsin, A.; Ghosh, S.; Urashima, S. H.; Nihonyanagi, S.; Yamaguchi, S.; Aoki, T.; Tahara, T., Structure of water and polymer at the buried polymer/water interface unveiled using heterodyne-detected vibrational sum frequency generation. *Phys Chem Chem Phys* **2020**, *22* (29), 16527-16531.
- 48. Senshu, K.; Yamashita, S.; Ito, M.; Hirao, A.; Nakahama, S., Surface Characterization of 2-Hydroxyethyl Methacrylate/Styrene Block Copolymers by Transmission Electron Microscopic Observation and Contact Angle Measurement. *Langmuir* **1995**, *11*, 2293-2300.

Acknowledgements

I would like to thank Prof. Dr. Martin Möller for being my doctoral father and giving me the opportunity to research in his group at DWI Leibniz Institute for Interactive Materials with its great facilities and devices learning numerous different analytic techniques. I am grateful for his mentorship and guidance on my PhD research. I would also like to thank Professor Dr. Andij Pich for being my second supervisor.

Furthermore, I would like to thank Dr. Smriti Singh for her guidance during my PhD. I am also thankful to my colleagues Puja, Aisa, Prachi, and Rahul for the collaborations and group meetings.

I would also like to thank Professor Dr. Dan Demco for fruitful discussions about thermoresponsitivity and his insights in NMR spectroscopy. I am also thankful to Dr. Jens Köhler and Dr. Helmut Keul for the introduction into the PVAm chemistry and helpful advices.

I am also thankful to the electron microscopy team Dr. Khosrow Rahimi, Michelle, Sabrina, Silke, and Marco.

I would also like to thank Petra Esser for her patience while several of my flasks exploded during lyophilization before knowing the optimum concentration of the polymer for lyophilization.

I would also like to thank Markus Reichelt for his competent answers in safety questions and his guidance for being lab responsible.